THE JOURNAL
OF
CHEMICAL PHYSICS

VOLUME 19, NUMBER 11 NOVEMBER, 1951

The Cataphoresis of Spherical Fluid Droplets in Electrolytes

F. BOOTH
Department of Theoretical Physics, Wheatstone Laboratory, King's College, London, England
(Received April 12, 1951)

A theory of the electrophoresis of spherical fluid droplets in an electrolyte is developed. A general formula is given for the electrophoretic velocity in terms of the applied field, the potential distribution in and near the drops, and the dielectric constants and coefficients of viscosity of the liquid and electrolyte. It is assumed that the liquid drop retains its spherical form in cataphoresis and also that relaxation effects in the electrolyte may be neglected.

Detailed formulas are worked out for the case of a Debye-Hückel potential in the electrolyte, and the following charge distributions in the fluid sphere.

(a) No charge within the sphere; the whole charge is concentrated on the interface.
(b) Uniform volume distribution of charge.
(c) Ionic double layer potential in the sphere.

It is shown that sundry special cases of the theory agree with previous computations and that it is not legitimate to apply theories of the cataphoresis of solid particles to fluid drops.

1. INTRODUCTION

In recent years a considerable amount of attention has been paid to the theory of the electrophoresis of solid charged particles in electrolytes. The problem of relating the zeta-potential and the rate of electrophoresis of spherical particles has been solved completely by Henry,[1] for the limiting case of small applied fields and low zeta-potentials. His work is an extension of earlier calculations by Smoluchowski.[2] More recently other writers have attempted to extend the range of application of Henry's work by taking into account relaxation effects[3] and the nonlinearity of the hydrodynamical equations of motion of the electrolyte.[4]

All the treatments mentioned above apply only to the cataphoresis of *solid* particles. However, in many cases of practical interest, for example emulsions, we have to deal with suspensions of fine *fluid* droplets. The results of theories of the cataphoresis of solids have sometimes been used to calculate the zeta-potentials of liquid droplets or even of air bubbles,[5] from electrophoretic measurements. This procedure is of course quite unjustified, since different boundary conditions apply in the two cases. For a solid particle the fluid velocity with respect to the center of the sphere vanishes at the interface; on the other hand, for a sphere of fluid the normal component of the velocity must vanish at the interface, but the tangential component is merely continuous. In this note we shall develop a theory of the electrophoresis of spherical fluid drops which is closely analogous to Henry's theory for solid particles. We shall not attempt to take into account the complicated refinements examined in the later papers. Even so, the analysis is more difficult than for solids since the motion of the fluid within the drop must be taken into account. The analysis will be based on the following assumptions.

(1) The fluid sphere remains spherical when the external field is applied. Although the solution we shall derive will be exact provided this assumption is satisfied, in practice, other solutions may be possible. The spherical form may become unstable when the field is applied and consequently the drop may take up less simple shapes. Any analysis of the stability or of the motion of nonspherical drops would be extremely difficult. It would seem to be very desirable therefore, before deductions are made from any experimental data, to verify by direct observation whether or not the shape is

[1] D. C. Henry, Proc. Roy. Soc. (London) **A133**, 106 (1931).
[2] M. v. Smoluchowski, Z. physik. Chem. **93**, 129 (1918).
[3] (a) J. Th. G. Overbeek, Kolloidbeihefte **54**, 287 (1943). (b) F. Booth, Proc. Roy. Soc. (London) **A203**, 514 (1950).
[4] F. Booth, J. Chem. Phys. **18**, 1361 (1950).
[5] (a) H. A. MacTaggart, Phil. Mag. (6) **27**, 297 (1914); **28**, 367 (1914). (b) T. Alty, Proc. Roy. Soc. (London) **A106**, 315 (1924); **A110**, 178 (1926).

altered appreciably by the external field. Since the surface energy arising from the interfacial tension of the two liquids is at a minimum for the spherical form, the the greater this surface tension, the less will be the tendency for the shape to alter.

(2) The charge and potential distribution both within and without the liquid sphere are spherically symmetrical in the steady state when there is no external field.

(3) The field distribution when an external field is applied is simply the vector sum of the field in the undisturbed state, and the field which would obtain if there were no charge in the liquid drop. This means that we shall neglect relaxation effects in the electrolyte and also any asymmetry of the charge distribution on the surface or within the drop, due to the fluid motion. This assumption corresponds to assumption (3) of Henry's paper.[1] The work on the relaxation effect for the cataphoresis of solid particles indicates that terms arising from the relaxation effect are of order ζ^2 or ζ^3, where ζ denotes the zeta-potential of the solid surface with respect to the electrolyte. It is easy to see by considering the way in which relaxation affects cataphoresis without examining the matter in detail, that the same result must obtain for liquid spheres. For the magnitude of the asymmetry of the charge distribution arising from relaxation must be of order ζ at most. The contribution of the relaxation effect to the electrophoretic velocity arises from the interaction between the asymmetrical part of the charge distribution and the symmetrical part. Since the latter is itself of order ζ, it follows that the effect on the velocity is at most of order ζ^2. Consequently we may take it that our analysis will be correct provided that the zeta-potential for the liquid-liquid interface is not too large.

(4) The inertia terms in the equation of motions of the fluid in the drop and of the electrolyte can be ignored. This assumption is almost certainly justified unless very intense fields are employed (see reference 4). The assumption is equivalent to postulating that the cataphoretic velocity is proportional to the strength of the applied field.

(5) Both fluids can be regarded as incompressible.

(6) The dielectric constant, viscosity, and electrical conductivity of the liquids both inside and outside the sphere, retain their macroscopic values right up to the interface between the two fluids.

In the next section a general formula for the cataphoretic velocity in terms of the charge distribution and the external field will be derived. The third section contains explicit formulas obtained by utilizing various suitable distribution functions for the charge in the fluid drop. Three cases will be dealt with.

(a) Charge concentrated in a thin layer at the interface.

(b) Charge distribution of uniform density.

(c) Charge and potential distribution, that of an electrical double layer.

For the potential in the electrolyte we shall use the Poisson-Boltzmann equation with the Debye-Hückel approximation. It will be shown that a wide variety of results are obtained, some of them very different from those for solid particles, depending on the ratios of the viscosities of the liquids and the way in which the charge is distributed in the drop.

2. GENERAL CALCULATION OF THE CATAPHORETIC VELOCITY

To find the rate of electrophoresis it is necessary to solve the equations of motion and of continuity for both the electrolyte and the liquid in the drop. For the electrolyte these equations are, taking into account our basic assumptions,

$$\eta_1 \operatorname{curl}\operatorname{curl}\mathbf{v}_1+\operatorname{grad}p_1+\rho_1\operatorname{grad}\Psi_1=0, \tag{2.1}$$

$$\operatorname{div}\mathbf{v}_1=0, \tag{2.2}$$

where η_1 is the coefficient of viscosity, $\mathbf{v}_1$ the velocity, p_1 the pressure, ρ_1 the charge density, and Ψ_1 the electrostatic potential. Both Eqs. (2.1) and (2.2) refer to axes fixed with respect to the center of the sphere. From assumption 3, it follows that Ψ_1 can be written in the form

$$\Psi_1=\psi_1-Er\cos\theta\left[1+(\lambda a^3/r^3)\right], \tag{2.3}$$

where

$$\lambda=(\sigma_1-\sigma_2)/(2\sigma_1+\sigma_2). \tag{2.4}$$

σ_1 is the specific conductivity of the electrolyte and σ_2 that of the liquid in the drop; r denotes distance measured from the center of the spherical drop, and θ the angle the radius vector makes with the direction of the applied field E. ψ_1 is the potential when the external field is not applied. The charge density ρ_1, and the potential ψ_1 are related by Poisson's equation

$$\nabla^2\psi_1=-4\pi\rho_1/\epsilon_1, \tag{2.5}$$

where ϵ_1 is the dielectric constant of the electrolyte.

General solutions appropriate for our purpose, apart from a few minor modifications, have already been derived by Henry[6] and so we shall merely write them down

$$p_1=\int_r^\infty \rho_1(z)\frac{d\psi_1(z)}{dz}dz+A_1 +\cos\theta\left[B_1r+\frac{C_1}{r^2}-\frac{\epsilon_1E}{4\pi}\left(3\frac{d\psi_1}{dr}-2\xi(r)\right)\right], \tag{2.6}$$

$$v_{1,r}=\cos\theta\left[\frac{B_1r^2}{10\eta_1}+\frac{C_1}{\eta_1 r}+D_1+\frac{F_1}{r^3}-\frac{\epsilon_1E}{6\pi\eta_1} \times\left(\int_r^\infty \xi(z)dz-\frac{1}{r^3}\int_r^\infty z^3\xi(z)dz\right)\right], \tag{2.7}$$

[6] See reference 1, p. 113.

$$v_{1,\theta}=\sin\theta\left[-\frac{B_1r^2}{5\eta_1}-\frac{C_1}{2\eta_1 r}-D_1+\frac{F_1}{2r^3}+\frac{\epsilon_1 E}{6\pi\eta_1}\times\left(\int_r^\infty \xi(z)dz+\frac{1}{2r^3}\int_r^\infty z^3\xi(z)dz\right)\right], \quad (2.8)$$

$$v_{1,\alpha}=0, \quad (2.9)$$

where

$$\xi(r)=\frac{d\psi_1}{dr}+\frac{4\pi\lambda a^3 r}{\epsilon_1}\int_r^\infty \frac{\rho_1(z)}{z^4}dz. \quad (2.10)$$

$v_{1,r}$, $v_{1,\theta}$, and $v_{1,\alpha}$ denote the velocity components along the r, θ, and α directions where (r, θ, α) are the usual spherical polar coordinates. The quantities A_1, B_1, C_1, D_1, and F_1 are integration constants which must be found from the boundary conditions.

Now consider the motion of the liquid in the spherical drop. Equations of the form of (2.1) and (2.2) again apply, but the potential is now

$$\Psi_2=\psi_2-Er\cos\theta(1+\lambda), \quad (2.11)$$

where now ψ_2 denotes the potential in the liquid when there is no external field. The solution for the pressure and the velocity components is quite straightforward and we shall merely set down the results. All symbols have the same physical meaning as assigned in Eqs. (2.1) and (2.2), but they are now distinguished by the suffix 2.

$$p_2=-\int_0^r \rho_2(z)\frac{d\psi_2(z)}{dz}dz+A_2+\cos\theta\left[B_2r+\frac{C_2}{r^2}-\frac{\epsilon_2E(1+\lambda)}{4\pi}\frac{d\psi_2}{dr}\right], \quad (2.12)$$

$$v_{2,r}=\cos\theta\left[\frac{B_2r^2}{10\eta_2}+\frac{C_2}{\eta_2 r}+D_2+\frac{F_2}{r^3}+\frac{\epsilon_2E(1+\lambda)}{6\pi\eta_2}\times\left(\int_0^r \frac{d\psi_2(z)}{dz}dz-\frac{1}{r^3}\int_0^r z^3\frac{d\psi_2(z)}{dz}dz\right)\right], \quad (2.13)$$

$$v_{2,\theta}=\sin\theta\left[-\frac{B_2r^2}{5\eta_2}-\frac{C_2}{2\eta_2 r}-D_2+\frac{F_2}{2r^3}-\frac{\epsilon_2E(1+\lambda)}{6\pi\eta_2}\times\left(\int_0^r \frac{d\psi_2(z)}{dz}dz+\frac{1}{2r^3}\int_0^r z^3\frac{d\psi_2(z)}{dz}dz\right)\right], \quad (2.14)$$

$$v_{2,\alpha}=0. \quad (2.15)$$

In Eqs. (2.12) to (2.14), A_2, B_2, C_2, D_2, and F_2 are again constants of integration. To fix these constants and the corresponding set for Eqs. (2.6) to (2.8), the boundary conditions must now be applied.

Since the velocity and pressure at both the origin and at infinity must remain finite we have

$$B_1=C_2=F_2=0. \quad (2.16)$$

At the boundary between the two liquids, the normal components of the velocity vanish for both liquids;

$$v_{1,r}(a,\theta)=v_{2,r}(a,\theta)=0, \quad 0\leqslant\theta\leqslant 2\pi. \quad (2.17)$$

The tangential component of the velocity is continuous;

$$v_{1,\theta}(a,\theta)=v_{2,\theta}(a,\theta), \quad 0\leqslant\theta\leqslant 2\pi. \quad (2.18)$$

Finally we have two further relations from the continuity of the tangential and normal stress across the interface.

$$\eta_1\left(\left.\frac{\partial v_{1,\theta}}{\partial r}\right|_a-\frac{v_{1,\theta}(a,\theta)}{a}\right)+\frac{\epsilon_1E(1+\lambda)}{4\pi}\sin\theta\left.\frac{d\psi_1}{dr}\right|_a=\eta_2\left(\left.\frac{\partial v_{2,\theta}}{\partial r}\right|_a-\frac{v_{2,\theta}(a,\theta)}{a}\right)+\frac{\epsilon_2E(1+\lambda)}{4\pi}\sin\theta\left.\frac{d\psi_2}{dr}\right|_a, \quad (2.19)$$

$$\frac{2T_{12}}{a}+p_1(a,\theta)-2\eta_1\left.\frac{\partial v_{1,r}}{\partial r}\right|_a-\frac{\epsilon_1}{8\pi}\left.\frac{d\psi_1}{dr}\right|_a\left(\left.\frac{d\psi_1}{dr}\right|_a-2E[1-2\lambda]\cos\theta\right)=p_2(a,\theta)-2\eta_2\left.\frac{\partial v_{2,r}}{\partial r}\right|_a-\frac{\epsilon_2}{8\pi}\left.\frac{d\psi_2}{dr}\right|_a\times\left(\left.\frac{d\psi_2}{dr}\right|_a-2E[1+\lambda]\cos\theta\right). \quad (2.20)$$

The last terms on each side of the above equations arise from the electrical stresses across the boundary surface due to the difference between the fields on opposite sides of the boundary. These stress components are easily derived from the potentials of Eqs. (2.3) and (2.11) by the use of the well-known maxwell stress tensor. Terms of small order involving E^2 have been dropped in accordance with our basic assumption 4. T_{12} denotes the interfacial tension between the two liquids.

Relations (2.17) to (2.20) furnish just sufficient equations to determine uniquely all the constants of integration not already determined by condition (2.16) apart from A_1 the value of which does not affect the cataphoretic velocity. The solution is straightforward but tedious; however, we do not need to know all the constants but only D_1, since in the steady state, the cataphoretic velocity U, which is the only quantity we required, is simply the velocity $(-\mathbf{v})$ at infinity. We finally obtain the following general expression for U.

$$U=-\frac{E}{6\pi\eta_1(3\eta_2+2\eta_1)}\left[3\epsilon_1\eta_2\int_a^\infty \xi(z)dz+\eta_1\left(\epsilon_1\left[2\int_a^\infty \xi(z)dz-a(1+\lambda)\left.\frac{d\psi_1}{dr}\right|_a+a\xi(a)\right]+\frac{5\epsilon_2(1+\lambda)}{a^3}\int_0^a z^3\frac{d\psi_2(z)}{dz}dz\right)\right]. \quad (2.21)$$

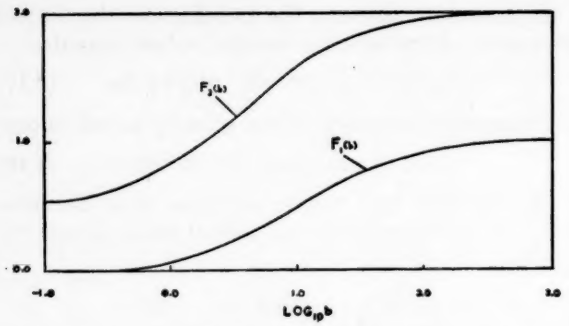

FIG. 1. Functions $F_1(b)$ and $F_2(b)$, Eqs. (3.5) and (3.6).

Before considering special cases of Eq. (2.21), it is interesting to note that it gives Henry's formula for solid particles. For in this case η_2 has the value infinity, and so

$$U=-E\epsilon_1\int_a^\infty \xi(z)dz/6\pi\eta_1. \tag{2.22}$$

3. FORMULAS IN SPECIAL CASES

Equation (2.21) is quite general provided that ψ_1 and ψ_2 have spherical symmetry. It is now necessary to examine the results when the special forms for ψ_1 and ψ_2 which are likely to arise in practice, are substituted in Eq. (2.21). First let us consider the potential outside the sphere. In the general case this potential will satisfy the Poisson-Boltzmann equation.

$$\frac{d^2\psi_1}{dr^2}+\frac{2}{r}\frac{d\psi_1}{dr}=-\frac{4\pi e}{\epsilon_1}\sum_{i=1}^{s} n_i z_i \exp(-ez_i\psi_1/\mathbf{k}T) \tag{3.1}$$

where n_i is the concentration of the ions of type i at infinity (where ψ_1 is set equal to zero), z_i their valency. The summation is over the ionic species in the electrolyte. Equation (3.1) may be investigated numerically,[7] or a power series solution in terms of the total charge in the sphere obtained.[8] If the charge is not too large, so that $e\psi/\mathbf{k}T$ is very small everywhere, the Debye-Hückel approximation can be applied and we may write

$$\psi_1=\frac{a\zeta}{r}\exp\kappa_1(a-r)+O(\zeta^2), \tag{3.2}$$

where

$$\kappa_1^2=4\pi e^2\sum_{i=1}^{s} n_i z_i^2/\epsilon_1\mathbf{k}T$$

and ζ is the potential at the interface where r equals a. The terms of order ζ^2 in expression (3.2) can be obtained explicitly. They are very complicated however, and the work on the cataphoresis of solid spheres indicates that if terms of this order were included, it would be necessary to take into account the distortion of the double layer field in the electrolyte.[9] If expression (3.2) is substituted in Eq. (2.10), $\xi(r)$ is easily calculated, and expression (2.22) now becomes, when terms of order ζ^2 are dropped

$$U=E\Big[\epsilon_1\zeta(3\eta_2[1+\lambda F_1(b)]+2\eta_1[1-\lambda F_2(b)])$$
$$-\frac{5\epsilon_2\eta_1(1+\lambda)}{a^3}\int_0^a z^3\frac{d\psi_2(z)}{dz}dz\Big]\Big/6\pi\eta_1(3\eta_2+2\eta_1), \tag{3.4}$$

where

$$F_1(b)=\frac{1}{8}b^2-\frac{5}{24}b^3-\frac{1}{48}b^4+\frac{1}{48}b^5$$
$$+\frac{1}{4}b^4e^bE_i(b)\left(1-\frac{1}{12}b^2\right), \tag{3.5}$$

$$F_2(b)=\frac{1}{2}+\frac{1}{2}b-\frac{1}{4}b^2+\frac{1}{4}b^3-\frac{1}{4}b^4e^bE_i(b), \tag{3.6}$$

and

$$b=\kappa_1 a. \tag{3.7}$$

The limiting forms of $F_1(b)$ and $F_2(b)$ are

$$\begin{aligned} F_1(b)&=0, \quad b\ll 1;=1, \quad b\gg 1.\\ F_2(b)&=\tfrac{1}{2}, \quad b\ll 1;=2, \quad b\gg 1.\end{aligned} \tag{3.8}$$

Both functions are plotted in Fig. 1.

Now consider the potential ψ_2. Three types of charge distribution would seem to be of practical interest and so we shall now consider each of them separately in some detail.

(a) No Charge within the Fluid Sphere

All the charge giving rise to the double-layer field in the outer electrolyte must reside on the interface. In addition there may be an adsorbed layer of dipole molecules which will give rise to a discontinuity in the potential across the interface. We have

$$\psi_2=\zeta+\psi_s, \tag{3.9}$$

where ψ_s is the potential discontinuity, and so

$$U=E\epsilon_1\zeta[3\eta_2(1+\lambda F_1(b))$$
$$+2\eta_1(1-\lambda F_2(b))]/6\pi\eta_1(3\eta_2+2\eta_1). \tag{3.10}$$

We see that U is entirely independent of ψ_s. Various special cases of this formula are of interest. For example, if λ equals zero, implying that the conductivities of the

[7] H. Müller, Kolloidchem. Beihefte **26**, 257 (1928).
[8] F. Booth, J. Chem. Phys. **19**, 821 (1951).

[9] See reference 3 (b), Fig. 2. In this graph the functions $F_3^*(b)$ and $Z_3^*(b)$ together, represent the corrections to U of order ζ^3 due to the distortion of the double layer field for *solid* spheres in a symmetrical electrolyte. $X_3^*(b)$ represents the contribution to U from terms of order ζ^3 in the equilibrium potential ψ_1 given by (3.2) above. It will be seen that the various corrections are of the same order of magnitude.

liquids are identical, then we have

$$U=E\epsilon_1\zeta/6\pi\eta_1. \tag{3.11}$$

This is identical with a formula originally obtained by Hückel[10] for *solid* particles under the same conditions, that is for σ_1 and σ_2 equal; hence for this case the velocity is independent of the viscosity of the fluid in the drop.

The limiting forms for very large or very small drops are easily derived from the limiting values (3.8) for b very small and very large, since the parameter b represents the ratio of the particle radius to the double-layer thickness. Thus for extremely fine droplets for which the double-layer thickness is much greater than the radius,

$$U=E\epsilon_1\zeta[3\eta_2+\eta_1(2-\lambda)]/6\pi\eta_1[3\eta_2+2\eta_1],\quad b\ll 1. \tag{3.12}$$

But for drops whose radius is much greater than the double layer thickness,

$$U=E\epsilon_1\zeta[3\eta_2(1+\lambda)+2\eta_1(1-2\lambda)]/6\pi\eta_1[3\eta_2+2\eta_1],\quad b\gg 1. \tag{3.13}$$

For nonconducting solid particles Eq. (3.13) gives, $U=E\epsilon_1\zeta/4\pi\eta_1$, which is Smoluchowski's well-known formula. For bubbles of gas in a liquid we have λ equal to $\frac{1}{2}$, since the gas will be effectively nonconducting compared with the electrolyte, and η_2 may be neglected in comparison with η_1. Also, since the double layer thickness is 10^{-4} cm or less we will have in general, b very large. From Eq. (3.13) we now see that U must vanish; consequently whatever the charge on the interface there is no electrophoresis. The contradiction between this result and some of the observations of McTaggart and Alty,[5] who certainly obtained electrophoresis of air bubbles, is of interest. The simplest explanation is that our basic assumption 6 is not justified in these cases. It is reasonable to postulate that there is a variation of the viscosity as the double layer is traversed, owing to the unbalanced intermolecular forces at the surface.

(b) Uniform Charge Distribution through the Sphere

In this case ψ_2 will not be constant and consequently there will be a contribution from the last integral in Eq. (2.21). Let ρ_2 denote the charge density per unit volume; then applying Gauss's theorem to a sphere of radius r, we find

$$\epsilon_2\frac{d\psi_2}{dr}=-4\pi\rho_2 r/3,\quad 0\leqslant r<a. \tag{3.14}$$

ρ_2 is related to ζ since the normal induction across the interface is continuous, if there is no charge residing on the boundary

$$\rho_2=3\epsilon_1\zeta(b+1)/4\pi a^2. \tag{3.15}$$

Combining Eqs. (3.14) and (3.15) gives

$$U=\frac{E\epsilon_1\zeta}{6\pi\eta_1(3\eta_2+2\eta_1)}[3\eta_2(1+\lambda F_1(b))+\eta_1(3+b+\lambda[1+b-2F_2(b)])]. \tag{3.16}$$

One case of this formula is of particular interest. Suppose that λ equals zero, so that the external field is uniform throughout the solution; also let the double-layer thickness be large compared with the radius, so that the parameter b is very small. Then the problem is equivalent to that of a sphere of fluid acted upon by a uniform body force

$$f_2=\rho_2 E \tag{3.17}$$

immersed in another fluid of different viscosity, with no body-force. In terms of f_2, Eq. (3.16) gives

$$U=\frac{2f_2a^2(\eta_1+\eta_2)}{3\eta_1(2\eta_1+3\eta_2)}. \tag{3.18}$$

But this case is equivalent to that of a sphere of fluid falling through another liquid of different density and viscosity. This particular problem has been examined by Hadamard,[11] and his result is equivalent to Eq. (3.18).

A slightly more complicated formula than Eq. (3.16) is obtained if we assume that there is also a *surface* charge on the interface. The only change in the analysis occurs in the relation between ζ and ρ_2; instead of Eq. (3.15) we have

$$\rho_2=3[\epsilon_1\zeta(b+1)-4\pi a\rho_s]/4\pi a^2, \tag{3.19}$$

where ρ_s is the surface charge density.

(c) Double-Layer Potential in the Sphere of Fluid

In many organic liquids ionic dissociation, and consequently double layer formation can occur exactly as in aqueous solutions. Provided that the organic liquid is immiscible with water, it can furnish the fluid of the interior sphere in our problem; this case will now give for the potential ψ_2 a more complex behavior than either of cases (a) or (b).

Let the ionic concentrations *inside* the sphere be denoted by $m_{2,i}$. The concentrations as functions of the potential will be given by

$$m_{2,i}=n_{2,i}\exp(-ez_i\psi_2/\mathbf{k}T),\quad i=1, 2\cdots s_2, \tag{3.20}$$

where $n_{2,i}$ denotes the concentration when ψ_2 is zero and s_2 the number of ionic species. Suppose we now form the sum

$$\sum_{i=1}^{s_2} m_{2,i}z_i=\sum_{i=1}^{s_2} n_{2,i}z_i\exp(-ez_i\psi_2/\mathbf{k}T). \tag{3.21}$$

As ψ_2 varies, this sum, which is proportional to the

[10] E. Hückel, Physik. Z. **25**, 204 (1924).

[11] J. Hadamard, Compt. rend. **152**, 1735 (1911).

charge density will alter. In general, at one particular value, ψ_n say, it will vanish. If we now write

$$\psi_2-\psi_n=\phi, \tag{3.22}$$

then the equation for ϕ is

$$\frac{d^2\phi}{dr^2}+\frac{2}{r}\frac{d\phi}{dr}-\kappa_2^2\phi=0, \tag{3.23}$$

where

$$\kappa_2^2=4\pi e^2\sum_{i=1}^{s2} n_{2,i}z_i^2\exp(-ez_i\psi_n/\mathbf{k}T)/\epsilon_2\mathbf{k}T. \tag{3.24}$$

In Eq. (3.24) we have assumed the Debye-Hückel approximation. The general solution of Eq. (3.24) is

$$\phi=\alpha e^{\kappa_2 r}/r+\beta e^{-\kappa_2 r}/r, \tag{3.25}$$

where α and β are constants of integration. At the origin we must have

$$\left.\frac{d\psi_2}{dr}\right|_o=\left.\frac{d\phi}{dr}\right|_o=0, \tag{3.26}$$

and so

$$\alpha=-\beta. \tag{3.27}$$

If there is no adsorbed charge on the interface, we have

$$\epsilon_2\left.\frac{d\psi_2}{dr}\right|_a=\epsilon_1\left.\frac{d\psi_1}{dr}\right|_a. \tag{3.28}$$

From Eqs. (3.2), (3.27), and (3.28), we find

$$\alpha=-a\epsilon_1\zeta(b_1+1)F_3(b_2)/\epsilon_2, \tag{3.29}$$

where

$$F_3(b_2)=[e^{b_2}(b_2-1)+e^{-b_2}(b_2+1)]^{-1}, \tag{3.30}$$

$$b_1=\kappa_1 a, \quad b_2=\kappa_2 a. \tag{3.31}$$

From Eq. (3.25) we now have

$$\int_0^a z^3\frac{d\psi_2(z)}{dz}dz=\frac{\alpha F_4(b_2)}{\kappa_2^2}, \tag{3.32}$$

where

$$F_4(b_2)=e^{b_2}(b_2^2-3b_2+3)-e^{-b_2}(b_2^2+3b_2+3). \tag{3.33}$$

The final formula for U in terms of ζ is now

$$U=\frac{E\epsilon_1\zeta}{6\pi\eta_1(3\eta_2+2\eta_1)}[3\eta_2(1+\lambda F_1(b_1))+\eta_1(2-2\lambda F_2(b_1)+5(1+\lambda)F_3(b_2)F_4(b_2)(b_1+1)b_2)^{-2}]. \tag{3.34}$$

For b_2 very small, corresponding to a very thick double layer; the limiting values of $F_3(b_2)$ and $F_3(b_2)$ are respectively, b_2^{-3} and $2b_2^5/15$. Substituting these values in Eq. (3.34) we regain Eq. (3.16). This is of course as it should be, since if the double layer thickness is very large compared with the radius, there is little variation of charge density through the drop, and the case (c) degenerates into case (b). For b_2 large, so that the double layer is near the interface, we find

$$U=\frac{E\epsilon_1\zeta}{6\pi\eta_1(3\eta_2+2\eta_1)}\left[3\eta_2(1+\lambda F_1(b_1))+\eta_1\left(2-2\lambda F_2(b_1)+\frac{5(1+\lambda)(b_1+1)}{b_2}\right)\right]. \tag{3.35}$$

When an absorbed charge resides on the interface, formula (3.34) is slightly modified. The only change in the analysis occurs in Eq. (3.28), where we now have

$$\epsilon_1\left.\frac{d\psi_1}{dr}\right|_a-\epsilon_2\left.\frac{d\psi_2}{dr}\right|_a+4\pi\rho_s=0, \tag{3.36}$$

where ρ_s is the surface density of the charge. The equation to determine α is easily found.

In common with cases (a) and (b), we see that the results are independent of the presence or absence of an adsorbed dipole layer on the interface.

Elastic Relaxation and Structure of Liquids. I. Ultrasonic Absorption in Some Halogenated Methylenes, Ethanes, and Ethylenes*

DANIELE SETTE
Istituto Nazionale di Ultracustica "O. M. Corbino," Rome, Italy

In order to obtain information on the presence of structural effects in the elastic relaxation phenomena observed in liquids, the ultrasonic absorption was studied as a function of temperature in some organic compounds whose structure is correlated in a simple way. Large differences of absorption coefficient and of its temperature dependence have been found. It is difficult, at the present time, to understand clearly the results, but they show that the liquid structure has a great importance in the relaxation phenomena present in liquids.

Moreover an increase in dipole moment of the molecules is often present with an increase of absorption, showing that the dipole moment is not related in a simple way with the characteristics of relaxation phenomena and that all the interactions among the molecules are to be taken in account.

1. INTRODUCTION

THE difference between experimental and classical values of the ultrasonic absorption coefficient in gases and liquids, as now seems fairly well established, is to be ascribed to the presence of relaxation phenomena. If such phenomena occur, the absorption coefficient for one wavelength attains a maximum when the period of ultrasonic waves is very near to the relaxation time and a noticeable dispersion can be detected in the velocity of propagation.

In the case of gases, it is possible to get the value of the maximum of the absorption coefficient for one wavelength and the velocity dispersion so that precise information is obtained on the nature of the phenomena involved.

In liquids, the relaxation times are usually so short that the measurements can be made only with acoustic waves whose period is much larger than the relaxation time. In the ordinary case no dispersion can be detected in the frequency range used, and the parameter α/ν^2 (α, absorption coefficient, ν, frequency) remains constant.

For this reason it is very difficult to have indications on the nature of the relaxation phenomena present in the liquids during the propagation of elastic waves.

In a complicated system like a liquid, many equilibria are present which may be altered by elastic waves and give origin to relaxation phenomena. Often when this happens, the relaxation times of the various phenomena are so different that only some particular one is really important in the frequency range in which the measurements are made. Anyway the assumption usually made that only one kind of relaxation phenomena is present each time, seems to be very restrictive.

Some indications of the coexistence of different phenomena were obtained studying binary mixtures.[1] It was in fact observed that the behavior of the absorption coefficient in mixtures formed by two liquids having similar absorption coefficients depends upon the nature of the two different molecules. Moreover, if strong interactions between the molecules of two unassociated liquids are present, the absorption of the mixtures cannot be explained by means of a treatment that seems to be valid for mixtures of unassociated and not interacting liquids.

Another way that can be useful in collecting information on the characteristics of relaxation phenomena in liquids is to consider how the absorption coefficient changes in a suitable series of organic compounds.

For these reasons we have studied the temperature dependence of the ultrasonic absorption coefficient in some methylenes, ethanes, and ethylenes in the range -20°C to 40°C. The experimental results are given in this paper.

2. METHOD OF MEASUREMENT

The measurements of the ultrasonic absorption coefficient were performed with a pulse method at about 30 Mc/s. Figure 1 gives the scheme of the experimental arrangement that does not essentially differ from those used by Pinkerton[2] and Litovitz.[3]

The measurements are made adjusting the electrical attenuation put before the receiver so that a pulse signal on the oscilloscope represents an acoustic echo of the same intensity at different distances between source and reflector.

As indicated in Fig. 1, a signal from the syncroscope

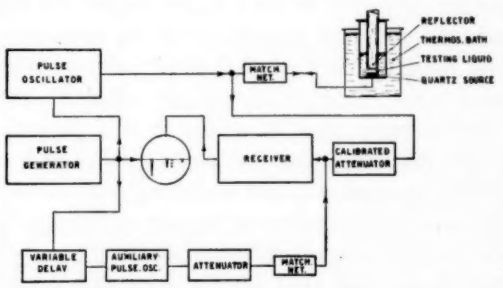

FIG. 1. Block diagram of equipment.

* Work done with the help of a grant of Italian Research Council at the Catholic University of America, Washington, D. C., aided by Contract N6 ONR-255III.

[1] D. Sette, J. Acoust. Soc. Am. **23**, 359 (1951).

[2] J. M. M. Pinkerton, Proc. Phys. Soc. (London) B **62**, 129 (1949).

[3] T. A. Litovitz, J. Acoust. Soc. Am. **23**, 75 (1951).

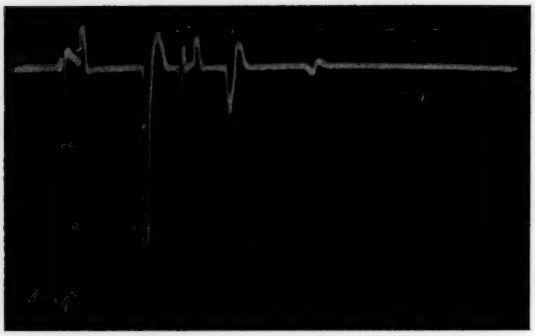

FIG. 2. Signals on the oscilloscope showing the main pulse, the echos, and the matching pulse.

drives through a variable delay system a second pulse oscillator whose output is fed directly into the receiver. Then a matching pulse is obtained on the scope that can easily be moved by means of the delay system, which is the reference signal level for the echo pulse used in measurements. Any influence of the receiver characteristics which depend on the value of the electric attenuation present between the main pulse oscillator and the receiver is therefore eliminated. The noncalibrated attenuator of the auxiliary pulse oscillator is used only to make the matching signal of suitable intensity. A picture of the signals, as seen on the oscilloscope is shown in Fig. 2.

The value of the absorption coefficient in some liquids has required an acoustic delay of the echo. A fused quartz rod was used for this purpose getting a delay of 25 μsec.

The absolute error in the measurements of the absorption coefficient with this experimental method is within the limits of 5 percent, while the accuracy in relative measurements is higher (2–3 percent).

In order to make possible the calculation of the classical value of the absorption coefficient also for liquids whose velocity of propagation is not available in the literature, a measurement of velocity was usually performed at 25°C. The method used for these measurements is the following one. The reflector is moved, remaining very near to the acoustic source. As it is well known, the electrical impedance of the source depends on the mechanically coupled fluid column. This impedence in fact changes periodically with the length of the fluid column, that is to say in the present case, with the distance between source and reflector, the period being equal to a half wavelength. If the distance between quartz and reflector is small these variations of impedance are very sensible so that the intensity of the emitted pulse and that of the echo are appreciably affected, and this makes possible a velocity measurement. These measurements of course are not very precise, but the accuracy (1–2 percent) is sufficient for our purpose.

3. EXPERIMENTAL RESULTS

The experimental results are reported in Table I for methylene chloride, methylene bromide, methylene iodide, 1,1 dichloroethane, 1,2 dichloroethane, 1,2 dibromoethane and for *cis*- and *trans*-dichloroethylene.

α is the amplitude absorption coefficient. The values of $(1/\alpha)(\partial\alpha/\partial t)$ indicated are calculated at $t=25$°C. The values of α_v/ν^2 are also calculated[4] because α_v, the absorption coefficient due to the viscosity of the liquid, is the principal part of the classical absorption coefficient. All the liquids tested have a low viscosity and from the table it appears that the excess of the experimental over the classical absorption coefficient is high.

4. DISCUSSION OF THE EXPERIMENTAL RESULTS

The temperature dependence of the absorption coefficient in methylene chloride is shown in Fig. 3. This liquid is one of the more absorbing liquids known; the value of the parameter α/ν^2 at 25°C is $1120\cdot10^{-17}$ sec^2/cm, about 200 times the absorption coefficient due to viscosity.

The value of the same parameter is about $900\cdot10^{-17}$ in benzene and $5500\cdot10^{-17}$ in carbon disulfide (at the same frequency). As it is known, the origin of relaxation phenomena in these two unassociated liquids seems due to the time required for the equipartition of energy among the internal degrees of freedom of the molecules. It has been suggested that the reasons of high absorption in these two liquids are to be found in the symmetry of the molecules and in the fact that only small couplings between translational and vibrational degrees of freedom are present in absence of electrostatic interactions, both liquids being nonpolar.

Different from benzene and carbon disulfide, the methylene chloride molecules do not have a large symmetry and they possess a dipole moment (1,55 D). Therefore, if the high absorption is mainly caused by the delay in the energy distribution among the internal degrees of freedom of the molecules, it may be the result of phenomena following a different scheme in which the interactions among more molecules are involved.

An indication of this possibility is obtained comparing the temperature dependences of the absorption coefficient in methylene chloride, benzene, and carbon disulfide. The absorption coefficient in benzene varies linearly throughout the temperature range between the melting and boiling points,[5] while the temperature coefficient of absorption, $(1/\alpha)(\partial\alpha/\partial t)$, in carbon disulfide goes to zero when the temperature approaches the boiling point.[6] The absorption coefficient in methylene chloride instead follows, at first, a linear law, but at higher temperature, when the boiling point is ap-

[4] For the velocity in the dichloroethylenes the values obtained by M. Baccaredda and A. Giacomini [Ricerca sci. **15**, 161 (1945)] were used.

[5] P. Bazulin, Compt. rend. acad. sci. URSS **14**, 273, (1937); H. Grobe, Physik Z. **39**, 333 (1938); B. J. Quinn, J. Acoust. Soc. Am. **18**, 185 (1946).

[6] D. Sette, J. Chem. Phys. **19**, 1342 (1951).

TABLE I. Ultrasonic absorption in halogenated methylenes, ethanes, and ethylenes.

Liquid	Chem. form.	ν (Mc/s)	t (°C)	Velocity $(m)/s$	α (cm^{-1})	$\alpha/\nu^2 \cdot 10^{17}$ sec^2/cm^{-1}	$(\alpha/\nu^2)_{visc} \cdot 10^{17}$ sec^2/cm	$1/\alpha(\partial\alpha/\partial\nu) \cdot 10^3$ (deg^{-1})	Manufacturer
Methylene chloride	CH_2Cl_2	29.9	−20.2		6.35	710			Eastman Kodak
			−13.7		6.82	763			
			−5.1		7.26	813			
			3.5		7.87	880			
			12.4		8.47	948			
			18.0		9.12	1020			
			22.0		9.82	1098			
			25.0	1100	9.96	1114	6.1	11.6	
			31.0		10.6	1191			
			36.2		11.8	1323			
Methylene bromide	CH_2Br_2	29.9	−17.0		3.39	379			Eastman Kodak
			−8.1		3.79	424			
			1.7		4.18	468			
			15.1		4.57	511			
			25.0	943	5.07	567	1.6	7.1	
			32.0		5.23	585			
			39.0		5.37	600			
Methylene iodide	CH_2I_2	29.9	8.3		2.10	234			Eastman Kodak
			16.2		2.16	242			
			25.0	963	2.24	250	23.2	4.3	
			33.4		2.31	258			
			41.3		2.41	269			
1,1 dichloroethane	CH_3CHCl_2	30.6	−20.4		0.723	77.2			Eastman Kodak
			−11.2		0.769	82.1			
			−1.3		0.810	86.5			
			9.2		0.846	90.4			
			18.8		0.892	95.2			
			25.0	1022			9.7	5	
			30.8		0.964	103			
			39.8		1.005	107			
1,2 dichloroethane	CH_2Cl-CH_2Cl	30.6	−27.4		1.60	171			Eastman Kodak
			−21.8		1.46	156			
			−16.6		1.38	148			
			−9.3		1.32	141			
			−1.4		1.29	138			
			10.0		1.27	136			
			12.0		1.28	136			
			22.5		1.28	136			
			25.0	1230			8.7		
			28.5		1.28	136			
			36.2		1.30	139			
1,2 dibromoethane	CH_2Br-CH_2Br	29.85	11.3		3.15	353			Amend Drug and Chemical Company
			16.6		2.97	334			
			20.8		2.85	320			
			25.0	983	2.77	311	20.3		
			31.7		2.57	289			
			38.7		2.47	278			
trans-dichloroethylene	CHCl−CHCl	31.05	−20.2		2.33	241			Matheson
			−10.0		2.58	267			
			0.0		2.83	294			
			10.0		3.14	326			
			19.8		3.43	356			
			20.0				8.5	7.5	
			21.7		3.50	363			
			30.0		3.64	377			
			37.6		3.87	401			
			45.2		4.06	421			
cis-dichloroethylene	CHCl−CHCl	30.6	−20.4		3.77	410			Matheson
			−11.5		4.07	443			
			−1.5		4.32	470			
			8.0		4.57	497			
			18.8		4.94	537			
			20.0				6.4	4.4	
			25.3		5.11	556			
			38.3		5.53	601			
			50.7		5.87	638			

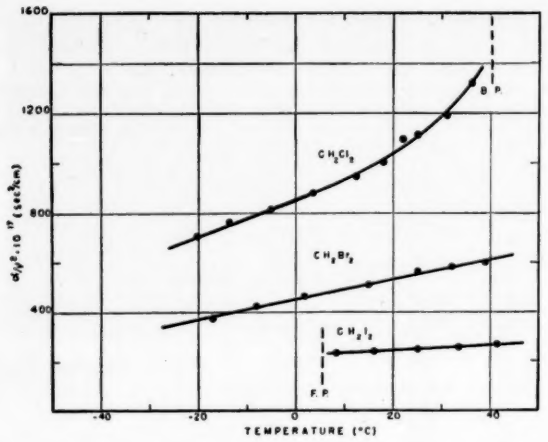

FIG. 3. Ultrasonic absorption in some halogenated methylenes.

proached, it increases more rapidly. This behavior indicates the presence of a particular action that affects the phenomena lowering the absorption, which is destroyed by thermal agitation. It seems, therefore, probable that the ultrasonic absorption in methylene chloride is not exclusively determined by phenomena that happen inside the molecules.

When a structural effect is present it is important to consider not only the dipole moments of the molecules but also the real distribution of charges in the molecules and all the various interactions among the molecules. This fact can be one of the reasons why in the methylene series (Fig. 3) the absorption decreases strongly going from the chloride to the bromide and to the iodide, while the dipole moment is decreasing in the same succession (1,55 D for chloride, 1,40 D for bromide, 1,15 D for iodide). Of course in the molecules of the last two liquids the chlorine atoms are replaced by the heavier bromine or iodine atoms and a change in the relaxation time of the vibrational degrees inside the molecules is to be expected independently from the possible influence of the forces among the molecules. It is to be observed however that in methylene chloride it seems that the intermolecular forces produce a decrease of absorption and that, if we take the boiling temperature as an index of the magnitude of the interactions among the molecules, the boiling point increases going from the chloride (40,1°C) to bromide (98,2°C) and iodide (180°C) in the succession in which the absorption decreases.

The possibility that interactions among the molecules play an important part in determining the particularities of relaxation phenomena is still more suggested by the behavior of the ultrasonic absorption in some halogenated ethanes.

The temperature dependence of the absorption coefficient in 1,1 dichloroethane ($CHCl_2-CH_3$) and in 1,2 dichloroethane (CH_2Cl-CH_2Cl) are shown in Fig. 4. The nature of the phenomena determining the absorption seems completely different in the two liquids. In 1,1 dichloroethane the absorption coefficient is linearly dependent on temperature, and it increases with temperature as usually happens in unassociated liquids. In the 1,2 dichloroethane, instead, the absorption coefficient decreases with temperature and this happens faster near the freezing point. The latter behavior is characteristic of the absorption coefficient in associated liquids, like water, where the relaxation phenomena are of structural nature. However, 1,2 dichloroethane has a high value of absorption coefficient in contrast to the small values found for all highly associated liquids having low viscosity on which measurements have been made. The analogy is not, therefore, complete and probably phenomena of structural origin are present together with phenomena of different kind.

The values of the dipole moment in 1,1 dichloroethane (1,95 D) and in 1,2 dichloroethane (1,7 D) do not differ so that the higher absorption in 1,2 dichloroethane and the complete change in the temperature dependence can be ascribed directly to the dipole moment. This confirms the importance of all interactions and of the short range forces among molecules and probably the more important rule of the dipole moments in these liquids is to fix the position in which the molecules are held one near the others.

The absorption coefficient in 1,2 dibromoethane also indicates the presence of a particular kind of phenomena in the 1,2 halogen substituted ethane (Fig. 4). The temperature dependence has the same aspect as in 1,2 dichloroethane near the freezing point while the value of the absorption coefficient is noticeably larger. The latter result is just opposite to that obtained in the methylene serie where the substitution of bromine for chlorine atoms produces a decrease of the absorption coefficient.

Figure 5 shows the absorption coefficient in *cis*- and *trans*-dichloroethylene as a function of temperature. There is no deflection from straight lines even near the boiling point. Both liquids present a large excess of the experimental over the classical value of the absorption coefficient. It is important also to observe that the *cis*-compound with a dipole moment (1,9 D) has a coefficient about 50 percent larger than the *trans*-dichloro-

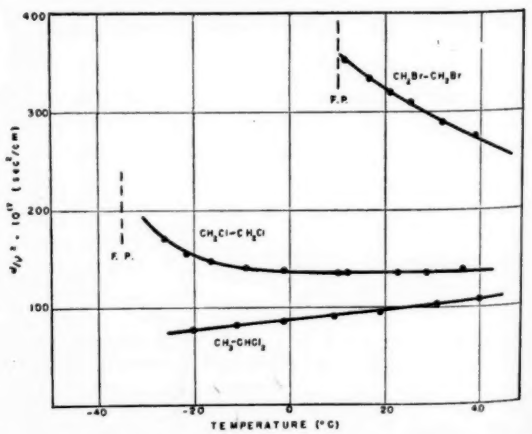

FIG. 4. Ultrasonic absorption in some halogenated ethanes.

ethylene which has no dipole moment.[7] This result shows clearly that often the dipole moment does not directly influence the absorption coefficient. The large difference between the absorption coefficients of the two liquids is, at least in part, due to a different efficiency of collisions among the molecules in producing inelastic transitions as it happens in the gaseous state. It is not possible to see if other kinds of relaxation phenomena are operative at the same time. However, if a structural effect is present it is not due to the dipole moment but to other forces among the molecules.

5. CONCLUSIONS

The temperature dependence of the ultrasonic absorption coefficient was measured in some series of halogenated methylenes, ethanes, and ethylenes.

The experimental results, even though at the present time they cannot be clearly understood, seem to indicate that often the relaxation phenomena determining the difference between experimental and classical values of the absorption coefficient are not exclusively inside the molecules. They seem to follow some scheme in which the interactions among the molecules are involved and some times independent relaxation phenomena might be present.

The absorption coefficients in 1,1 dichloroethane and in 1,2 dichloroethane present a completely different temperature dependence. The replacement of chlorine with bromine atoms has opposite consequences on the absorption in the methylene and ethane series.

Many times, but not always, an increase in dipole moment of the molecules is accompanied by an observed increase in the absorption, showing that the phenomena

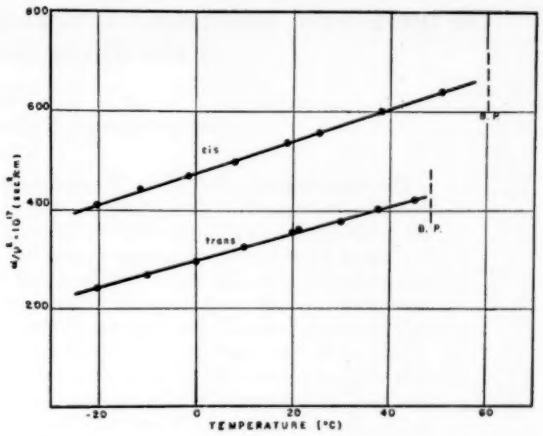

FIG. 5. Ultrasonic absorption in *cis*- and *trans*-dichloroethylenes.

are not related in a simple way to the dipole forces and that all the forces among the molecules, such as the short-range forces need to be taken into account.

The experimental results, as seen, do not permit one to get more precise conclusions on the nature and the characteristics of relaxation phenomena in liquids for which further experimental data are necessary. However, the measurements of the absorption coefficients and their temperature dependence in suitable series of organic compounds appears to be a good method for these purposes.

ACKNOWLEDGMENTS

Grateful acknowledgment is made to the Italian Research Council and to the Catholic University of America who have made this research possible. The author also wishes to thank Dr. K. F. Herzfeld and the staff of the Department of Physics for much assistance and valuable discussions and Dr. Virginia Griffing of the Chemistry Department for supplying some of the organic liquids used in this work.

[7] Some measurements in vapors of *cis*- and *trans*-dichloroethylene show that also in the gaseous state the energy equilibrium is attained quicker in the *trans* than in the *cis* form. These measurements made by J. C. Hubbard and the author will be reported in another paper.

On the Elastic Relaxation in Carbon Disulfide: The Temperature Dependence of the Ultrasonic Absorption Coefficient*

DANIELE SETTE
Istituto Nazionale di Ultracustica "O. M. Corbino," Rome, Italy

The experimental values of the ultrasonic absorption coefficient given in the literature for carbon disulfide show the presence of dispersion in the frequency range 1–100 Mc/sec, but large differences are present in the values obtained by various authors at the same frequencies so that it is difficult to analyze the behavior of this liquid. In order to discriminate among the various results more information is needed. For this reason a measurement of the absorption coefficient was performed at 30 Mc/sec. The value obtained for α is in agreement with the higher values of the absorption coefficient obtained by other authors at various frequencies and, therefore, it gives more credence to them in comparison with others.

The absorption coefficient as a function of temperature does not follow a linear law as it does in other unassociated liquids. The temperature coefficient $(1/\alpha)(\partial\alpha/\partial t)$ goes from $7.3\cdot10^{-3}$ deg^{-1} at -23°C to almost zero near the boiling point. These results can be used to examine the theoretical explanations of absorption in carbon disulfide based on the assumption that all the vibrational modes relax together or on the hypothesis that they have different relaxation times. The value of the temperature coefficient at 25°C seems to be better explained with the first treatment.

1. INTRODUCTION

CARBON disulfide, as is known, is particularly important for studying the characteristics of relaxation phenomena in liquids because the high experimental value of the absorption coefficient shows it to be one of the few liquids in which the period of the acoustic waves we are using is sufficiently near to the relaxation time.

Nonetheless carbon disulfide has not been sufficiently studied from the experimental point of view and, moreover, the results obtained often are not in good agreement.

It seemed worthwhile, therefore, to measure the ultrasonic absorption coefficient in carbon disulfide at 30 Mc/sec and to study experimentally its temperature dependence for which there are no indications in literature.

This paper presents the results of the measurements.

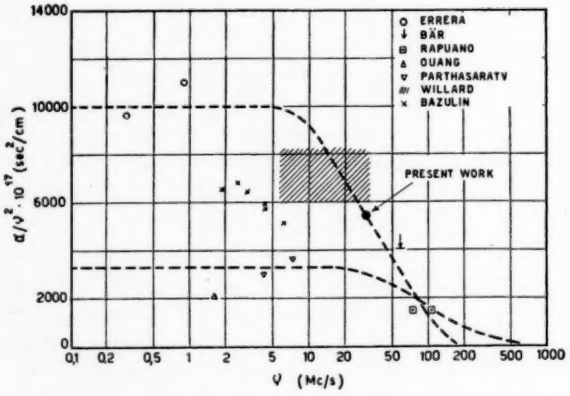

FIG. 1. Ultrasonic absorption in carbon disulfide as a function of frequency.

* Work done with the help of a grant of Italian Research Council at the Catholic University of America, Washington, D. C., aided by Contract N6-ONR-225III.

2. METHOD OF MEASUREMENT

The measurements of the ultrasonic absorption coefficient were made using a pulse method at about 30 Mc/sec.

The experimental arrangement does not differ essentially from that used by Pinkerton[1] and by Litovitz,[2] as described in the preceding paper.

The high values of the absorption coefficient in the liquid made it necessary to use a reflector made of a quartz rod that gives an acoustic delay of 25 μsec.

Particular care was used in order to avoid contamination of the specimen. A completely metallic tank was designed with a pressed cotton cover to close the container without preventing the free movement of the reflector.

In order to check the accuracy of the apparatus calibration measurements were made in distilled water. The value of the parameter α/ν^2 (α amplitude absorption coefficient, ν frequency) obtained at 25°C is $22.5\cdot10^{-17}$ sec^2/cm in very good agreement with literature.

With this experimental disposition the absolute error is less than 5 percent while the accuracy in relative measurements is about 1–2 percent.

3. EXPERIMENTAL RESULTS

The values of the ultrasonic absorption coefficient obtained in carbon disulfide are given in Table I. α is the amplitude absorption coefficient.

The specimen used was produced by The Matheson Company.

4. DISCUSSION OF RESULTS

In Fig. 1 the results of measurements of absorption coefficient in carbon disulfide made by various authors[3]

[1] J. M. M. Pinkerton, Proc. Phys. Soc. (London) **B62**, 129 (1949).
[2] T. A. Litovitz, J. Acoust. Soc. Am. **23**, 75 (1951).
[3] Claeys, Errera, and Sack, Trans. Faraday Soc. **33**, 136 (1937); R. Bär, Helv. Phys. Acta **10**, 332 (1937); P. Bazulin, Zhur. Eksptl'i Teoret. Fiz. URSS **9**, 1147 (1939); S. Parthasarathy,

are shown. While it is clear that in the range 1–100 Mc/sec a definite decrease of the parameter α/ν^2 is present, it is also easy to see that there is a noticeable scattering of the experimental points, and more information is necessary in order to discriminate between these results.

Kneser[4] has calculated two curves that seem to represent sufficiently well two different sets of experimental points. These curves, also drawn in Fig. 1, are obtained supposing that the excess of the experimental absorption coefficient over the classical value is produced by relaxation of the vibrational heats and that the different vibration modes have the same relaxation time. The relaxation times corresponding to the higher and lower curves are 5 and $1.6\cdot10^{-9}$ sec, respectively.

The range of frequency near 30 Mc/sec appears very important in order to discriminate between the two curves. The result obtained in the present work is $\alpha/\nu^2=5480\cdot10^{-17}$ sec^2/cm at 20°C and it fits very well on the higher curve of Kneser. It gives, therefore, more credance to the higher values of the absorption coefficient quoted by some authors at different frequencies. This seems to be in good agreement with the observation that can be made studying binary systems having an unassociated very absorbing liquid as one component.[5] In these cases the addition of a second liquid produces always a strong decrease of the absorption whatever its nature. It is possible, therefore, that, notwithstanding the accuracy of the experimental arrangement used, values of α lower than the true ones have been obtained because of the presence of small amounts of impurities.

The assumption made by Kneser that all the vibration modes relax together is the one normally used in order to simplify the treatment, but obviously it may not be satisfactory in carbon disulfide.

Bauer[6] has tried to work out the calculation assuming the presence of multiple dispersion and he succeeded in explaining a set of experimental results that are the same used for the higher curve of Kneser. The value found for α in the present work can be, therefore, well inserted in this treatment.

It seems however difficult to decide at this point what treatment fits better the experimental results and probably more information will be needed.

The temperature dependence of the absorption coefficient probably can furnish some suggestions to explain the absorption in this liquid. Figure 2 gives the temperature dependence at 30 Mc/sec. The absorption coefficient does not increase linearly with temperature and the temperature coefficient, $(1/\alpha)(\partial\alpha/\partial t)$, goes from $7.3\cdot10^{-3}$ deg^{-1} for −23°C, to almost zero near the boiling point.

Current Sci. (India) **6**, 501 (1938); T. Ouang, Compt. rend. **222**, 1215 (1946); G. W. Willard, J. Acoust. Soc. Am. **12**, 438 (1941); R. A. Rapuano, Phys. Rev. **72**, 78 (1947).

[4] H. O. Kneser, Ergeb. exakt. Naturwiss., Band **XXII**, p. 169.

[5] D. Sette, Nature **166**, 116 (1950); Nuovo cimento Suppl. Vol. 7, 318 (1950); J. Acoust. Soc. Am. **23**, 359 (1951).

[6] E. Bauer, Proc. Phys. Soc. (London) **A62**, 141 (1949).

TABLE I. Ultrasonic absorption in carbon disulfide.

ν (Mc/sec)	t (°C)	α (cm^{-1})	$\alpha/\nu^2\cdot10^{17}$ (sec^2 cm^{-1})
31.05	−22.8	44.0	4560
	−18.0	46.0	4770
	−10.8	47.5	4930
	−8.2	47.3	4910
	−1.3	49.1	5090
	5.7	50.0	5190
	10.0	51.8	5370
	14.4	51.2	5310
	16.2	51.9	5380
	20.1	53.0	5500
	20.8	52.8	5480
	21.0	52.6	5460
	24.2	52.8	5480
	25.4	53.0	5500
	30.0	52.8	5480
	33.2	53.0	5500
	33.7	53.0	5500
	37.8	53.2	5520
	40.4	53.7	5570
	43.6	53.2	5520

Bauer has made some theoretical considerations on the variation of the absorption in carbon disulfide with temperature, but they are founded on the assumption that the value of $(1/\alpha)(\partial\alpha/\partial t)$ is equal to 10^{-2} at about 25°C as in some other unassociated liquid. The calculation of $(1/\alpha)(\partial\alpha/\partial t)$ gives to Bauer one argument to suggest the presence of multiple relaxation and therefore it is interesting to see how this argument is affected by our results.

The expression of the temperature coefficient of α calculated by Bauer[6] for unassociated liquids using the hypothesis of a single relaxation time is

$$(1/\alpha)(\partial\alpha/\partial t)=-1/c(\partial c/\partial t)+1/T(\bar{D}-n) \qquad (1)$$

where $1/c(\partial c/\partial t)$ is the temperature coefficient of the velocity of propagation; $\bar{D}/T$ is equal to $(\partial \log\sum C_i)/(\partial T)$, the C_i being the vibrational specific heats. n is the exponent that fixes the temperature dependence of the probabilities of inelastic transition in the collisions of the molecules. These probabilities in fact increase with absolute temperature approximately as T^n, being n of order 1 to 2.

As mentioned above, Bauer, in the absence of any experimental indication, assumed the value 10^{-2} deg^{-1} for $(1/\alpha)(\partial\alpha/\partial t)$ and $-3.5\cdot10^{-3}$ deg^{-1} for $1/c(\partial c/\partial t)$ in order to carry on the calculation for carbon disulfide at $T=300K$.

The value of $(\bar{D}-n)$ deduced applying Eq. (1) is 1.95 and because $\bar{D}$ for carbon disulfide in the condition of the calculation is equal to 0.878, the calculation would indicate a negative value of n, which of course is wrong. From this conclusion Bauer was led to examine the possibility of different relaxation times for the various vibrational modes. The modes with higher vibrational frequency would present a lower dispersion frequency, a lower specific heat and a larger temperature coefficient of specific heats. He carried out the calculation of the dispersion frequencies of three vibrational modes and of

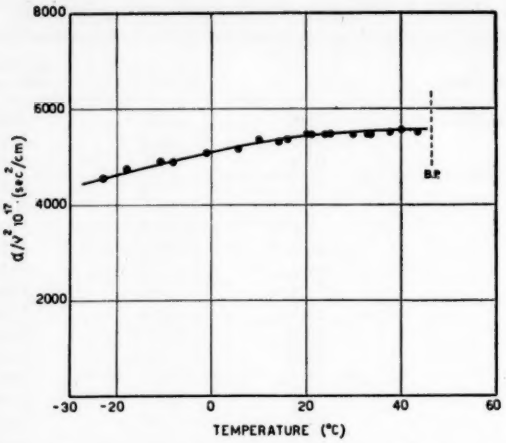

FIG. 2. Temperature dependence of ultrasonic absorption in carbon disulfide.

a new value for $\bar{D}$ equal to $D_{eff}=2.76$. This value of $\bar{D}$ would give for $1/\alpha(\partial\alpha/\partial t)$ the value 9.10^{-3} deg^{-1} assuming n equal 1. This temperature coefficient is sufficiently near to what Bauer thought was the actual one.

As it was pointed out before, the experimental results in carbon disulfide show that the value of $(1/\alpha)(\partial\alpha/\partial t)$ changes with temperature and its value at $T=300K$ is about $1.5\cdot10^{-3}$ deg^{-1}.

If we apply Eq. (1) keeping, for want of a better value, $-3.5\cdot10^{-3}$ deg^{-1} for the temperature coefficient of velocity, $(\bar{D}-n)$ is equal to -0.6 and, $\bar{D}$ being 0.874, this means n equal to 1.474. This value seems sufficiently satisfactory.

If instead we assume the validity of the scheme with different relaxation time for three vibrational modes $\bar{D}$ is 2.76 and therefore n must have the value 3.36 which seems too high.

From the precedent discussion it appears that the experimental results do not support Bauer's idea, at least in the present form of the calculation, and that they seem more in agreement with the treatment that assumes only one relaxation time for all the vibrational modes.

5. CONCLUSION

Measurements of the ultrasonic absorption coefficient in carbon disulfide were performed at 30 Mc/sec in the temperature range -23 to $+46$°C.

The value of α/ν^2 at 20°C fits well with the set of higher values obtained by different authors at various frequencies, and therefore it gives more credence to them in comparison with measurements that have furnished lower values.

The temperature dependence of the absorption coefficient is not linear. The value of $1/\alpha(\partial\alpha/\partial t)$ at room temperature seems to agree better with the theoretical treatment carried on the hypothesis of one relaxation time for the different vibrational modes than with the other founded on the assumption of multiple dispersions.

ACKNOWLEDGMENT

Grateful acknowledgment is made to the Italian Research Council and the Catholic University of America who have made this research possible. The author also wishes to thank Dr. K. F. Herzfeld and the staff of the Department of Physics for much assistance and valuable discussion.

Vapor Pressures below 1 mm Hg of Several Aromatic Compounds*†

E. R. HOPKE‡ AND G. W. SEARS§
Department of Physics, Duke University, Durham, North Carolina
(Received March 26, 1951)

Vapor pressures of the three isomeric picolines and *p*-di-tert-butylbenzene were determined over a pressure region of approximately 5–250 microns Hg using a Rodebush manometer and an effusion manometer for each compound. The experimental results of the two methods show good agreement. A comparison of the two manometers is made and the merits of each method are discussed.

IN connection with the spectroscopic studies of polyatomic molecules which are being undertaken in this department, it is desirable to have vapor pressure data available in the range 0.01–1.0 mm Hg.

In many cases, measurements have been made previously for the pressure region of 10–760 mm Hg. An excellent compilation of this work has been published by Stull.[1] The pressure region below 10 mm has been the subject of very little investigation. The purpose of the present investigation was to obtain experimental data over the region of approximately 0.01–1.0 mm Hg and to subsequently evaluate the methods used. A literature search showed very little data for polyatomic molecules over this region.

A modification of the Rodebush manometer[2] has been used previously by the authors.[3] Similar instruments have been used by Dietz[4] and by Balson.[5] This manometer is an electromagnetic balance which measures the force exerted by a pressure acting upon a movable quartz plate. The force or pressure is measured in terms of electric current passing through a solenoid. The quartz plate serves as a tightly fitting valve separating two chambers. One chamber is evacuated and the other one is maintained at the pressure to be measured.

Using the Rodebush manometer, each pressure measurement involved opening the valve between the two chambers. Thus, when a sample of the compound in the liquid or solid phase was placed in the pressure chamber, each pressure measurement also served to pump out adsorbed gases or other volatile impurities that were present in the condensed phase. In the course of previous measurements, it had been observed that organic substances regardless of the care with which they had been purified, still evolved slight traces of volatile impurities. A few parts per million of such impurities were observed to cause the initial measurements to be appreciably high. This was evidenced by the fact that continued measurements at a single temperature gave decreasing values of pressure which finally reached a minimum value. The time required for attainment of equilibrium in the presence of these outgassing effects was about five minutes while only a few seconds were required with a sample that had been completely outgassed. Outgassing effects have also been observed by Dietz[4] for potassium chloride and by Balson[5] for several organic compounds.

For comparison purposes it seemed desirable to use an effusion manometer. Such an instrument would tend to circumvent the outgassing difficulties, and, at the same time, permit comparison of a dynamic method with the quasi-static Rodebush method.

EXPERIMENTAL

Eastman Kodak's highest grade naphthalene was further purified by vacuum sublimation. Samples of α-picoline 99.85 percent pure (bp 129.44°C) and β-picoline 99 percent (bp 143.0–143.5°C) were contributed by Dr. J. J. McGovern of the Mellon Institute of Pittsburgh. The γ-picoline was obtained from a lot purified (bp 144.5–145.0°C) by Dr. J. C. Shivers of the Chemistry Department of Duke University. *P*-di-tert-butylbenzene of unknown purity was obtained from the Chemical Products Department of the Standard Oil Company (Indiana). A sample of the last compound was purified by recrystallization from ethyl alcohol, separation from distilled water, and vacuum sublimation. After these purification processes, the *p*-di-tert-butylbenzene had a melting point range of 76.5–76.8°C. Temperatures were recorded with mercury-in-glass thermometers which were graduated in either 0.1 or 0.2°C intervals. This set of thermometers was calibrated by the Precision Thermometer and Instrument Company.

Procedure

The Rodebush manometer used has been described in a previous paper.[3] Before the new series of measure-

* Taken from part of a thesis submitted by E. R. Hopke in partial fulfillment of the requirements for the degree of Doctor of Philosophy at Duke University.

† This investigation was assisted by the ONR under Contract N6ori-107, Task Order I, with Duke University.

‡ Present address: Spectroscopy Department, The Dow Chemical Company, Midland, Michigan.

§ Present address: Research Laboratory, General Electric Company, Schenectady, New York.

[1] D. R. Stull, Ind. Eng. Chem. **39**, 517 (1947).

[2] W. H. Rodebush and C. E. Coons, J. Am. Chem. Soc. **49**, 1953 (1927); W. H. Rodebush and W. F. Henry, J. Am. Chem. Soc. **52**, 3159 (1930).

[3] G. W. Sears and E. R. Hopke, J. Phys. Colloid Chem. **52**, 1137 (1948); E. R. Hopke and G. W. Sears, J. Am. Chem. Soc. **70**, 3801 (1948); G. W. Sears and E. R. Hopke, J. Am. Chem. Soc. **71**, 1632 (1949); G. W. Sears and E. R. Hopke, J. Am. Chem. Soc. **71**, 2575 (1949).

[4] V. Dietz, J. Chem. Phys. **4**, 575 (1936).

[5] E. W. Balson, Trans. Faraday Soc. **43**, 48 (1947).

ments was made, the manometer was calibrated with mercury. The vapor pressure of mercury was taken from the International Critical Tables. The vapor pressure of distilled water (ice) was then measured and the results were compared with values given in the International Critical Tables. The deviations of the two sets of data were both positive and negative, the average deviation being 1.7 percent.

The various samples were maintained in the Rodebush manometer for 24 hours under a high vacuum

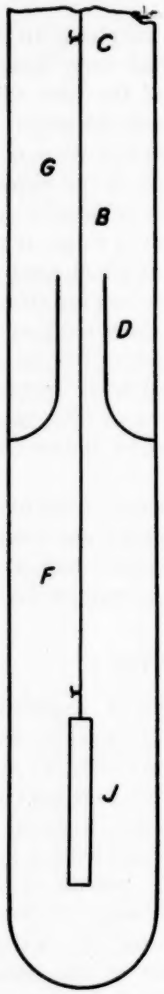

FIG. 1. Effusion manometer.

before any measurements were begun. After this waiting period, the samples of β-picoline and γ-picoline were frozen, melted and then refrozen, this process being followed by a 3-minute pump-out period. This outgassing process was carried out ten times for each of these two samples. α-picoline was liquid over the temperature range of investigation and the melting point of p-di-tert-butylbenzene is above room temperature, so that this procedure of outgassing was not followed for these latter compounds.

Apparatus

A diagram of the effusion manometer is shown in Fig. 1. *G* is used to refer to the vacuum chamber and *F* refers to the lower chamber. The outside Pyrex tubing is 28 mm in diameter. *D* is a Pyrex tube of small bore which was ring-sealed to the outside tubing at a point about 12 cm from the bottom of the apparatus. *B* is a fine Pyrex fiber with hooks on both ends. *J* is the effusion vessel which is suspended by the fiber *B*. The fiber in turn is suspended from a hook at *C* on the end of a helical nichrome spring, which is not shown in the diagram. The spring is suspended by a Pyrex hook at the top of the 28 mm outside tubing. This hook was made on the end of a 1 cm diameter tube which was ring-sealed to the larger tube. The distance from the hook to the ringseal was about 4 inches and thus permitted the outside tube to be heated in this vicinity without affecting the temper of the suspending nichrome spring. The outside larger tube was connected to a vacuum system consisting of a dry-ice trap, a two stage mercury diffusion pump, a vacuum stop-cock, and a Hy-vac mechanical pump, in that order.

The nichrome spring was $\frac{3}{4}$ inch in diameter. It had a free length of about 13 cm and consisted of about 40 turns of 0.005-inch nichrome wire. Over the load range of this investigation the spring obeyed Hooke's law. The sensitivity of the spring was approximately 1.5 mg/mm.

The effusion vessel was a cylindrical nickel tube which had a length of 5 cm, a diameter of 0.25 cm, and a wall thickness of 0.0038 cm. An orifice was made with a 0.013-inch twist drill. After one end of the tube had been sealed by spotwelding, the tube was coated with "Aquadag." A small area about the orifice was left uncoated so as to leave the effective wall thickness unchanged. After baking out the tube for about 4 hours at 100°C and inserting the compound, the other end was sealed by spotwelding. The filled vessel was inserted into the system by cracking the outside Pyrex wall and then resealing it.

In order to eliminate formation of burrs, while drilling the orifice, a snug fitting brass rod was inserted into the nickel tube before the drilling operation. After drilling, the wall around the orifice was smoothed by pushing the tightly fitting brass rod through the tube. This operation was done very carefully so as to avoid changing the wall thickness near the orifice. The tubes were washed with ether and boiled in distilled water to clean them. After preparing the orifice the wall thickness at the orifice was measured with a measuring microscope. In all cases it was found that the wall thickness was not altered by the orifice preparation and the wall thickness was always taken as 0.0038 cm.

In operation, a thermostat was placed about the lower part of the apparatus. The thermostat consisted of a four inch internal diameter Dewar flask filled with acetone or water at the desired temperature, the bath temperature being maintained uniform with a high speed glass stirrer. Small bits of ice or dry ice added at about five-minute intervals sufficed to maintain the temperature constant to within 0.1°C below room

temperature. Above room temperature, the bath was heated electrically.

The motion of a fiducial mark on the lower end of the spring was followed with a measuring microscope by setting the cross-hair above the fiducial point and noting the time when the two came again into coincidence. Repeated observations at constant temperature gave the rate of motion, which, when multiplied by the spring constant, gave the mass rate of effusion. Spring vibration, when it occurred, was minimized by attracting the nickel tube to one side with a small magnet, so that friction against the wall of the apparatus damped the vertical motion.

RESULTS

The vapor pressure was calculated from data taken with the effusion manometer with the aid of the equation, known in kinetic theory,

$$q=\alpha_0 A_0(M/2\pi RT)^{\frac{1}{2}}\Delta P, \tag{1}$$

where q is the rate of effusion (mass/time), α_0 is a factor dependent upon the geometry of the tubular orifice, A_0 is the orifice area, M is the molecular weight of the gas, T is the absolute temperature, and ΔP is the difference in pressure in and outside the effusion vessel. Values of α_0 for various tubular geometries have been tabulated in an article by Clausing.[6] In computing ΔP, cgs units have been used in Eq. (1) and the pressure then converted from dynes/cm^2 to microns Hg.

The constriction D, shown in Fig. 1, was inserted to insure that all of the Pyrex tubing which can radiate heat to the effusion vessel would be at the same temperature as the thermostat. Due to this constriction, the pressure in chamber F was about 2 percent of the pressure in the effusion vessel. To calculate this pressure, let P be the pressure in the effusion vessel, P' the pressure in chamber F, A' the cross-sectional area of the tube D, α' the corresponding correction due to finite length, A_0 the orifice area, and α_0 the corresponding correction factor. Then P' is determined by the flow of vapor into the chamber from the effusion vessel and out of the chamber into the vacuum and effusion vessel. We write

$$\frac{PA_0\alpha_0}{(2\pi RMT_0)^{\frac{1}{2}}}=\frac{P'A_0\alpha_0}{(2\pi RMT)^{\frac{1}{2}}}+\frac{P'A'\alpha'}{(2\pi RMT)^{\frac{1}{2}}}, \tag{2}$$

where the term on the left represents flow into chamber F and the terms on the right represent flow out of chamber F. Because P' is about 0.02 P and T is not very different from T_0, T can be set equal to T_0 without seriously affecting the calculated pressure. We have then

$$P'=\frac{A_0\alpha_0}{A'\alpha'}\Delta P, \tag{3}$$

[6] P. Clausing, Physica **9**, 65 (1929).

where we have set $\Delta P=P-P'$. ΔP is obtained from Eq. (1). With P' from Eq. (3), P is immediately obtained.

When a finely ground solid was used as sample in the effusion vessel, the area of the sample was large as compared to the orifice area and the steady-state pressure in the effusion vessel was the vapor pressure. However, when a liquid such as water was frozen after insertion into the vessel, the surface area of the sample could no longer be considered large as compared to the orifice area. The cross-sectional area of the nickel tube, which represented the minimum surface area available to the sample, was 0.051 cm^2 whereas the orifice area available to the sample, was 0.051 cm^2 whereas the orifice area was about 0.001 cm^2. With a ratio of only 50 to 1 the question also arose as to whether the sample was at a uniform temperature. Measurements taken to examine this question did not indicate this to be an effect. For purposes of calculating the vapor pressure, it was assumed that the pressure everywhere in the vessel was constant and that it was determined by a balance of the maximum rate at which molecules could evaporate from the sample surface and the combined rates at which molecules were lost through the orifice

TABLE I. Vapor pressure of ice.

T °C (bath)	P(meas) microns Hg	δT °C (Calc) $\epsilon=0.65$	$\epsilon=0.60$	$\epsilon=0.55$	$\delta T'$ °C I.C.T.
−40.1	56.5±0.5	4.4	4.7	5.2	4.6
−45.1	36.4±0.3	3.0	3.3	3.6	3.2
−50.1	22.1±0.5	2.0	2.2	2.4	2.2
−55.1	13.2±0.1	1.3	1.4	1.5	1.3

and recondensed on the sample surface. On this basis, it may be written that

$$P_0=P+\frac{\alpha_0 A_0}{A_1}\Delta P, \tag{4}$$

where P_0 is the vapor pressure, P is the steady-state pressure in the effusion vessel, and A_1 is the cross-sectional area of the nickel tube.

Since the effusion vessel was suspended in a low pressure region, heat transfer to and from the effusion vessel occurred mainly by radiation and vaporization. Under these conditions, the vessel temperature is slightly lower than that of the thermostat. The temperature difference may be quantitatively determined by the following argument.

The vessel was assumed to be suspended in a blackbody cavity whose temperature equals that of the thermostat. Let the vessel temperature be T_0 and the thermostat temperature be T. At equilibrium we have

$$A\epsilon\sigma T^4=A\epsilon\sigma T_0^4+qL, \tag{5}$$

where A is the surface area of the vessel, ϵ is its emissivity, σ is the Stefan-Boltzmann constant, q is the rate

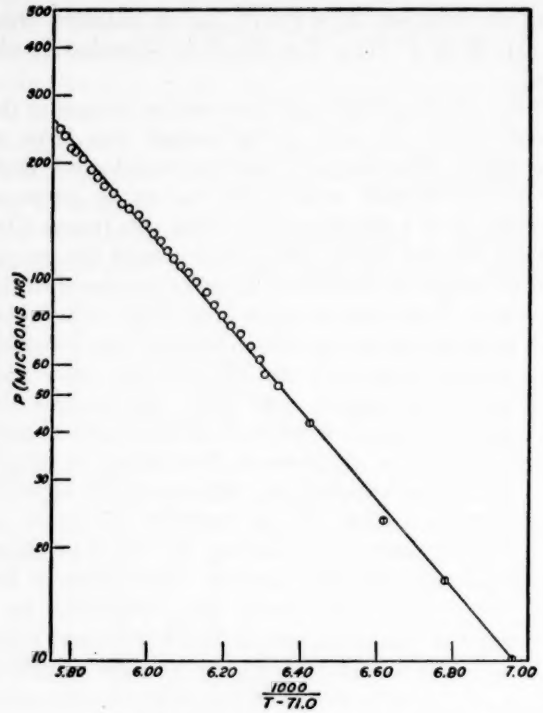

FIG. 2. Vapor pressure of α-picoline.

of effusion, and L is the heat of vaporization for 1 g of substance. The term on the left gives the rate of heating and the terms on the right give the rate of cooling. Equation (5) may be rewritten

$$A\epsilon\sigma(T^4-T_0^4)=qL. \tag{6}$$

Now let T_0 be represented by $T-\delta T$. Since δT is a very small quantity, we can approximate $T^4-T_0^4$ by $4T^3\delta T$ and Eq. (6) may be rewritten to a good approximation

$$\delta T=qL/(4A\epsilon\sigma T^3). \tag{7}$$

All quantities in this expression except ϵ are known or may be estimated from experimental data rather accurately. Volmer,[7] using a comparable apparatus, has given an argument similar to the above to show that his results were not seriously affected by temperature deviations which may be caused by vaporization. In the present case, however, the temperature corrections are not negligible.

In order to test the validity of Eq. (7), it was decided to measure the vapor pressure of ice, the values of which are known rather accurately over the region of interest. The large heat of sublimation of ice and the low temperatures in the region of interest would give large calculated temperature corrections. Measurements were made at -40, -45, -50, and -55°C. With the aid of the foregoing equations, the vapor pressure and temperature corrections were calculated and are shown in Table I. The values are presented in such a way as to make the choice of the best value of ϵ evident. The first column gives the bath temperature, the second column the measured pressures as calculated with the aid of Eqs. (1), (3) and (4), the third, fourth, and fifth columns the value of the temperature corrections calculated with Eq. (7) where a different value of ϵ was used to determine the value of δT in each of these columns. The sixth column was determined with the aid of the International Critical Tables in the following manner. Using values of the measured pressure given in the second column, corresponding temperatures were obtained from the I. C. T., and $\delta T'$ is the difference between these temperatures values and the bath temperature. The indicated uncertainties given in the second column indicate the maximum deviation of measured pressures from the average value. Three determinations were made at each temperature.

The necessity for applying temperature corrections for the vapor pressure of ice is at once evident. Over the range of temperatures used in Table I, a temperature difference of 0.1°C is equivalent to a pressure deviation of about 1.2 percent. A comparison of the third and sixth columns shows that corresponding values of δT and $\delta T'$ agree to within 0.2°C for $\epsilon=0.65$. This temperature difference is equivalent to 2.4 percent error in pressure. 2 percent of this may be involved in the determination of the factor $\alpha_0 A_0$. An additional 3 percent possible error involved in using Eq. (7) was already indicated. A comparison of the fourth and fifth columns with the sixth shows good agreement between δT and

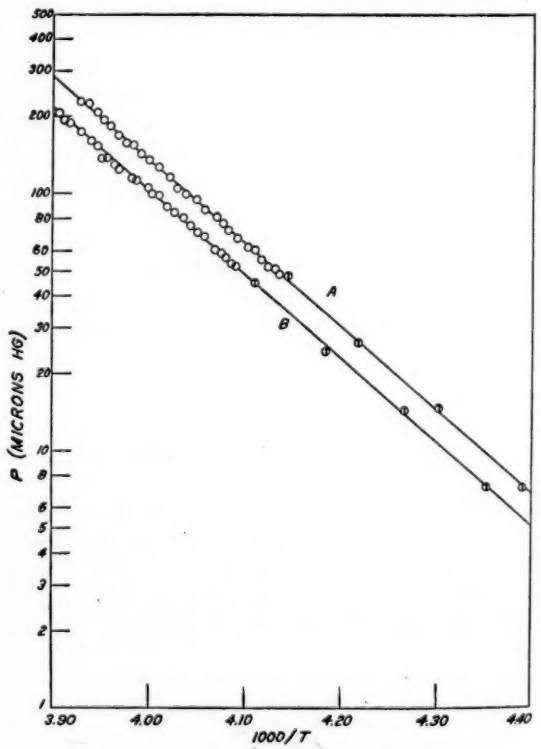

FIG. 3. (A) Vapor pressure of β-picoline.
(B) Vapor pressure of γ-picoline.

[7] M. Volmer, Z. physik. Chem. p. 863 (1931).

$\delta T'$ for $\epsilon=0.6$ with the comparison becoming less favorable for $\epsilon=0.55$.||

Since the pressure in chamber F is about 2 percent of the pressure in the effusion vessel, heat transfer by conduction is possible and an approximate calculation was made to see if this effect would seriously influence the above results. It was assumed that the vapor in chamber F was in thermal equilibrium with the walls of chamber F and that the mean free path of the vapor molecules was large as compared to the linear dimensions of chamber F. The accommodation coefficient of water vapor on carbon was taken as 0.5. Values of δT were again calculated considering the effect of heat conduction for the special case of $\epsilon=0.55$. The results in order of decreasing temperatures are 4.6, 3.3, 2.3, and 1.4°C and the effect of heat conduction is shown to be small. These values show very good agreement with the values of $\delta T'$. In view of the favorable results obtained when ϵ takes a range of 0.65 to 0.55, the best value was here taken as 0.60.

The vapor pressures of α-picoline, β-picoline, γ-picoline, and p-di-tert-butylbenzene were measured with the Rodebush manometer over the temperature ranges of -23 to -44, -19 to -31, -16 to -29, and 40 to 52°C, respectively. The temperature ranges covered with the effusion manometer are -47 to -59, -32 to -45, -30 to -43, and 12 to 41°C for α-picoline, β-picoline, γ-picoline, and p-di-tert-butylbenzene, respectively. The results are plotted in Figs. 2, 3, and 4 where circles indicate measurements on the Rodebush manometer and circles with one diameter drawn indicate effusion measurements.

When the data for α-picoline were plotted on a $\log P$ *vs* $1/T$ graph, a smooth line drawn through the data was somewhat curved. Therefore, these measurements were fitted to an Antoine's equation which may be written

$$\log P=-A/(T-B)+C, \tag{8}$$

where P is the pressure in microns Hg, T is the absolute temperature, and A, B, and C are constants. Since the measurements were taken by two different methods for which the ranges of pressure do not overlap B, which is a measure of the curvature, was considered separately. For this, a smooth curve was drawn through the data on a $\log P$ *vs* $1/T$ plot. Three points taken from this curve, two of them at the end points of the measurable temperature range and the third near the center of this range, sufficed to determine B. The slope of this smooth curve was then determined at two points which were taken near the midpoint of the measurable temperature range of each apparatus. The ratio of these slopes, together with the temperature at which the slopes were measured, gave a second value of B. The final B was taken as an average of the two results. A and C were then determined by the method of least squares. When data for the other compounds were plotted on a $\log P$ *vs* $1/T$ graph, there appeared no observable curvature for the vapor pressure curves and therefore B was set equal to zero in these cases before A and C were determined by the method of least squares. These constants, together with the derived heats of vaporization, are given in Table II.

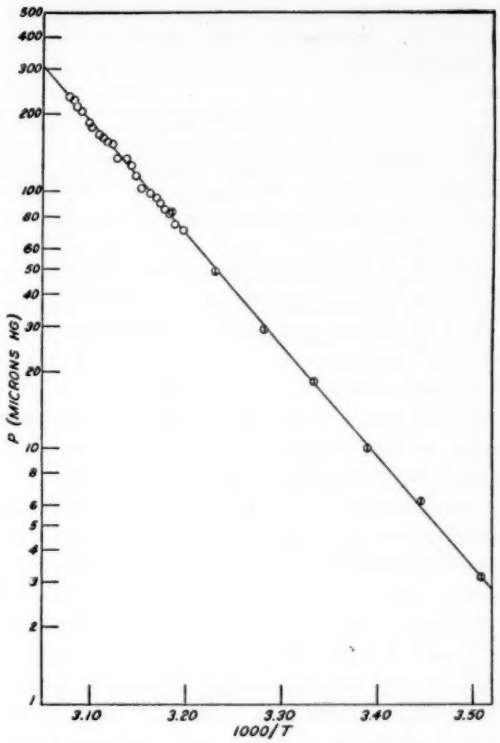

FIG. 4. Vapor pressure of p-di-tert-butylbenzene.

Each pressure measured with the effusion manometer represents the average of three measurements, and in the least-squares calculations these measurements, and in the least-squares calculations these measurements were given a weight of 3 as compared to 1 for measurements with the Rodebush manometer. This procedure was followed because the two methods were considered to give about equally reliable values. The maximum deviation of data used in obtaining the calibration curve for the Rodebush manometer was 3 percent. Since 3 percent also represents a random effect in the measurement of any other compound, the maximum possible error for the Rodebush method was considered 6 percent. The maximum error involved in measurements with the effusion manometer was previously indicated as 5 percent.

The average deviation of the vapor pressure of α-picoline as determined with the Rodebush manometer and the least-squares equation is 2.6 percent. The corresponding deviation with the effusion method is 3.1 percent. Stull[2] has fitted the date of Anschütz and

|| I. Langmuir and K. Blodgett, Rev. Sci. Instr. 5, 321 (1934), report $\epsilon=0.6$ for Aquadag coated tungsten at 1100°C in comparison to $\epsilon=0.12$ for clean tungsten at the same temperature.

TABLE II. Vapor pressure constants and heats of vaporization L (sublimation).

Compound	A	B	C	L (meas. temp. range)
α-picoline	1164.1	71.0	9.106	9.0 kcal/mole (−38°C)
β-picoline	3246.9	0	15.120	14.9 kcal/mole (−45 to −19°C)
γ-picoline	3277.6	0	16.121	15.0 kcal/mole (−43 to −16°C)
p-di-tert-butylbenzene	4346.4	0	15.746	19.8 kcal/mole (12 to 52°C)

Reitter[8] and of Kahlbaum[9] to a curve. In Stull's compilation, the vapor pressure of α-picoline is 1 mm Hg at −11.1°C. Riley and Bailey[10] measured the vapor pressure of α-picoline to a lower limit of 6 mm Hg. Their values were extrapolated downward to give 0.94 mm at this temperature. An upward extrapolation of our data to this temperature gives 1.03 mm Hg. The agreement was considered very satisfactory.

For measurements on β-picoline with the Rodebush manometer, the average deviation of the data from the least-squares equation is 1.2 percent. The corresponding deviation with the effusion manometer is 2.5 percent. For γ-picoline the corresponding deviations are 1.8 percent and 3.1 percent. Over the temperature range covered by our measurements, β-picoline and γ-picoline are solids. Brown and Barbaras[11] have determined the vapor pressure of these two compounds in their liquid phase at 0 and 20°C. Straight line curves were drawn for their data and ours on a $\log P$ *vs* $1/T$ plot. These curves intersect at −15.2 and −6.5°C for β-picoline and γ-picoline, respectively. Dühring's rule, together with our vapor pressure equation for α-picoline, was used to predict the vapor pressure of the other two isomers at their melting points which were taken as −15.2 and −6.5°C for β-picoline and γ-picoline, respectively. This procedure gave a value of 347 microns Hg for β-picoline as compared to 345 obtained by extrapolating our data upward. Dühring's rule gives a value of 714 microns Hg for γ-picoline as compared to 679 obtained by an upward extrapolation of our data. This agreement was considered very good.

The average deviation of the vapor pressure of p-di-tert-butylbenzene obtained with the Rodebush manometer and as calculated from the least-squares equation is 1.9 percent. The corresponding deviation with the effusion manometer is 3.4 percent. Hennion and Auspos[12] have measured the vapor pressure of p-di-tert-butylbenzene at 109 and 237°C. Their values were extrapolated downward graphically on a $\log P$ *vs* $1/T$ plot to give 3.4 mm Hg at the melting point. Extrapolating the data obtained in this investigation upward yields 2.1 mm Hg. The agreement is only within 50 percent, but considering the uncertainties involved in the extrapolation of the two sets of data, it was considered satisfactory.

It was at first decided to limit the pressure measurements with the effusion manometer so as to make applied temperature corrections less than 1°C. However, in order to completely cover the temperature range, it was necessary to exceed this limitation. The largest corrections used were 1.5, 1.8, 1.7, and 1.3°C for α-picoline, β-picoline, γ-picoline, and p-di-tert-butylbenzene, respectively. They apply for the highest pressures and Figs. 2, 3, and 4 show that these points fit our curves very well. It is also an indication that our chosen value of ϵ was a good one.

COMPARISON OF MANOMETERS

The two manometers used in this investigation were fundamentally very different. The Rodebush instrument was quasi-static and required a calibration whereas the effusion instrument was dynamic and absolute. The Rodebush manometer used here was limited at high temperature since very involatile substances condensed on the fibers of the high vacuum side, thus changing the effective calibration. The effusion apparatus was especially designed for work with involatile substances. The Rodebush manometer measured pressure directly while pressure measurements on the effusion manometer were indirect and the calculations required that the molecular mean free path be large as compared to the orifice's linear dimensions. Any unknown molecular association would make the pressure calculation erroneous.

In operation, the Rodebush manometer required experience in observations in order to obtain reproducible results. The adjustment of the suspension in this apparatus was rather critical, and any disturbance that affected the seating of the quartz plate changed the calibration somewhat. The effusion manometer required no prior experience and its operation did not involve any critical adjustments. Our Rodebush instrument could be used from 50 to 230 microns Hg whereas the effusion manometer could be employed to a lower limit of about 0.1 micron and an upper pressure limit of about 100 microns.

Since the Rodebush manometer was calibrated and the measurements were more difficult at the ends of the pressure range, there was a risk that the data would be more in error at these ends of the pressure range than in the intermediate range, possible causing a slightly erroneous slope for the vapor pressure curve. This effect was less likely with the effusion manometer.

Working with the effusion manometer, it was observed that the rates of effusion at a given temperature remained constant in time, within experimental error. This observation confirmed our original assumption that an effusion method would circumvent the outgassing difficulties encountered with the Rodebush manometer. The agreement of the data obtained with

[8] Anschütz and Reitter, *Die Destillation unter vermindertem Druck im Laboratorium,*" 2nd Edition, Cohen, Bonn, 1895.
[9] G. W. A. Kahlbaum, Ber. deut. chem. Ges. **17**, 1245 (1884).
[10] F. C. Riley and K. C. Bailey, Proc. Roy. Irish Acad. **388**, 450 (1929).
[11] H. C. Brown and G. K. Barbaras, J. Am. Chem. Soc. **69**, 1137 (1947).
[12] G. F. Hennion and L. A. Auspos, J. Am. Chem. Soc. **65**, 1603 (1943).

the two methods was taken to indicate that the outgassing procedure followed with the Rodebush method effectively eliminated volatile impurities as a source of error.

In measurement of the picolines, the pressure regions of the two methods were not made to overlap because of the large temperature corrections necessary with the effusion method. The methods were strictly complementary here, and it would not have been desirable to use the effusion manometer alone for these low temperatures. While the two methods were equally applicable for work with *p*-di-tert-butylbenzene, the region of overlap of the pressure ranges by each method is small. The plotted data in Figs. 2, 3, and 4 in general show both positive and negative deviations from the plotted curve for both methods over the entire pressure range.

ACKNOWLEDGMENTS

The authors wish to thank Dr. H. Sponer of Duke University for her continued interest in this work. We should like to acknowledge the kindness of Dr. J. J. McGovern of the Mellon Institute and Dr. J. C. Shivers of Duke University for making samples of the picolines available to us. We thank the Standard Oil Company for giving us the sample of *p*-di-tert-butylbenzene.

THE JOURNAL OF CHEMICAL PHYSICS VOLUME 19, NUMBER 11 NOVEMBER, 1951

Quantitative Line-Width Measurements in the Infrared. I. Carbon Monoxide Pressurized with Infrared-Inactive Gases*

S. S. PENNER AND D. WEBER
Jet Propulsion Laboratory, California Institute of Technology, Pasadena, California
(Received August 3, 1951)

Quantitative infrared-intensity measurements on CO pressurized with gases such as H_2, He, and A have been carried out at room temperature. For pressures up to 100 psia the experimental absorption measurements are correlated quantitatively by the use of theoretical relations derivable from the dispersion formula. Thus, for a fixed value of the total pressure, the observed absorption is a linear function of the square root of the optical density. Similarly, at constant optical density, the absorption is a linear function of the square root of the total pressure. Using Elsasser's treatment for equally spaced and equally intense rotational lines, lower limits have been determined for the rotational half-widths of CO broadened by various infrared-inert gases.

The determination of rotational half-widths from spectroscopic measurements can be refined by allowing for the variation of integrated absorption per rotational line from one line to another in a given vibration-rotation band. By carrying out numerical calculations, with the rotational half-width treated as a variable parameter, a direct comparison between calculated and observed infrared absorption can be used to determine the rotational half-width δ^0 for pressures which are small enough to justify a treatment for nonoverlapping rotational lines. In this manner it was found that $(\delta_F)_{H_2}=0.077$ cm^{-1} atmos^{-1}, $(\delta_F)_A=0.040$ cm^{-1} atmos^{-1}, $(\delta_O)_{H_2}=0.063$ cm^{-1} atmos^{-1}. Here the subscripts F and O denote measurements on the fundamental and the first overtone, respectively. The subscripts H_2 and A identify the broadening agent used for study.

I. INTRODUCTION

THE experimental technique and apparatus used for carrying out quantitative infrared-intensity measurements have been described in a previous publication.[1] For a given partial pressure of CO the total pressure was varied systematically up to 700 psia by the addition of infrared-inactive gases such as H_2, He, A, N_2, and O_2. Measurements were performed in absorption cells of special design fitted with mechanical stirrers to assure uniform mixing of the gases. Representative gas mixtures were also analyzed by use of a mass spectrograph to verify relative compositions computed from the partial pressure changes associated with introduction of gases into the infrared-absorption cell. Some of the experimental data used in reference 1 for the determination of integrated absorption have also been used for the study of line broadening.

It is well known that the rotational half-widths of molecules such as CO are very small at atmospheric pressure, in fact so small that the direct measurement of line shape is beyond the resolving power attainable with most spectrographic instruments. For this reason it has become customary to estimate rotational half-widths indirectly by studying the dependence of apparent absorption on total pressure.[2–7] The basic theo-

* This paper presents the results of one phase of research carried out at the Jet Propulsion Laboratory, California Institute of Technology, under Contract No. DA-04-495-ORD 18, sponsored by the U. S. Army Ordnance Department.

[1] S. S. Penner and D. Weber, J. Chem. Phys. **19**, 807, 817, 974 (1951).

[2] L. A. Matheson, Phys. Rev. **40**, 813 (1932).

[3] W. M. Elsasser, Harvard Meteorological Studies No. 6, Milton (Massachusetts), 1942.

[4] A. M. Thorndike, J. Chem. Phys. **16**, 211 (1948).

[5] J. Strong and K. Watanabe, Phys. Rev. **57**, 1049 (1940).

[6] E. Lindholm, Arkiv Math. Astron. Fys. **32A**, No. 17 (1946).

[7] E. Lindholm, dissertation, Uppsala, 1942.

retical relations which are used for this work have been given by Elsasser,[3] whose discussion is, however, restricted to equally intense and equally spaced rotational lines obeying a dispersion formula. Elsasser also assumed that the incident intensity is constant and independent of ν. Extensions to more general types of vibration-rotation bands have been given by Schnaidt[8] and by Matossi and collaborators.[9] However, it has been pointed out by Elsasser and verified experimentally by other investigators that the results derived from the idealized line shape distribution of Elsasser lead to the correct functional relation between absorption, pressure, and optical density. Accordingly this simplified treatment will be used for the determination of apparent rotational half-widths from available experimental data.

Derivation of appropriate line shapes for collision broadening, broadening associated with the Doppler effect, van der Waals broadening, etc., may be found in the literature[3,6,7,10–13] and need not be repeated here. For the present purposes, only those parts of the theory will be reproduced and amplified which refer to results

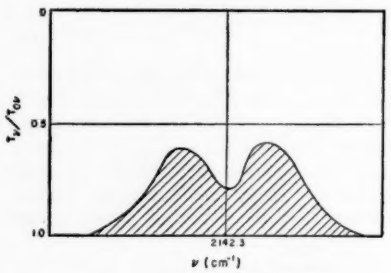

FIG. 1. Plot for the determination of $\int_{\Delta\nu}[1-(T_\nu/T_{0\nu})]d\nu$.

useful in interpreting available experimental data. Interpretation of experimental data in terms of a band spectrum consisting of equally intense and equally spaced rotational lines is presented in Sec. II.

The calculation of rotational half-widths using equally spaced and equally intense rotational lines suffers from the fact that no allowance is made for the variation of integrated absorption per rotational line from one line to another in a given vibration-rotation band. The correct value of the integrated absorption for each of the rotational lines of an anharmonic, vibrating and rotating diatomic molecule is calculable by utilizing theoretical studies carried out by Oppenheimer.[14,15] Furthermore, it is possible to determine with relative ease the actual intensity of radiation absorbed for nonoverlapping rotational lines broadened by molecular impacts.[3,15] By carrying out calculations of this type, with the rotational half-width treated as a variable parameter, a direct comparison between calculated and observed infrared absorption can be used to determine δ for pressures which are small enough to justify a treatment for nonoverlapping rotational lines. This procedure for the determination of rotational half-width is described in Sec. III. It is found that $(\delta_F)_{H_2}=0.077$ cm^{-1} atmos^{-1}, whereas $(\delta_F)_A=0.040$ cm^{-1} atmos^{-1}. Similarly, for the first overtone, $(\delta_O)_{H_2}=0.063$ cm^{-1} atmos^{-1}. These results are seen to be somewhat smaller than the values $(\delta_F)_{air}=0.10$ cm^{-1} atmos^{-1} and $(\delta_O)_{air}=0.12$ cm^{-1} atmos^{-1} reported by Matheson.[2]

II. DETERMINATION OF LOWER LIMITS FOR ROTATIONAL HALF-WIDTHS, ASSUMING EQUALLY SPACED AND EQUALLY INTENSE LINES

A. Outline of Theory

The theoretical studies of Elsasser for equally intense and equally spaced rotational lines lead to the conclusion that, in the most general case, the transmission function τ is given by the relation

$$\tau=\sinh\beta\int_{S\beta l/q\sinh\beta}^{\infty}[\exp(-y\cosh\beta)]J_0(iy)dy \quad (1)$$

where

$$\tau=1-A=\int_{\Delta\nu}I_\nu d\nu\Big/\int_{\Delta\nu}I_{0\nu}d\nu\simeq\int_{\Delta\nu}I_\nu d\nu/I_0\Delta\nu \quad (2)$$

and

$$\beta=2\pi\delta^0/q. \quad (3)$$

Here I_ν and $I_{0\nu}$ represent, respectively, the transmitted and incident spectral intensities, $\Delta\nu$ = effective width of the vibration-rotation band, I_0 = average value of the nearly constant incident intensity in the spectral interval of width $\Delta\nu$, δ^0 = rotational half-width, q = distance between the equally spaced rotational lines composing the vibration-rotation band of width $\Delta\nu$, J_0 = bessel function of order zero, and S = integrated absorption of each of the equally intense rotational lines.

In view of the approximation involved in the representation of a vibration-rotation band by a system of equally spaced and equally intense rotational lines, it is apparent that there is no such thing as a "correct" value for S. However, since the functional form of the relation derivable from Eq. (1) is correct, it is of some interest to determine an apparent rotational half-width by assuming the validity of the relation

$$S=\alpha/(\Delta\nu/q), \quad (4)$$

where α is the integrated absorption of an entire vibration-rotation band and $\Delta\nu/q$ represents the number of equally intense rotational lines in $\Delta\nu$. The relation given in Eq. (4) is probably a reasonably good approxi-

[8] F. Schnaidt, Gerl. Beiträge zur Geophysik **54**, 203 (1939).
[9] Matossi, Mayer, and Rauscher, Phys. Rev. **76**, 760 (1949).
[10] V. Weisskopf, Z. Physik **75**, 287 (1932).
[11] H. Margenau and W. W. Watson, Revs. Modern Phys. **8**, 22 (1936).
[12] J. H. Van Vleck and V. F. Weisskopf, Phys. Rev. **17**, 227 (1945).
[13] P. W. Anderson, Phys. Rev. **76**, 647 (1949).
[14] J. R. Oppenheimer, Proc. Cambridge Phil. Soc. **23**, 327 (1926); D. M. Dennison, Phys. Rev. **31**, 503 (1928).
[15] S. S. Penner, J. Chem. Phys. **19**, 272 (1951).

mation at very high pressures[16] but undoubtedly overestimates the value of S for low pressure data of the type useful for estimating rotational half-widths. Since S always occurs as a multiplier of δ^0, the choice of too large a value for S will lead to a lower limit for δ^0. The value of the half-width obtained by the use of Eq. (4) will be called an apparent rotational half-width and will be identified by a prime in order to distinguish it from the "true" rotational half-width δ^0. With this qualification the following analysis may be regarded as an empirical check on the validity of the functional form of the relations derivable from Eq. (1).

Elsasser[3] has shown how a number of limiting forms can be derived from Eq. (1) for various special cases. Thus, at low total pressures, δ^0 is small compared with q, whence β and $\sinh\beta$ are also small. The range of integration in Eq. (1) is therefore restricted to large values of y. But in this case it can be shown[3] that

$$\tau=1-A=1-\phi[(\pi S\delta^0 pl)^{\frac{1}{2}}/q] \simeq 1-2(S\delta^0 pl)^{\frac{1}{2}}/q+\cdots, \quad (5)$$

where $\phi(x)$ is the error integral defined by

$$\phi(x)=\frac{2}{\pi^{\frac{1}{2}}}\int_0^x [\exp(-x^2)]dx.$$

On the other hand, for large values of δ^0/q corresponding to large values of the total pressure, it can be shown[3] that

$$\tau\simeq\exp(-Spl/q)=\exp(-\alpha pl/\Delta\nu). \quad (6)$$

Here Eq. (6) is a satisfactory approximation for $\beta\geq 2$, whereas, for $\beta\leq\frac{1}{2}$, Eq. (5) forms a reasonable approximation. Finally, for values of β in the range $\frac{1}{2}\leq\beta\leq 2$, Elsasser recommends the relation

$$\tau=1-(Spl/q)\exp(-y)[J_0(iy)-iJ_1(iy)] \quad (7)$$

where

$$y=Spl/q\,\sinh\beta \quad (8)$$

and J_1 is a bessel function of order 1.

For collision broadening, the rotational half-width will be approximately proportional to the total pressure p_T at constant temperature.[3,11] Thus

$$\delta^0=\delta p_T \quad \text{and} \quad \delta^{0\prime}=\delta' p_T \quad (9)$$

where δ and δ' are the "true" and apparent rotational half-widths, respectively, at a pressure of 1 atmos. Replacing δ^0 in Eq. (5) by the value given in Eq. (9), it is evident that

$$\tau=1-A\simeq 1-2(S\delta pl p_T)^{\frac{1}{2}}/q$$

or

$$-d\tau/d(p_T)^{\frac{1}{2}}=dA/d(p_T)^{\frac{1}{2}}\simeq 2(S\delta pl)^{\frac{1}{2}}/q. \quad (10)$$

Thus the transmission τ is seen to vary as the square root of the total pressure at constant optical density for small values of δ, corresponding to small values of p_T. Since all of the quantities appearing on the right-hand side of Eq. (10) are known except δ, the slope of a τ *vs* $p_T^{\frac{1}{2}}$ plot can be used to estimate δ. Furthermore, Eq. (6) can be used to determine α for very large values of p_T. This method of determining α has been used successfully for CO.[16]

B. Experimental Results and Calculations for the Fundamental of CO

It should be noted that it is not possible to measure τ or A directly. The experimentally determined transmission is τ', and the experimentally observed absorption is A' where

$$\tau'=1-A'=\int_{\Delta\nu} T_\nu d\nu \Big/ \int_{\Delta\nu} T_{0\nu} d\nu \quad (11)$$

TABLE I. Experimental results of $A'\Delta\nu$ for CO-He mixtures (fundamental of CO).

p (mm Hg)	pl (cm atmos)	$(pl)^{\frac{1}{2}}$ (cm atmos)$^{\frac{1}{2}}$	p_T (psia)	$(p_T)^{\frac{1}{2}}$ (psia)$^{\frac{1}{2}}$	$\Delta\nu$ (cm^{-1})	$A'\Delta\nu$ (cm^{-1})
3	0.0203	0.142	700	26.46	210	2.03
60	0.407	0.638	16	4.00	240	30.0
↓	↓	↓	20	4.47	250	31.7
↓	↓	↓	25	5.00	250	34.9
↓	↓	↓	40	6.32	250	42.2
↓	↓	↓	50	7.07	250	48.3
↓	↓	↓	75	8.66	250	53.7
↓	↓	↓	100	10.00	250	56.7
↓	↓	↓	300	17.32	255	65.9
↓	↓	↓	500	22.36	260	67.6
↓	↓	↓	700	26.46	260	66.5
200	1.355	1.165	3.87	1.97	250	34.9
↓	↓	↓	15	3.87	250	46.5
↓	↓	↓	20	4.47	250	59.8
↓	↓	↓	25	5.00	250	65.4
↓	↓	↓	30	5.48	250	69.8
↓	↓	↓	50.5	7.11	250	82.2
↓	↓	↓	75	8.66	255	99.2
↓	↓	↓	100	10.00	260	105.7
↓	↓	↓	300	17.32	260	123.3
↓	↓	↓	500	22.36	270	123.6
↓	↓	↓	700	26.46	270	124.9; 122.7

and T_ν and $T_{0\nu}$ represent, respectively, the intensities of radiation with and without absorber to which the instrument responds. Furthermore, since $T_{0\nu}$ is approximately constant in the wave number interval $\Delta\nu$, it is apparent that

$$A'=1-\tau'\simeq(1/\Delta\nu)\int_{\Delta\nu}[1-(T_\nu/T_{0\nu})]d\nu. \quad (11a)$$

The quantity $A'\Delta\nu$ defined by Eq. (11a) can be obtained conveniently from a plot of the type shown in Fig. 1. The area of the entire rectangle is $\Delta\nu$, where $\Delta\nu$ is chosen large enough to assure that $T_\nu/T_{0\nu}$ has increased to 1 in the wings of the vibration-rotation band. The unshaded area in Fig. 1 evidently represents the quantity $\int_{\Delta\nu}(T_\nu/T_{0\nu})d\nu$, whence the shaded area has

[16] S. S. Penner, J. Appl. Phys. **21**, 685 (1950). S. S. Penner and D. Weber, J. Appl. Phys. **22**, 1164 (1951).

TABLE II. Experimental results of $A'\Delta\nu$ for CO-H_2 mixtures (fundamental of CO).

p (mm Hg)	pl (cm atmos)	$(pl)^{\frac{1}{2}}$ (cm atmos)$^{\frac{1}{2}}$	$A'\Delta\nu$ (cm^{-1}) at p_T =50 psia	at p_T =100 psia	at p_T =700 psia
3	0.0203	0.142	...	...	2.92
5	0.0339	0.184	6.34	...	4.67
10	0.0678	0.260	14.7	16.5	15.3
15	0.102	0.319	19.3	19.1	20.0
20	0.136	0.369	22.4; 23.0	24.6	25.8
40	0.271	0.521	35.9; 36.4	46.1	48.6
60	0.407	0.638	48.1; 44.9	66.6	65.8
80	0.542	0.736	57.5	76.6	81.1
200	1.355	1.165	...	...	119.4
40	0.271	0.521	37.0	43.0	...
150	1.016	1.008	77.2	...	109.1

the value $A'\Delta\nu$. It is found experimentally that the effective band width $\Delta\nu$ is practically constant and independent of partial pressure and total pressure.[16] This statement is verified by the results given in Table I. It is seen that only a small error will be made by setting $\Delta\nu=250$ cm^{-1} for all values of p and p_T.

The experimental data of $A'\Delta\nu$ for CO-H_2 mixtures are shown in Table II and plotted in Fig. 2. If Eq. (5) is assumed† to hold for A' as well as for A, it is apparent that

$$d(A'\Delta\nu)/d(pl)^{\frac{1}{2}}\simeq\Delta\nu dA'/d(pl)^{\frac{1}{2}}=2\Delta\nu(S\delta' p_T)^{\frac{1}{2}}/q \quad (10a)$$

where the validity of Eq. (9) has been assumed. Reference to Fig. 2 clearly shows that $A'\Delta\nu$ is a linear function of $(pl)^{\frac{1}{2}}$ for constant values of the total pressure. Furthermore, the validity of Eq. (10a) for pressures of

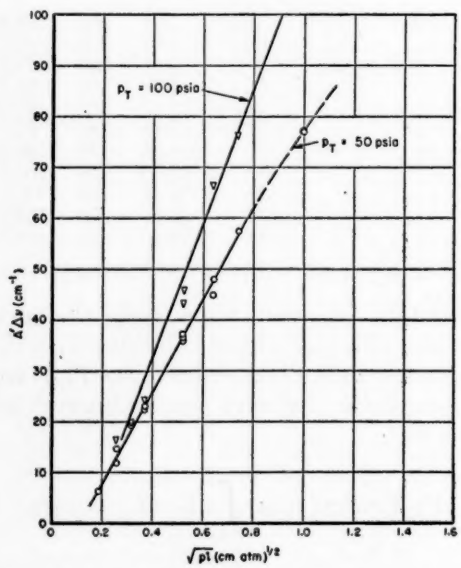

FIG. 2. $A'\Delta\nu$ for CO-H_2 mixtures as a function of $(pl)^{\frac{1}{2}}$ at $p_T=50$ and 100 psia (fundamental of CO).

† Replacing A by A' can be justified independently of the exact dependence of T_ν on instrumental factors. Thus $A'\Delta\nu$ is essentially an integrated transmittance obtained over a wave-number interval large compared with the instrumental slit width. The proof that $A'\Delta\nu\simeq A\Delta\nu$ under these conditions has been given by Nielsen, Thornton, and Dale, Revs. Modern Phys. 16, 307 (1944).

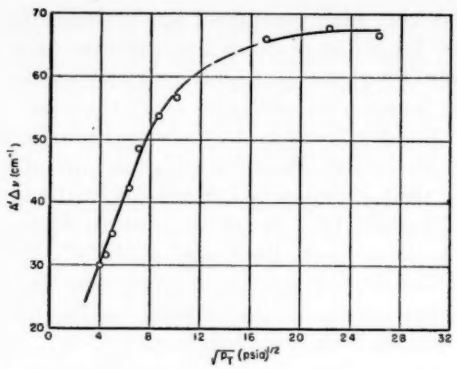

FIG. 3. $A'\Delta\nu$ for CO-He mixtures as a function of $(p_T)^{\frac{1}{2}}$ at $pl=0.407$ cm atmos (fundamental of CO).

50 and 100 psia is seen to be verified approximately. Thus

$$\{d[(A'\Delta\nu)/d(pl)^{\frac{1}{2}}]\}_{p_T=100\text{ psia}}/\{d[A'\Delta\nu/d(pl)^{\frac{1}{2}}]\}_{p_T=50\text{ psia}}=1.46$$

compared with a value of 1.41 computed from Eq. (10a).

It should be noted that the experimental values corresponding to $p_T=700$ psia cannot be used to evaluate δ^0 since δ^0/q is no longer small enough to justify the use of Eq. (5).

The value of $S=S_F$ for the fundamental[1] calculated from Eq. (4), with $\Delta\nu=250$ cm^{-1} and $q=4$ cm^{-1}, is $S_F=237/(250/4)=3.79$ cm^{-2} atmos^{-1}. Using this value of S_F and the slopes $d(A'\Delta\nu)/d(pl)^{\frac{1}{2}}$ determined from Fig. 2, it is found that $(\delta_F')_{H_2}=0.041$ cm^{-1} atmos^{-1}, where the subscript H_2 on δ_F' identifies the broadening agent which was present in large excess for the current studies.

The data of Table II may also be used to determine

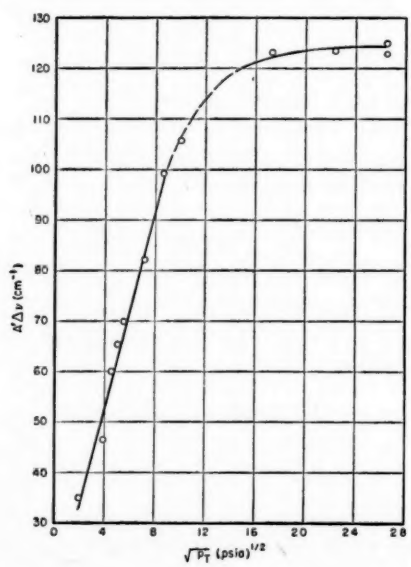

FIG. 4. $A'\Delta\nu$ for CO-He mixtures as a function of $(p_T)^{\frac{1}{2}}$ at $pl=1.355$ cm atmos (fundamental of CO).

TABLE III. Experimental results of $A'\Delta\nu$ for CO-A mixtures (fundamental of CO).

p (mm Hg)	pl (cm atmos)	$(pl)^{\frac{1}{2}}$ (cm atmos)$^{\frac{1}{2}}$	p_T (psia)	$(p_T)^{\frac{1}{2}}$ (psia)$^{\frac{1}{2}}$	$\Delta\nu$ (cm^{-1})	$A'\Delta\nu$ (cm^{-1})
80	0.541	0.736	50	7.07	240	50.1
↓	↓	↓	100	10.00	250	64.8
↓	↓	↓	300	17.32	255	75.3
↓	↓	↓	700	26.46	270	76.9
100	0.678	0.823	50	7.07	240	57.2
↓	↓	↓	100	10.00	250	72.8
↓	↓	↓	300	17.32	255	87.2
↓	↓	↓	700	26.46	270	90.5
200	1.355	1.165	700	26.46	270	123.0
40	0.271	0.521	50	7.07	240	32.7
80	0.542	0.736	↓	↓	240	50.1
100	0.678	0.823	↓	↓	240	57.2
300	2.033	1.43	↓	↓	240	94.2

$\delta^{0\prime}$ by using Eq. (5) with A replaced by A' whence

$$\delta^{0\prime} \simeq \left[\frac{q}{2\Delta\nu}\frac{A'\Delta\nu}{(pl)^{\frac{1}{2}}}\right]^2 \frac{1}{Sp_T}.$$

Alternately Eq. (10) can be applied to the two points corresponding to $p_T=50$ and 100 psia at constant pl. For the set of data shown in Table II this type of calculation is evidently less satisfactory than the method illustrated in Fig. 2, where a large number of experimental points are used to determine $\delta^{0\prime}$.

The experimental results for CO-He mixtures are summarized in Table I. The observed values of $A'\Delta\nu$ are plotted as a function of $(p_T)^{\frac{1}{2}}$ for $pl=0.407$ and 1.355 cm atmos in Figs. 3 and 4, respectively. Reference to Figs. 3 and 4 shows that $A'\Delta\nu$ is a linear function of $(p_T)^{\frac{1}{2}}$ for pressures up to about 80 psia. These results may be interpreted to mean that for pressures less than about 80 psia the ratio δ^0/q or $\delta^{0\prime}/q$ is small enough to permit the use of Eq. (5), whereas for higher pressures the rotational lines have become broadened sufficiently to necessitate consideration of overlapping rotational lines.

By the use of Eq. (10) the slopes of the linear regions in Figs. 3 and 4 may be used to compute δ_F'. Using the value previously given for S_F and again setting $\Delta\nu=250$ cm^{-1}, it is found that $\delta_F'=0.019$ cm^{-1} atmos^{-1} from the slope of Fig. 3 or $\delta_F'=0.017$ cm^{-1} atmos^{-1} from the slope of Fig. 4. Thus $(\delta_F')_{He}\simeq 0.018$ cm^{-1} atmos^{-1}. The fact that the values of δ_F' obtained from Figs. 3 and 4 agree well with each other immediately suggests that $A'\Delta\nu$ varies with pl approximately according to Eq. (10a). Thus the data given in Table I could be used to calculate δ' for each value of $p_{T'}$ up to $p_T=75$ psia, by comparing the experimentally determined results for $A'\Delta\nu$ at the two different values of pl used. It is apparent that the results obtained in this manner would be less accurate for the set of data given in Table I than results obtained by the method exemplified in Figs. 3 and 4, since calculations would be based on only two experimental points.

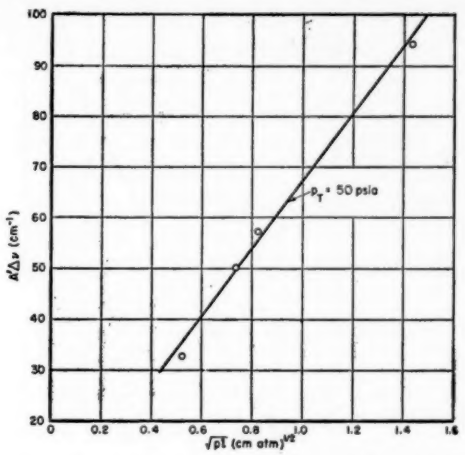

FIG. 5. $A'\Delta\nu$ for CO-A mixtures as a function of $(pl)^{\frac{1}{2}}$ at $p_T=50$ psia (fundamental of CO).

The experimental results obtained for CO-A mixtures are summarized in Table III. Of the data given in this table the last set, corresponding to four different values of pl at constant p_T, appears to be suitable for the determination of δ' by using Eq. (10a) in the same way as it has already been used for CO-H_2 mixtures (see Fig. 2). Accordingly $A'\Delta\nu$ is plotted as a function of $(pl)^{\frac{1}{2}}$ in Fig. 5 for $p_T=50$ psia. From the slope of the line in Fig. 5 it is found that $\delta'=0.021$ cm^{-1} atmos^{-1} if $S_F=3.79$ cm^{-2} atmos^{-1} and $\Delta\nu=250$ cm^{-1}. The half-width for CO broadened by the addition of A, *viz.*, $(\delta_F')_A=0.021$ cm^{-1} atmos^{-1}, is seen to be approximately as large as the half-width for CO broadened by the addition of He, whereas the rotational lines of CO are broadened more rapidly by the addition of H_2.

TABLE IV. Experimental results of $A'\Delta\nu$ for CO-He and CO-H_2 mixtures at $p_T=300$ psia (first overtone of CO).

p (psia)	pl (cm atmos)	$(pl)^{\frac{1}{2}}$ (cm atmos)$^{\frac{1}{2}}$	$A'\Delta\nu$ (cm^{-1})	Added gas
7.73	2.71	1.65	4.16	He
15.5	5.43	2.33	9.22	↓
20	7.01	2.65	10.5	↓
40	14.00	3.74	20.1	↓
60	21.0	4.58	29.2	↓
80	28.0	5.29	37.0; 36.1	↓
100	35.1	5.92	44.5	↓
20	7.01	2.65	10.6	H_2

TABLE V. Experimental results of $A'\Delta\nu$ for CO-He and CO-H_2 mixtures at $p_T=700$ psia (first overtone of CO).

p (psia)	pl (cm atmos)	$(pl)^{\frac{1}{2}}$ (cm atmos)$^{\frac{1}{2}}$	$A'\Delta\nu$ (cm^{-1})	Added gas
7.73	2.71	1.65	4.68	He
15.5	5.43	2.33	9.80	↓
20	7.01	2.65	10.2	↓
40	14.0	3.74	21.2	↓
60	21.0	4.58	30.3	↓
80	28.0	5.29	37.0; 37.8	↓
100	35.1	5.92	45.0	↓
20	7.01	2.65	12.7	H_2

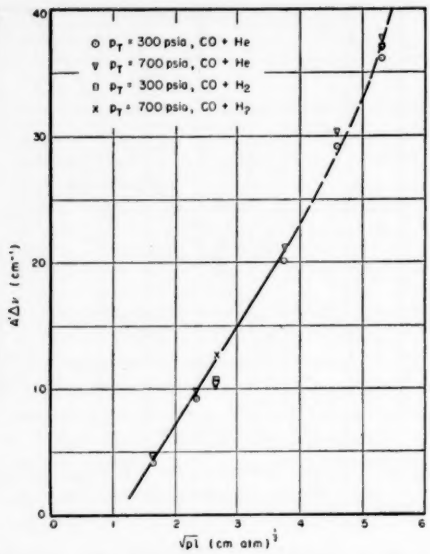

FIG. 6. $A'\Delta\nu$ as a function of $(pl)^{\frac{1}{2}}$ at $p_T=300$ and 700 psia (first overtone of CO).

The results of the present analysis of rotational half-widths are evidently not in agreement with Matheson's conclusion[2] that $(\delta_F)_{air}=0.10$ cm^{-1} atmos^{-1} since available infrared-transmission data indicate that $(\delta_F)_{air}$ should be roughly of the same magnitude as $(\delta_F)_A$ or $(\delta_F)_{He}$. As mentioned earlier in this section, the observed discrepancies are the result, in part, of the fact that the use of Eq. (4) overestimates S and hence leads to excessively small apparent half-widths. More reliable estimates of rotational half-widths require numerical calculations with proper allowance for the change in integrated absorption from one rotational line to another in a given vibration-rotation band (see Sec. III).

C. Experimental Results and Calculations for the First Overtone of CO

The experimental data of $A'\Delta\nu$ for CO-He and CO-H_2 mixtures at $p_T=300$ and 700 psia are given in Tables IV and V, respectively. At pressures between 300 and 700 psia, the transmission is practically independent of p_T. Hence the data of Tables IV and V were combined and plotted in Fig. 6. Reference to Fig. 6 shows that $A'\Delta\nu$ is a linear function of $(pl)^{\frac{1}{2}}$, at least for small values of $(pl)^{\frac{1}{2}}$. However, it is evident that the data plotted in Fig 6 are not suitable for the evaluation of the apparent rotational half-width since p_T is so large that the use of Eq. (5) or of any of the relations derived from it is no longer justifiable. The observation that the data of Fig. 6 are unsuitable for the calculation of the variation of half-width with pressure is particularly obvious if note is taken of the fact that for pressures in excess of about 100 psia the infrared transmission does not vary appreciably with total pressures, whereas it should vary as $(p_T)^{\frac{1}{2}}$ if Eq. (10) applied.

In order to obtain a satisfactory estimate of the change of apparent rotational half-width with pressure for the first overtone of CO, resulting from collision broadening by an added gas, it is necessary to determine the infrared transmission as a function of pl for p_T less than about 80 psia, retaining a vast excess of added gas. Measurements of this type cannot be carried out readily in the small infrared-absorption cells designed for high-pressure work (see Figs. 1, 2, and 3 of reference 1). For this reason a special set of infrared-transmission measurements was made for CO-H_2 mixtures in a 100-cm cell at a constant total pressure of 760 mm. The results of these studies, which are not considered to be suitable for the determination of integrated absorption, are summarized in Table VI and plotted in Fig. 7.

TABLE VI. Experimental results of $A'\Delta\nu$ for CO-H_2 mixtures at $p_T=760$ mm of Hg for $l=100$ cm (first overtone of CO).

p (mm Hg)	pl (cm atmos)	$(pl)^{\frac{1}{2}}$ (cm atmos)$^{\frac{1}{2}}$	$A'\Delta\nu$ (cm^{-1})
50	6.58	2.565	6.76
100	13.16	3.627	11.06
150	19.74	4.443	14.80
200	26.32	5.130	17.24
250	32.90	5.735	20.78
300	39.47	6.283	22.32
400	52.63	7.254	26.98
500	65.79	8.111	29.32
600	78.95	8.885	34.32
700	92.11	9.597	38.50

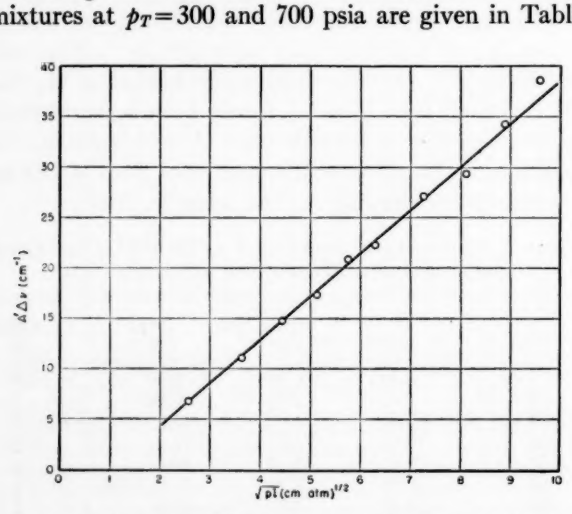

FIG. 7. $A'\Delta\nu$ for CO-H_2 mixtures as a function of $(pl)^{\frac{1}{2}}$ at $p_T=760$ mm of Hg (first overtone of CO).

Reference to Fig. 7 shows that $A'\Delta\nu$ is a linear function of $(pl)^{\frac{1}{2}}$ for the entire range of partial pressures of CO from 50 to 700 mm of Hg. For small concentrations of CO there is a sufficient excess of H_2 to permit the calculation of $(\delta_O')_{H_2}$. Here the subscript O identifies the spectral half-width of the first overtone. Since the plot of Fig. 7 is linear with the same slope, also, for partial pressures of CO which are so large that appreciable self-broadening must occur, it appears that H_2 and CO are nearly equally efficient broadening agents for the rotational lines of CO. This statement is further

supported by the experimental results on self-broadening which will be described in the second report of this series.

Using Eqs. (5) and (9) and setting[1] $S_O=1.64/(250/4)=2.62\times10^{-2}$ cm^{-2} atmos^{-1} with $\Delta\nu=250$ cm^{-1} and $q=4$ cm^{-1}, it is found that $(\delta_O')_{H_2}=0.044$ cm^{-1} atmos^{-1}. Thus the change of the apparent rotational half-width of CO with pressure for CO-H_2 mixtures is roughly the same for the fundamental as for the first overtone. Similar results have also been obtained by Matheson.[2]

D. Apparent Optical Collision Diameters for Collisions between CO Mixtures with H_2, He, or A

In the impact theories of line broadening the optical collision diameter is defined as the average distance between the centers of two colliding atoms at which the radiative process stops. The optical collision diameter σ is related to the half-width δ^0 through the relation

$$\delta^0=0.78\sigma^2\bar{v}N, \tag{12}$$

where $\bar{v}$ represents the appropriate mean velocity of impact and N is the total number of molecules per unit volume. Substituting the kinetic-theory value for $\bar{v}$, it can be shown[2] that

$$\sigma^2=\frac{\delta}{N_0}\left(\frac{2\pi}{7.60kT}\right)^{\frac{1}{2}}\left(\frac{mM}{m+M}\right)^{\frac{1}{2}}, \tag{13}$$

where N_0 represents the number of molecules per unit volume at atmospheric pressure, m is the mass of the absorbing atom, and M is the mass of the perturbing molecule.

By use of the experimental data for δ_F' and δ_O' given in Secs. II-B and II-C, it is possible to calculate the corresponding apparent optical collision diameters from Eq. (13). The results of these calculations are contrasted in Table VII, with the kinetic-theory collision diameters calculated from viscosity measurements.[17] Reference to Table VII shows that the apparent optical and kinetic-theory collision diameters do not agree with each other, a fact which is not surprising since they correspond to different physical processes and since the values of δ' represent lower limits. It is to be noted, however, that the relative order of the sizes of the collision diameters is the same for the optical and kinetic-theory values.

III. DETERMINATION OF ROTATIONAL HALF-WIDTHS FOR COLLISION-BROADENED ROTATIONAL LINES

A. Theoretical Relations for Diatomic Molecules with Collision-Broadened Lines

For collision broadening of diatomic molecules which do not possess a Q branch, the spectral absorption coefficient P_ν of the fundamental is given by the relation

$$P_\nu=\frac{\delta^0}{\pi}\sum_j\left[\frac{S_{j\to j-1}^{0\to1}}{(\nu-\nu_{j\to j-1}{}^{0\to1})^2+\delta^{0^2}}+\frac{S_{j-1\to j}^{0\to1}}{(\nu-\nu_{j-1\to j}{}^{0\to1})^2+\delta^{0^2}}\right], \tag{14}$$

where [14,15]

$$S_{j\to j-1}^{0\to1}=\frac{\nu_{0\to1}}{\nu_e}\frac{N_T\pi\epsilon^2}{3\mu cQ(T)}\frac{\nu_{j\to j-1}^{0\to1}}{\nu_{0\to1}}j[\exp-E_{0,j}/kT]FG \tag{15}$$

$$S_{j-1\to j}^{0\to1}=\frac{\nu_{0\to1}}{\nu_e}\frac{N_T\pi\epsilon^2}{3\mu cQ(T)}\frac{\nu_{j-1\to j}^{0\to1}}{\nu_{0\to1}}\times j[\exp-E_{0,j-1}/kT]F'G'. \tag{15a}$$

Here N_T = total number of molecules per unit volume per unit of total pressure, μ = reduced mass of diatomic molecule under discussion, c = velocity of light, ϵ = effective charge, $\nu_{0\to1}$ = wave number corresponding to the (forbidden) transition $j=0\to j=0$ and $n=0\to n=1$, ν_e = wave number corresponding to an infinitesimal oscillation at the equilibrium interatomic distance, $E_{n,j}$ = energy of n'th vibrational and j'th rotational level, $F=1+4\gamma j[1+(5\gamma j/8)-(3\gamma/8)]$, $F'=1-4\gamma j[1-(5\gamma j/8)-(3\gamma/8)]$, $\gamma=h/4\pi^2Ic\nu_e$ where I represents the moment of inertia, $G=1-\exp(-hc\nu_{j\to j-1}{}^{0\to1}/kT)$, $G'=1-\exp(-hc\nu_{j-1\to j}{}^{0\to1}/kT)$, and $Q(T)$ = complete internal partition function at temperature T. The wave numbers $\nu_{j\to j'}{}^{n\to n'}$ are determined by use of the Bohr frequency relation from the expression for $E_{n,j}$; i.e.,

$$E_{n,j}=(n+\tfrac{1}{2})hc\nu_e-(n+\tfrac{1}{2})hcx_e\nu_e+j(j+1)hc\beta_e-j^2(j+1)hcD_e-(n+\tfrac{1}{2})j(j+1)hc\zeta \tag{16}$$

where ν_e, x_e, β_e, D_e, and ζ are empirical constants which are known with a high degree of accuracy.[18–20]

TABLE VII. Collision diameters for collisions between CO and H_2, He, or A (fundamental and first overtone of CO).

	Added gas	Apparent optical collision diameter (cm $\times10^8$)	Kinetic-theory collision diameter, calculated from viscosity data* (cm $\times10^8$)
Fundamental of CO	H_2	2.0	3.25
Fundamental of CO	He	1.5	2.97
Fundamental of CO	A	2.5	3.72
First overtone of CO	H_2	2.1	3.25

* See reference 17, p. 229.

[17] S. Chapman and T. G. Cowling, *The Mathematical Theory of Non-Uniform Gases* (Cambridge University Press, Cambridge, 1939).

[18] Lagemann, Nielsen, and Dickey, Phys. Rev. **72**, 284 (1947).
[19] H. Sponer, *Molekülspektren* (Verlag. Julius Springer, Berlin, 1935).
[20] K. N. Rao, J. Chem. Phys. **18**, 213 (1950).

TABLE VIII. Numerical values of A^0 and S for the fundamental of CO at 298.7°K.

Rotational transitions $j \rightarrow j-1$	$10^3 A^0_{j\rightarrow j-1}$	$S_{j\rightarrow j-1}{}^{0\rightarrow 1}$ (cm^{-2} $atmos^{-1}$)	Rotational transitions $j-1 \rightarrow j$	$10^3 A^0_{j-1\rightarrow j}$	$S_{j-1\rightarrow j}{}^{0\rightarrow 1}$ (cm^{-2} $atmos^{-1}$)
1→ 0	5.4000	1.986	0→ 1	5.4433	2.002
2→ 1	10.462	3.847	1→ 2	10.627	3.908
3→ 2	14.919	5.486	2→ 3	15.277	5.617
4→ 3	18.563	6.826	3→ 4	19.158	7.044
5→ 4	21.265	7.819	4→ 5	22.107	8.129
6→ 5	22.934	8.433	5→ 6	24.041	8.840
7→ 6	23.621	8.685	6→ 7	24.947	9.173
8→ 7	23.372	8.594	7→ 8	24.888	9.151
9→ 8	22.355	8.220	8→ 9	23.994	8.823
10→ 9	20.733	7.624	9→10	22.423	8.245
11→10	18.681	6.869	10→11	20.365	7.488
12→11	16.388	6.026	11→12	18.004	6.620
13→12	14.012	5.152	12→13	15.516	5.705
14→13	11.693	4.300	13→14	13.047	4.797
15→14	9.5279	3.503	14→15	10.714	3.940
16→15	7.5888	2.790	15→16	8.5972	3.161
17→16	5.9095	2.173	16→17	6.7475	2.481
18→17	4.5009	1.655	17→18	5.1796	1.905
19→18	3.3559	1.234	18→19	3.8902	1.430
20→19	2.4490	0.901	19→20	2.8265	1.039
22→21	1.2252	0.450	21→22	1.3867	0.510
24→23	0.5645	0.208	23→24	0.6795	0.250
26→25	0.2400	0.088	25→26	0.2932	0.108
28→27	0.0943	0.035	27→28	0.1168	0.043
30→29	0.0342	0.013	29→30	0.0430	0.016
32→31	0.0115	0.004	31→32	0.0147	0.005
34→33	0.0036	0.001	33→34	0.0034	0.001
36→35	0.0010	0.000	35→36	0.0014	0.001
38→37	0.0003	0.000	37→38	0.0004	0.000
40→39	0.0001	0.000	39→40	0.0001	0.000
42→41	0.0000	0.0000	41→42	0.0000	0.000

The quantity A defined by Eq. (2) can also be written as

$$A\Delta\nu=\int_{\Delta\nu}[1-\exp(-P_\nu X)]d\nu, \tag{17}$$

where $X=pl$ represents the optical density. For nonoverlapping rotational lines, Eq. (17) can be integrated[3,15] with the result

$$A\Delta\nu=2\pi\delta^0\sum_j Z_j\exp(-Z_j)[J_0(iZ_j)-iJ_1(iZ_j)], \tag{18}$$

where the summation over j includes all of the transitions contributing to absorption of radiation by the vibration-rotation band. The quantity Z_j is defined through either of the relations

$$Z_j=S_{j\rightarrow j-1}{}^{0\rightarrow 1}X/2\pi\delta^0 \tag{19}$$

$$Z_j=S_{j-1\rightarrow j}{}^{0\rightarrow 1}X/2\pi\delta^0 \tag{19a}$$

depending upon the energy transition involved. The symbols J_0 and J_1 denote bessel functions of order zero and 1, respectively.

For the first overtone, relations analogous to Eqs. (14), (15), (15a), (19), and (19a) hold with $S_{j\rightarrow j-1}{}^{0\rightarrow 1}$ and $S_{j-1\rightarrow j}{}^{0\rightarrow 1}$ replaced by $S_{j\rightarrow j-1}{}^{0\rightarrow 2}$ and $S_{j-1\rightarrow j}{}^{0\rightarrow 2}$, respectively.

In this connection it should be noted that an approximate method for the calculation of $A\Delta\nu$ has been developed by Matheson[2] for nonoverlapping rotational lines obeying a dispersion formula. Matheson's method is more accurate than the procedure described in Sec. II because allowance is made for the change in integrated absorption from one rotational line to the next. However, since Matheson uses the results of the old quantum theory for the integrated absorption per rotational line, his method is less precise than that used in deriving Eq. (18).

Equation (18) was derived on the assumption that no overlapping of rotational lines occurs. Since some overlapping may occur even for small values of the optical density, it is to be expected that the values of $A\Delta\nu$ calculated from Eq. (18) give an upper limit for $A\Delta\nu$. However, $A\Delta\nu$ increases with rotational half-width δ^0. Hence comparison of results calculated from Eq. (18) with experimental data will lead to a lower limit for the rotational half-width δ^0. Overlapping of rotational lines is minimized by small values of δ^0, whence calculations using Eq. (18) should be restricted to the smallest values of p_T for which reliable experimental data are available.

B. Integrated Absorption for Individual Rotational Lines

Equations (15) and (15a) for the integrated absorption of individual rotational lines can be written, respectively, as

$$S_{j\rightarrow j-1}{}^{0\rightarrow 1}=\psi A^0{}_{j\rightarrow j-1} \tag{20}$$

and

$$S_{j-1\rightarrow j}{}^{0\rightarrow 1}=\psi A^0{}_{j-1\rightarrow j}, \tag{20a}$$

where

$$A^0{}_{j\rightarrow j-1}=j\frac{\nu_{j\rightarrow j-1}{}^{0\rightarrow 1}}{\nu_{0\rightarrow 1}}\exp(-E_{0,j}/kT)FG \tag{21}$$

$$A^0{}_{j-1\rightarrow j}=j\frac{\nu_{j-1\rightarrow j}{}^{0\rightarrow 1}}{\nu_{0\rightarrow 1}}\exp(-E_{0,j-1}/kT)F'G' \tag{21a}$$

$$\psi=\alpha/Q(T). \tag{22}$$

The quantities $A^0{}_{j\rightarrow j-1}$ and $A^0{}_{j-1\rightarrow j}$ do not depend on the effective charge ϵ and hence can be calculated quite accurately from the spectroscopic constants of Sponer.[19] Since these data have been revised recently by Lagemann *et al.*[18] and by Herzberg and Rao,[20] all of the wave numbers for the various transitions will be somewhat shifted (by about 1 cm^{-1}). The effect of revised values of $E(n, j)$ on the calculated integrated absorption is exceedingly small and may be neglected in the present application.

The complete internal partition function $Q(T)$ is readily obtained by standard statistical methods.[21] At 298.7°K it is found that $Q(298.7°K)=0.6445$. Hence

[21] J. E. Mayer and M. G. Mayer, *Statistical Mechanics* (John Wiley and Sons, Inc., New York, 1946).

for the fundamental

$$\psi_F = 237/0.6445 = 367.7 \text{ cm}^{-2} \text{ atmos}^{-1}. \quad (23)$$

The absolute value of the integrated absorption for each rotational line of the first overtone will be assumed to be equal to the intensity ratio for the integrated absorption over the entire vibration-rotation band, *viz.*, $1.64/237 = 6.92\times10^{-3}$, times the value for the corresponding rotational transition of the fundamental. This last remark is in rough agreement with the results of calculations on overtone intensities.[22,23]

The absolute values of $A^0_{j\to j-1}$, $A^0_{j-1\to j}$, $S_{j-1\to j}{}^{0\to1}$, and $S_{j\to j-1}{}^{0\to1}$ for the fundamental vibration-rotation band of CO at 298.7°K are given in Table VIII, whereas the values of $S_{j-1\to j}{}^{0\to2}$ and $S_{j\to j-1}{}^{0\to2}$, calculated according to the procedure described in the preceding paragraph, are summarized in Table IX. The numerical values given in Tables VIII and IX will now be used to calculate $A\Delta\nu$ and hence to determine rotational half-widths by direct comparison with available experimental data.

C. Determination of Rotational Half-Width from Comparison between Calculated and Observed Values of $A\Delta\nu$

The quantity $A\Delta\nu$ can be calculated according to Eq. (18) by using the data on integrated absorption given in Tables VIII and IX.

In order to determine the rotational half-width of the fundamental, the optical density pl was chosen as 0.10 or 1.355 cm atmos. Calculations of $A\Delta\nu$ have been carried out for assumed values of the half-width δ_F ranging from 0.2 to 0.7 cm^{-1}. The results of this laborious numerical work are summarized in Table X. Similarly, in order to estimate the rotational half-width for the first overtone, pl was set equal to 30 cm atmos, and δ_O was assumed to have values of 0.05, 0.1, and 0.2 cm^{-1}. The results of calculations for the first overtone are summarized in Table XI.

Reference to Fig. 2 shows that at $p_T = 50$ psia the observed value of $A'\Delta\nu$ of the fundamental for CO-H_2 mixtures at $pl = 0.10$ (i.e., $(pl)^{\frac{1}{2}} = 0.316$ cm$^{\frac{1}{2}}$ atmos$^{\frac{1}{2}}$) is 18.0 cm^{-1}. Comparison with the data listed in Table X shows that for $\delta_F{}^0 = 0.263$ cm^{-1} the calculated and observed values of $A\Delta\nu$ agree if it is assumed that $A'\Delta\nu = A\Delta\nu$ and that a smooth curve is drawn through the calculated data for $A\Delta\nu$ as a function of δ^0. Since the lower limit for $\delta_F{}^0$ is 0.263 cm^{-1} at 50 psia, it follows that $(\delta_F)_{H_2} \geq 0.077$ cm^{-1} atmos^{-1}. Furthermore, from Fig. 5 it is seen that for CO-A mixtures $A'\Delta\nu$ for the fundamental has the value 78.0 cm^{-1} at $pl = 1.355$ cm atmos (i.e., $(pl)^{\frac{1}{2}} = 1.164$ cm$^{\frac{1}{2}}$ atmos$^{\frac{1}{2}}$). Comparison with the data of Table X therefore leads to the conclusion that the lower limit of $\delta_F{}^0$ is 0.135 cm^{-1} for CO-A mixtures at $p_T = 50$ psia. Hence $(\delta_F)_A \geq 0.040$ cm^{-1} atmos^{-1}.

Proceeding similarly for the first overtone and CO-H_2 mixtures, it can be seen from Fig. 7 that $A'\Delta\nu = 19.2$ cm^{-1} at $p_T = 1$ atmos and $pl = 30$ cm atmos (i.e., $(pl)^{\frac{1}{2}} = 5.477$ cm$^{\frac{1}{2}}$ atmos$^{\frac{1}{2}}$). Hence comparison with the data listed in Table XI shows that $(\delta_O)_{H_2} \geq 0.063$ cm^{-1} atmos^{-1}. The lower limits for the half-widths given above are seen to be appreciably smaller than the rotational half-widths reported by Matheson, *viz.*, $(\delta_F)_{air} = 0.10$ cm^{-1} atmos^{-1} and $(\delta_O)_{air} = 0.12$ cm^{-1} atmos^{-1}.

The method for determining lower limits for rotational half-widths described in this section does not appear to have been used by other investigators. If the total pressure is sufficiently small, it seems to be a simple and reliable procedure, since $A\Delta\nu$ has been found to be a relatively sensitive function of δ^0 (see Tables X and XI).

The optical collision diameters calculated from the rotational half-widths of the fundamental found by numerical calculations are 2.65×10^{-8} cm for collisions between H_2 and CO, and 3.45×10^{-8} for collisions between A and CO. Reference to Table VII shows that these optical collision diameters are smaller than the kinetic-theory values. One might be tempted to account for this observation by noting that numerical calculations according to Eq. (18) will yield only a lower limit for δ and also for the optical collision diameter. However, this supposition is hardly in accord with the relative results obtained for the rotational half-widths of CO-H_2 collisions for the fundamental and the first overtone of CO. Since the experimental data for the fundamental were obtained at $p_T = 3.401$

TABLE IX. Numerical values of S for the first overtone of CO at 298.7°K.

Rotational transition $j \to j-1$	$S_{j\to j-1}{}^{0\to2}$ (cm^{-2} atmos^{-1})	Rotational transition $j-1 \to j$	$S_{j-1\to j}{}^{0\to2}$ (cm^{-2} atmos^{-1})
1→ 0	0.01374	0→ 1	0.01385
2→ 1	0.02663	1→ 2	0.02705
3→ 2	0.03797	2→ 3	0.03888
4→ 3	0.04724	3→ 4	0.04878
5→ 4	0.05412	4→ 5	0.05626
6→ 5	0.05837	5→ 6	0.06118
7→ 6	0.06012	6→ 7	0.06349
8→ 7	0.05948	7→ 8	0.06334
9→ 8	0.05689	8→ 9	0.06016
10→ 9	0.05277	9→10	0.05707
11→10	0.04754	10→11	0.05183
12→11	0.04171	11→12	0.04582
13→12	0.03566	12→13	0.03949
14→13	0.02976	13→14	0.03320
15→14	0.02425	14→15	0.02727
16→15	0.01931	15→16	0.02188
17→16	0.01504	16→17	0.01717
18→17	0.01145	17→18	0.01297
19→18	0.00854	18→19	0.00974
20→19	0.00623	19→20	0.00708
22→21	0.00312	21→22	0.00347
24→23	0.00144	23→24	0.00170
26→25	0.00061	25→26	0.00073
28→27	0.00024	27→28	0.00029
30→29	0.00009	29→30	0.00011
32→31	0.00003	31→32	0.00004
34→33	0.00001	33→34	0.00001
36→35	0.00000	35→36	0.00000

[22] K. Scholz, Z. Physik 28, 751 (1932).
[23] B. L. Carwford, Jr., and H. L. Dinsmore, J. Chem. Phys. 18, 983, 1682 (1950).

TABLE X. $A\Delta\nu$ calculated from Eq. (18) for the fundamental of CO at $pl=0.10$ and 1.355 cm atmos for various values of δ^0.

δ^0 (cm^{-1})	$A\Delta\nu$ (cm^{-1}) for $pl=0.10$ cm atmos	$A\Delta\nu$ (cm^{-1}) for $pl=1.355$ cm atmos
0.2	17.23	...
0.3	18.38	...
0.5	19.50	...
0.7	19.88	...
0.1	...	68.1
0.2	...	93.3
0.4	...	126.2

atmos and those for the first overtone at 1 atmos, it is apparent that the numerical calculations of $A\Delta\nu$ according to Eq. (18) would tend to overestimate $A\Delta\nu$ considerably more for the fundamental than for the first overtone because of more extensive overlapping of rotational lines at the higher pressure. Hence it would be expected that if the present method of calculation did not yield a reasonably good approximation to the true values of the rotational half-width, the discrepancy should be appreciably greater for the fundamental than for the first overtone. This line of reasoning leads to the conclusion that either the true rotational half-width for the fundamental is appreciably larger than for the first overtone for CO-H_2 collisions, or the use of Eq. (18) constitutes a useful method of calculation. Since there are no apparent reasons for postulating much larger rotational half-widths for the fundamental than for the first overtone (Matheson's data indicate the reverse behavior), the small calculated optical collision diameters are probably reasonable approximations to the "true" optical collision diameters.

TABLE XI. $A\Delta\nu$ calculated from Eq. (18) for the first overtone of CO at $pl=30$ cm atmos for various values of δ^0.

δ^0 (cm^{-1})	$A\Delta\nu$ (cm^{-1})
0.05	17.65
0.1	23.58
0.2	29.93

Comparison of the results of apparent half-width calculations for the fundamental given in Sec. II with the results obtained in this section shows that the present values for the half-widths are roughly twice as large as the apparent half-width data computed in Sec. II. Hence, referring to Sec. II, it is apparent that if Eq. (4) for the calculation of S had been replaced by the relation

$$S=\alpha/2(\Delta\nu/q) \tag{4a}$$

the apparent half-widths computed in Sec. II would have been doubled and would therefore have been in good agreement with the results of numerical calculations on the fundamental described in this section. The use of an integrated absorption per rotational line roughly equal to one-half of the arithmetic mean value for the region where the transmission varies as the square root of the optical density is thus seen to be indicated. The fact that a correction factor for S in Eq. (4) larger than one-half is required in order to achieve agreement between the overtone half-widths $(\delta_0')_{H_2}$ and $(\delta_0)_{H_2}$ is the result of the larger optical densities which were employed for the experimental investigations on the first overtone.

Quantitative Line-Width Measurements in the Infrared. II. Unpressurized Carbon Monoxide*

S. S. PENNER AND D. WEBER
Jet Propulsion Laboratory, California Institute of Technology, Pasadena, California

(Received July 3, 1951)

Experimental measurements on self-broadening of CO are correlated quantitatively by the use of a dispersion formula for line-shape representation. Interpretation of experimental data in terms of a simplified line-intensity distribution leads to the conclusion that the apparent rotational half-width of CO changes with the pressure of CO at approximately the same rate as with the pressure of H_2 for the fundamental. Similar calculations for the first overtone lead to relatively small values for the apparent rotational half-width. Numerical calculations for a realistic line-intensity distribution have not been carried out.

I. INTRODUCTION

THE experimental technique and apparatus used for quantitative intensity measurements have been described previously.[1] Methods for determining rotational half-widths from a simplified line-intensity distribution, as well as numerical methods for more accurate calculations, have been discussed in Part I.[2]

The absorption A is again defined by the relation

$$1-A=\int_{\Delta\nu} I_\nu d\nu \Big/ \int_{\Delta\nu} I_{0\nu} d\nu \simeq \int_{\Delta\nu} I_\nu d\nu / I_0 \Delta\nu, \quad (1)$$

where I_ν and $I_{0\nu}$ represent, respectively, the transmitted and the incident spectral intensities, $\Delta\nu$ is the effective width of the vibration-rotation band, and I_0 represents an average value for the nearly constant incident intensity in the spectral interval of width $\Delta\nu$. For self-broadening of the rotational lines, it is readily shown[3] that Eq. (10) of reference 2 becomes

$$d(A\Delta\nu)/dp \simeq 2\Delta\nu(S\delta' l)^{\frac{1}{2}}/q, \quad (2)$$

where δ' is the apparent rotational half-width per atmosphere of broadening agent, p is the pressure, S is the integrated absorption per rotational line, l is the path length, and q represents the distance between the centers of adjacent rotational lines. Equation (2) shows that for self-broadening the absorption is a linear function of the pressure for a constant path length. Since this relation was derived by retaining only the first two terms of the expansion of the error function of $\phi[p(\pi S\delta' l)^{\frac{1}{2}}/q]$, it is to be expected that Eq. (2) will hold only for relatively small values of the pressure at fixed path length.†

TABLE I. Experimental results for self-broadening on the fundamental of CO ($l=6.22$ cm).

p (mm Hg)	pl (cm atmos)	$A'\Delta\nu$ (cm^{-1})
50	0.409	8.48
100	0.818	17.65
150	1.228	27.26
200	1.637	34.21
300	2.455	51.58
400	3.274	67.97
500	4.092	80.88
600	4.911	93.72
700	5.729	103.1
1292	10.574	141.1

II. EXPERIMENTAL RESULTS AND INTERPRETATION OF DATA

A. Absorption Studies on the Fundamental of Unpressurized CO

Experimental results obtained for the fundamental of unpressurized CO are summarized in Tables I and II. Measurements on the fundamental were made in cells 6.22 and 10.1 cm in length. The data of Tables I and II are plotted in Fig. 1.‡ The relation given in Eq. (2) is borne out by the linear plots shown in Fig. 1 up to pressures of about 500 mm of Hg. Furthermore, the ratio of the slopes for cell lengths of 10.1 and 6.22

TABLE II. Experimental results for self-broadening on the fundamental of CO ($l=10.1$ cm).

p (mm Hg)	pl (cm atmos)	$A'\Delta\nu$ (cm^{-1})
25.1	0.334	8.78
50.1	0.666	13.68
100.3	1.333	21.22
149.5	1.987	33.94
198.5	2.638	46.98
299.5	3.980	56.52
348.1	4.626	71.04
496.8	6.602	97.40
719.6	9.563	117.10

* This paper presents the results of one phase of research carried out at the Jet Propulsion Laboratory, California Institute of Technology, under Contract No. DA-04-495-ORD 18, sponsored by the U. S. Army Ordnance Department.

[1] S. S. Penner and D. Weber, J. Chem. Phys. **19**, 807, 817, 974 (1951).

[2] S. S. Penner and D. Weber, J. Chem. Phys. **19**, 1351 (1951).

[3] W. M. Elsasser, Harvard Meteorological Studies No. 6, Milton (Massachusetts), 1942.

† According to Elsasser (see reference 3), Eq. (2) forms a satisfactory approximation if $2\pi\delta' p/q \leq \frac{1}{2}$.

‡ All of the experimental data refer to the apparent absorption A' rather than to the true absorption A. Compare references 1 and 2.

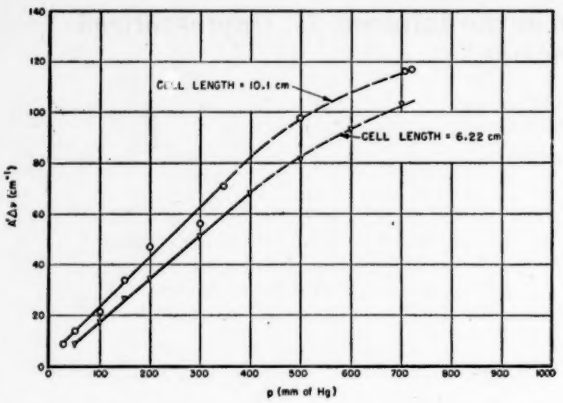

FIG. 1. Dependence of $A'\Delta\nu$ on p for the fundamental of CO.

cm, respectively, is

$$\frac{d(A'\Delta\nu)_{l=10.1}/dp}{d(A'\Delta\nu)_{l=6.22}/dp}=1.17,$$

which is seen to be in rough agreement with the theoretical value of $(10.1/6.22)^{\frac{1}{2}}=1.27$. Finally the value of $(\delta_F')_{CO}$, the change in rotational half-width with pressure for self-broadening of the fundamental, should be calculable, approximately, from the slopes of the plots shown in Fig. 1. The result is found to be $(\delta_F')_{CO}=4\times10^{-2}$ cm^{-1} atmos^{-1}. The experimental data for the infrared absorption by pure CO therefore lead to the conclusion that the apparent rotational half-width of the fundamental changes with the pressure of CO at approximately the same rate as with the pressure of H_2 for CO mixed with a large excess of hydrogen.[2] The apparent optical collision diameter is found to be 3.25×10^{-8} cm compared with the kinetic-theory value of 3.78×10^{-8} cm. Thus, although the apparent optical collision diameter for self-broadening is again smaller than the kinetic-theory value, it is relatively larger than the corresponding results for collisions[2] between CO and either H_2, He, or A. This conclusion is in agreement with the idea that some resonance broadening may occur for collisions between identical molecules,

TABLE III. Experimental results for self-broadening on the first overtone of CO ($l=3.57$ cm).

p (psia)	$A'\Delta\nu$ (cm^{-1})
15	4.52
20	7.10
30	9.68
40	12.5
60	18.2
70	20.4
100	30.1
200	58.7
300	79.4
400	93.4
500	103
600	118
700	125

TABLE IV. Experimental results for self-broadening on the first overtone of CO ($l=6.22$ cm).

p (psia)	$A'\Delta\nu$ (cm^{-1})
20	16.1
30	20.2
40	25.8
60	29.3
70	32.8
100	50.2
200	83.7
300	108
400	122
500	141
600	148
700	148

thus leading to large values for the apparent optical collision diameter.

B. Absorption Studies on the First Overtone of Unpressurized CO

Experimental results obtained for the first overtone of unpressurized CO are summarized in Tables III and IV. Measurements on the first overtone were made in cells 3.57 and 6.22 cm in length. The quantity $A'\Delta\nu$ is plotted as a function of pressure in Fig. 2. Reference to Fig. 2 shows that $A'\Delta\nu$ is a linear function of p at least up to pressures of 100 psia, thus showing that the rotational half-width is a linear function of pressure. It is found from Fig. 2 that

$$\frac{d(A'\Delta\nu)_{l=6.22}/dp}{d(A'\Delta\nu)_{l=3.57}/dp}=1.31,$$

which is seen to be in excellent agreement with the theoretical value of $(6.22/3.57)^{\frac{1}{2}}=1.32$. Finally, from the slopes[1,2] of Fig. 2 with $S=2.62\times10^{-2}$ cm^{-2} atmos^{-1} and $\Delta\nu=250$ cm^{-1}, it is possible to calculate $(\delta_O')_{CO}$. The result is $(\delta_O')_{CO}=0.013$ cm^{-1} atmos^{-1}. Comparison of $(\delta_F')_{CO}$ and $(\delta_O')_{CO}$ shows that the apparent rotational half-width for the first overtone is only about one-third as large as the apparent rotational half-width for the fundamental. This discrepancy may well be caused by the arbitrary choice[2] for the calculation of S, which does not necessarily lead to proportionate results for the fundamental and the first overtone of

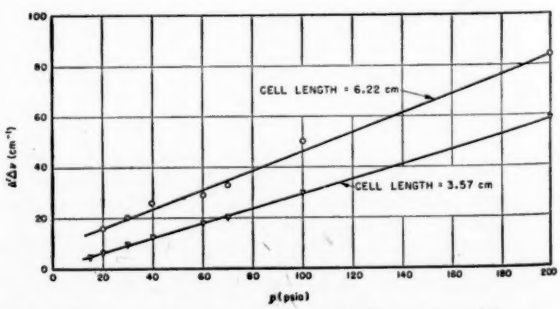

FIG. 2. Dependence of $A'\Delta\nu$ on p for the first overtone of CO.

CO if different ranges of total pressures are involved. The only safe conclusion which can be drawn is that the use of a simplified line-intensity distribution will yield correct functional forms but not necessarily valid quantitative values.

In order to obtain more realistic estimates for the rotational half-widths than are provided by calculations based on the assumptions of equally intense and equally spaced rotational lines, it is necessary to carry out numerical calculations similar to those discussed in reference 2. On the basis of the results obtained previously, it is to be expected that $(\delta_F)_{CO} \sim 0.08$ cm^{-1} atmos^{-1} and that $(\delta_O)_{CO} \sim 0.03$ cm^{-1} atmos^{-1}.

In conclusion it appears desirable to determine the over-all pressure dependence of $A'\Delta\nu$ in order to ascertain the high pressure limit above which $A'\Delta\nu$ can no longer be considered to be dependent on the square root of the product of $S\delta' p^2 l$. Reference to the plot of $\log A'\Delta\nu$ as a function of $\log p$ given in Fig. 3 shows that up to pressures of several hundred pounds per square inch the functional form $A'\Delta\nu = sp^n$ applies. Here s and n are constants. As is to be expected, n has a value close to unity at least for the data obtained in the cell 3.57 cm in length. On the other hand, the data obtained in the 6.22-cm cell are correlated by a value for n of approximately 0.82, probably because of

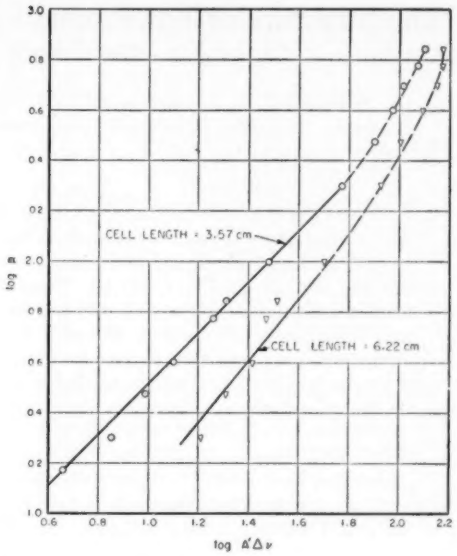

FIG. 3. Dependence of $\log A'\Delta\nu$ on $\log p$ for the first overtone of CO.

significant experimental scatter and error. From the plots of Fig. 3 it is apparent that Eq. (2) should apply for unpressurized CO up to pressures of the order of 100 psia.

The Structure of Trifluoromethyl Acetylene from the Microwave Spectrum and Electron Diffraction Pattern

J. N. Shoolery,* R. G. Shulman,† William F. Sheehan, Jr.,‡ Verner Schomaker, and Don M. Yost
Gates and Crellin Laboratories of Chemistry, California Institute of Technology, Pasadena, California

(Received July 16, 1951)

Measurements, in the microwave region, of the $J=3\rightarrow4$ rotational transitions of trifluoromethyl acetylene and several of its isotopic modifications have been made, and the moments of inertia, I_B (in a.m.u.-Å^2), have been found for the ground vibrational state: for CF_3CCH, 175.61_3, $CF_3C^{13}CH$, 177.02_4, $CF_3CC^{13}H$, 181.30_2, and for CF_3CCD, 187.46_2. Three lines corresponding to $J=3\rightarrow4$ transitions of CF_3CCH in the excited vibrational state $v_{10}=1$, and two lines corresponding to $v_{10}=2$ and $v_{10}=3$, have also been measured and interpreted according to Nielson's theory of l-type doubling in symmetric tops. From Stark effect measurements at different electric field strengths the dipole moment of CF_3CCH in the ground vibrational state has been found to be 2.36 ± 0.04 Debye units. For the ground vibrational state the microwave data lead to the following bond distances: C–H, 1.056 ± 0.005Å; C≡C, 1.201 ± 0.002A. The C–C and C–F distances were calculated from the measured moments of inertia for several assumed values of the FCF angle. Electron diffraction experiments were also made, and the intensity curves calculated for the assumed microwave models were compared with the observed visual curve. From the combination of microwave and electron diffraction results the best agreement was obtained with the following set of parameters: ∠FCF, $107.5°\pm1°$; C–C, 1.464 ± 0.02A; C–F, 1.335 ± 0.01A.

INTRODUCTION

Substituted acetylenes have long been known to show pronounced shortening of the single bond distances adjacent to the triple bonds; this has been nicely confirmed in several cases by recent microwave studies.[1–4] Fluorine compounds often show anomalous bond distances. Of interest in both these respects is trifluoromethyl acetylene, CF_3CCH, for which Anderson, Trambarulo, Sheridan, and Gordy[4] reported bond lengths C–F = 1.330A and C–C = 1.493A on the basis of measurements on two isotopic species, and on the assumption that C–H = 1.056A, C≡C = 1.207A, and ∠FCF = 109°28′. The complete structure of this molecule has now been determined in this laboratory from the combined experimental data afforded by electron diffraction results and by microwave absorption lines for four isotopic species. The acetylenic C–H and C≡C distances together with two relations between the other three parameters were evaluated directly from the microwave spectra. In this way, and for the compound studied, the electron diffraction problem was reduced to one which could be handled relatively rapidly and accurately.

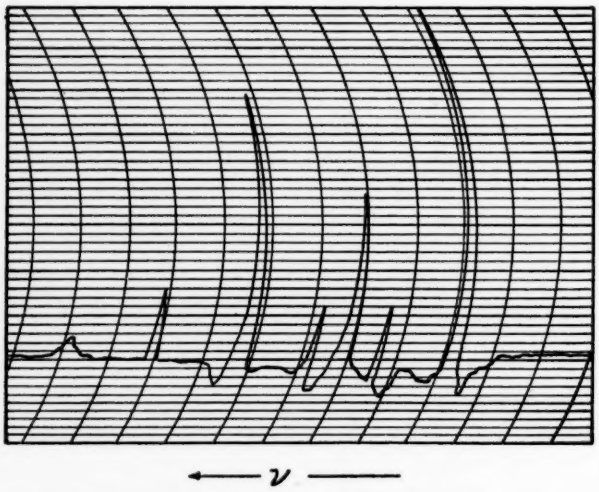

Fig. 1. Microwave absorption of CF_3CCH in the region between 22,980 and 23,200 mc.

MICROWAVE EXPERIMENTAL PROCEDURE

Since the particular microwave spectroscope used in this research has not previously been described in the literature, a few words about it are in order. Microwave energy is generated by a 2K-50 (K-band) reflex klystron; the radiation passes through a 12-foot absorption cell of X-band copper wave guide provided with an accurately centered steel Stark electrode supported by slotted Teflon strips, and the resulting 50 kc square wave modulated, absorption line envelope is preamplified and detected with a heterodyne detector. Provision is made for either oscilloscope or recording meter presentation. A slow motor drive allows frequency sweep rates of 40 mc/min. Frequencies are measured by comparing with the harmonics of a thermostated 10 mc crystal multiplied to the microwave region. The frequency markers are calibrated on the absorption lines of NH_3 gas, which is permanently sealed in a one foot long Stark modulation cell at 50 microns pressure.

A sample of trifluoromethyl acetylene, B.P. = −45°, was obtained through the good offices of Professor

* General Electric Company Swope Fellow.
† AEC Post Doctoral Fellow, 1949–1950. Present address: Hughes Aircraft Company, Culver City, California.
‡ U. S. Rubber Company Predoctoral Fellow.
[1] R. Trambarulo and W. Gordy, J. Chem. Phys. 18, 1613 (1950).
[2] A. A. Westenberg and E. B. Wilson, Jr., J. Am. Chem. Soc. 72, 199 (1950).
[3] Westenberg, Goldstein, and Wilson, Jr., J. Chem. Phys. 17, 1319 (1949).
[4] Anderson, Trambarulo, Sheridan, and Gordy, Phys. Rev. 82, 58 (1951).

A. L. Henne of Ohio State University. Isotopic molecular species, in which C^{13} is substituted for C, are present in 1.1 percent natural abundance.§ CF_3CCD was prepared by condensing several cubic centimeters of CF_3CCH vapor at S.T.P. into a tube containing one cubic centimeter of a 50 percent solution of NaOH and NaOD in D_2O. Approximately 50 percent conversion was obtained overnight.

RESULTS OF THE MICROWAVE EXPERIMENTS

Trifluoromethyl acetylene is expected to be a symmetric top similar to methyl acetylene,[1] and observation of a simple microwave spectrum indicates that this is indeed the case. The $J=3\rightarrow4$ rotational transitions of several isotopic species were found with the Stark modulated sweep spectroscope, and their frequencies were measured with the harmonic frequency standard. These are given in Table I. A recording meter trace of the absorption for the most abundant species of CF_3CCH appears in Fig. 1. Lines of the same J and different K values should appear at slightly different frequencies, but are not resolved. This results in a broadening of the lines and limits the accuracy of the frequency measurements.

TABLE I. Measured frequencies for the $J=3\rightarrow4$ transition in several isotopic species of CF_3CCH.

Species	Transition	Frequency[a] (mc/sec)
CF_3CCH	$J=3\rightarrow4$ Ground state	23,023.4
	$J=3\rightarrow4$ Excited state $v_{10}=1$ ($C-C'\equiv C''$ bending)	23,053.5 23,067.7 23,082.4
	$J=3\rightarrow4$ Excited state $v_{10}=2$	23,111.2
	$J=3\rightarrow4$ Excited state $v_{10}=3$	23,153.0
$CF_3C^{13}CH$	$J=3\rightarrow4$ Ground state	22,839.9
$CF_3CC^{13}H$	$J=3\rightarrow4$ Ground state	22,301.0
CF_3CCD	$J=3\rightarrow4$ Ground state	21,568.2

[a] Absolute frequencies were measured to ±0.3 mc and relative frequencies to ±0.1 mc.

Most of the measurements were made with the square wave amplitude set at 10 to 20 volts and with the bottom of the square wave based on ground potential. A first-order Stark effect was observed. However, the rotational transition of CF_3CCH in the ground vibrational tate was completely resolved into its four second-order Stark components by the application of 700 volts dc (1150 volts/cm) to the Stark electrode in addition to the square wave modulation. This identifies it as the $J=3\rightarrow4$ transition. The corresponding transitions in the isotopic species $CF_3C^{13}CH$ and $CF_3CC^{13}H$ were identified by their appearance near the predicted frequencies, by their possession of first-order Stark components, and by the presence of excited vibrational state absorptions at slightly higher frequencies. These excited vibrational lines can be seen clearly in Fig. 2.

§ The most abundant isotope of carbon, C^{12}, is denoted by the simple symbol C.

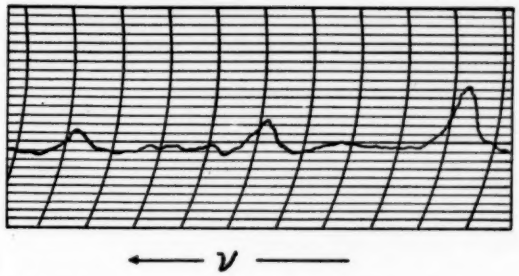

FIG. 2. Microwave absorption of $CF_3CC^{13}H$ in region between 22,280 and 22,380 mc.

From relative intensity measurements at room and dry ice temperatures (about −73°), the five lines between 23,053.5 mc and 23,152.9 mc are shown to arise from $J=3\rightarrow4$ rotational transitions in CF_3CCH molecules with the degenerate bending vibration v_{10} excited. The assignments are presented in Table I.

Rotational constants and moments of inertia for the ground vibrational state of four different isotopic species of CF_3CCH are given in Table II.

EXCITED VIBRATIONAL TRANSITIONS

Nielsen's[5] theory of l-type doubling in symmetric top molecules predicts that the $J=3\rightarrow4$ transition for molecules in the first excited degenerate bending vibrational state will consist of six closely spaced lines flanked by two lines split out at nearly equal distances on either side. A broad central line and lines 14.2 mc lower and 14.7 mc higher were actually observed. Solutions for the secular equations given by Nielsen[5] have been obtained for $J=3$ and $J=4$. Energy levels are obtained which give rise to transitions at the following frequencies:

$$\nu=8B_v-256D_J-\frac{60(B_e^2a/\omega_{10})^2}{(1-\xi)C_v-B_v};\quad K=0,\ l=\pm1$$

$$\nu=8B_v-256D_J-8D_{JK}+16(2D_J+D_{JK})\xi \pm 8B_e^2a/\omega_{10};\quad K=\pm1,\ l=\pm1$$

TABLE II. Rotational constants for various isotopic species of CF_3CCH in the ground vibrational state, from the $J=3\rightarrow4$ transition.

Species	B_0 (mc/sec)	I_B (amu-Å^2)
CF_3CCH	2877.93±0.04[a]	175.61$_3$
$CF_3C^{13}CH$	2854.99±0.04	177.02$_4$
$CF_3CC^{13}H$	2787.63±0.04	181.30$_2$
CF_3CCD	2696.02±0.04[a]	187.46$_4$

[a] These values agree, within experimental error, with those previously reported[4] for the $J=4\rightarrow5$, $6\rightarrow7$, and $8\rightarrow9$ transitions of CF_3CCH, and $J=5\rightarrow6$ and $8\rightarrow9$ transitions of CF_3CCD.

[5] H. H. Nielsen, Phys. Rev. **77**, 130 (1950).

TABLE III. Relative intensities I of $v_{10}=2$ and $v_{10}=0$ lines for CF_3CCH.

Temperature	$I(v_{10}=2)/I(v_{10}=0)$ observed	ω_{10}(calc)cm^{-1}
300°K	24/40	170
200°K	13/40	156

$$\nu=8B_v-256D_J-8D_{JK}-16(2D_J+D_{JK})\xi - \frac{24(B_e^2a/\omega_{10})^2}{(1-\xi)C_v-B_v};\quad K=\pm1,\ l=\mp1$$

$$\nu=8B_v-256D_J-32D_{JK}+32(2D_J+D_{JK})\xi + \frac{60(B_e^2a/\omega_{10})^2}{(1-\xi)C_v-B_v};\quad K=\pm2,\ l=\pm1$$

$$\nu=8B_v-256D_J-32D_{JK}-32(2D_J+D_{JK})\xi - \frac{28(B_e^2a/\omega_{10})^2}{3[(1-\xi)C_v-B_v]};\quad K=\pm2,\ l=\mp1$$

$$\nu=8B_v-256D_J-72D_{JK}+48(2D_J+D_{JK})\xi + \frac{24(B_e^2a/\omega_{10})^2}{(1-\xi)C_v-B_v};\quad K=\pm3,\ l=\pm1$$

$$\nu=8B_v-256D_J-72D_{JK}-48(2D_J+D_{JK})\xi;\quad K=\pm3,\ l=\mp1.$$

The $K=\pm1$, $l=\pm1$ transitions give rise to two absorption lines spaced 16 B_e^2a/ω_{10} mc apart. These are the two widely split lines of the l-type multiplet at 23,053.5 and 23,082.4 mc. The other six lines all fall within a one megacycle region centered at 23,067.7 mc. From this assignment B_e^2a/ω_{10} is 1.81 mc. This value was also obtained for the $J=4\rightarrow5$ and $8\rightarrow9$ rotational transitions for molecules in the same excited vibrational state by Anderson *et al.*[4] If we assume that a is 1.15, as in methyl acetylene,[1] then $\omega_{10}=176$ cm^{-1}.

Relative intensities were measured for the $v_{10}=2$ and ground vibrational lines at two different temperatures. These are given in Table III along with values calculated for ω_{10} assuming a Boltzmann distribution. The frequency of the degenerate C−C≡C bending vibration in trifluoromethyl acetylene determined in this way is in the vicinity of 170 cm^{-1}, and is in satisfactory agreement with the theoretical value 176 cm^{-1} for ω_{10}.

TABLE IV. Dipole moment μ from Stark effect measurements for $J=3\rightarrow4$ transition of CF_3CCH in ground vibrational state.

E^2(ESU/cm)^2	$\Delta\nu_{M=3}-\Delta\nu_{M=2}$ mc/sec	μ, Debye	$\Delta\nu_{M=3}-\Delta\nu_{M=1}$ mc/sec	μ, Debye
32.40	12.39	2.314	19.82	2.315
23.25	9.49	2.415	14.77	2.378
20.20	7.92	2.362	12.47	2.343
16.55	6.45	2.360	10.30	2.356
Average $\mu=2.36\pm0.04$ Debye				

STARK EFFECT MEASUREMENTS AND DIPOLE MOMENT

When the electric field in the absorption cell was increased from zero to 1700 volts/cm by the application of a dc voltage to the Stark electrode, the first-order Stark components of the $J=3\rightarrow4$ transition of CF_3CCH in the ground vibrational state could be seen to move away rapidly from the original frequency, and then second order components gradually appeared. Complete resolution of the second-order pattern was obtained at 1150 volts/cm.

The change in energy of the levels of a symmetric top molecule haveing a dipole moment μ and in an electric field E is given by[6]

$$W_{JKM}=-\mu E\frac{KM}{J(J+1)}+\frac{\mu^2E^2}{2B}\left\{\frac{\left(\frac{3K^2}{J(J+1)}-1\right)\left(\frac{3M^2}{J(J+1)}-1\right)}{(2J-1)(2J+3)}-\frac{M^2K^2}{J^3(J+1)^3}\right\}. \quad (1)$$

Since the electric field is parallel to the electric vector of the microwave radiation, the selection rule $\Delta M=0$ applies. Transitions for which only the second-order Stark effect occurs are those with either K or M equal to zero; therefore, Eq. (1) reduces to the expression for the frequency shift in a linear molecule

$$\Delta\nu=\frac{3M^2(16J^2+32J+10)-8J(J+1)^2(J+2)}{J(J+2)(2J-1)(2J+3)(2J+5)}\frac{\mu^2E^2}{h^2\nu_0} \quad (2)$$

where the transition is from $J\rightarrow J+1$, M is the spatial quantum number, ν_0 is the frequency of the rotational transition when $E=0$, and $\Delta\nu$ is the difference in frequency between ν_0 and the frequency of the Stark component. For $J=3$, $|M|=0$ and $|M|=1$, the components move to lower frequencies; and for $|M|=2$ and $|M|=3$, the components move to higher frequencies. When $M=0$, values of K should be substituted for M in equation (2). Measurements of the difference in frequency of the $M=3$ and $M=2$ components, and of the $|M|=3$ and $|M|=1$ components were made at four different field strengths. From Eq. (2) and the appropriate numerical values for ν_0 and h the expressions

$$\mu^2=14.02(\Delta\nu_{M=3}-\Delta\nu_{M=2})/E^2 \quad (3)$$

$$\mu^2=8.76(\Delta\nu_{M=3}-\Delta\nu_{M=1})/E^2 \quad (4)$$

are easily derived. Table IV gives the splittings at different field strengths and the values of μ corresponding to these measurements. The error quoted is the sum of the precision error of the measurement and the systematic error due to uncertainty in the electrode spacing.

[6] D. K. Coles, *Advances in Electronics* (1950), Vol. II, p. 310.

MICROWAVE CONTRIBUTION TO DETERMINATION OF THE MOLECULAR STRUCTURE

In a rigid molecule with a figure axis, the distance of a particular atom on the figure axis from the center of gravity of the unsubstituted molecule is given by

$$Z=\{(I_B'-I_B)(M+\Delta m)/M\Delta m\}^{\frac{1}{2}}, \quad (5)$$

where $I_B'-I_B$ is the difference in the moments of inertia for the unsubstituted molecule and one in which the particular atom has been replaced by a different isotope, M is the original molecular weight, and Δm is the increase in mass as a result of the substitution.

The total moment of inertia of the symmetric top $F_3C-C'\equiv C''-H$ may be written

$$I_B=\tfrac{3}{2}M_FX_F^2+3M_FZ_F^2+M_CZ_C^2 +M_{C'}Z_{C'}^2+M_{C''}Z_{C''}^2+M_HZ_H^2, \quad (6)$$

where X_F is the perpendicular distance of the fluorine atoms from the figure axis, and the Z's are the components of the distance of each atom from the center of mass, measured along the figure axis.

Interatomic distances were computed using the following atomic masses ($O^{16}=16.00000$): H, 1.00813; D, 2.01471; C^{12}, 12.00382; C^{13}, 13.00761; and F, 19.00450. From Eq. (5) and the data of Table II the distance from the center of mass can be calculated for the atoms C', C'', and H. The following two bond distances are immediately determined:

$$r_0(C\equiv C)=1.201\pm0.002\text{A}$$

$$r_0(C-H)=1.056\pm0.005\text{A}.$$

In estimating the limits of error, it must be remembered that Eqs. (5) and (6) hold strictly only for a rigid molecule. We have calculated average, or effective, values for the bond distances for molecules in the ground vibrational state. These effective bond distances differ by very small amounts in going from one isotopic species to another because of changes in zero point vibration frequencies. In carrying out the calculation we multiply these small uncertainties by a factor which depends upon the sensitivity of the calculation to small changes in the moments of inertia. The net result is that, even though the moments of inertia are measured with an accuracy of one part in 10^5, the interatomic distances calculated from these quantities will not retain this accuracy.

There are five structural parameters in CF_3CCH and measurements have been made for four isotopic species. If one parameter is assumed, the other four can be calculated. The C−H and C≡C distances have already been determined unequivocally; therefore, the problem is reduced to one of calculating two of the remaining three parameters for various assumed values of the third. We have chosen to assume several different values for the FCF angle and to calculate the F−C and C−C distances for each of these assumed values from equation (6) and from I_B for CF_3CCH. The results are plotted in Fig. 3. Each and every set of three parameters obtained by interesecting the two curves and the horizontal coordinate axis of Fig. 3 with a vertical line will be consistent with the measured moments of inertia for CF_3CCH.

A choice of the FCF angle can easily be made by means of electron diffraction results, if the microwave data are assumed to be correct, for there then remains only one shape parameter. It is also true that, except perhaps for the C−H distance, a complete structure determination could be accomplished by means of electron diffraction alone, but the accuracy and elegance of the determination would be decreased.

ELECTRON DIFFRACTION PROCEDURES

Photographs were taken in the apparatus described by Brockway[7] with sample-bulb temperatures of −68° to −100°. The camera distance was 10.94 cm, and the electron wavelength, calibrated by means of zinc oxide,[8] was 0.0606A. Corrections for film expansion were made.

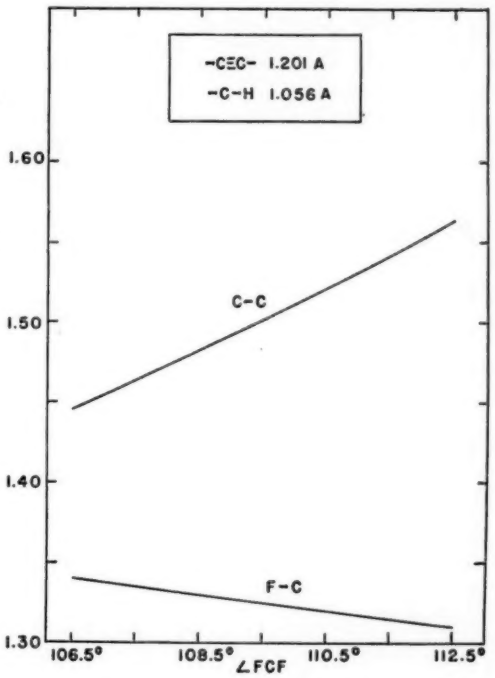

FIG. 3. Parameters of CF_3CCH from microwave spectrum.

The radial distribution curve of Fig. 4 was calculated from the equation,[9,10]

$$rD(r)=\sum_{q=1,\,2,\,\cdots}^{q_{\max}} I(q)\exp(-aq^2)\sin\frac{\pi qr}{10}$$

[7] L. O. Brockway, Revs. Modern Phys. **8**, 231 (1936).
[8] C. S. Lu and E. W. Malmberg, Rev. Sci. Instr. **14**, 271 (1943). ($a=3.2492$A, $c=5.20353$A.)
[9] R. Spurr and V. Schomaker, J. Am. Chem. Soc. **64**, 2693 (1942).
[10] Shaffer, Jr., Schomaker, and Pauling, J. Chem. Phys. **14**, 659 (1946).

by the use of punched cards.[10,11] The visual intensity curve, $I(q)$, was drawn to represent the appearance of the photographs, and the constant a was chosen to make $\exp(-aq^2)$ equal to 0.1 at q equals 100. Peaks

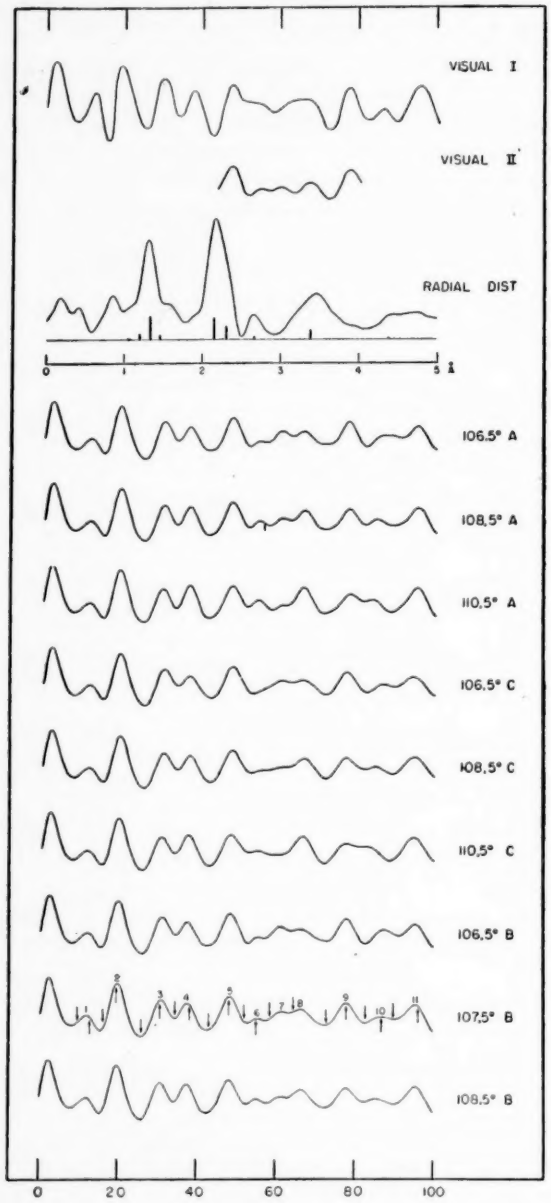

FIG. 4. Electron diffraction intensity functions and radial distribution function.

occur at 0.86A (error), 1.315A (C—F), 2.18A (F···F and C′···F), 2.66A (C···C″), and 3.46A (C″···F and error). The heavy lines below the radial distribution curve indicate distances and weights nZ_iZ_j/r_{ij} of the final model.

[11] Shaffer, Jr., Schomaker, and Pauling, J. Chem. Phys. **14**, 648 (1946).

CORRELATION OF VISUAL AND THEORETICAL INTENSITY CURVES

Intensity curves were calculated[10,11] from the equation[9]

$$I(q)=\sum_{i,j}{}' Z_iZ_jr_{ij}^{-1}\exp(-a_{ij}q^2)\sin\frac{\pi r_{ij}q}{10}$$

for models consistent with the microwave data (see Fig. 3) for FCF angles in the range 106.5°–112.5° and the three sets of a_{ij} values shown in Table V. Curves for $\angle$FCF=107.5° with further variations of a_{ij} for C′···F and C″···F were also calculated. The significant variations, however, are the ones shown in the Table for C′···F, C″···F, and F···F.

Models 110.5°A and 110.5°C are clearly unacceptable in the region of maxima 8–11 and in the relative heights of maxima, 2, 3, 4, and 5, and only models with the FCF angle less than 108.5° are acceptable if maximum 8 is to be considerably weaker than maximum 9. Since maxima 6, 7, and 8 appear to increase in intensity in the order, 6, 7, 8, models with the FCF angle less than 106.5° are unacceptable. Besides, a weak ring appears at about $q=72$ on model 106.5°A, and maximum 7 disappears in 106.5°C: two objections to 106.5° models which, however, could perhaps be overcome by careful adjustment to the temperature factors.

Maximum 10 and the neighboring minima change very rapidly with $\angle$FCF and so are very important for the choice of best value and limits of error. According to Visual I they would lead to a choice of about 108°, but it is not certain that the relative depths of the minima are just those shown: the photographs sometimes give the impression that minimum 11 is the weaker, possibly as much as would correspond to an angle of 107°. The position of maximum 10 seems to afford the most sensitive indication, the measured value (which seems to be quite precise) definitely favoring the 107.5° models over the others. In general, all the 107.5° curves calculated are in good agreement with the visual curve. The lack of agreement in the relative depths of minima 2 and 3 and of minima 6 and 7 apparently cannot be resolved by changes in the

TABLE V. Relative temperature factor coefficients, in $Å^2$.

Atom pair	$a_{ij}\cdot10^4$ Set A	Set B	Set C
CF	0.15	0.15	0.15
C′F	1.04	0.90	2.08
C″F	2.00	2.55	5.53
FF	0.68	0.68	1.04
FH	5.94	7.25	7.68
CC′	0.10	0.10	0.10
CC″	0.46	0.46	0.46
(C′C″	0.00	0.00	0.00)
CH	3.04	3.04	3.04
C′H	2.58	2.58	2.58
C″H	2.22	2.22	2.22

model and presumably arise from errors in the visual curve.[12]

Table VI shows the comparison of measured q values with those read from Curve 107.5°B. The average deviations for 106.5°B and 108.5°B are 0.0075 and 0.0074, both appreciably greater than that, 0.0057, for 107.5°B. The value 1.002 of $\langle q_{calc}/q_{obs}\rangle_{Av}$ is in excellent agreement with the microwave data. This average is satisfactorily stable with respect to changes in the weights, and, perhaps significantly, more so for 107.5°B than for any of the other curves. The parameters of the structure of trifluoromethyl acetylene, with limits of error, are given in Table VII.

ADVANTAGES OF COORDINATED STRUCTURE DETERMINATIONS

The interrelation of electron diffraction and microwave data may be expressed in terms of the intersection of a geometric surface, which defines limits of error for electron diffraction, in the N-dimensional parameter space, with the sheet of $(N-n)$ dimensions which approximately represents the freedom remaining in the choice of parameters when n moments of inertia are known from microwave spectra. On this microwave sheet, limits based on more general knowledge of molecular structures may be drawn; these limits are equally available for the electron diffraction determination. In the ideal case, the model in best agreement with the electron diffraction data lies on the microwave sheet and at the center of the electron diffraction limiting surface.

The advantage accruing from the use of electron diffraction data is the reduction of limits based on a general knowledge of molecular structure to diffraction limits of error; the advantages accruing from the use of microwave data are the usually very sharp limitation of the position of the model with respect to certain directions in parameter space, including often some corresponding to the positions of atoms which do not scatter electrons strongly. The most valuable sort of combination is one which minimizes the area of the microwave sheet included by the diffraction limit-of-error surface and the fraction of the volume bounded by this limit-of-error surface which is allowed by the microwave sheet. For particular arbitrary parameters the total range of allowed variation may be minimized under circumstances which do not correspond to this criterion. In any case, the situation for a certain molecule will not be a matter of choice unless the possibility of using only some of the accessible isotopic species is under consideration.

In trifluoromethyl acetylene there is a fortunate combination of methods. Two parameters of direct interest (C−H and C≡C), neither one well determined by electron diffraction, are accurately determined by the microwave data, and the fifth, the sole remaining one, being easily found from electron diffraction.

TABLE VI. Electron diffraction data.

Min (See Fig. 4)	Max	q(obs), Å^{-1}	q(calc)/q(obs)[a]	Min (See Fig. 4)	Max	q(obs), Å^{-1}	q(calc)/q(obs)[a]
1		9.5	(0.844)	8		64.1	(0.985)
	1	12.6	(0.942)		8	...	...
2		15.9	(0.961)	9		72.5	0.995
	2	19.2	1.019		9	77.7	1.001*
3		25.7	1.001*	10		82.4	1.003
	3	30.3	1.017		10	86.6	1.003*
4		34.17	1.002*	11		89.5	1.008
	4	37.9	0.987		11	95.8	0.995
5		42.8	0.989*	12		99.9	1.008
	5	47.8	1.009*		12	105.6	1.006
6		51.7	(1.016)				
	6	54.8	(1.008)	Average			1.002
7		58.1	(0.980)				
	7	...	...	Average deviation			0.0057

[a] Model 107.5°B. Values in parentheses were omitted from average; those with an asterisk were given double weight.

TABLE VII. Structure of trifluoromethyl acetylene.

Parameter	Value	Limits of error[a]
C−F	1.335Å	±0.01Å
C−C′	1.464Å	±0.02Å
C′≡C″	1.201Å	±0.002Å
C″−H	1.056Å	±0.005Å
∠FCF	107.5°	±1.0°

[a] The C−F, C−C′, and ∠FCF values are less certain than the C′≡C″ and C″−H values because the electron diffraction data only restrict the three related parameters of Fig. 3 to a region of parameter space, of size corresponding to the listed limits of error.

ACKNOWLEDGMENTS

The authors wish to express their gratitude to Professor Albert L. Henne of Ohio State University for generously supplying the sample of trifluoromethyl acetylene. Thanks are due also to Professors W. H. Pickering and H. V. Neher and Mr. Bart Locanthi for valuable counsel concerning electronic problems, and to Dr. Kenneth W. Hedberg for his help with the interpretation of the electron diffraction photographs. This work was supported in part by a grant from the Research Corporation, for which we are very grateful.

[12] Having inspected the theoretical intensity curves before studying the photographs, V. S. was unable to make as unbiased an interpretation as was desired, but it seems obvious to him that minimum 6 is very much deeper than shown by Visual I, which was drawn by W. S. Dr. Kenneth Hedberg, who was unacquainted with the details of the investigation, was asked to examine the photographs over the region between what we here call maxima 5 and 9. His representation (Visual II) confirms the conclusion that Visual I is in error in regard to the depths of minima 6 and 7. The concensus on the relative depths of minima 7 and 8, however, is that in this regard Visual I is more nearly correct than Visual II.

Thermodynamic Data and Some Notes on the Nature of Adsorbed Helium*

S. V. R. MASTRANGELO† AND J. G. ASTON
The Barrett Division, Allied Chemical and Dye Corporation, Philadelphia, Pennsylvania
(Received April 6, 1951)

The adsorption isotherms and heat capacities of helium on TiO_2 in the rutile crystalline form have been obtained. On the basis of the observed shift in lambda-point with coverage, the behavior of the adsorbed phase has been correlated with the behavior of the bulk liquid and solid under pressure.

I. INTRODUCTION

DATA obtained at Leiden[1a,b] on the adsorption isotherms and heat capacities of helium adsorbed on jewelers' rouge between 1.0°K and 3.0°K indicate an anomalously dense first layer with no lambda-point but with lambda-points in the higher layers. The lambda-points of the higher layers were shifted to lower temperatures by amounts decreasing with increasing coverage. The shift in the lambda-point with coverage has been attributed to a change in the surface pressure of the film.[2] This idea was extended to explain the anomalously high density of the first layer. The absence of any pronounced lambda-point in this layer and its low heat capacity[1a,b] indicate that the film is essentially solid.

Figure 1 reproduces the experimental specific heats (open circles) in cal per g of adsorbed helium obtained at Leiden[1b] for a film having 12.86 cc of liquid helium on 4430 m² of jewelers' rouge.[1b] This film is estimated to consist of three solid layers and four liquid layers. This estimate was made as follows. It has been shown that[3] the ordinary Brunauer, Emmett, and Teller[4] theory predicts the practically simultaneous completion of layers or groups of layers (one, two, or three) if each layer has an adsorption energy greater than the liquid. When there are two or more such layers, they will act like an ordinary B.E.T. monolayer. Such a "multilayer" will therefore appear to have an anomalous density if it be treated as a monolayer. The data of Frederikse[1b] shows that, between 1.3 and 2.0°K, the first ordinary B.E.T. "layer" consists of exactly three layers with solid density; this amount corresponds to 4.96 cc out of a total of 12.86 cc of liquid helium, leaving 7.90 cc of liquid helium to form four layers, with liquid density, above the three solid layers. The relative pressure of this coverage amounts to 0.82 at 2.0635°K.

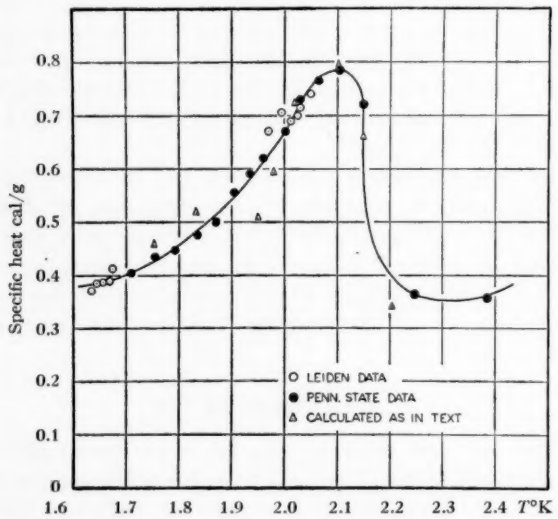

FIG. 1. Specific heat of adsorbed helium compared with liquid and solid in bulk (adsorbent: high surface area TiO_2).

On the same graph are included experimental points (filled circles) obtained on TiO_2 with surface area of 230 m²/g in this laboratory.[5] While this coverage corresponds to 17.9 cc of liquid helium on 9075 m² of surface or 8.75 cc on 4430 m², the relative pressure is 0.82 at 2.0635°K, i.e., the same as that above. However, the adsorption isotherms on this system, when treated by the modified version[3] of the Brunauer, Emmett, and Teller[4] method, indicate that only the first two layers are solid and that two-and-one-half layers are liquid, so that the coincidence of the heat capacities with those above must be fortuitous. Our data do however, indicate a definite lambda-point shift and confirm the Leiden finding that the lambda-point of the adsorbed phase is lowered.

On the same graph are also included the values of the heat capacity curves computed for an amount of helium adsorbed on jewelers' rouge corresponding to that at Leiden. These points were computed as follows. The lambda-points obtained by Frederikse[1b] were plotted as a function of coverage; and the average lambda-point for each layer was obtained, assuming that the lambda-point of the outermost layer occurs

* This research was carried out under Contract N6ONR, Task Order X, of the ONR.
† DuPont Fellow (1949–50). Partial fulfillment of degree of Doctor of Philosophy. Present address, The Barrett Division, Allied Chemical and Dye Corporation, Philadelphia, Pennsylvania.
[1a] H. P. R. Frederikse, Physica **15**, No. 10, 860 (1949).
[1b] H. P. R. Frederikse, thesis submitted in partial fulfillment of the requirements for the degree of Doctor of Philosophy at the University of Leiden.
[2] S. V. R. Mastrangelo, J. Chem. Phys. **18**, 896 (1950).
[3] J. G. Aston and S. V. R. Mastrangelo, J. Chem. Phys. **19**, 1067 (1951).
[4] Brunauer, Emmett, and Teller, J. Am. Chem. Soc. **60**, 309 (1938).
[5] These points were obtained as part of an investigation now in progress to obtain the complete thermodynamic data on such films at many different coverages.

at the maximum in the heat capacity curve of the entire film. From the data of Keesom and Keesom[6] on the specific heats of liquid helium under pressure, specific heat curves with lambda-points corresponding to those of the four liquid layers were interpolated. These four curves were used to obtain values of the total heat capacity of each of the layers at various temperatures. Regions near the lambda-points of the layer were avoided because of the uncertainty caused by the discontinuity. The values thus obtained for each of the four liquid layers and the contributions of the three solid layers obtained from data on bulk solid helium[7] (which is very small compared with the liquid) were added at each of the temperatures. The result was divided by the weight of helium to obtain the specific heat. These are the points plotted as triangles in Fig. 1.

In a preliminary way this indicates the qualitative correctness of the explanation of the anomalously dense "first" layer and the lambda-point shift. With such high surface areas, part of the adsorbed phase could be held by capillary condensation at points where small particles had aggregated. It therefore was desirable to obtain data on low surface areas where capillary condensation would be greatly reduced.

In the present investigation a sample of TiO_2 (rutile) having a surface area of 10.2 m^2/g, used previously[8] was chosen. The increased dead space correction inevitably reduced the accuracy of the results so that their significance is little more than qualitative, for reasons discussed below. However, they do show the drift in lambda-point with coverage and qualitatively verify Frederikse's results.

II. EXPERIMENTAL

The apparatus used in making this study has a cryostat with a built-in helium liquefier employing the Simon[9a,b] method of adiabatic expansion. A description of the apparatus has been given in a previous publication.[10] The sample of rutile (10.2 m^2/g) weighed 116.2 g.

The pressures above 3.5 mm were read on a manometer of diameter 12.5 mm, in a copper case with a plate glass window, using a Société Génévoise comparison cathetometer, with two telescopes equipped with micrometer eyepieces sensitive to 0.005 mm, to compare with a standard meter. The lower pressures were read on a McLeod gauge whose "capillary" had a diameter of 4 mm so that the meniscus height corrections could be made according to the data of Kistemaker.[11] This was also in a copper case with a plate glass window. The mercury levels of the McLeod gauge were read by comparison with a calibrated scale on a Goertner cathetometer with two telescopes equipped with micrometer eyepieces, sensitive to 0.01 mm. In calculating the pressure from the McLeod gauge readings, the temperature of all parts of the system was carefully taken into account.

TABLE I. Specific heats of helium films (rutile) (surface area 10.2 m^2 per g).

T°K	Coverage g He	Specific heat cal/g	Calculated cal/g
A. 0.956 cc/m^2 at S.T.P. at 1.841°K			
1.740	0.208	0.37	0.40
1.793	0.205	0.51	0.54
1.922	0.197	0.41	0.23
2.035	0.191	0.39	0.20
2.155	0.184	0.36	0.21
2.255	0.178	0.36	0.22
2.364	0.172	0.39	0.23
B. 1.157 cc/m^2 at S.T.P. at 1.865°K			
1.973	0.235	0.60	0.50
2.033	0.228	0.48	0.27
2.096	0.220	0.46	0.27
C. 1.362 cc/m^2 at S.T.P. at 1.927°K			
1.799	0.306	0.52	0.50
1.855	0.299	0.57	0.57
1.927	0.288	0.67	0.61
2.007	0.276	0.73	0.72
2.094	0.261	0.63	0.42
2.179	0.250	0.60	0.26
2.286	0.235	0.61	0.25
2.421	0.209	0.55	0.26

The temperatures are based on the 1937 vapor pressure scale[12] of liquid helium above 1.6°K. No measurements were obtained below this temperature. A constantan thermometer was calibrated against the helium vapor pressures during each run at several temperatures, and the linear relationship obtained between temperature and resistance was used to obtain interpolated temperatures. To our surprise, the resistance thermometer maintained its calibration at the normal boiling point of helium within 0.004° in spite of warming many times to room temperature over a period of several months, during which time about 15 runs were made.

The corrections for both the thermal and mass effect of evaporation into the dead space of the system were made using the virial coefficients calculated by de Boer and Michels[13] according to the equation given by Bleaney and Simon.[14] The variation of mass of adsorbed helium with temperature and coverage is shown in column 2 of Table I. Thermomolecular pressure corrections were made according to the data of Weber and Schmidt,[15] and a second-order correction for the volume of the adsorbed phase in the calorimeter dead

[6] W. H. Keesom and A. P. Keesom, Comm. Leiden, No. 235d.
[7] W. H. Keesom and A. P. Keesom, Comm. Leiden, No. 240b.
[8] J. A. Morrison and G. J. Szasz, J. Chem. Phys. **16**, 280 (1948).
[9a] F. Simon, Z. ges. Kälte-Ind. **39**, 816 (1933).
[9b] F. Simon, Physik. Z. **34**, 232 (1933).
[10] Aston, Metlay, and Mastrangelo, Rev. Sci. Instr., submitted for publication.
[11] J. Kistemaker, Comm. Leiden, No. 268d.
[12] W. H. Keesom, *Helium* (Elsevior Publishing Company, Inc., New York, 1942), p. 196.
[13] J. de Boer and A. Michels, Physica 's Grav. **6**, 409 (1939).
[14] B. Bleaney and F. Simon, Trans. Faraday Soc. **35**, No. 221, Part 9, 1205 (1939).
[15] S. Weber and G. Schmidt, Comm. Leiden, No. 246c.

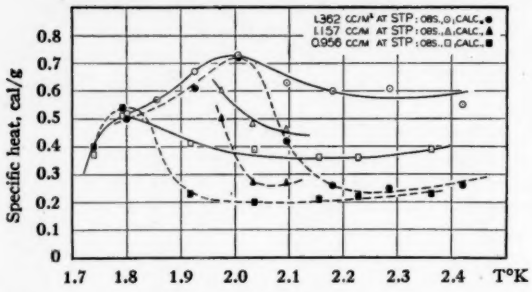

FIG. 2. Specific heat of adsorbed helium compared with liquid and solid in bulk (adsorbent: low surface area TiO_2).

space was made according to the data of Keesom and Keesom.[16a,b]

The experimental technique used is essentially that of Morrison and Szasz.[8]

III. RESULTS

The results of the heat capacity data uncorrected to constant coverage are shown in Table I. Column 1 gives the temperature, column 2 the amount of helium on the titanium dioxide at this temperature, and column 3 the specific heat. Figure 2 shows the same specific heat data, uncorrected to constant coverage, plotted against the temperature. The tabulated data have been corrected for evaporation of helium into the dead spaces and for the heat capacity of the calorimeter filled with gas at the corresponding temperatures and pressures. Certain points on the 1.157 cc/m² at S.T.P. coverage have been omitted because of abnormal drifts and small rises observed in the lower region and uncertainty in the isosteric heats used in correcting the points in the higher temperature region for evaporation of helium into the dead spaces. These isosteric heats were obtained from our own isotherms. The values calculated at 2.41°K are shown in Table II.

In the last column of Table III are given values computed as for the high surface area TiO_2 for the coverages shown in the second column which were computed from the equilibrium pressures and temperatures along with the dead space volumes and the total helium in the system. The points are shown by crosses in Fig. 2. The shape of the experimental curves constitutes a semiquantitative agreement with the conclusion reached from the results obtained at Leiden[1a,b] and on high surface area TiO_2 in this laboratory that there is a shift in the lambda-point of the adsorbed phase. The agreement of the calculated heat capacities with experimental ones, although poor at the higher temperatures, in no way conflicts with the idea that the shift in lambda-point is a result of the increased density resulting from some sort of pressure effect in the film.

TABLE II. Isosteric heat of adsorption for helium on TiO_2, 10.2 m²/g at 2.41°K.

Coverage cc/m² at S.T.P.	Isosteric heat cal/mole
0.757	28.6
0.800	27.9
0.841	27.5
0.886	27.1
0.927	25.7
0.971	24.0
1.021	23.9
1.052	23.6
1.093	24.0
1.138	24.4
1.178	24.6
1.220	24.6
1.262	24.6

The position of the lambda-point of each layer could also be determined by means of the equilibrium pressures observed during the heat capacity measurements. Plots were made of the log of the equilibrium pressure against the reciprocal of the temperature for the systems having a *constant number of moles* of helium distributed between the adsorbent and calorimeter dead space and filling line; i.e., the data are not corrected to constant coverage. Each consists of two straight lines which intersect at the lambda-point of the film as shown in Fig. 3 for the 1.157 coverage. The intersection of the lines for each coverage agrees with the position of the peak in the heat capacity curve and serves to check these data.

Because they are not constant coverage, these curves have no actual significance. The curves can be corrected to constant coverage as follows.

Let $P=P(T, V_s)$, where P is the equilibrium pressure, T is the equilibrium temperature, and V_s is the coverage in cc at S.T.P. Then, we have

$$d\ln P/d(1/T)=[\partial \ln P/\partial(1/T)]_{V_s} + (\partial \ln P/\partial V_s)_T dV_s/d(1/T), \quad (1)$$

where $d\ln P/d(1/T)$ is the slope of the curve uncorrected to constant coverage, $[\partial \ln P/\partial(1/T)]_{V_s}$ is the slope of the curve corrected to constant coverage, $(\partial \ln P/\partial V_s)_T$ is the slope of the reduced pressure isotherm at temperature T and coverage V_s, and $dV_s/d(1/T)$ is the slope of the curve of V_s plotted against $1/T$. In order to compute $[\partial \ln P/\partial(1/T)]_{V_s}$, it is necessary to obtain values for the other terms. The value at $dV_s/d(1/T)$ was found to be constant below and above the lambda-point of the film with the discontinuity where the two straight lines intersected, $(\partial \ln P/\partial V_s)_T$ was obtained from our isotherm at 2.41°K, and this was assumed to be constant. This assumption is valid only if the reduced pressure isotherms do not change shape with temperature and is therefore an approximation with only qualitative justification. The value of $d\ln P/d(1/T)$ was obtained, of course, from the slope of the curves uncorrected for constant coverage shown by the open circles in Fig. 3. The dashed curve shown in Fig. 3 is the curve cor-

[16a] W. H. Keesom and A. P. Keesom, Proc. Roy. Acad. Amsterdam **36**, 483 (1933).
[16b] W. H. Keesom and A. P. Keesom, Proc. Roy. Acad. Amsterdam **36**, 612 (1933).

rected to constant coverage by the above method. The break in this curve could easily be a result of the inaccuracies in the method of correction and may be no more evident in the properly corrected isotherms for helium on this sample of TiO_2, on jewelers' rouge at Leiden[1b] or on high surface area TiO_2 in this laboratory than for bulk helium. The breaks in the uncorrected curve are then due to the difference in the equilibrium pressure relations of the adsorbed helium on either side of the lambda-point as they affect the correction with this particular dead space.

The isotherm at 2.41°K has been obtained with a total of about 35 points. The curve is shown in Fig. 4 and the data are listed in Table II. The surface area was obtained from a nitrogen isotherm at the normal boiling point[8] using the B.E.T.[4] theory. The helium isotherm shows two inflections, a weak one at a point at about 3 mm agreeing with the completion of the first B.E.T. layer for helium to within the experimental accuracy of 0.5 percent. It would seem, from this, that the B.E.T. theory yields the correct point of completion of the first layer and hence that the surface area determined using nitrogen is correct. The density of this layer is $V_s=0.62$ cc/m² at S.T.P.

Another inflection occurs at $V_s=0.94$ cc/m² at S.T.P. The second inflection probably indicates the beginning of a third layer. It should be emphasized that to draw any other curve without the inflection places about six points off the curve by ten times our experimental error. The difference between the two values of V_s is 0.32 cc/m² at S.T.P. This is the density of the second layer and, according to the data of Keesom and Keesom,[9a,b] corresponds to the He—He spacing in the liquid when it is subjected to a pressure of 25 atmospheres. The surface pressure calculated by the lambda-point shift and the P, T phase diagram of liquid helium is also 25 atmospheres for this layer.

The density of the first layer, $V_s=0.62$ cc/m² at S.T.P., is anomalously high and, if it is a single layer, would correspond to the solid under a pressure of several hundred atmospheres. Anomalous values of the density of the first layer have also been obtained by other investigators. A summary of these is given by Frederikse and Gorter.[17]

This anomalous density is taken to indicate the formation of solid multilayers as discussed above.

IV. DISCUSSION OF RESULTS

A plot of the pressure on bulk He II to produce the observed shift in the lambda-point was made against coverage. The difference between the pressure acting on the second and on the third layers, based on the shift in λ-point, was thus found to be −1.3 atmospheres. The formation of the third layer begins in the region of the second inflection in the isotherm. The inflection can then be ascribed to this change of pressure on the layers of −1.3 atmospheres over a range in equilibrium pressure of 10.00 mm.

[17] H. P. R. Frederikse and C. J. Gorter, Physica **16**, 403 (1950).

TABLE III. The isotherm of helium on titanium dioxide at 2.41°K.

P corrected mm of Hg	Temperature correction (percent)	Thermomolecular pressure correction (percent)	V_s cc at S.T.P.
	April 17, 1950, points—circles		
0.2	0	11.0	475.7
2.48	0	8.70	704.8
7.49	0.14	2.30	824.0
15.61	0.58	1.00	945.2
23.83	0.09	0.50	1048.8
33.24	2.04	0.25	1162.1
48.63	1.51	0	1496.9
	April 26, 1950, points—triangles		
3.39	0	6.20	753.3
9.39	0	2.3	853.2
12.79	0	1.30	903.4
22.12	0	0.50	1021.8
33.23	0.4	0.10	1254.2
60.35	0.6	0	2122.9
63.26	0.7	0	2721.9
	May 25, 1950, points—shaded half-circles		
5.28	0	3.30	783.1
7.40	0	2.30	823.7
	May 31, 1950, points—squares		
5.37	0	3.40	773.5
13.88	0	1.20	912.6
24.75	0	0.50	1049.6
28.33	0	0.35	1095.7
31.23	0	0.25	1123.1
33.12	0	0.15	1165.9
34.45	0	0.10	1203.7
36.72	0	0.07	1237.6
39.57	0	0.03	1290.8
42.76	0	0.01	1345.4
45.36	0	0	1411.8
47.86	0	0	1475.6
50.30	0	0	1543.9
59.63	0	0	2016.0
62.40	0	0	2580.6
	October 17, 1950, points—squares open at bottom		
31.21	0	0.25	1132.6
32.56	0	0.17	1168.4
33.67	0	0.11	1181.4

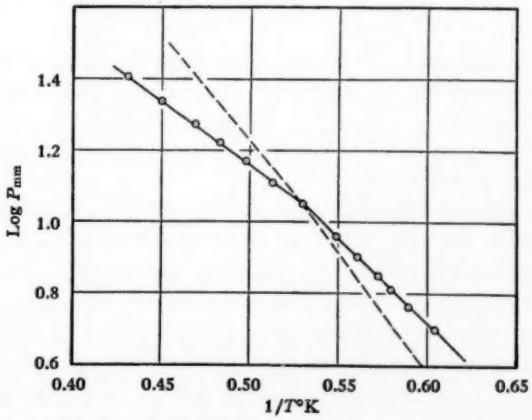

FIG. 3. Log of equilibrium *versus* reciprocal temperature in °K at 1.157 cc/m² at S.T.P.

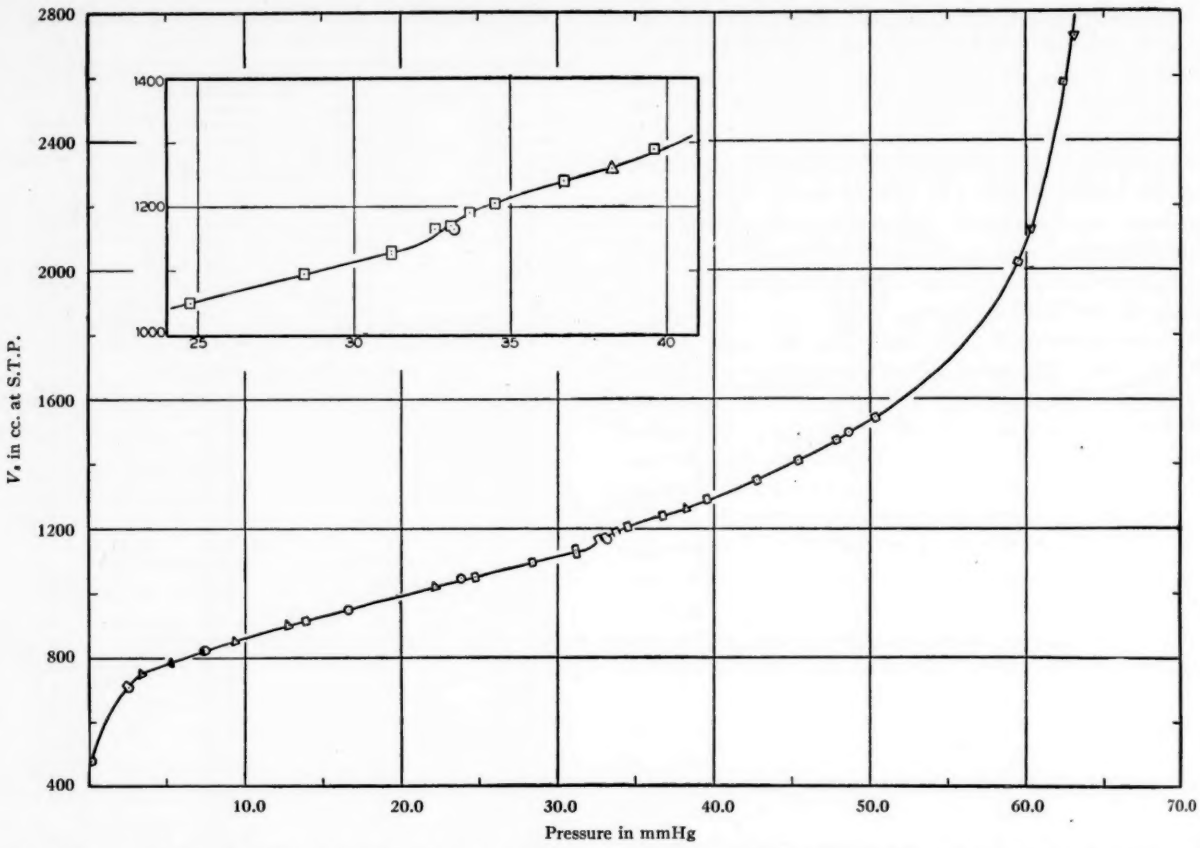

FIG. 4. Isotherm of helium on TiO_2 at 2.41°K. Circles: April 17, 1950. Triangles: April 26, 1950. Shaded half-circles: May 25, 1950. Squares: May 31, 1950. Squares open at bottom: October 17, 1950.

The isotherm is reasonably straight for about 15-mm change in equilibrium pressure below and 5 mm above the second inflection and has about the same slope. It is therefore reasonable to assume that

$$(\partial P/\partial V_s)_{\rho_s} = \text{constant}, \tag{2}$$

where P is the equilibrium pressure of helium, V_s is the coverage, and ρ_s is the surface density of the film. Let $P=P(V_s, \rho_s)$; then, we have

$$\delta P = (\partial P/\partial V_s)_{\rho_s}\delta V_s + (\partial P/\partial \rho_s)_{V_s}\delta\rho_s, \tag{3}$$

where $(\partial P/\partial V_s)_{\rho_s}$ is the reciprocal of the slope of the isotherm which is constant in the region of the second inflection according to Eq. (2) and $(\partial P/\partial \rho_s)_{V_s}\delta\rho_s$ is the change in equilibrium pressure caused by a change in surface density of $\delta\rho_s$.

It proved difficult to calculate $(\partial P/\partial \rho_s)_{V_s}$ alone; however, $(\partial P/\partial \rho_s)\delta P_s$ was obtained over the region of the second inflection by substituting in Eq. (3) the total change in equilibrium pressure, P, for an increment of gas adsorbed over this region and using the slope of the isotherm to calculate $(\partial P/\partial V_s)_{\rho_s}$. For this computation δV_s was taken as 167 cc at S.T.P. and the total change in pressure δP is then 10.00 mm for this increment of gas. The slope of the isotherm is 11.5 cc per mm and $(\partial P/\partial V_s)_{\rho_s}=0.087$ mm per cc. Substituting these quantities in Eq. (3), the value obtained for $(\partial P/\partial \rho_s)_{V_s}\delta\rho_s$ is -4.6 mm.

In order to calculate the change in surface pressure necessary to cause this change in equilibrium pressure of -4.6 mm, the Gibbs equation

$$d\gamma = 1/\sigma RT d\ln P \tag{4}$$

was used with the relationship

$$P' = n\gamma, \tag{5}$$

where P' is the three-dimensional analog of the surface pressure and corresponds to the pressure causing the shift in the lambda-point, n is the number of surface layers per centimeter depth of film, $d\gamma$ is the change in surface tension in dynes per centimeter caused by a change in the logarithm of the equilibrium pressure, P, and σ the molar surface area of the film in square centimeters. Using Eq. (4), the change in γ caused by a change in equilibrium pressure of -4.6 mm is -4.75×10^{-2} dyne/cm, and, assuming hexagonal packing in the liquid, $n=3\times10^7$ layers/cm, as calculated from the density of the second layer. The value calculated for $\Delta P'$ by Eq. (5) is -1.42×10^6 dynes/cm^2 or -1.4 atmospheres. Thus, a change in equilibrium pressure

of -1.4 atmospheres. Naturally, the value for $\Delta P'$ calculated using the formula for the change in vapor pressure with applied pressure,

$$dP/dP' = V'/V \tag{6}$$

(where P is the equilibrium pressure above a liquid on which a pressure P' is exerted, while V and V' are, respectively, the molar volumes of vapor and liquid), is also -1.40 atmospheres. This is obvious, since Eq. (4) is the two-dimensional analog of Eq. (6). Both of these values are in excellent agreement with the value of -1.3 atmospheres calculated from the shift in lambda-point of bulk helium. The inflection in the isotherm appears, therefore, as a result of a rather abrupt change in surface density on going from the second to the third layer as calculated by means of the lambda-point shift.

This last result is given as evidence for the contention that the first few layers tend to complete themselves before starting to build new layers. It assumes that the effective density of the film is equal to that of the completed films. This means that the film consists largely of regions of the surface completely filled as predicted by Halsey.[18]

ACKNOWLEDGMENT

The authors are indebted to Mr. R. J. Tykodi for his collaboration in the determination of the heat capacities of helium adsorbed on the high surface area TiO_2.

[18] G. Halsey, J. Chem. Phys. **16**, 931 (1948).

THE JOURNAL OF CHEMICAL PHYSICS VOLUME 19, NUMBER 11 NOVEMBER, 1951

I. Normal Frequencies of a One-Dimensional Crystal. II. An Approximation to the Lattice Frequency Distribution in Isotropic Solids

J. O. HALFORD

Chemistry Department, University of Michigan, Ann Arbor, Michigan

(Received March 19, 1951)

I. The accurate expression for the individual frequencies of a linear crystal of any number of particles is derived.

II. It is shown that, for an isotropic three-dimensional array of uniform masses, the root-mean-square frequency is easily evaluated and the maximum square must always be less, but not much less, than twice the mean square. For two commonly studied simple cubic systems, the maximum square is evaluated and shown to be twice the mean square. The Debye expression for the frequencies in terms of standing wave components is modified empirically to give the correct maximum and mean squares by substituting linear crystal frequencies for the components and introducing a second force constant.

The resulting expression, a simplified form of the factored secular equation, should yield a more realistic and probably therefore a more widely useful distribution function than the Debye equation.

I.

IN connection with the normal frequency distribution in solids, it has proved to be useful and instructive to examine the frequencies of a so-called one-dimensional crystal. This has been done by Born and von Kármán[1] and is discussed by Mayer and Mayer.[2] For N point masses m with a restoring force k for unit relative displacement of neighbors, the nth normal frequency is given by the equation

$$\nu_n = (k/\pi^2 m)^{\frac{1}{2}} \sin[n\pi/2(N-1)]; \quad (1 \leqslant n \leqslant N-2). \tag{1}$$

Since the equation expresses $N-2$ frequencies for a model which must have $N-1$ vibrations, the result is an approximation which is claimed to approach accuracy only for large values of N.

The accurate solution, with this restriction removed, is readily obtained. As might be expected, the correction, for large N, is negligible; but the effect of the approximation is exactly evaluated, and the new result is valid for all N down to the diatomic molecule and may find application in future studies of limited chains of particles.

For the model, as described, the kinetic energy is $m\sum\dot{X}_i^2/2$ and the potential energy is $k\sum(X_i - X_{i-1})^2/2$. With the substitution, $u(=4\pi^2\nu^2 m/k)-2$, the secular equation takes the form

$$D_N \equiv \begin{vmatrix} u+1 & 1 & & & & & \\ 1 & u & 1 & & & & \\ & 1 & u & 1 & & & \\ & & 1 & u & 1 & & \\ & & & 1 & u & 1 & \\ & & & & 1 & u+1 \end{vmatrix}_N = 0, \tag{2}$$

with N denoting the number of rows or columns in the determinant.

[1] M. Born and Th. von Kármán, Physik. Z. **13**, 297 (1912).

[2] J. E. Mayer and M. G. Mayer, *Statistical Mechanics* (John Wiley and Sons, Inc., New York, 1946), p. 248.

The translation, $u+2=0$, can be factored out. Let E_N be defined as

$$E_N \equiv \begin{vmatrix} u & 1 & & & & & \\ 1 & u & 1 & & & & \\ & 1 & u & 1 & & & \\ & & 1 & u & 1 & & \\ & & & 1 & u & 1 & \\ & & & & 1 & u & \end{vmatrix}_N . \tag{3}$$

Then, by means of expansion by minors, we obtain

$$\begin{aligned} D_N &= (u+1)^2 E_{N-2} - 2(u+1)E_{N-3} + E_{N-4} \\ &= (u^2+2u)E_{N-2} - (u+2)E_{N-3} = (u+2)E_{N-1}. \end{aligned} \tag{4}$$

From Eq. (4) it is seen that the normal frequencies for the N-particle chain are the roots of the equation $E_{N-1}=0$. To factor this equation it is assumed that Eq. (1) has the correct form except that the angle may be wrong. The frequency is then taken to be $(k/\pi^2 m)^{\frac{1}{2}} \sin\theta/2$, so that $(4\pi^2\nu^2 m/k)-2=-2(1-2\sin^2\theta/2)$, leading to the substitution $u=-2\cos\theta$.

For $N=2$, $E_1=-2\cos\theta=-\sin 2\theta/\sin\theta$, and, for $N=3$, $E_2=4\cos^2\theta-1=\sin 3\theta/\sin\theta$. Now, through expansion by minors,

$$\begin{aligned} \sin\theta E_3 &= -2\cos\theta \sin 3\theta + \sin 2\theta \\ &= -2\cos\theta \sin 3\theta + \sin 3\theta \cos\theta - \cos 3\theta \sin\theta \\ &= -\sin 3\theta \cos\theta - \cos 3\theta \sin\theta = -\sin 4\theta \end{aligned}$$

and

$$\begin{aligned} \sin\theta E_4 &= 2\cos\theta \sin 4\theta - \sin 3\theta \\ &= 2\cos\theta \sin 4\theta - \sin 4\theta \cos\theta + \cos 4\theta \sin\theta \\ &= \sin 4\theta \cos\theta + \cos 4\theta \sin\theta = \sin 5\theta. \end{aligned} \tag{5}$$

Since this operation can be extended indefinitely with increasing values of N, the general secular equation for the internal motions takes the form, for N particles,

$$E_{N-1} = (-1)^{N-1} \sin N\theta/\sin\theta = 0. \tag{6}$$

As an alternative, it is readily shown that if $E_{N-1} = \pm\sin N\theta/\sin\theta$ and $E_N = \mp\sin(N+1)\theta/\sin\theta$, then $E_{N+1} = \pm\sin(N+2)\theta/\sin\theta$, which, in conjunction with the known values of E_1 and E_2, leads to the same conclusion.

Equation (6) is satisfied when $\sin N\theta=0$ and $\sin\theta\neq 0$, for which the condition is that $\theta=n\pi/N$, where n must not be zero nor a multiple of N. Although the number of such angles is infinite, they yield only $N-1$ values of u, which lie between -2 and $+2$ and are all encountered in the range $0<\theta<\pi$, for which $1\leqslant n\leqslant N-1$. Since the secular equation $E_{N-1}=0$ can have only $N-1$ roots, there are no other values of u, real or imaginary, which will satisfy it. It follows from the definition of θ that the nth frequency is

$$\nu_n = (k/\pi^2 m)^{\frac{1}{2}} \sin(n\pi/2N). \tag{7}$$

Evidently, the approximation involved in deriving Eq. (1), namely, the arbitrary restriction of the terminal masses to zero amplitude, has given an equation for the N-particle chain which is actually correct for $N-1$ particles. In the same way, if, instead of factoring out the translation, the end corrections of Eq. (2) had been neglected by replacing each element $u+1$ by u, the resulting frequency distribution would be correct for $N+1$ instead of N particles. Since, for N sufficiently large, the distribution function is independent of the chain length, it is evident that under this condition the end corrections are negligible. It is reasonable, then, to assume that they will also be negligible in two- and three-dimensional systems.

In deriving Eq. (7), no end corrections have been neglected, nor have any approximations other than those implied in the potential energy function been introduced. Consequently, Eq. (7) must yield correctly the frequency of a symmetrical diatomic molecule, for which $n=1$ and $N=2$. The frequency becomes $\nu=(k/\pi^2 m)^{\frac{1}{2}} \sin\pi/4$ or $(1/2\pi)(2k/m)^{\frac{1}{2}}$, which is the familiar expression for this case. By Eq. (1), as well as by inspection, this is also the frequency for a single mass m connected to two fixed points by bonds of force constant k.

II.

In solving for the distribution of lattice frequencies in a solid, it is necessary to work with a particular model involving a defined distribution of atoms and an assumed potential energy function. The formidable features of the derivation may lead to approximations which widen the gap between the model and physical reality.

When the problem has been solved for a particular model, it is of interest to ask if the result is applicable to other models as well, that is, if the distributions of a representative set of models are similar enough to permit the substitution of one for another. To obtain an adequate number of derived distributions to resolve this question appears at present to be too difficult, but the general usefulness of a particular distribution can be judged by the number and variety of solid substances for which the thermal properties can be calculated successfully.

Frequency distributions, or partial descriptions of the distribution, have been proposed by Debye,[3] Born and von Kármán,[1] Blackman,[4] Houston,[5] Leighton,[6] Montroll,[7] and others. Of these, the relatively simple Debye description has been most widely tested and used. The Debye theory stands out from the others because of the highly simplified model, an isotropic continuum which can represent reality only in the limit for very low frequencies. Since the Debye distribution cannot

[3] P. P. Debye, Ann. Physik **39**, 789 (1912).
[4] M. Blackman, Proc. Roy. Soc. (London) **A159**, 416 (1937).
[5] W. V. Houston, Revs. Modern Phys. **20**, 161 (1948).
[6] R. B. Leighton, Revs. Modern Phys. **20**, 165 (1948).
[7] E. W. Montroll, J. Chem. Phys. **15**, 575 (1947).

be accurate in the higher frequency range, the use of his equations to predict thermal properties at higher temperatures must be regarded as empirical. Each of the other distributions is likewise a property of a particular model. Most of the available distributions are incomplete because of difficulties of computation, but the application of a complete accurate one to the prediction of thermal properties of other models would, like the Debye theory, have to be made upon an empirical basis.

It would seem, therefore, that, for success in predicting thermal properties, it makes little difference whether the distribution is merely set down empirically or is arrived at in some more elegant and complicated fashion. In either case, a proposal that the function is generally usable must be validated empirically.

That the frequency distribution, for the calculation of thermal properties, does not have to be accurate throughout the range is evident from the success of the Debye theory in predicting the entire heat capacity curve for some simple crystals with fair accuracy in spite of the unreal model upon which the theory is based.

It is further evident, from the Einstein function, the Nernst-Lindemann equation, and the recent calculations of Raman[8] and his collaborators, that considerable success is possible even with a severely oversimplified function. The sensitivity of the thermal properties to the frequency distribution has been analyzed in detail by Katz.[9]

The present purpose is to modify the Debye distribution empirically in the direction indicated by the study of more realistic models than the Debye continuum. To effect an improvement, it is necessary only to make changes in the right directions and clearly unnecessary to include specific features of any particular distribution, such as, for example, the "infinities" of the Montroll function.

For a cubic Debye model, three sets of standing waves which can be set up parallel to the edges of the cube are recognized. The propagation vector of a characteristic standing wave of the model is taken to be the sum of three component propagation vectors, one taken from each of the sets parallel to the edges. The components are combined in all possible ways. Since the propagation vector is proportional to the frequency, the characteristic frequencies can be expressed by the vector summation

$$\nu^2=\nu_x^2+\nu_y^2+\nu_z^2, \tag{8}$$

in which ν_x, etc., are the frequencies of the component standing waves. Equation (8) defines spherical surfaces of constant frequency and sets the number of frequencies between ν and $\nu+d\nu$ proportional to the volume of a spherical shell of radius ν. If this proportionality is assumed to persist all the way to an arbitrarily imposed maximum frequency ν_0, the distribution function z becomes

$$z=9N\nu^2d\nu/\nu_0^3, \tag{9}$$

which is the original Debye relation, used subsequently without change in most published discussions.

In this form, however, the function does not properly represent the model. The assumption of a maximum frequency requires, for the vector additions, that each component be limited to a maximum value. All of the vectors of Eq. (8) must then terminate within a cube and the number of frequencies in the interval ν to $\nu+d\nu$ will be proportional to the part of the area of a spherical shell which lies within the cube. Equation (9) can be valid only for frequencies less than the maximum component. The distribution function should contain two discontinuities, at $(\frac{1}{3})^{\frac{1}{2}}\nu_0$ and $(\frac{2}{3})^{\frac{1}{2}}\nu_0$, with the function diminishing to zero at the maximum frequency. These features have been discussed in detail by Slater,[10] along with related interpretations. It is surprising that they have been rather generally ignored in publications of later date than Slater's discussion.

The use of the simple Debye distribution over the whole range sets the mean frequency too high by neglecting the discontinuities and consequently including a large number of extraneous high frequencies. The well-known success of the function in certain cases must then mean that at least one compensating factor has been included which tends to lower the mean frequency. The nature of this second factor can be inferred from a comparison of the linear crystal distribution with that of a continuous rod. In the continuous one-dimensional model, the standing wave frequencies are equally spaced, with the numerical mean at half the maximum and the root mean square at $\nu(\max)/\sqrt{3}$. In the linear crystal, by Eq. (7), for each frequency proportional to $\sin(n\pi/2N)$ there is always another proportional to $\sin[(N-n)\pi/2N]$ or $\cos(n\pi/2N)$, unless $n=N/2$, which is trivial. The sum of the squares of these two frequencies is the square of the maximum frequency, the mean square is half the maximum square, and the root mean square is $\nu(\max)/\sqrt{2}$, showing that the mean frequency of the continuous model is too low. This property will certainly appear in the continuous two- or three-dimensional model, at least to some degree, and will account qualitatively for a cancellation of inadequacies in the Debye distribution in favorable cases.

In deference to the considerable success of the Debye equation, it seems to be in order to retain the form of Eq. (8), but to attempt to find a set of components ν_x, etc., which will give a more realistic mean frequency. Equation (8) represents a factored form of the secular equation which is undoubtedly severely oversimplified, since in certain cases the secular equation has been reduced to a cubic in ν^2 which is not readily factored

[8] C. V. Raman and others, J. Indian Acad. Sci. **A14** (1941); A15 (1942).

[9] E. Katz, J. Chem. Phys. **19**, 488 (1951).

[10] J. C. Slater, *Introduction to Chemical Physics* (McGraw-Hill Book Company, Inc., New York, 1939), pp. 225 *ff*.

in any general way to give the individual frequencies explicitly. It could still be true, however, that Eq. (8) with the right set of components would give a distribution which could be used for more than one model.

At this point, it will be useful to examine the secular equation for an isotropic array of uniform masses. In any such array, if end corrections are neglected, each particle is symmetrically surrounded by neighbors, and the restoring force for unit displacement of a single particle when the entire model is motionless will be independent of the direction of the displacement. With any specified potential energy function and any chosen cartesian coordinates, the secular determinant must contain the unknown squared frequency in a uniform element which appears at every point on the principal diagonal. For any reasonable potential energy function, it should always be easy to express this diagonal element. All other elements of the determinant will be potential constants. If every element is divided by the principal force constant k, the diagonal element will be $u=(4\pi^2\nu^2 m/k)-A$, in which A is a dimensionless quantity made up of the sum of ratios of potential constants. The secular equation has the degree $n=3N$ for N particles and the first term in the polynomial form is u^n. There can be no term in u^{n-1}, however, since in a term by term expansion it is not permissible to accept at any time two elements from the same row or column and the selection of u, $(n-1)$ times, blocks out all elements except the remaining u.

As a consequence the sum of the roots u_i is zero, the mean value of $\lambda_i'(4\pi^2\nu_i^2 m/k)$ is A and the average squared frequency is $kA/4\pi^2 m$. This evidently gives the frequency with which a single particle would vibrate if the rest of the model was motionless.

There are some models in which it is possible to vibrate all the particles simultaneously in this same manner against the same set of forces. If the displacement has a component directed toward a neighbor, the neighbor will have a like component directed back toward the particle. If, however, there is no component toward a particular neighbor, the two can move in the same direction. Evidently, all the relative displacements are twice as large as they were when the particle was moving alone, and the restoring force must also have been doubled for unit displacement of the particle. Consequently, the squared frequency of the general motion is twice that of the individual particle which has been evaluated from the diagonal element. For such models, then, the squared maximum frequency is twice the numerical mean square.

Two simple cubic models which have been studied extensively fulfill this condition. In Houston's[5] model, a unit relative displacement of neighbors along their line of centers is resisted by a force k, while a displacement perpendicular to the connecting line sets up a force $k\alpha$, where α is a fraction. The two squared frequencies, by inspection, are $\lambda'(\text{mean})=2+4\alpha$ and $\lambda'(\text{max})=4+8\alpha$. Each row of particles, at the maximum frequency, executes the highest frequency motion of the linear crystal, but any two neighboring rows are always out of phase. For the central force model introduced by Born and von Kármán[1] and used by Blackman[4] and Montroll,[7] a restoring force k is assigned to the unit displacement toward a nearest neighbor, and a force $k\alpha$ to the displacement toward a second neighbor across the diagonal of a square. Here again, by inspection, the squared frequencies are $\lambda'(\text{mean})=2+4\alpha$ and $\lambda'(\text{max})=4+8\alpha$; but, for motion parallel to an edge of the cubical model, while each row again executes the motion of maximum frequency of the linear crystal, the rows are now all in phase when the frequency is at the maximum.

If only forces between nearest neighbors were important, it would be generally true that the mean square is half the maximum square, and it should always be true that the contribution of the principal force constant to the mean square frequency is half its contribution to the maximum square in an isotropic array. Every force constant must contribute to the mean square, but there will be second and more distant neighbors in some models which suffer no relative displacement in the highest frequency motion. This can be seen by examining the linear crystal with an additional force $k\alpha$ introduced for the relative displacement of second neighbors, resulting in $\lambda'(\text{mean})=2+2\alpha$ and $\lambda'(\text{max})=4$. It is concluded, for isotropic arrays, that the mean square frequency is at least half the maximum square and may be larger, but not much larger.

With a reasonable potential energy function, it will always be possible to write the diagonal element of the secular determinant which evaluates the root mean square frequency, and it will usually also be possible to find the maximum frequency. An acceptable distribution function and simplified secular equation should express these two frequencies with reasonable accuracy in a nearly correct ratio.

In the first approximation the maximum square is twice the mean square. A wide variety of distributions will meet this condition, from something like the linear crystal distribution at one extreme to a heavy concentration about two principal frequencies at the other. The latter extreme is suggested by Montroll's[7] "infinities," but the former, intuitively, seems more in line with the widely variable situations presumably represented by the normal coordinates. It is possible that the distributions for real systems may vary all the way from one extreme to the other, and still possible also that the representation of thermal properties may not be sensitive to the particular distribution chosen within the prescribed limits.

The limiting value of the required ratio can be imposed upon the Debye distribution by interpreting the components of Eq. (8) as linear crystal frequencies, according to Eq. (7). Since the one-dimensional frequencies are arranged in complementary pairs which meet the requirement, it is obvious that the sums can

be arranged as similar complementary pairs. At the same time the expected discontinuities appear in the distribution. The vector additions still outline a cube whose geometry requires the discontinuities, but the density of frequencies within the cube is no longer constant, but instead varies with the coordinates. This change alone should effect an improvement in the Debye distribution by introducing some features required of a real system, and the resulting distribution might very well fit the thermal properties of a wider selection of models without further modification.

In this form, however, Eq. (8) as an approximation to the secular equation is too highly simplified, since it implies a potential energy function with only the one constant introduced through Eq. (7), and no one would attempt to describe a reasonable approximation to a real system without at least two constants. A further modification is therefore suggested, in order to bring Eq. (8) into line with the common maximum frequency of the Houston[5] and central force models of the simple cubic system without altering the ratio of the maximum to the mean square. This can be done by rewriting Eq. (8) in the form

$$\nu^2=\nu_x^2+\alpha(\nu_y^2+\nu_z^2) \tag{9}$$

with the components still taken from Eq. (7).

Equation (9) is still an oversimplified secular equation in respect to real systems and presumably also most mathematical models, but it should now be markedly better than the Debye equation and should be usable to express the thermal properties of a wide variety of isotropic models adequately. The equation implies a potential energy function, and therefore a model, without specifying what they are. There are preliminary indications that Eq. (9) is the exact form of the factored secular equation for Houston's[5] model; but the proof requires further development, and, if achieved, will be reported at a later date.

To obtain all the normal frequencies, Eq. (9) must be applied three times, once with each set of components in the leading term. For a cube of N^3 particles, there will be N^3 vector additions each time, leading to the correct total of $3N^3$ frequencies. The first set of frequencies is obtained by adding the vectors ν_x, $\alpha^{\frac{1}{2}}\nu_y$ and $\alpha^{\frac{1}{2}}\nu_z$. All of the vectors must terminate within a rectangular parallelipiped of square cross section, a construction which will introduce four discontinuities into the distribution curve, at $\alpha^{\frac{1}{2}}\nu_x(\max)$, $(2\alpha)^{\frac{1}{2}}\nu_x(\max)$, $\nu_x(\max)$ and $(1+\alpha)^{\frac{1}{2}}\nu_x(\max)$. The density of frequencies within the parallelipiped increases with the distance from each of the coordinate reference planes. Surfaces of constant frequency are still spherical, with the pertinent surface area increasing rapidly up to the first discontinuity, more slowly from the first to the second, than decreasing slightly from the second to the third, decreasing more sharply between the third and the fourth, and dropping rapidly to zero between the fourth discontinuity and the maximum frequency. Such a distribution has more acute discontinuities than the Debye distribution, but will not show the extreme "infinities" indicated by Montroll's analysis. The result deviates from the Debye distribution in the direction of the Montroll type of curve and should be an improvement over the Debye function which is probably about as near as one can expect to come to a general function for isotropic crystals.

At very low frequencies, and therefore for thermal properties at very low temperatures, with the components ν_x, etc., in the region where $\theta=\sin\theta$, it is evident from Eq. (7) that the distribution follows the Debye quadratic form. How low the temperature must be, however, depends upon the value of α which, if small enough, would lead to a linear crystal distribution in the limit. Such a distribution appears at present to be extremely unlikely for any real system. Consequently, no change in the commonly used method of extrapolating low temperature thermal data has been suggested.

Small-Angle X-Ray Scattering from Argon*

WALTER GRAHAM AND LOUIS H. LUND
Missouri School of Mines and Metallurgy, Rolla, Missouri
(Received August 13, 1951)

A correlation function as introduced by Debye in the case of light scattering is used to characterize the inhomogeneities in liquid argon for those cases showing excessive small-angle x-ray scattering. This method of characterizing the inhomogeneities is compared with the method of characterizing the inhomogeneities as droplets. Curves showing the correlation functions for the various cases are also presented.

INTRODUCTION

SIGNIFICANT among the features of the x-ray scattering by liquid argon[1] has been the excessive small-angle scattering in the neighborhood of the critical temperature. More recently, a careful series of measurements has been made of the x-ray scattering of liquid nitrogen[2] at various pressures and temperatures in the general region of the critical point. Here, too, the scattering at small angles is quite large. In both cases, a theory of small-angle x-ray scattering by amorphous substances by Vineyard[3] has been applied to this small-angle scattering.

In this theory,[4] the small-angle scattering from an amorphous substance is ascribed to widely separated macroscopic regions of inhomogeneities, such as clumps of molecules, pockets, or foreign inclusions. In particular, in the application of the theory to the cases of small-angle scattering of liquid argon and nitrogen, a physical model of spherical droplets of vapor in the liquid or of liquid in the vapor has been used to characterize the inhomogeneities. Ascribing the intensity from zero angle (extrapolated) to the first minimum on the intensity curve as the small-angle scattering from the droplets, it is possible by the usual method of particle size determination[5] to calculate the radius of the droplet. This droplet radius has turned out to be quite small; too small, in fact, for one to attribute to the droplets the properties of a distinct phase. The conjecture,[6] however, has been made that the inhomogeneities need not be so sharply delineated and that the inhomogeneities are perhaps equally well described physically by a temporary, dynamic association of the molecules into various irregular ways of clumping.

In what follows, the inhomogeneities responsible for the small-angle scattering from liquid argon have been characterized by a "correlation function" as introduced by Debye[7] and the essential similarity as well as a difference of this method to that of Vineyard's considered.

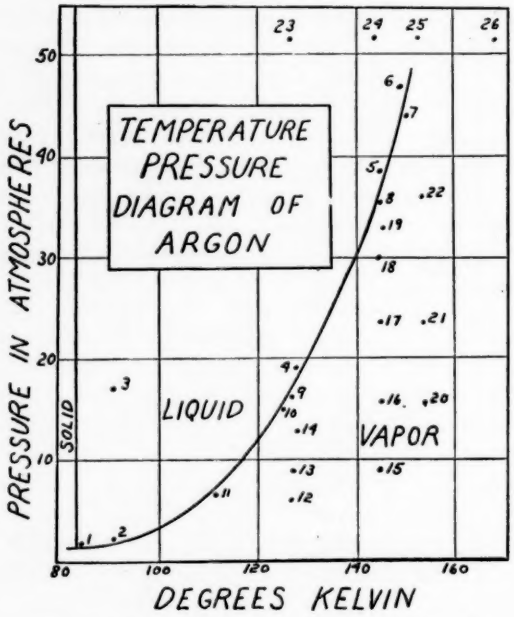

FIG. 1. *P-T* diagram for argon with datum points corresponding to x-ray scattering patterns.

METHOD OF CALCULATION

Let us take the average electron density of the liquid (or vapor) to be ρ_0 upon which is superimposed a small fluctuation Δ which may, especially in the neighborhood of the critical temperature, be considered to a rapidly varying function of position. Taking the electron fluctuation at point 1; multiplying by the fluctuation at point 2 a distance r away and moving the two points 1 and 2 throughout the liquid with fixed r, we obtain a large number of these products, $\Delta_1\Delta_2$, which we can designate as $\langle\Delta_1\Delta_2\rangle_{Av}$. Now, as in the case of scattering of light by an inhomogeneous solid, we can define a correlation function $\gamma(r)$[8] through the relation $\langle\Delta_1\Delta_2\rangle_{Av}=\bar{\Delta}^2\gamma(r)$ where $\gamma(r)$ ranges from unity at $r=0$ to zero for large r. The function $\gamma(r)$ obviously provides a way of characterizing the average extension of the inhomogeneities.

Suppose the sample to be irradiated by a collimated,

* Part of this work is from a thesis submitted to the Missouri School of Mines and Metallurgy by Walter Graham towards the M.S. degree.

[1] A. Eisenstein and N. S. Gingrich, Phys. Rev. **62**, 261 (1942).
[2] R. L. Wild, J. Chem. Phys. **18**, 1627 (1950).
[3] G. H. Vineyard, Phys. Rev. **74**, 1076 (1948).
[4] See reference 3.
[5] A. Guinier, Radiocrystallographie (Dunod, Paris, France, 1945), Chapter XII.
[6] See reference 3.
[7] P. Debye and A. M. Bueche, J. Appl. Phys. **20**, 518 (1949).
[8] See reference 7.

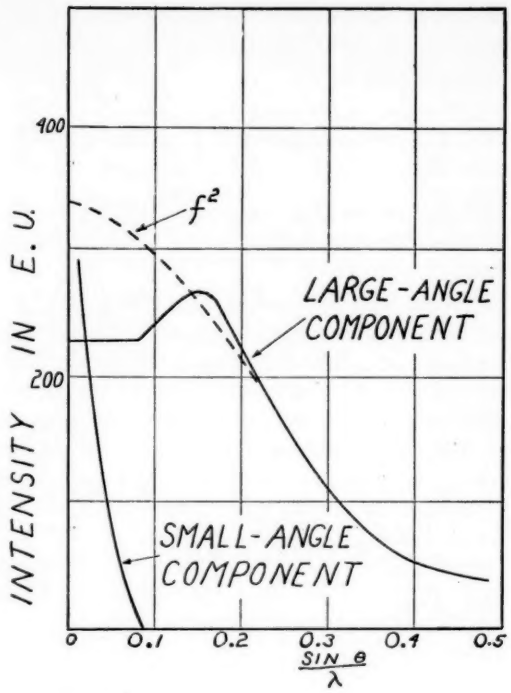

FIG. 2. Subdivision of intensity into large-angle and small-angle components.

monochromatic beam of x-rays having the direction of the unit vector $\mathbf{S}_0$. The coherent part of the electric field scattered in the direction of the unit vector $\mathbf{S}$ by the volume V may easily be shown to be proportional to the average of the square of the following:

$$E=\int_V(\rho_0+\Delta)e^{i\mathbf{k}\cdot\mathbf{r}'}dv, \tag{1}$$

where $\mathbf{k}=2\pi/\lambda(\mathbf{S}-\mathbf{S}_0)$, is the wavelength of the x-rays, 2θ is the angle between $\mathbf{S}$ and $\mathbf{S}_0$, $\mathbf{r}'$ is a vector from a fixed origin and the magnitude of $k=(4\pi/\lambda)\sin\theta$. We may then write that the scattered intensity is proportional to

$$\int_0^R 4\pi r^2 e^{i\mathbf{k}\cdot\mathbf{r}}dr\int_0^\pi\int_0^{2\pi}\left\{\int(\rho_0+\Delta_1)(\rho_0+\Delta_2)dv\right\}\times\frac{1}{4\pi}\sin\theta d\theta d\varphi, \tag{2}$$

where the second volume element has been replaced by the corresponding spherical volume element, R is the largest linear dimension of the sample, and $\mathbf{r}=\mathbf{r}_1'-\mathbf{r}_2'$ is the vector connecting the two points 1 and 2. Now remembering the way the correlation function is formulated, one has, if the integral in the curly brackets is performed first, followed by the integrations over θ and φ

$$\int_0^R 4\pi r^2\rho_0^2 e^{i\mathbf{k}\cdot\mathbf{r}}dr+\bar{\Delta}^2\int_0^R 4\pi r^2\gamma(r)e^{i\mathbf{k}\cdot\mathbf{r}}dr, \tag{3}$$

where the integrations over the volume of $\Delta_1\rho_0$ and $\Delta_2\rho_0$ will yield zero if the fluctuations Δ are purely random. No special orientation will be discernable so one may average the result over all possible directions of $\mathbf{k}$ to obtain an average intensity

$$I(k)\sim\int_0^R 4\pi r^2\rho_0^2\frac{\sin kr}{kr}dr+\bar{\Delta}^2\int_0^R 4\pi r^2\gamma(r)\frac{\sin kr}{kr}dr. \tag{4}$$

Now the first term, for any sample of macroscopic size, may be shown to contribute to the scattering at an angle so small as to be physically insignificant for the case considered here. Further, since $\gamma(r)$ will go to zero for values of r which are very small compared to the size of the sample, we may replace the upper limit in the second integral by infinity and we will have

$$I(k)\sim\bar{\Delta}^2\int_0^\infty 4\pi r^2\gamma(r)\frac{\sin kr}{kr}dr. \tag{5}$$

The last may be rewritten through the aid of a fourier transform theorem as

$$r\gamma(r)\sim\int_0^\infty kI(k)\sin krdk. \tag{6}$$

The last relation has been applied in what follows to a number of the argon x-ray scattering curves[9] showing a large small-angle scattering for a determination of the correlation function $\gamma(r)$.

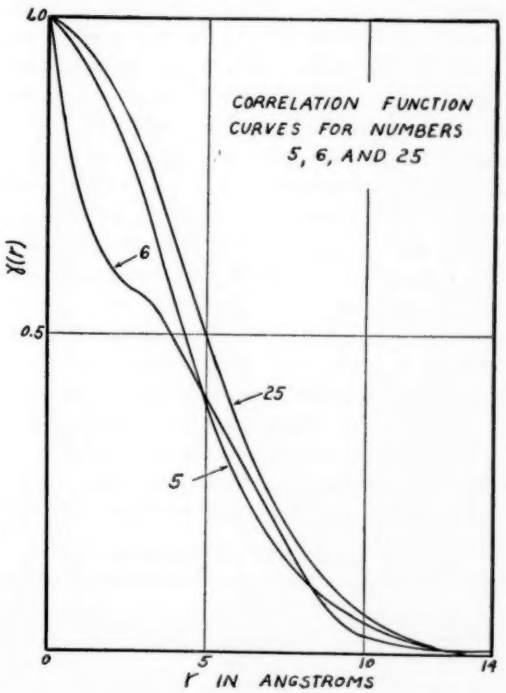

FIG. 3. Correlation functions corresponding to datum points 5, 6, and 25.

[9] See reference 1.

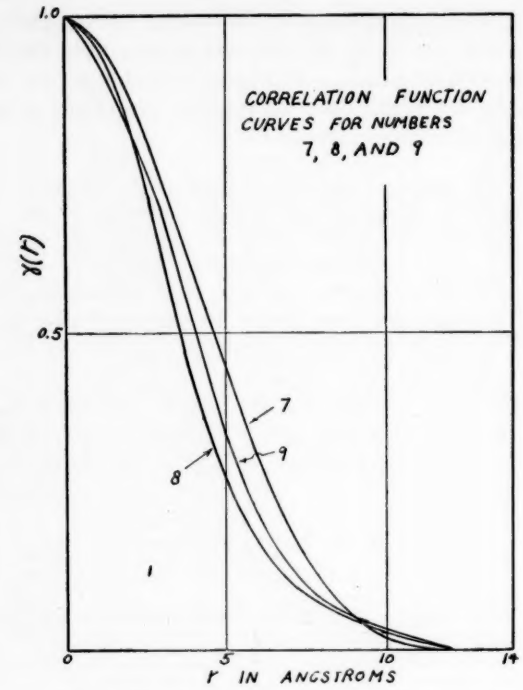

FIG. 4. Correlation functions corresponding to datum points 7, 8, and 9.

DISCUSSION

The x-ray scattering curves examined are those corresponding to datum points 5, 6, 7, 8, 9, and 25 in Fig. 1 on the liquid-vapor transition curve. These scattering curves, all showing excessive small-angle scattering, permit examination of the correlation functions as one approaches the critical temperature from the liquid and vapor sides of the liquid-vapor transition curve. One datum point, 25, corresponding to the gaseous state, is also included. The scattering due to the inhomogeneities here also is taken to be that from zero angle (extrapolated) to the first minimum of the scattering curve (see Fig. 2). This division of the intensity into large and small angle components is, of course, an arbitrary one. However, both components of the intensity curve have zero slopes at zero angle and hence a horizontal extrapolation of the large-angle component is not unreasonable. Using this small-angle intensity corresponding to a particular datum point, the integral in (6) may be evaluated in steps of r of $\frac{1}{2}A$ and the resulting $\gamma(r)$ normalized to unity at $r=0$. The resulting correlation functions are shown in Figs. 3 and 4. To characterize the average extension of the inhomogeneities obtained here, an average r^2 has been calculated from

$$\overline{r^2}=\left(\int_0^\infty r^2 4\pi r^2\gamma(r)dr\right)\Big/\left(\int_0^\infty 4\pi r^2\gamma(r)dr\right) \quad (7)$$

for each correlation function and $\overline{r^2}^{\frac{1}{2}}$ shown in Table I along with the spherical droplet radii obtained by Vineyard.[10]

TABLE I. Extension of inhomogeneities (argon).

Datum point	$\overline{r^2}^{\frac{1}{2}}$(A)	Droplet radius (A)
5	6.85	6.2
6	8.51	7.1
7	6.03	6.2
8	6.61	5.4
9	6.45	5.7
25	7.15	6.5

It is seen that $\overline{r^2}^{\frac{1}{2}}$ compares favorably with the droplet radii. The correlation functions, however, sensibly vanish at distances about twice that of the droplet radii in each case. It might be noted that all the correlation functions have nearly the same shape except that corresponding to curve 6 which lies nearest the critical temperature in the liquid state. Its somewhat anomalous shape might be attributed to its proximity to the critical temperature.

It seems clear that so far as the average size of the inhomogeneities is concerned both methods give essentially the same result. It is, however, perhaps interesting to notice the way the two methods of characterizing the inhomogeneities differ in their physical models. If one imagines the inhomogeneities occurring in the liquid or vapor to be truly droplets the small-angle scattering formula attributed to a droplet may be obtained from (4) by taking Δ everywhere zero in a sphere of radius equal to the droplet radius and extending the integration over the volume of the droplet. One is left with the first term where this term may, of course, not now be neglected. The scattering of N independently scattering droplets is then obtained by multiplying the single droplet intensity by N. The function ρ_0^2, involving the radius of the sphere, may be calculated and hence a fitting of this term to the small-angle scattering, enables the droplet size to be calculated.[11] Similarly, if one begins with the droplet model and takes the droplet to be large (essentially infinite), it is necessary to introduce a fluctuation of electron density within the sphere since one does not have now a true droplet. Since the spheres effectively overlap the integration may be extended over the whole volume and the final result is (4) where the first term is neglected as before.

Although either model may be used to characterize the average size of the inhomogeneities, the small droplet size obtained in the cases of liquid argon and nitrogen does not lead to the droplet model as being a particularly tenable physical model. The correlation functions obtained here are consistent with the notion of regions of inhomogeneities, less sharply defined than the droplet model, somewhat larger, and which merge more or less continuously into one another. The correlation function thus appears to be a more physically reasonable way of characterizing the inhomogeneities.

[10] See reference 3.

[11] The same procedure would hold for the case of N independently scattering particles such as in colloidal solutions.

Rotational Temperatures of OH in Methane-Air Flames*

HERBERT P. BROIDA
National Bureau of Standards, Washington, D. C.

(Received July 6, 1951)

Rotational line intensity distributions in emission and absorption of the $0\leftrightarrow0$ band of the $^2\Sigma\leftrightarrow{}^2\Pi$ transition of OH have been measured in methane-air flames. The number of electronically excited OH radicals in the inner cone greatly exceeds the equilibrium concentration, and the intensity distribution of the high quantum numbers gives a temperature of 5200°K. However, OH radicals in the ground state were in thermal equilibrium at 2000°K. A break in the intensity distribution indicates a two stage combustion reaction. It is suggested that the excessive amount of excited OH is due to its formation in the intermediate reaction steps. Line reversal temperatures using Na, Hg, and OH have been measured in the same flame for purposes of comparison. Also the rotational temperature of excited OH in a methane-oxygen flame was measured.

1. INTRODUCTION

CURRENT expansion in the use of power units driven by hot gases has stimulated in physicists and chemists a renewed interest in flame phenomena. One of the major obstacles to a complete understanding of the operation of gas turbines, jet engines, and rockets is the lack of an adequate theory of flame propagation. Furthermore, limitations of conventional immersion type pyrometric devices and radiation pyrometers have hindered the development and practical use of such propulsion units. Because of the promise appearing in research methods involving optical spectroscopic analysis of burning regions, many laboratories have undertaken programs of spectroscopic studies of flames. Such studies have contributed greatly to the present knowledge of intermediate particles within the flame zone, and also have led to various methods for determining temperatures in burning gases. Although quantitative measurements of intensities in both emission and absorption are necessary to an understanding of the relative importance of excited and unexcited intermediate particles of the chemical reactions within the flame zone, only a small number of absorption studies have been made because of the many experimental difficulties inherent in such work.

Since neither thermal nor chemical equilibrium exists in a flame region, there is not a flame temperature because, in a strict thermodynamic sense, temperature applies only to an equilibrium state. However, less precise use of the word temperature has become commonly accepted in order to simplify discussions concerning the measurement of radiation intensities from hot gases. The temperature of a flame generally depends upon the technique of measurement and, therefore, it is common practice to use a modifying adjective or phrase descriptive of the method by which the number associated with the temperature was obtained. For example "OH rotational temperature" refers to the temperature obtained from the distribution of intensity among the various rotational states of an OH band. This paper reports investigations of the rotational energy distribution of the $0\leftrightarrow0$ band of the $^2\Sigma\leftrightarrow{}^2\Pi$ transition (between 3064 and 3133 angstrom units) of the hydroxyl radical in absorption and emission in flames at atmospheric pressure of methane pre-mixed with air and oxygen.

The OH radical was selected for initial studies of radiation from flames for the following reasons:

1. It occurs strongly in most hydrocarbon flames;
2. It is an important intermediate in reaction chains;
3. There is evidence[1] that in some flames, the OH produced is chemiluminescent;
4. Its electronic transition is in a convenient region to observe spectroscopically;
5. Its spectrum[2] is well known;
6. Experimental "f numbers"[3] have been measured; and
7. The rotation distribution is in a relatively narrow wavelength interval, but the lines are separated sufficiently for temperature determinations.

The band specified above, which is degraded to the red and which has a head at 3064 angstrom units is not only the most intense band of the OH electronic transition but also is very prominent in the ultraviolet spectra of hydrocarbon flames. For temperature measurements, the R_2 branch is the most usable of the 12 branches since it has many lines which do not overlap in a small region (22 A.U.). A spectrograph of fairly high dispersion is required both to separate these lines and to measure absorption coefficients.

A search of the literature has revealed no information on rotational intensity distributions in absorption by OH in a flame. Failure to apply this technique to combustion studies is probably the result of the difficulties of bringing together the appropriate apparatus. One

* This work was done under the sponsorship of the Navy, Bureau of Aeronautics.

[1] A. G. Gaydon and H. G. Wolfhard, *Third Symposium on Combustion Flame and Explosion Phenomena* (Williams and Wilkins, 1949), pp. 504–508.
[2] G. H. Dieke and H. M. Crosswhite, *The Ultra-Violet Bands of OH*, Bumblebee Series, Report No. 87 (Bur. Ord., USN, 1948).
[3] O. Oldenberg and F. F. Rieke, J. Chem. Phys. **6**, 439, 779 (1938). O. Oldenberg and R. J. Dwyer, J. Chem. Phys. **12**, 351 (1944).

major problem is the need of an intense source of continuum that is steady with time, and has no superimposed emission or absorption lines. Another outstanding need is a sensitive detecting instrument of high resolution. Since no continuum source of the intensity and uniformity required for studies with oxygen flames was available, it was necessary to cool the flame with nitrogen (i.e., by using air), so that a tungsten lamp could be used. A direct reading monochromator with high resolution capable of detecting absorption of 1 percent with relative ease served as the needed detector.

In addition to the determination of the OH rotational temperatures in emission and absorption, three separate line reversal temperatures have been measured

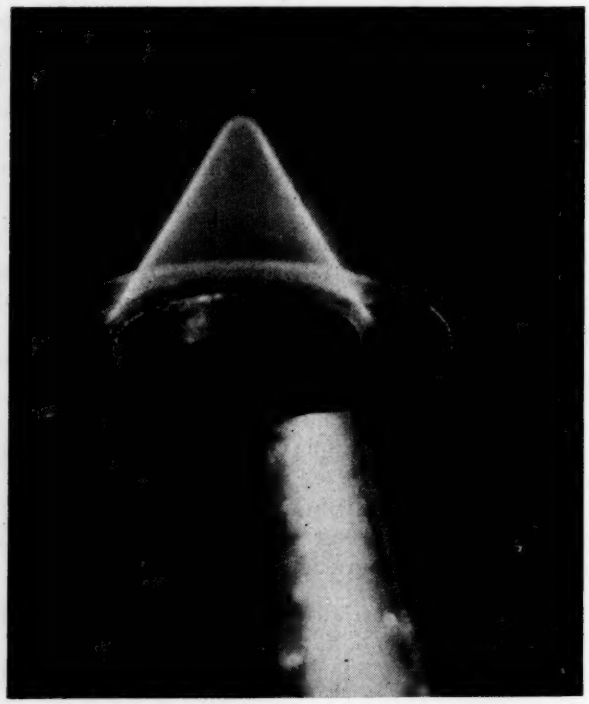

FIG. 1. Flame of stoichiometric mixture of methane and air burning above a ½-inch nozzle.

by comparing the emission from added sodium, from added mercury and from rotational lines of OH with a calibrated tungsten strip lamp. Analysis of the data indicates that thermal equilibrium exists in the outer cone and that, in the inner cone, there is a two stage reaction in which OH is formed in an excited electronic state.

2. METHOD AND EXPERIMENTAL RESULTS

2.1 Apparatus

Figure 1 is a photograph of the flame used in these studies. A homogeneous mixture of dried air and methane (99.6 percent purity) flowing upward through 1 meter of steel tube 38 mm in diameter, is burned above an accelerating nozzle having a throat diameter of 12.7 mm. A more complete description of the apparatus for controlling the flame has been given elsewhere.[4] This flame differs from the conventional Bunsen flame burning above a tube in that the gas emerges from the nozzle with a uniform velocity rather than with a parabolic velocity distribution. A more nearly conical burning zone results from this uniform velocity pattern. It is of interest to note that the visible region begins about 0.6 mm above the nozzle and has a diameter greater than the throat of the nozzle by about 2.5 mm. Both emission and absorption measurements were made along the side of the inner cone where the intensity is greatest, and near the base where the effects of the surrounding outer cone are least. Measurements on the outer cone were made about one cm above the tip of the inner cone.

The portion of the flame to be studied was focused by a quartz lens having a magnification of two, upon the entrance slit (6 mm high) of a direct reading monochromator.[5,†] The desired spectral region is scanned by rotating the grating. Radiation is detected by a 1*P*28 photomultiplier tube behind the exit slit, and intensity is recorded directly as a function of wavelength. Although this monochromator has a resolving power of 55,000, the full resolution could not be used because the weak intensity of this flame (due to the cooling by the nitrogen in the air) made it necessary to use relatively wide slits (0.015 mm). For absorption spectra, radiation from a tungsten strip lamp was focused by either a spherical mirror or a quartz lens on the region of the flame being studied. A quartz lens focused both the flame and the image of the lamp on the slit of the monochromator.

2.2 Rotational Distribution of OH

If there is thermal equilibrium in a flame, the intensity distribution of an emission or absorption band of a molecular species can be used to determine temperature.[6] For a fixed electronic and vibrational transition of the molecule, the intensity $I_{K\to L}$ of an emitted line depends only upon the number of molecules N_K in the Kth rotational level of the excited state and upon the transition probability A_{KL}. Thus

$$I_{K\to L}=\text{constant}\times A_{KL}\times N_K. \quad (1)$$

Although the constant term is linear with frequency, the change in frequency over a small frequency range is negligible and need not be considered. The equilibrium number of molecules in an excited state with

[4] Caldwell, Broida, Dover, and Fiock, "Symposium on combustion cemistry," Cleveland (April 12, 1951).

[5] W. Fastie, J. Opt. Soc. Am. 40, 800(A) (1950).

† This instrument was constructed by the research department of Leeds and Northrup Company and was loaned to the National Bureau of Standards on a field trial basis.

[6] G. Herzberg, *Molecular Spectra and Molecular Structure I* (D. Van Nostrand Company, Inc., 1950), second edition, pp. 124, 204.

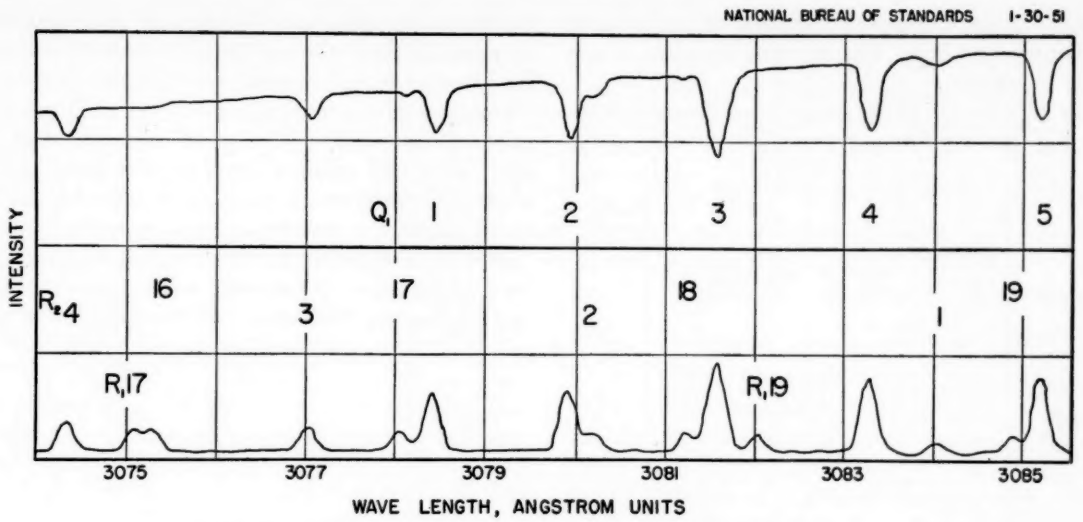

FIG. 2. Absorption and emission spectra of OH from a stoichiometric methane-air flame. Upper curve is absorption. The resolved branches are marked.

an energy E_K is determined by the Maxwell-Boltzmann distribution and is given by

$$N_K = N_0(2K+1)\exp(-E_K/kT) = N_0 q \exp(-E_K/kT). \quad (2)$$

Where k is the Boltzmann constant, T is the absolute temperature, and N_0 is the total number of molecules. Equations (1) and (2) can be combined and written in an experimentally useful form as

$$\log_{10}(I_{K\to L}/qA_{KL}) = \text{constant} - (E_K/kT)\log_{10}e. \quad (3)$$

Thus a plot of $\log_{10}(I_{K\to L}/qA_{KL})$ as a function of E_K can be made from the known transition probabilities and measured intensities. This is a straight line, the slope of which is proportional to $1/T$. When experimental errors have been eliminated, a lack of linearity of this plot may be an indication of non-equilibrium. Equation (3) for absorption differs from that in emission only in that the transition depends upon the number of molecules N_L in the energy level E_L in the unexcited or ground state. There is also a difference in the constant term but this is unimportant for temperature measurement over a narrow wavelength interval.

Figure 2 is a 10 angstrom region of the OH spectrum, in both emission and absorption, from the inner cone of a stoichiometric methane-air flame. The lower curve shows the intensities of emitted radiation, and the upper curve shows the absorption of the strip lamp continuum by the flame. The absorption curve was obtained with less amplification than the emission curve. The resolved lines of the three branches in this region are marked; the satellite lines of the Q_1 branch are not shown. It will be noticed that transitions from the higher rotational levels are not observable in absorption even though transitions from the lower levels are of an intensity comparable to that of emission. This relative weakness of lines from the higher rotational levels is a clear indication that in the ground state, the OH is at a much lower rotational temperature than the excited state.

A quantitative measure of this difference can be obtained from the logarithmic plot suggested by Eq. (3). Figure 3 shows the results of intensity measurements of the R_2 branch of OH emitted from the inner cone of a stoichiometric mixture of methane and air. The observed points lie on two distinct straight lines; one line corresponds to the intensities from the lower rotational states and the other line of completely different slope corresponds to the intensities from the higher states. From the slopes of the two lines "temperatures" of 2350°K and 5200°K are found for the lower and higher states, respectively. Repeated measurements show a precision in each of these "temperatures" of approximately ±5 percent. The line marked 1550°K will be discussed later.

An analysis of possible experimental errors that might have caused a break in the logarithmic plot indicated that the break was real and is characteristic of the flame itself. No error was introduced by the small amount of emitted continuum, since intensities were measured directly as heights above this continuous background. Although there was only small self-absorption (of the order of 5 percent) by the weak methane-air flame, a correction factor for this type of error was easily obtained from the absorption measurements of the continuum from the strip lamp. Such corrections did not change the characteristics of lines and did not affect the slopes by as much as the experimental error. Although there was some overlapping of lines, a weak line only 0.2 A.U. removed from a line 6 times as strong was still resolved, and a sufficient number of lines were resolved and measured so that the lack of resolving power was of no consequence. Circles in Fig. 3 represent lines completely resolved and the squares represent lines

that either are not completely resolved or which have weak superimposed lines. The straight lines are drawn to best fit the circles.

Another manner of illustrating the non-equilibrium is by using the iso-intensity method developed by

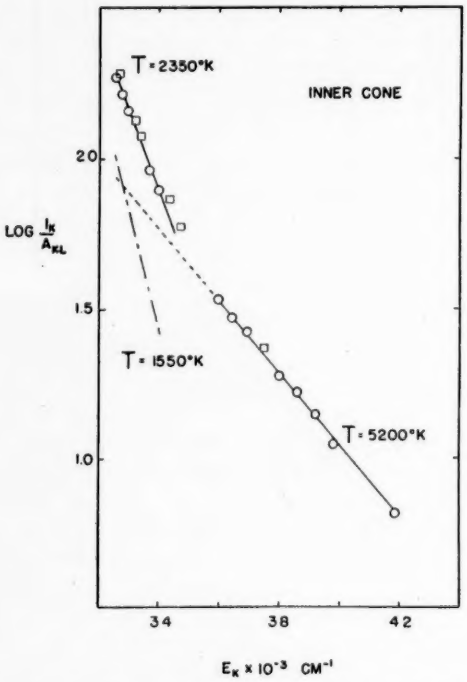

FIG. 3. A plot of $\log(I_K/A_{KL})$ *vs* E_K for the R_2 branch of the $(0\leftrightarrow 0)$ band of OH($^2\Sigma\leftrightarrow{}^2\Pi$) in the inner cone of a stoichiometric methane-air flame.

Dieke and Crosswhite.[2] This method has the advantage that for lines of equal intensity, the effect by self-absorption will cancel out in the first approximation. Shuler[7] has shown for lines of equal intensity and small difference in wavelength that

$$A_{K'}/A_K=\exp[(E_{K'}-E_K)/kT]. \quad (4)$$

A plot of $E_{K'}-E_K$ *vs* $\log(A_{K'}/A_K)$ will be a straight line going through the origin for an equilibrium rotational distribution. Figure 4 shows such a plot for the emission from the methane-air inner cone. Since a straight line cannot be drawn through the experimental points and the origin, a non-equilibrium is indicated.

The persistence of a non-equilibrium distribution as indicated by Figs. 3 and 4 can be interpreted as showing that the large number of collisions which the OH radical undergoes during its lifetime are not sufficient to bring about rotational equilibrium. Since the radiative lifetime of electronically excited OH is of the order of 10^{-6} second[8] and the time between collisions at atmospheric pressure is of the order of 10^{-10} second (10^{10} collisions per second), the observed non-equilibrium rotational temperature would mean that 10,000 collisions per lifetime of the excited OH are not very effective for bringing about thermal equilibrium. Such a lag in the equipartition of rotational energy with other forms of energy is consistent with the observation of Oldenberg[9] that OH radicals show an abnormal rotational intensity distribution in electric discharges through water vapor.

Breaks in logarithmic curves similar to Fig. 3 have been observed in flames with other gases, particularly by Gaydon and Wolfhard,[1] but the cause is unexplained

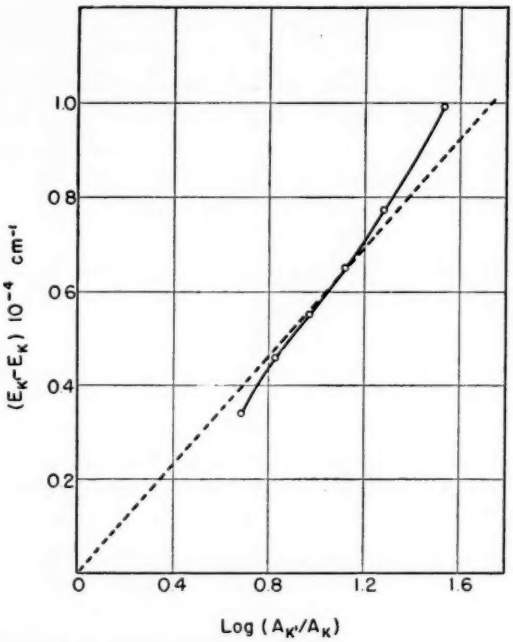

FIG. 4. A plot of $E_{K'}-E_K$ *vs* $\log(A_{K'}/A_K)$ for the R_2 branch of the $(0\leftrightarrow 0)$ band of OH in the inner cone of a stoichiometric mixture.

when experimental errors have been eliminated. Continuous temperature gradients in the flame would not be expected to cause such an abrupt change in the intensity distribution but Dr. Henry Crosswhite (by private communication) of the Johns Hopkins University has suggested that such a distribution would be expected from two distinct temperature regions. Assuming that there are two temperature regions, it is possible to separate the effect of the intensity of the "cold" region from that of the "hot." When the straight line for the higher rotational states of Fig. 3 is extrapolated to the lower states, and these extrapolated intensities are subtracted from the measured values, the intensity of the "cold" region alone (lower curve on the left side of Fig. 3) is found to correspond to a temperature of 1500°K.

It might be expected that this "cold" region would be associated with the cooler outer cone, but the intensity of emitted radiation in the outer cone was of

[7] K. E. Shuler, J. Chem. Phys. **11**, 1466 (1950).

[8] A. G. Gaydon, *Spectroscopy and Combustion Theory* (Chapman and Hall, Ltd., London, 1948), second edition, pp. 138–141.

[9] O. Oldenberg, Phys. Rev. **46**, 210 (1934).

the order of 1/25 of that in the inner cone. Consequently its effect on the distribution would not be observed. This extremely low intensity of emission made it impossible to obtain a meaningful intensity distribution in the outer cone since even the intensity from the inner cone was so weak that thermal noise from the first surface of the photomultiplier tube was troublesome. The entire measured radiation must come from the inner cone, since the radiation from the outer cone alone was too weak to be observed on the background of the more intense emission from the inner cone. Consequently, it seems reasonable to assume that the two temperature regions are evidence of a two-stage combustion process occuring within the narrow region of the inner cone. A two-stage reaction is known to occur in compression-ignition engines[10] and under some conditions a "pre-flame" reaction appears to be completed before the final burning occurs. In flames of ether mixed with air, Powling[11] has separated the "cool flame" from the ordinary "hot" flame. Although there is no evidence from low temperature reaction studies[8] of methane-air mixtures that a two stage process exists, it is known that acetylene is formed in a methane flame. The formation of these larger molecules might lead to conditions under which a two stage reaction could take place. Another possibility which exists for the formation of a two temperature region, and which would account for the experimental facts, is the existence of two different intermediate reactions giving rise to excited OH with separate rotational distributions. Until more experimental evidence is available, it is not possible to consider and eliminate all reasonable possibilities for the two temperatures.

For the purpose of discussion, let the reaction producing excited OH with a rotational distribution corresponding to 1550°K be called reaction *a* and that producing radicals with a rotational distribution corresponding to 5200°K be called reaction *b*. The relative numbers of radicals formed in these two reactions can be calculated from the experimental results if it is assumed that the only loss of excited OH is by radiation to the ground state. Following the approximation of Herzberg[6] which is sufficiently good at the high temperatures found in this flame, it is possible to find the total number of radicals, N, from the rotational state sum, Q_r, and the number of radicals, N_K, in some particular level, K.

$$N=\frac{N_K Q_r}{2K+1}\exp(E_K/kT)$$

$$=\frac{K(K+1)N_K}{(2K+1)E_K}kT\exp(E_K/kT). \quad (5)$$

According to Eq. (1), N_K is proportional to I_K/A_{KL} and therefore the intersection in Fig. 3 of the curves for the two reactions gives the energy, E_3, at which the reactions form the same number of radicals. E_3 is the rotational contribution to the energy, whereas, Fig. 3 shows the total energy. The ratio of the number of OH radicals formed in reaction *a* to the number formed in reaction *b* is

$$N_a/N_b=(T_a/T_b)\exp[E_3/k(1/T_a-1/T_b)]$$
$$=(1550/5200)\exp[(163/0.695)(1/1550-1/5200)]=0.3. \quad (6)$$

Thus for every OH radical formed by reaction *a*, three are formed by reaction *b*.

Absorption measurements in the inner and outer cone of the same stoichiometric flame gave a rotational temperature of 2000±100°K in both cones, as shown by the representative results in Fig. 5. The uncertainty of ±100°K is estimated from data of over 30 measurements of the inner and outer cones. Since the same temperatures were observed in the inner and outer cones, the rotational states of unexcited OH are probably in thermal equilibrium in both regions.

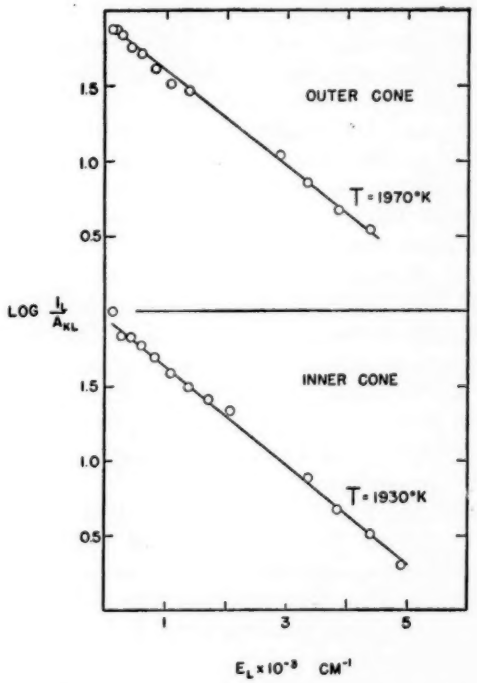

FIG. 5. Plots of $\log(I_L/A_{KL})$ *vs* E_L for the R_2 branch in absorption of the $(0\leftrightarrow 0)$ band of OH($^2\Sigma\leftrightarrow{}^2\Pi$) in the inner and outer cones of a stoichiometric methane-air flame.

In addition to giving the temperature of the ground state, absorption measurements can be used to determine the concentration of the absorbing molecules. Following the approximation given by Gaydon[8] for the integrated absorption coefficient, the number of OH radicals per cubic centimeter, in the Lth state

[10] J. Levedahl and F. Howard, J. Research Natl. Bur. Standards **46**, 301 (1951).
[11] J. Powling, Fuel **28**, 25 (1949).

N_L, is given in terms of the observable quantities as

$$N_L \cong \left(\frac{\mu c^2}{2e^2 f}\right)\left(\frac{I_{abs}/I_0}{\Delta x}\right)\Delta\nu \qquad (7)$$

μ and e are respectively the mass and charge of an electron; c is the speed of light; I_{abs}/I_0 is the fraction of light absorbed at the center of a spectral line of half-width $\Delta\nu$ by an absorbing region of thickness Δx; and f is the "f-number" of the absorbed line. Neglecting the change of temperature within the hot gases and using the edge of the visible cone as the extent of the absorbing region, Δx of the outer cone was approximately 2 cm. For the R_2 (3) line, the measured values of $\Delta\nu$ and I_{abs}/I_0 were of the order of 0.8 cm^{-1} and 0.06, respectively. Using the corrected "f-number," 4.6×10^{-4}, of Oldenberg and Dwyer[3] for this line, N_3 is found to be 0.9×10^{14} OH radicals per cm^3. The total number of OH radicals per cm^3 in the ground state as calculated from Eq. 5 is 8×10^{14}. This value is in reasonable agreement with that of 2×10^{15} given in the tables calculated from thermodynamic data by Hottel, Williams, and Satterfield[12] for the equilibrium concentration at 2000°K.

It is difficult to estimate with any certainty the accuracy of the calculated concentration, because of the numerous possible sources of error. In addition to the errors inherent in the assumptions used in deriving Eqs. (5) and (7), the largest uncertainties are: in lack of knowledge of the temperature and its distribution in the hot region; in the measurements of the half-width of the spectral line; and in the fraction of radiation absorbed at the center of the line. The effect of the latter appears to be negligible, because it was found that the monochromator slit could be increased to more than double its optimum width for maximum resolution before the overlapping of radiation from adjacent wavelengths reduced the absorption noticeably. The resultant of all these errors is not likely to cause the measured concentration to be in error by more than a factor of five.

It is difficult to determine quantitatively the difference in concentrations of OH in the inner and outer cones because the inner cone cannot be observed except through a region of the outer cone. However, the relative absorption intensity in the two regions indicate that the concentration of OH in the inner cone is greater by a factor of at least 2.5. This value was estimated from measurements which show that intensities of absorption lines in the inner cone were 25 percent greater than those in the outer cone. The thickness of the outer cone surrounding the inner cone was about $\frac{1}{2}$ that of the outer cone above the tip of the inner cone. At atmospheric pressure the visible region of the inner is about 0.2 mm thick.

It will be noticed that the experimental value for the first absorption lines in the inner cone (lower curve of Fig. 5) do not lie on the straight line through the other points, but are somewhat higher. Although the separation of these points from the straight line is only slightly greater than the experimental error, the effect was found only for the inner cone and never for the outer cone alone. These facts show that there are more OH radicals in the first (and possibly other lower levels) than is to be expected from a maxwellian distribution of the radicals among the energy states. An average of six measurements showed an excessive absorption of the first state of about 30 percent. This extra population of the first state in the inner cone may be due to the superposition of two temperature regions, as has been postulated for the excited state. Also it is possible that this extra population may come about as a result of the type of phenomena that would be expected from Golden's[13] quantum-mechanical theory of reaction rates.

Measurements made with methane-air mixtures varying from 0.75 to 1.25 of stoichiometric fuel gave results similar to those made on stoichiometric mixtures, and need not be presented here.

2.3 Line Reversal Temperatures

The line reversal method[14] of measuring gas temperature is probably used more widely than any other spectroscopic means because of the relative simplicity of the apparatus and of interpreting the measured quantities. Essentially the method consists of comparing the intensity of monochromatic radiation emitted by the hot gases with the intensity of light of the same wavelength emitted by a continuum source at a known temperature. This method gives the excitation temperature of the atoms or molecules whose radiation is being observed. For gases in equilibrium, this temperature is equal to the thermodynamic temperature. Although various reversal temperatures of methane-air flames were determined, the procedure for making such measurements is so well known that the method need not be described in detail.

A large number of careful determinations of temperature were made using a flame totally colored with sodium (5890, 5896 A.U.). The sodium was introduced into the air stream as sodium-chloride vapor. These measurements showed that the measured temperature depended upon the region of the flame that was observed. The maximum temperature was found about 3 mm above the tip of the inner cone. Care was taken with the optical alignment and apertures of the lenses so that no errors from these sources would enter. For a stoichiometric mixture of methane and air, this measured maximum temperature was 2075 ± 10°K. The uncertainty of 10°K is the accidental error in the measured temperature of a given flame, and does not include the unknown systematic errors of the method of meas-

[12] Hottel, Williams, and Satterfield, *Thermodynamic Charts for Combustion Processes* (John Wiley and Sons, Inc., New York, 1949).

[13] S. Golden, J. Chem. Phys. **17**, 630 (1949).

[14] For example, see E. Griffith and J. H. Awberry, Proc. Roy. Soc. (London), **123A**, 401 (1929).

urement. Determinations made through the inner cone yielded temperatures about 35°C less than the maximum. This is probably due to a lack of thermal equilibrium between the newly formed sodium atoms and the hot gases. The measured temperature is some 125°C lower than that calculated from specific heat data. This difference is probably the result of the cooling of the gases by the surrounding atmosphere.

Mercury was introduced into the flame by allowing the air to bubble through liquid mercury; and by a mercury line reversal method (at 2537 A.U.) the temperature in the inner cone was observed to be 2500°K. This value may include an error by as much as 10 percent because of the uncertainty in the value of the reflectivity at this wavelength of the concave aluminum mirror used to focus the image of the strip lamp on the flame. Because of the large amount of cold mercury within the inner cone, it was expected that the measured temperature might be much lower than the theoretical flame temperature. However the high measured value is another indication of excess energy in some energy states within the reaction zone. The non-equilibrium amount of emitted mercury radiation might be caused by collisions of the second kind between mercury atoms and highly excited molecules. It is also possible that the mercury may actually enter into the chemical reactions.

Using an OH line, the reversal temperature was found to be 2300°K, a high value that might be expected from the excessive radiation already mentioned. There was also a measurable difference in temperature depending upon the OH rotational level observed, the temperature being higher for higher energy levels. For example, the temperature determined from the R_2 (9) transition was 20° higher than that determined from the Q_1 (6) line. This difference is not significant as a temperature but emphasizes the lack of meaning of the measured value when thermal equilibrium has not been attained.

A study of the line reversal method is being undertaken at this laboratory and further details will be published in the future.

2.4 Methane-Oxygen

As a check upon the emission from methane-air flames, measurements were made of the rotational distribution of the OH band in a stoichiometric methane-oxygen flame burning above an acetylene torch having a port diameter of 1.6 mm. Although there is a small amount of self-absorption of the intense lines of the R_2 branch, the iso-intensity method[2] shows that the temperatures of the inner and outer cone were respectively 3000°K and 2700°K. The temperature in the outer cone is in good agreement with the rotation temperature of approximately 2600°K measured by Shuler[7] in a similar flame. The lower temperature of the outer cone probably is a result of the cooling by the surrounding atmosphere. No indication of abnormal distribution was found in this flame. Absorption measurements were not made on the flame of methane and oxygen because no appropriate light source with a brightness temperature greater than 3000°K was available.

Gaydon and Wolfhard[8] report that rotational temperatures of OH at low and high energy levels are 2800°K and 7500°K, respectively, in flames of methane and oxygen at low pressure. The values reported here for flames at atmospheric pressure agree well with the low energy value, but no evidence of abnormal intensity at higher levels was noticed, even though the R_2 branch was measured to the 27th line.

The various temperatures of the stoichiometric mixtures are summarized in Table I. All the measured temperatures are affected by the averaging over the cooler regions surrounding the hotter core of the flame.

3. DISCUSSION AND CONCLUSIONS

In methane-air flames, the emission of OH is stronger in the inner cone than in the outer cone. This phenomenon and the abnormally high rotational temperature of the higher energy state may be due to chemiluminescence. Gaydon and Wolfhard[1] have suggested that OH may be formed in the electronically excited state as a result of the strongly exothermic reaction

$$CH+O_2 \rightarrow OH'+CO. \quad (8)$$

Although this suggestion is reasonable, a mechanism to account for a distribution of energy states that will lead to the straight lines shown in Fig. 3 is difficult to conceive. Perhaps this distribution can be explained by Eq. (8) and calculations of the type that Golden and Peiser[13] used to predict an abnormal rotational distribution of HBr produced by the reaction between atomic bromine and molecular hydrogen at 500°C. The HBr is predicted to have a temperature below that of the ambient temperature, whereas in methane-air flames the abnormal temperature is greater than the equilibrium value. This might be due to the formation of OH in an exothermic reaction. In the hotter methane-oxygen flame at atmospheric pressure the intensity of

TABLE I. Temperatures in methane-air flames.

OH rotational distribution	Temperatures °K Inner cone	Outer cone
Emission		
Low quantum numbers	1550	
High quantum numbers	5200	
Absorption	2000	2000
Reversal		
Na (5890, 5896)	2040	2075
Hg (2537)	2600	
OH (3089)	2400	
Calculated (methane-air)[12]		2200 (max)
Calculated (methane-oxygen)[12]		3050 (max)

emission from OH in thermal equilibrium is probably sufficiently high to mask the weaker chemiluminescence. This does not rule out the possibility of detecting such abnormal distribution at low pressures, where the number of OH radicals produced thermally is much smaller.

Although absorption measurements show thermal equilibrium so far as the rotational energy of the ground state of OH is concerned, the non-equilibrium number of unexcited radicals in the inner cone indicates that OH is not in chemical equilibrium within the burning zone. This increased amount of unexcited OH in the inner cone might be caused by the transition of radicals from the excessive number in the excited state. The radicals in the ground state may reach thermal equilibrium by collisions before being consumed in chemical reactions. The excessive absorption of the first rotational level in the inner cone again can be considered as evidence of a two stage combustion or it might come about from the lack of time to reach thermal equilibrium.

The available experimental evidence does not permit a firm choice among the various possible explanations that can be advanced for the observed abnormal conditions. However, one consistent and plausible explanation of the experimental facts is as follows. Electronically excited OH may be formed in two reactions, occurring simultaneously within the flame. Both reactions may form OH with a Boltzmann distribution of rotational energy in the excited state. One reaction may form OH with a rotational distribution equivalent to 5200°K, while the other reaction may form OH with a rotational distribution in the neighborhood of 1550°K. The excited OH may radiate before reacting with other particles in the flame zone and before the excess rotational energy is distributed among the other modes of energy by collision. In the ground state, OH reacts with the other molecules and except for the lowest rotational states, assumes an equilibrium rotational energy distribution.

Until both the intermediate reaction steps and the energy distribution of products from these steps are known, it will be difficult to interpret fully the complicated conditions within a flame region. However, attempts to interpret spectra of flames may prove to be an important step in the development of tenable theories of flame propagation. Experimental studies using fuels that are simpler than methane may yield data which are less involved, and thus lead to more rapid progress. Such studies with hydrogen are now in progress at the National Bureau of Standards.

On the Electron Affinity of Fluorine*

REED H. JOHNSTON†
Department of Chemistry, Stanford University, Stanford, California
(Received April 23, 1951)

The hamiltonian for systems isoelectronic with neon is treated by perturbation methods. The energy of ionization of such systems is represented by a four-term expression (i.e., to third order of perturbation); the two leading terms are calculated, spectroscopic data for isoelectronic systems are used to evaluate the constants in the two remaining terms. The electron affinity of fluorine is estimated to be 73±3 kcal/g atom. The corresponding dissociation energy of fluorine, as inferred by the Born-Haber cycle, is estimated to be 18 kcal/mole, to an accuracy believed better than ±12 kcal/mole.

PRINCIPLE OF THE CALCULATION[1]

CHOOSING as the unit of mass the reduced mass of an electron with respect to its atomic system, and taking the electronic charge to be of unit magnitude, then the hamiltonian for the relative motion of n point electrons, about a point nucleus of charge Z, may be written as $H+H'$ where

$$H=\sum_i\left[\tfrac{1}{2}p_i^2-(Z-S)r_i^{-1}\right]$$

and

$$H'=\sum_{i<j}\left[r_{ij}^{-1}-\epsilon p_i\cdot p_j\right]-\sum_i Sr_i^{-1}.$$

Herein ϵ denotes the reciprocal of the atomic mass, and the shielding constant S is a separation artifice. H' is regarded as a perturbation on the exactly soluble system. Setting Planck's constant equal to 2π, and adopting the second as the unit of time, completes the definition of units.

Let $u_j(i)$ denote the unperturbed wave function of the jth electron having quantum numbers n^i, l^i, m^i, and s^i.

Let

$$\phi(A)=(n!)^{-\frac{1}{2}}\begin{vmatrix} u_1(a) & \cdots & u_n(a)\\ u_1(c) & \cdots & u_n(c)\\ u_1(d) & \cdots & u_n(d)\\ u_1(n) & \cdots & u_n(n)\end{vmatrix}.$$

Let

$$\phi(B)=(n!)^{-\frac{1}{2}}\begin{vmatrix} u_1(\alpha) & \cdots & u_n(\alpha)\\ u_1(\nu) & \cdots & u_n(\nu)\end{vmatrix},$$

and suppose that several rows of $\phi(B)$ appear also in $\phi(A)$, though they need not be corresponding rows. By $\phi(B')$ is denoted the expression derived by permuting the rows of $\phi(B)$ so that rows common to $\phi(B)$ and $\phi(A)$ are in corresponding positions.

Thus

$$\phi(B')=(n!)^{-\frac{1}{2}}\begin{vmatrix} u_1(a) & \cdots & u_n(a)\\ u_1(\gamma) & \cdots & u_n(\gamma)\\ u_1(\delta) & \cdots & u_n(\delta)\\ u_1(n) & \cdots & u_n(n)\end{vmatrix},$$

which is row for row identical with $\phi(A)$, except that rows $u_1(\gamma)\cdots u_n(\gamma)$, $u_1(\delta)\cdots u_n(\delta)$, etc., differ from $u_1(c)\cdots u_n(c)$, $u_1(d)\cdots u_n(d)$, etc., as they must since they pertain to quantum numbers not common to $\phi(B)$ and $\phi(A)$. Clearly,

$$\phi(B)=(-1)^t\phi(B'),$$

where t denotes the number of interchanges required to bring $\phi(B)$ to $\phi(B')$.

The perturbation is seen to consist of terms of type $G=\sum_{i<j}g_{ij}$ and of type $F=\sum_i f_i$. Slater's treatment[1] shows that[2]

$$\begin{aligned}(A/G/B)&=\textstyle\sum_{c<d}\left[(cd/g/cd)-(cd/g/dc)\right]\text{ if }\phi(B')=\phi(A)\\ &=(-1)^t\textstyle\sum_c\left[(cd/g/c\delta)-(cd/g/\delta c)\right]\text{ if }\phi(B')\\ &\quad\text{and }\phi(A)\text{ differ by one row }(\delta\neq d)\\ &=(-1)^t\left[(cd/g/\gamma\delta)-(cd/g/\delta\gamma)\right]\text{ if }\phi(B')\text{ and}\\ &\quad\phi(A)\text{ differ by two rows }(\gamma\neq c;\ \delta\neq d)\\ &=0\text{ if }\phi(B')\text{ and }\phi(A)\text{ differ by more than two}\\ &\quad\text{rows.}\\ (A/F/B)&=\textstyle\sum_c(c/f/c)\text{ if }\phi(B')=\phi(A)\\ &=(-1)^t(d/f/\delta)\text{ if }\phi(B')\text{ and }\phi(A)\text{ differ by one}\\ &\quad\text{row }(\delta\neq d)\\ &=0\text{ if }\phi(B')\text{ and }\phi(A)\text{ differ by more than one}\\ &\quad\text{row.}\end{aligned}$$

Since L_z, L^2, S_z, and S^2 commute with the hamiltonian, the wave functions may be chosen to be single expressions of the type $\phi(A)$.

The energy of the ground state is given (to third order of Rayleigh-Schroedinger perturbation) by

$$E\cong H_{00}+H_{00}'+\sum_k'\frac{H_{0k}'H_{k0}'}{H_{00}-H_{kk}}+\left[\sum_k'\sum_n'\frac{H_{0k}'H_{kn}'H_{n0}'}{(H_{00}-H_{kk})(H_{00}-H_{nn})}-H_{00}'\sum_k'\frac{H_{0k}'H_{k0}'}{(H_{00}-H_{kk})^2}\right]\quad(1)$$

where the subscript 0 refers to the ground state, while

* Extract from dissertation submitted to Leland Stanford, Jr., University, in partial fulfillment of requirement for degree of Doctor of Philosophy.

† The writer is indebted to his employer, The Defence Research Board of Canada, for generous financial support without which his studies at Stanford University would have been impossible. Present address: Experimental Station, Suffield, Alberta, Canada.

[1] Development follows as closely as possible notation of E. U. Condon and G. H. Shortley, *Theory of Atomic Spectra* (Cambridge University Press, Cambridge, England, 1935).

[2] $(A/G/B)\equiv\int\cdots\int\phi^*(A)G\phi(B)d\tau_1\cdots d\tau_n$ and $(cd/g/\gamma\delta)\equiv\Sigma_{s_1}\Sigma_{s_2}\int\int\int\int\int\int u_1^*(n^c,\ l^c,\ m^c,\ s^c)u_2^*(n^d,\ l^d,\ m^d,\ s^d)\times g_{12}u_1(n^\gamma,\ l^\gamma,\ m^\gamma,\ s^\gamma)u_2(n^\delta,\ l^\delta,\ m^\delta,\ s^\delta)d\tau_1d\tau_2$ etc., after the Dirac notation.

subscripts $_k$ and $_n$ refer to excited states. It is proposed to estimate the difference in energies between systems in the $1s^22s^22p^6$, $^1S_0$ state, and the corresponding systems with an electron removed, in the $1s^22s^22p^5$, $^2P_{\frac{3}{2}}$ state, by use of this expression. (The configurations $1s^22s^22p^5$ and $1s^22s2p^6$ are degenerate in the unperturbed system; this leads to no complication, however, since these configurations are of opposite parity, while H' is of even parity.) The summations are assumed to converge. Since $\epsilon \ll 1$, contributions from the term $\epsilon \sum_{i<j} p_i \cdot p_j$ are neglected.

For all members of an isoelectronic sequence the various terms in the Rayleigh-Schroedinger expression (1) will differ only by powers of the scale factor $(Z-S)$. Specifically, the energy of any member of an isoelectronic sequence, having nuclear charge Z, is given by an expression of the form,

$$E(Z) \cong A(Z-S)^2+B(Z-S)+C+D(Z-S)^{-1}, \quad (2)$$

where A, B, C, and D (all of which, of course, pertain to the same specific electronic configuration) are finite and independent of Z, and pertain to perturbation contributions of orders zero through three, respectively.

In the simplest of variation treatments, the energy of an atomic system is estimated using, as trial function, an antisymmetric function composed of products of hydrogenic functions for the individual electrons; and the nuclear charge is regarded as the parameter of variation. The first-order perturbation treatment of this paper, with optimum choice of S, is equivalent to such a variation calculation. In the variation calculation of the energy of the ground state, the optimum screening constant S is such that the decrease in the estimate of the binding energy of the system, due to first-order terms in the interelectronic repulsion is $2A(Z-S)S$. (This latter term being the increase in binding energy associated with the increase of nuclear charge from the unperturbed $(Z-S)$ to the actual Z, treating this increase of nuclear charge as an infinitesimal.) But S so determined, is optimum for the estimation of the energy of the entire system; in a neon-like structure the $1s$ electrons will experience a field greater than that due to a nuclear charge $(Z-S)$, while the $2p$ electrons will be less tightly bound.

To obtain the S appropriate to the estimation of the ionization potential, the energies of the interactions of the six $2p$ electrons with the $1s$ and the $2s$ electrons and with one another are calculated; one-sixth of the sum gives an average energy of repulsion per $2p$ electron. S is so chosen that the perturbation of the nuclear charge increases the binding energy of each $2p$ electron to cancel exactly this average energy of repulsion, S again being treated as an infinitesimal. The fact that the field from a nuclear charge $(Z-S)$ fails to approximate closely that experienced by the $1s$ and $2s$ electrons is of minor consequence, since terms not involving the $2p$ electrons will not appear in the expression for the ionization energy.

S is chosen the same for the fluorine configuration as for the neon-like structure, then termwise subtraction of expressions of type (2) appropriate to the $1s^22s^22p^6$ and to the $1s^22s^22p^5$ configurations yields an estimate of the ionization energy $I(Z)$:

$$I(Z) \cong a(Z-S)^2+b(Z-S)+c+d(Z-S)^{-1}. \quad (3)$$

Define

$$Q(Z) \equiv I(Z)-a(Z-S)^2-b(Z-S)$$

and

$$Q'(Z) \equiv c+d(Z-S)^{-1}.$$

$I(Z)$ is known from spectroscopic data for systems isoelectronic with the ground state of neon for $Z \geq 10$; hence, $Q(Z)$ is known for $Z \geq 10$. The constants c and d are evaluated by setting $Q'(10)=Q(10)$ and $Q'(11)=Q(11)$. Using the values of c and d so determined, $Q'(12)$ and $Q'(13)$ are calculated; it is found that these approximate $Q(12)$ and $Q(13)$ so closely that one sets $Q'(9) \cong Q(9)$ with considerable confidence. The estimate of the electron affinity of fluorine is then determined from

$$I(9) \cong Q'(9)+a(9-S)^2+b(9-S).$$

The spin-orbit interaction is excluded from the hamiltonian deliberately—for when this is present the contribution to the nth order of perturbation is no longer proportional to $(Z-S)^{2-n}$. To compensate for this omission the spectroscopic term values must be referred to the center of gravity of the multiplet, for purpose of determining $I(Z)$.

DETAILS OF CALCULATION

From the theory of the hydrogen atom it is evident that

$$a=0.125000.$$

It is readily seen that b must satisfy

$$b(Z-S)=-2J(2p, 1s)-2J(2p, 2s)-4J(2p_x, 2p_z) -J(2p_z, 2p_z)+K(2p, 1s)+K(2p, 2s) +2K(2p_x, 2p_z)+S(2p_z/r^{-1}/2p_z),$$

where $J(2p, 1s)$ denotes the direct integral $(2p, 1s/r_{ij}^{-1}/2p, 1s)$ and $K(2p, 1s)$ denotes the exchange integral $(2p, 1s/r_{ij}^{-1}/1s, 2p)$ etc. Substituting termwise, we have

$$b=-2(0.242798)-2(0.162109)-4(0.174609) -0.195703+0.017070+0.029297 +2(0.010547)+0.250000S.$$

Similarly, S is determined from

$$12J(2p, 1s)+12J(2p, 2s)+12J(2p_x, 2p_z) +3J(2p_z, 2p_z)-6K(2p, 1s)-6K(2p, 2s) -6K(2p_x, 2p_z)-6S(2p_z/r^{-1}/2p_z)=0,$$

i.e.,

$$12(0.242798)+12(0.162109)+12(0.174609) +3(0.195703)-6(0.017070)-6(0.029297) -6(0.010547)-1.500000S=0.$$

From these one finds

$$S=4.799878,$$
$$b=-0.436522.$$

To convert from term values to the unit of energy herein employed one has only to divide the term value by twice the Rydberg constant appropriate to the system. The spectroscopic term values of the $1s^22s^22p^6$, $^1S_0$ state with respect to the $1s^22s^22p^5$, $^2P_{\frac{3}{2}}$ state for various Z values are tabulated in Table I; also tabulated is one third of the $1s^22s^22p^5(^2P_{\frac{3}{2}}-^2P_{\frac{1}{2}})$ separation.[3] These must be added to give the term value from which $I(Z)$ is obtained.

By substituting for a, b, S, and $I(Z)$, the value of $Q(Z)$ is determined. Table II presents the details of the calculation; $Q'(Z)$ is identified with $Q(Z)$ at $Z=10$ and 11; $Q'(12)$ and $Q'(13)$ are included for comparison with $Q(12)$ and $Q(13)$. $Q(12)$ and $Q(13)$ straddle the $Q'(Z)$ line and the agreement is within the accuracy of the term values used to evaluate $Q(12)$ and $Q(13)$.

Estimating from column $(Z=9)$, $I(9)\cong 0.11679$. Converting this to wave numbers, and subtracting one third of the doublet separation in F spectrum, one obtains a term value corresponding to 72.86 kcal/g atom for the electron affinity of fluorine.

It is not a straightforward matter to assign a probable error to this estimate. It will be noted that, in estimating the electron affinity, relativistic effects have been ignored. The Thomas term has, of course, been taken into account in referring the term value to the center of gravity of the multiplet. The term in $\partial\phi/\partial r$ of the Dirac hamiltonian affects the energy levels of the s states only, for first-order perturbation of a coulomb potential. Consequently, the only neglected term is that corresponding to the relativistic mass correction. Inclusion of this term as a perturbation, increases the estimate of the affinity of fluorine by less than 1 kcal/g atom. If any systematic error is anticipated, surely this will be a tendency to overestimate the electron affinity, since the extrapolation formula is singular at $Z=4.799878$. The writer believes the electron affinity of fluorine to be 73 ± 3 kcal/g atom.[4]

THE INFERRED DISSOCIATION ENERGY OF FLUORINE

Mayer and Helmholz[5] have applied the Born-Haber cycle to the estimation of electron affinities of the halogens. They assert that their calculated values of lattice energies are reliable to ±3 kcal/mole; since the principal source of error in the thermochemical cycle lies in the lattice energy this is probably the error that should be assigned to the cycle. The excellent agreement between the directly measured affinities of chlorine,[6] bromine,[7] and iodine[8] and the estimates by Mayer and Helmholz suggest that this is indeed the case.

Accepting this accuracy, and assuming the electron affinity of fluorine to be 73 ± 3 kcal/g atom, the inferred dissociation energy of fluorine would be about 18 ± 12 kcal/mole.

An excellent review of the existing state of confusion on the thermochemistry of fluorine and related compounds as they affect the estimation of the dissociation energy of fluorine is due to Evans *et al.*[9] They conclude "that the experimental data *at present available* as a whole indicate strongly a value for $D(F_2)$ of about 37 kcals g mole^{-1}, certainly not greater than about 45 kcals g mole^{-1}." Their recommendation of 37 ± 8 kcal/mole is barely compatible with the estimate of this paper.

More recently Schumacher[10] has reported that, on the assumption that the complete dissociation of fluorine oxide requires approximately twice the energy of dissociation of one fluorine atom, the energy for complete dissociation of fluorine oxide is 81 ± 6 kcal/mole. The heat of formation of fluorine oxide he gives as -7 ± 2 kcal/mole. The inferred dissociation energy of fluorine is 30 ± 8 kcal/mole.

Note added in proof:—In a letter to this Journal (J. Chem. Phys. **19**, 1070 (1951), Doescher reports an experimental determination of the heat of dissociation of fluorine. His results indicate that the error in the calculated lattice energy for alkali fluorides together with the error in the writer's estimate of the electron affinity of fluorine must be about 10 kcal/mole rather than 6 kcal/mole as the writer had estimated.

TABLE I. Spectroscopic data for the determination of $I(Z)$.

Z	$(^1S_0-^2P_{3/2})$ cm^{-1}	$\frac{1}{3}(^2P_{3/2}-^2P_{1/2})$ cm^{-1}	$I(Z)$
9		135	
10	173930	261	0.793694
11	381528	455	1.740483
12	646364	742	2.948497
13	967783	1147	4.414860

TABLE II. Parameters in Eq. (3) for isoelectronic series.

	$Z=9$	$Z=10$	$Z=11$	$Z=12$	$Z=13$
$I(Z)$	?	0.79369	1.74048	2.94850	4.41486
$-a(Z-S)^2$	−2.20513	−3.38016	−4.80519	−6.48022	−8.40525
$-b(Z-S)$	1.83345	2.26997	2.70649	3.14301	3.57953
$Q(Z)$	?	−0.31650	−0.35822	−0.38871	−0.41086
$Q'(Z)$*	−0.25489	−0.31650	−0.35822	−0.38838	−0.41117

* $c=-0.57527$; $d=1.34563$.

[3] Taken from R. F. Bacher and S. Goudsmit, *Atomic Energy States* (McGraw-Hill Book Company, Inc., New York, 1932), and from *Annual Tables of Physical Constants and Numerical Data* (Frick Chemical Laboratory, Princeton, New Jersey, 1942). This latter source contains a typographical error in that the term values for Na II are stated to be with respect to $^2P_{\frac{3}{2}}$ state of Na III, while in fact they are referred to the $^2P_{\frac{3}{2}}$ ground state of Na III, as is apparent from a paper by J. E. Mack and R. A. Sawyer, Phys. Rev. **35**, 299 (1930).

[4] Discussed more fully in writer's dissertation, "On the Electron Affinity of Fluorine—an Estimate of the Electron Affinity with a Discussion of the Inferred Dissociation Energy," Stanford University, 1951.

[5] J. E. Mayer and L. Helmholz, Z. Physik. **75**, 19 (1932).

[6] McCallum and Mayer, J. Chem. Phys. **11**, 56 (1943).

[7] Weissblatt, dissertation, The Johns Hopkins University, Baltimore, Maryland, 1938.

[8] Sutton and Mayer, J. Chem. Phys. **3**, 20 (1935).

[9] Evans, Warhurst, and Whittle, J. Chem. Soc., 1524 (June 1950).

[10] H. J. Schumacher, Chem. Abstracts **45**, 2300^b (1951).

THE JOURNAL OF CHEMICAL PHYSICS VOLUME 19, NUMBER 11 NOVEMBER, 1951

The Ultraviolet Absorption Spectra of Gaseous Diazomethane and Diazoethane. Evidence for the Existence of Ethylidine Radicals in Diazoethane Photolysis

R. K. Brinton and D. H. Volman
Department of Chemistry, University of California, Davis, California
(Received August 23, 1951)

The absorption of gaseous diazoethane begins at about 5400A, increases to a broad maximum of $\epsilon=3.5$ at 4500A and falls to a minimum of $\epsilon=0.15$ at 3200A. At wavelengths shorter than 3000A a second region of rapidly increasing absorption is found. The absorption curve of diazomethane is similar in general shape to this curve but shifted somewhat toward shorter wavelengths. The absorption of diazoethane is continuous over its entire region while in the visible region diazomethane shows a number of broad and very diffuse bands from about 4300A to 3200A which probably overlie a continuum. The presence of 2-butene in the photolysis products of diazoethane is explained by the combination of ethylidine radicals formed by the primary photochemical process

$$CH_3CHN_2+h\nu\rightarrow CH_3CH+N_2.$$

A DETERMINATION of the gaseous ultraviolet and visible absorption spectra of diazomethane and diazoethane has been made as a preliminary to the investigation of the photolysis of diazoethane. The quantitative evaluation of the spectra was carried out similar to the method employed by Blacet, Young, and Roof.[1] A Bausch and Lomb large littrow spectrograph with interchangeable glass and quartz optics was used to take nine photographic plates covering the room temperature (about 27°C) absorption of the two compounds from 2500 to 6000A. The diazoalkanes were introduced into a silica cell with plane parallel windows which was in the almost parallel light beam from a Beckman hydrogen discharge or an incandescent lamp. Cell lengths of 25 cm and 56 cm and diazoalkane pressures from 5 mm to 200 mm of mercury were used. Each plate was calibrated by recording a series of exposures in which the source intensity was reduced to different fraction transmissions with moving calibrated screens interposed in the light path. A reference spectrum from a mercury arc was used for wavelength calibration. Tracings made by a Henson[2] recording microphotometer of both the intensity calibrations and the absorption spectra were used to calculate the molecular extinction coefficients from the equation

$$\epsilon=1/cl\,\log_{10}I_0/I,$$

where c is expressed in moles/liter and l in cm. These coefficients are plotted as a function of wave number in Fig. 1.

The similar spectra of the two compounds consisting of a visible region of moderate absorption followed by an ultraviolet region of rapidly increasing absorption compare well in general form to the gaseous diazomethane spectrum determined by Kirkbride and Norrish[3] and the absorption of both compounds in cyclohexane solution given by Adamson and Kenner.[4]

The absorption of diazoethane was continuous in both the visible and ultraviolet regions. Atlhough careful observation of the diazomethane spectrographic plates seemed to indicate continuous absorption also, the microphotometer tracings showed a number of very weak, broad, and diffuse bands between 4300 and 3200A which appeared to overlie a continuum. The series of eight diffuse bands found by Kirkbride and Norrish between 4710 and 4250A could not be detected by either careful visual inspection of the plates or from the microphotometer tracings. In addition, the extinction coefficients given by Kirkbride and Norrish are about double those determined in the present study. It is believed that these differences could possibly be explained by the presence of impurities in the diazomethane used by Kirkbride and Norrish. In our study the diazoethane prepared by the action of sodium cyclohexoxide on N-nitroso-β-ethylaminoisobutyl methyl ketone in cyclohexanol solvent[4] had to be carefully purified by repeated distillation in order to remove impurities which caused significant differences in the absorption curve. Diazomethane prepared by reacting aqueous sodium hydroxide and nitrosomethyl urea[5] in di-*n*-butyl ether solvent seemed to contain negligible amounts of impurities.

The presence of radicals in the low temperature pyrolysis[6] and the ultraviolet photolysis[6,7] of diazoethane has been indicated by the removal of metallic mirrors. The similarity of the absorption of diazoethane and diazomethane could well indicate that the primary photochemical reactions of the two compounds are

$$CH_2N_2+h\nu\rightarrow CH_2+N_2 \quad (1)$$

$$CH_3CHN_2+h\nu\rightarrow CH_3CH+N_2. \quad (2)$$

[1] Blacet, Young, and Roof, J. Am. Chem. Soc. **59**, 608 (1937).
[2] Leighton, Smith, and Henson, Rev. Sci. Instr. **5**, 431 (1934).
[3] F. W. Kirkbride and R. G. W. Norrish, J. Chem. Soc. **1933**, 119 (1933).
[4] D. W. Adamson and J. Kenner, J. Chem. Soc. **1937**, 1551 (1937).
[5] Newer Methods of Preparative Organic Chemistry (Interscience Publishers, Inc., New York, 1948), p. 564.
[6] Barrow, Pearson, and Purcell, Trans. Faraday Soc. **35**, 880 (1935).
[7] Volman, Leighton, Blacet, and Brinton, J. Chem. Phys. **18**, 203 (1950).

Study[3,8,9] of the reaction kinetics and the ultimate products from the first of these reactions seems to establish the occurrence of methylene radicals of appreciable stability. If the radicals causing the mirror removal observed in the diazoethane photolysis are ethylidine radicals of some stability, the reaction products should include compounds resulting from combination of this radical

$$2CH_3CH \rightarrow CH_3CHCHCH_3 \qquad (3)$$

or reactions of ethylidine with other molecules in the mixture.

Several gas phase photolyses of diazoethane at about 200 mm pressure were run almost to completion. The unfiltered light of a Hanovia-Type A medium pressure arc was used to irradiate the gas in a cylindrical silica cell. The gaseous reaction products obtained were analyzed by a Consolidated Mass Spectrometer. A typical analysis obtained on basis of nitrogen as 1.00 is $N_2=1.00$, $C_2H_4=0.61$, $CH_3CHCHCH_3=0.06$, $H_2=0.08$, and $C_2H_2=0.06$.

The presence of 2-butene in the products is best explained by the formation and combination of ethylidine radical by reaction (2) and (3). The large amount of ethylene may indicate that a fast rearrangement of this radical occurs

$$CH_3CH \rightarrow C_2H_4 \qquad (4)$$

to give ethylene or that a second primary process

$$CH_3CHN_2 + h\nu \rightarrow C_2H_4 + N_2 \qquad (5)$$

[8] Norrish, Crone, and Saltmarsh, J. Chem. Soc. **1933**, 1533 (1933).

[9] G. B. Kistiakowsky and N. W. Rosenberg, J. Am. Chem. Soc. **72**, 321 (1950).

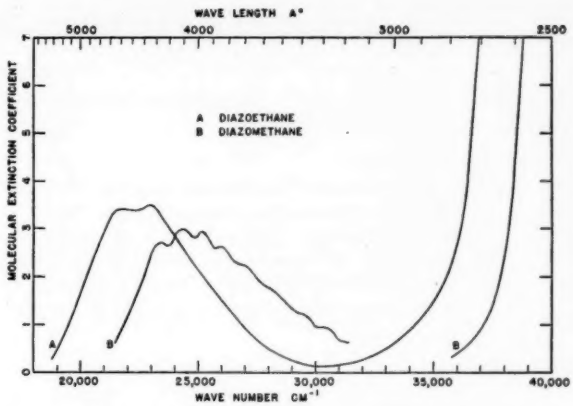

FIG. 1. Absorption spectra of diazoethane and diazomethane.

produces the major products by a direct intramolecular decomposition. The formation of hydrogen and acetylene is probably the result of some related process but more study is needed in order to clarify the actual mechanism.

Further investigation of the photolysis of diazoethane was discontinued because of the hazard from frequent detonations of gas itself and also the liquid even at −180°C. Samples containing impurity were generally stable but the danger of explosion seemed to increase as the purity was enhanced.

The authors wish to express their appreciation to Dr. J. E. Eastmond of the Western Regional Laboratory for the use of the Henson microphotometer, to Dr. Amos Newton and Mr. Laurin Tolman of the Radiation Laboratory, Berkeley, for assistance in the mass spectrometric analyses, and to the Research Corporation for financial aid.

THE JOURNAL OF CHEMICAL PHYSICS VOLUME 19, NUMBER 11 NOVEMBER, 1951

A Note on the Quantum-Mechanical Perturbation Theory*

PER-OLOV LÖWDIN
Department of Physics, Duke University, Durham, North Carolina†

(Received July 23, 1951)

The solution of the quantum-mechanical eigenvalue problem is discussed for cases when a series of approximate eigenfunctions is known. If these "unperturbed" states are divided into two classes, a perturbation formula is derived giving the influence of one class of states on the other in the final solution. The formula contains as special cases: (i) the Schrödinger-Brillouin formula for the eigenvalue of a nondegenerate state, (ii) a new simple formula for treating a class of degenerate states, and (iii) the splitting of the secular equation in cases where the system naturally consists of two independent parts in mutual interaction.

1. INTRODUCTION

ONE of the most important tools for treating the fundamental quantum-mechanical eigenvalue problem

$$H\psi=\mathfrak{E}\psi \tag{1}$$

is the perturbation method due to Schrödinger.[1] In its conventional form, the operator H has the form $H=H_0+V$, and, for the derivation of the perturbation formulas, it is usually assumed[2] that V can be expressed as a power series in a perturbation parameter λ. Another type of derivation of these formulas has been given by Lennard-Jones[3] and by Brillouin,[4] who used the secular equation and the theory of bordered determinants. Here we will show that a still simpler treatment of the perturbation theory can be given by using the system of linear equations[5] corresponding to the secular equation. Dividing the given "unperturbed" states into two classes, we will derive a formula which explicitly gives the influence of one class of states on the other in the final solution of (1). As special cases we will obtain the Schrödinger-Brillouin formula[4] for the eigenvalue of a nondegenerate state, a new formula for the treatment of a class of degenerate states, and finally a formula for the splitting of the secular equation for a system which naturally consists of two independent parts in mutual interaction. Even if these formulas are here derived mainly for the application in the theory of molecules, they may be useful in other parts of quantum mechanics.

* Work supported by the ONR, under Contract N6ori-107, Task Order I, with Duke University.

† Permanent address: Institute of Mechanics and Mathematical Physics, University of Uppsala, Uppsala, Sweden.

[1] E. Schrödinger, Ann. Physik (4) **80**, 437 (1926).

[2] See, for instance, Pauling and Wilson, *Introduction to Quantum Mechanics* (McGraw-Hill Book Company, Inc., New York, 1935); Kemble, *Principles of Quantum Mechanics* (McGraw-Hill Book Company, Inc., New York, 1937); Mott and Sneddon, *Wave Mechanics and its Applications* (Oxford University Press, Oxford, 1948).

[3] J. E. Lennard-Jones, Proc. Roy. Soc. (London) **129**, 604 (1930).

[4] L. Brillouin, J. Phys. radium (7) **3**, 373 (1932). See also E. Wigner, Math. naturw. Anz. ungar. Akad. Wiss. **53**, 477 (1935).

[5] This idea has previously been used for special purposes by E. Gora, Z. Physik **120**, 121 (1942–43) and by H. Feshbach, Phys. Rev. **74**, 1548 (L), (1948).

2. THE VARIATIONAL PRINCIPLE

Here we will not restrict the Hermitian operator H to having any special form, and we will only assume that we know a system of orthonormalized functions $\psi_n^{(0)}$ $(n=1, 2, \cdots N)$, which are *approximate* eigenfunctions of H. This system may be finite or infinite, but it must not necessarily be complete.[6] We will then investigate the *best* eigenfunctions of H which can be formed by linear combinations of the given functions:

$$\psi=\sum_{n=1}^{N}\psi_n^{(0)}c_n. \tag{2}$$

For this purpose we introduce the matrix elements of the total operator H with respect to the given set:

$$H_{mn}=\int\psi_n^{*(0)}H\psi_n^{(0)}d\tau. \tag{3}$$

The coefficients c_n can now be determined by the variational principle, which says that the integral

$$E=\int\psi^*H\psi d\tau\Big/\int\psi^*\psi d\tau$$

$$=\sum_{mn}c_m^*H_{mn}c_n/\sum_{mn}c_m^*\delta_{mn}c_n \tag{4}$$

gives an approximate value of $\mathfrak{E}$, and that the best approximation is obtained when $\delta E=0$. If $E=A/B$, we have $\delta E=(\delta A-E\delta B)/B$, which, for the coefficients c_n, gives the system of linear equations:

$$\sum_{n=1}^{N}(H_{mn}-E\delta_{mn})c_n=0, \quad m=1, 2\cdots N. \tag{5}$$

The condition for the existence of a non-trivial solution of (5) is $\mathrm{Det}(H_{mn}-E\delta_{mn})=0$, an equation previously used by Lennard-Jones[3] and by Brillouin.[4] Here we will instead base our treatment directly on the linear system (5).

[6] This is of special importance in the theory of molecules, where, for instance in the MO-LCAO-method, we usually know only a few approximate wave functions.

3. A PERTURBATION FORMULA FOR THE MUTUAL INFLUENCE OF TWO CLASSES OF STATES

Let us assume that, in some definite way, we have divided the series of indices n of $\psi_n^{(0)}$ into two classes, (A) and (B). Let us for a moment be mainly interested in the class (A), and let us try to derive a formula by means of which we can treat the influence of the states in (B) as a perturbation. The system (5) can be written

$$(E-H_{mm})c_m=\sum_n^A H_{mn}'c_n+\sum_n^B H_{mn}'c_n, \tag{6}$$

if the sign $'$ on a matrix means that we omit all diagonal elements, so that $H_{mn}'=H_{mn}(1-\delta_{mn})$. Using the notation

$$h_{mn}=H_{mn}/(E-H_{mm}), \tag{7}$$

we get then

$$c_m=\sum_n^A h_{mn}'c_n+\sum_n^B h_{mn}'c_n. \tag{8}$$

We will now eliminate the states in the class (B) by a process of iteration, expressing the coefficients c in all sums exclusively over B by the formula (8) itself. In this way we obtain the formal expansion

$$c_m=\sum_n^A (h_{mn}'+\sum_\alpha^B h_{m\alpha}'h_{\alpha n}'+\sum_{\alpha\beta}^B h_{m\alpha}'h_{\alpha\beta}'h_{\beta n}'+\cdots)c_n. \tag{9}$$

Introducing the new notation

$$U_{mn}{}^A=H_{mn}+\sum_\alpha^B \frac{H_{m\alpha}'H_{\alpha n}'}{E-H_{\alpha\alpha}} +\sum_{\alpha\beta}^B \frac{H_{m\alpha}'H_{\alpha\beta}'H_{\beta n}'}{(E-H_{\alpha\alpha})(E-H_{\beta\beta})}+\cdots \tag{10}$$

we get

$$c_m=\sum_n^A \frac{U_{mn}{}^A-H_{mn}\delta_{mn}}{E-H_{mm}}c_n. \tag{11}$$

For the two cases of m in (A) or (B), we have, therefore, the two basic formulas

$$\begin{cases} \sum_n^A (U_{mn}{}^A-E\delta_{mn})c_n=0, & m \text{ in } (A). \qquad (12) \\ c_m=\sum_n^A \dfrac{U_{mn}{}^A}{E-H_{mm}}c_n, & m \text{ in } (B). \qquad (13) \end{cases}$$

The first formula is formally identical to (5), but it is limited only to the class (A). This gives the theorem:

An eigenvalue problem (5) with respect to a system of states belonging to two classes, (A) and (B), can be reduced only to the class (A), if the matrix elements H_{mn} are replaced by the elements $U_{mn}{}^A$, where the influence of the class (B) is taken into account by expansion (10).

When the coefficients c_n belonging to (A) have been determined, we get the coefficients c_n belonging to (B) according to (13).

We note that series (10) is here only formally derived and that, when the series is interrupted after a finite number of terms, there is a remainder containing sums exclusively over (B). A necessary condition for the validity of (10) is therefore that, for the value of E under consideration and for m and n in (B), the matrix elements h_{mn}' are small in comparison to the unity:

$$|H_{mn}'/(E-H_{mm})|\ll 1. \tag{14}$$

The problem of the convergency of (10) remains still to be investigated.

Matrix elements of the type (10), where the summation is carried out only over a restricted number of states, have previously been considered by Feenberg[7] in his perturbation formulas without repetitive elements. It may be noted that even his formulas can simply be derived by using (5), as has been shown by Feshbach.[5] Here we will now consider some special cases of (10), (12), and (13) in greater detail.

(i) (A) = Single Nondegenerate State k

In the case the whole class (A) consists of a single nondegenerate state, the whole system (5) is reduced to a single term, and the secular equation takes the form

$$U_{kk}{}^k-E=0. \tag{15}$$

According to (10) this gives for our approximate eigenvalue $E=E_k$

$$E=U_{kk}{}^k=H_{kk}+\sum_{\alpha\neq k}\frac{H_{k\alpha}'H_{\alpha k}'}{E-H_{\alpha\alpha}} +\sum_{\alpha,\beta\neq k}\frac{H_{k\alpha}'H_{\alpha\beta}'H_{\beta k}'}{(E-H_{\alpha\alpha})(E-H_{\beta\beta})}+\cdots. \tag{16}$$

This formula was first derived in another way by Brillouin,[4] and we note that E can be computed by iteration. If we introduce the conventional form $H=H_0+V$, we have

$$H_{mn}=\begin{cases} H_{mm}{}^{(0)}+V_{mm} & \text{for } m=n \\ V_{mn} & \text{for } m\neq n. \end{cases} \tag{17}$$

Putting these expressions into (16), using iteration, and developing the right-hand member in a power-series in V_{mn}, we obtain the well-known perturbation formulas first given by Schrödinger.[1] In this way not only the first- and second-order terms but even the third- and fourth-order terms[8] can be easily derived. However, we note that in general it has been recommended

[7] E. Feenberg, Phys. Rev. **74**, 206, 664 (1948).

[8] The explicit form of the third- and fourth-order terms in Schrödingers theory may be found, e.g., in K. F. Niessen, Phys. Rev. **34**, 253 (1929).

to use formula (16) instead of the original Schrödinger formula, since (16) is simpler and seems to have better convergence properties. Equation (13) gives directly the best form of the corresponding eigenfunction.

(ii) (A) = Class of Degenerate States

Let us now consider the case that the eigenvalue problem (1) shows a degeneracy. This means here that a class of diagonal elements H_{kk} are exactly or almost the same, i.e.,

$$H_{kk} \approx E_A \tag{18}$$

but for quantities of the first or higher orders. In the conventional theory it is recommended to treat the degeneracy by performing linear transformations of the approximate wave functions $\psi_n^{(0)}$ in such a way that the matrix H becomes *diagonal* with respect to the class of degenerate states, whereafter the ordinary perturbation formulas can be applied. This means that

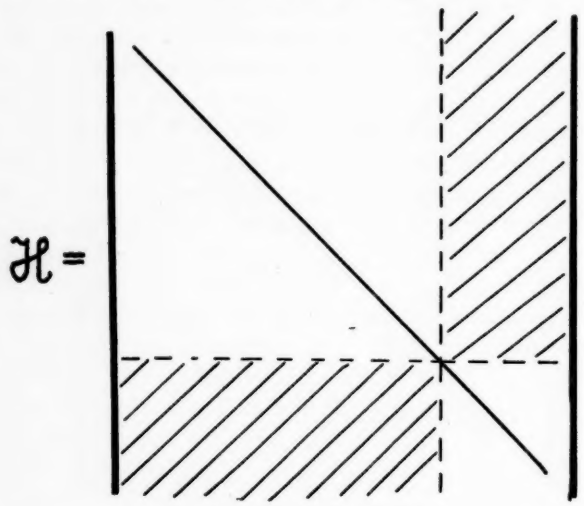

FIG. 1. Form of the matrix.

one first removes the degeneracy and then treats the perturbation problem. This theoretically simple procedure can often be rather complicated in the applications,[9] and considerable simplifications have therefore been worked out by Van Vleck.[10]

The general process described in this paper gives another method of treating the degeneracy in a very simple and natural way. It takes things in the reverse order: first the perturbation problem, i.e., the influence of the states not belonging to the degenerate class under consideration, is treated according to formula (10), and then the degeneracy is removed by solving the secular equation corresponding to the system (12). For the latter step only algebraic methods are, in general, available. The coefficients c_n for the states in (A) are determined from the linear system (12), and, finally, the remaining coefficients are found by using (13).

The second-order approximation takes a particularly simple form in the method given here. According to (18) we have $E \approx E_A$, but for quantities of the first and higher orders, and in the second-order approximation, (10) gives therefore

$$U_{mn}^A = H_{mn} + \sum_{\alpha}^{B} \frac{H_{m\alpha}' H_{\alpha n}'}{E_A - H_{\alpha\alpha}}. \tag{19}$$

Since all these matrix elements are numerically given, the secular equation corresponding to (12) can be directly solved without any iterations. We have applied this method to the treatment of the one-electron wave functions in the MO-LCAO-theory of conjugated organic compounds; the results will be published elsewhere.

(iii) (A) = Class of Arbitrary States

Let us for a moment assume that the system has naturally or arbitrarily been divided into two classes, (A) and (B), and that k is a nondegenerate state in (A). According to (10) we can first eliminate the system (B), and using (16) we can then solve the perturbation problem (12). For the approximate eigenvalue $E = E_k$ we get in this way

$$E = U_{kk}^A + \sum_{\alpha \neq k}^{A} \frac{U_{k\alpha}^A U_{\alpha k}^A}{E - U_{\alpha\alpha}^A} + \sum_{\alpha\beta \neq k}^{A} \frac{U_{k\alpha}^A U_{\alpha\beta}^A U_{\beta k}^A}{(E - U_{\alpha\alpha}^A)(E - U_{\beta\beta}^A)} + \cdots. \tag{20}$$

Since the result must be the same as in (16), formula (20) gives one of the possible ways of *regrouping* the terms in (16); compare reference 7.

Finally we will treat the case that our system naturally consists of two independent parts (A) and (B) in mutual interaction. We will assume that the wave functions $\psi_n^{(0)}$ have been chosen in such a way that the matrix H is diagonal with respect to (A) and (B), respectively (see Fig. 1). Since the elements $H_{\alpha\beta}'$, for α and β both in (B), are then vanishing, the expansion (10) reduces exactly to its first two terms:

$$U_{mn}^A = H_{mn} + \sum_{\alpha}^{B} \frac{H_{m\alpha}' H_{\alpha n}'}{E - H_{\alpha\alpha}}. \tag{21}$$

It is also easily checked that the remainder in (9) vanishes.

As an application we will consider a problem in the MO-LCAO-theory of conjugated compounds, let us say a mono-substituted benzene. Let H be the one-electron Hamiltonian for the π-electrons and let ψ be the MO formed by LCAO from the six benzene π-orbitals

[9] For a detailed description see, for instance, Kemble, *Principles of Quantum Mechanics* (McGraw-Hill Book Company, Inc., New York, 1937).

[10] J. H. Van Vleck, Phys. Rev. **33**, 467 (1929); O. M. Jordahl, Phys. Rev. **45**, 87 (1934).

$\psi_1^{(0)}$, $\psi_2^{(0)}$, $\cdots\psi_6^{(0)}$, and the π-orbital $\psi_7^{(0)}$ of the substituent. The matrix H has then the form:

$$H=\begin{vmatrix} H_{11} & 0 & \cdot & & |H_{17} \\ 0 & H_{22} & \cdot & & |H_{27} \\ \cdot & \cdot & H_{33} & & |H_{37} \\ & & & \cdot & |\ \cdot \\ & & & \cdot & \cdot \\ & & & H_{66} & |H_{67} \\ \hline H_{71} & H_{72} & H_{73}\cdots H_{76} & & |H_{77} \end{vmatrix}$$

The secular equation has been treated in the first approximation in the wave functions by Sklar[11] and by Herzfeld,[12] and recently Matsen,[13] using conventional perturbation theory, has shown that, for instance, E_7 is given by:

$$E_7=H_{77}+\sum_{i=1}^{6}\frac{|H_{7i}|^2}{H_{77}-H_{ii}}. \tag{22}$$

This perturbation theory breaks down when H_{77} is close in value to any of the H_{ii}.[14]

However, if we here apply formula (10) to a class (A) consisting of the only state 7, we get directly without any approximation:

$$E=H_{77}+\sum_{i=1}^{6}\frac{H_{7i}H_{i7}}{E-H_{ii}}, \tag{23}$$

a formula which holds even when (22) breaks down. The energy E can be found by iteration, and we note that even the derivatives of E, which are of importance, e.g., in calculating the charge distribution, can be found by implicit derivation. This example shows that the methods developed here may be useful in the theory of molecules.

Since Eq. (23) must be *exactly* contained in the secular equation $\mathrm{Det}(H_{mn}-E\delta_{mn})=0$, there must exist a more elementary way of finding this relation from the determinant itself. This problem will be treated in the next section.

4. THE CONNECTION WITH THE THEORY OF BORDERED DETERMINANTS

In the previous section we have treated problems which are closely connected with the theory of bordered determinants. Recently Dewar[15] has given some useful transformations of determinants $\mathrm{Det}(H-E\cdot 1)$ when H has the same form as in Fig. 1. However, the general formula for the expansion of a bordered determinant was given already 1896 by Arnaldi.[16] According to this formula,[17] we obtain directly

$$\begin{vmatrix} H_{11}-E & & & |H_{1,\,n+1}\cdots & H_{1,\,n+p} \\ & H_{22}-E & & |H_{2,\,n+1}\cdots & H_{2,\,n+p} \\ & & \cdot & |\cdots\cdots\cdots\cdots & \\ & & \cdot & | & \\ & & H_{nn}-E & |H_{n,\,n+1}\cdots & H_{n,\,n+p} \\ \hline H_{n+1,\,1} & H_{n+1,\,2}\cdots & H_{n+1,\,n} & |H_{n+1,\,n+1}-E & \\ \cdots\cdots\cdots\cdots & & & | & \\ H_{n+p,\,1} & H_{n+p,\,2}\cdots & H_{n+p,\,n} & | & H_{n+p,\,n+p}-E \end{vmatrix} = \prod_{i}^{A+B}(H_{ii}-E)$$

$$\cdot\left\{1-\sum_{r}^{A}\sum_{s}^{B}\frac{|H_{rs}|^2}{(E-H_{rr})(E-H_{ss})}+\sum_{r_1r_2}^{A}\sum_{s_1s_2}^{B}\frac{\begin{Vmatrix} H_{r_1s_1} & H_{r_1s_2} \\ H_{r_2s_1} & H_{r_2s_2} \end{Vmatrix}^2}{(E-H_{r_1r_1})(E-H_{r_2r_2})(E-H_{s_1s_1})(E-H_{s_2s_2})}-+\cdots\right.$$

$$\left.+(-1)^p\sum_{r_1r_2\cdots r_p}^{A}\sum_{s_1s_2\cdots s_p}^{B}\frac{\begin{Vmatrix} H_{r_1s_1} & H_{r_1s_2}\cdots & H_{r_1s_p} \\ H_{r_2s_1} & H_{r_2s_2}\cdots & H_{r_2s_p} \\ \cdots\cdots & \cdots\cdots & \cdots\cdots \\ H_{r_ps_1} & H_{r_ps_2}\cdots & H_{r_ps_p} \end{Vmatrix}^2}{(E-H_{r_1r_1})(E-H_{r_2r_2})\cdots(E-H_{r_pr_p})}\right\}. \tag{24}$$

[11] A. L. Sklar, J. Chem. Phys. **7**, 984 (1939).
[12] K. F. Herzfeld, Chem. Rev. **41**, 233 (1947).
[13] F. A. Matsen, J. Am. Chem. Soc. **72**, 5243 (1950).
[14] See reference 13, footnote 9.
[15] M. J. S. Dewar, Proc. Cambridge Phil. Soc. **45**, 638 (1949).
[16] M. Arnaldi, Giornale di Mat. Battaglini **34**, 209 (1896).
[17] See, for instance, G. Kowalewski, *Determinantentheorie* (Leipzig, 1909), pp. 89–99, or T. Muir, *Theory of Determinants* (London, 1923), IV, p. 432.

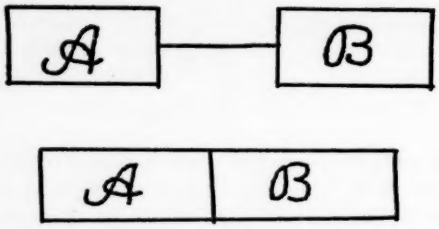

FIG. 2. Schematic diagram of singly or tightly linked molecule parts.

with $r_1<r_2<\cdots<r_p$ and $s_1<s_2<\cdots<s_p$. Formula (24) is given for $p\leq n$, and the sign $\| \ \|$ means that we take the absolute value of a determinant. This relation can also be easily derived by using Laplace's expansion theorem with respect to the first n rows of the given determinant. We note that our formula (23) is contained as a special case for $p=1$; compare also Dewar.[15] Putting the second factor in (24) equal to zero and multiplying the relation with the factor $(E-H_{kk})$, we get again a formula analogous to (16) and (20) but this time containing only a finite number of terms.

If our system is a molecule, the linkage between its two parts is of special interest. Let us as an example consider the one-electron wave functions. The MO ψ is, according to Dewar's terminology, formed by LCMO (=linear combination of molecular orbitals) from the given MO $\psi_m{}^{(0)}$, which again are formed by LCAO from the given atomic orbitals φ_μ:

$$\psi_m{}^{(0)}=\sum_\mu \varphi_\mu a_{\mu m}. \tag{25}$$

Introducing the matrix elements of H with respect to this AO,

$$\mathfrak{H}_{\mu\nu}=\int \varphi_\mu{}^* H \varphi_\nu d\tau \tag{26}$$

we get directly

$$H_{mn}=\sum_{\mu\nu} a_{m\mu}\dagger \mathfrak{H}_{\mu\nu} a_{\nu n} \tag{27}$$

or

$$H=a\dagger \mathfrak{H} a. \tag{28}$$

The last relation gives the MO-matrix H expressed in the AO-matrix $\mathfrak{H}$.

With respect to the atoms, the molecule may now consist of two natural parts ($\mathfrak{A}$) and ($\mathfrak{B}$), which may be separated or which may have atoms in common (see Fig. 2). From the AO in ($\mathfrak{A}$) we will build up the MO in class (A) in such a way that the operator H will be diagonalized; from the AO in ($\mathfrak{B}$) we will then form the MO in class (B) in the same way.† We will further introduce linkage classes $L\mathfrak{A}$ and $L\mathfrak{B}$ by the definition that an AO φ_μ in ($\mathfrak{A}$) belongs to $L\mathfrak{A}$ if, for at least one AO φ_ν in ($\mathfrak{B}$), the matrix element $\mathfrak{H}_{\mu\nu}$ in (26) is essentially different from zero; the class $L\mathfrak{B}$ is defined analogously.

Using a well-known theorem, we can now expand the determinants in (24) in sums of products of determinants of the three factors in (27):

$$\begin{vmatrix} H_{r_1s_1} & H_{r_1s_2}\cdots & H_{r_1s_k} \\ H_{r_2s_1} & H_{r_2s_2}\cdots & H_{r_2s_k} \\ \cdots & \cdots & \cdots \\ H_{r_ks_1} & H_{r_ks_2}\cdots & H_{r_ks_k} \end{vmatrix}$$

$$=\sum_{\mu_1\mu_2\cdots\mu_k}^{L\mathfrak{A}}\ \sum_{\nu_1\nu_2\cdots\nu_k}^{L\mathfrak{B}} \begin{vmatrix} a_{r_1\mu_1}\dagger & a_{r_1\mu_2}\dagger\cdots & a_{r_1\mu_k}\dagger \\ a_{r_2\mu_1}\dagger & a_{r_2\mu_2}\dagger\cdots & a_{r_2\mu_k}\dagger \\ \cdots & \cdots & \cdots \\ a_{r_k\mu_1}\dagger & a_{r_k\mu_2}\dagger\cdots & a_{r_k\mu_k}\dagger \end{vmatrix} \begin{Vmatrix} \mathfrak{H}_{\mu_1\nu_1} & \mathfrak{H}_{\mu_1\nu_2}\cdots & \mathfrak{H}_{\mu_1\nu_k} \\ \mathfrak{H}_{\mu_2\nu_1} & \mathfrak{H}_{\mu_2\nu_2}\cdots & \mathfrak{H}_{\mu_2\nu_k} \\ \cdots & \cdots & \cdots \\ \mathfrak{H}_{\mu_k\nu_1} & \mathfrak{H}_{\mu_k\nu_2}\cdots & \mathfrak{H}_{\mu_k\nu_k} \end{Vmatrix} \begin{vmatrix} a_{\nu_1s_1} & a_{\nu_1s_2}\cdots & a_{\nu_1s_k} \\ a_{\nu_2s_1} & a_{\nu_2s_2}\cdots & a_{\nu_2s_k} \\ \cdots & \cdots & \cdots \\ a_{\nu_ks_1} & a_{\nu_ks_2}\cdots & a_{\nu_ks_k} \end{vmatrix}, \tag{29}$$

where $\mu_1<\mu_2<\cdots<\mu_k$ and $\nu_1<\nu_2<\cdots\nu_k$. The terms in (24) can now be factorized, and, introducing the notations

$$Q^A_{\substack{\mu_1'\mu_2'\cdots\mu_k' \\ \mu_1\mu_2\cdots\mu_k}}=\sum_{r_1r_2\cdots r_k}^{A} \frac{\begin{vmatrix} a_{\mu_1'r_1} & a_{\mu_1'r_2}\cdots & a_{\mu_1'r_k} \\ \cdots & \cdots & \cdots \\ a_{\mu_k'r_1} & a_{\mu_k'r_2}\cdots & a_{\mu_k'r_k} \end{vmatrix} \begin{Vmatrix} a_{r_1\mu_1}\dagger & a_{r_1\mu_2}\dagger\cdots & a_{r_1\mu_k}\dagger \\ \cdots & \cdots & \cdots \\ a_{r_k\mu_1}\dagger & a_{r_k\mu_2}\dagger\cdots & a_{r_k\mu_k}\dagger \end{Vmatrix}}{(E-H_{r_1r_1})(E-H_{r_2r_2})\cdots(E-H_{r_kr_k})},$$

$$Q^B_{\substack{\nu_1\nu_2\cdots\nu_k \\ \nu_1'\nu_2'\cdots\nu_k'}}=\sum_{s_1s_2\cdots s_k}^{B} \frac{\begin{vmatrix} a_{\nu_1s_1} & a_{\nu_1s_2}\cdots & a_{\nu_1s_k} \\ \cdots & \cdots & \cdots \\ a_{\nu_ks_1} & a_{\nu_ks_2}\cdots & a_{\nu_ks_k} \end{vmatrix} \begin{Vmatrix} a_{s_1\nu_1'}\dagger & a_{s_1\nu_2'}\dagger\cdots & a_{s_1\nu_k'}\dagger \\ \cdots & \cdots & \cdots \\ a_{s_k\nu_1'}\dagger & a_{s_k\nu_2'}\dagger\cdots & a_{s_k\nu_k'}\dagger \end{Vmatrix}}{(E-H_{s_1s_1})(E-H_{s_2s_2})\cdots(E-H_{s_ks_k})}, \tag{30}$$

we can write the determinant D in the left-hand side of (24) in the form

† We note that the MO in the total system $(A+B)$ must be chosen in such a way that they are linearly independent.

$$D=\prod_{i}^{A+B}(H_{ii}-E)\cdot\Big\{1-\sum_{\mu\mu'}^{L_{\mathfrak{A}}}\sum_{\nu\nu'}^{L_{\mathfrak{B}}}Q^{A}_{\mu\mu'}\,\mathfrak{H}_{\mu\nu}Q^{B}_{\nu\nu'}\,\mathfrak{H}_{\nu'\mu'}$$

$$+\sum_{\substack{\mu_1\mu_2\\ \mu_1'\mu_2'}}^{L_{\mathfrak{A}}}\sum_{\substack{\nu_1\nu_2\\ \nu_1'\nu_2'}}^{L_{\mathfrak{B}}}Q^{A}_{\mu_1'\mu_2'}{}_{\mu_1\mu_2}\begin{vmatrix}\mathfrak{H}_{\mu_1\nu_1} & \mathfrak{H}_{\mu_1\nu_2}\\ \mathfrak{H}_{\mu_2\nu_1} & \mathfrak{H}_{\mu_2\nu_2}\end{vmatrix}Q^{B}_{\nu_1\nu_2}{}_{\nu_1'\nu_2'}\begin{vmatrix}\mathfrak{H}_{\nu_1'\mu_1'} & \mathfrak{H}_{\nu_1'\mu_2'}\\ \mathfrak{H}_{\nu_2'\mu_1'} & \mathfrak{H}_{\nu_2'\mu_2'}\end{vmatrix}-+\cdots$$

$$+(-1)^{p}\sum_{\substack{\mu_1\mu_2\cdots\mu_p\\ \mu_1'\mu_2'\cdots\mu_p'}}^{L_{\mathfrak{A}}}\sum_{\substack{\nu_1\nu_2\cdots\nu_p\\ \nu_1'\nu_2'\cdots\nu_p'}}^{L_{\mathfrak{B}}}Q^{A}_{\mu_1'\mu_2'\cdots\mu_p'}{}_{\mu_1\mu_2\cdots\mu_p}\begin{vmatrix}\mathfrak{H}_{\mu_1\nu_1} & \mathfrak{H}_{\mu_1\nu_2}\cdots & \mathfrak{H}_{\mu_1\nu_p}\\ \cdots & \cdots & \cdots\\ \mathfrak{H}_{\mu_p\nu_1} & \mathfrak{H}_{\mu_p\nu_2}\cdots & \mathfrak{H}_{\mu_p\nu_p}\end{vmatrix}Q^{B}_{\nu_1\nu_2\cdots\nu_p}{}_{\nu_1'\nu_2'\cdots\nu_p'}\begin{vmatrix}\mathfrak{H}_{\nu_1'\mu_1'} & \mathfrak{H}_{\nu_1'\mu_2'}\cdots & \mathfrak{H}_{\nu_1'\mu_p}\\ \cdots & \cdots & \cdots\\ \mathfrak{H}_{\nu_p'\mu_1'} & \mathfrak{H}_{\nu_p'\mu_2'}\cdots & \mathfrak{H}_{\nu_p'\mu_p'}\end{vmatrix}\Big\}. \tag{31}$$

If the linkage between $(\mathfrak{A})$ and $(\mathfrak{B})$ is of a simple type, this expansion will reduce to a few terms. Formula (31) may be considered as a generalization of the formulas given by Dewar.[15] We note that if the coefficients c_n for the class (A) have been determined, we get directly the coefficients for the class (B) according to (13) and (21):

$$c_m=\sum_{n}^{A}\frac{H_{mn}}{E-H_{mm}}c_n. \tag{32}$$

The example treated here is concerned with the one-electron wave functions, but we wish to emphasize that the general perturbation theory, contained in the formulas (10), (12), and (13), even can be applied to the molecular wave functions.

In conclusion, we wish to remark that, even if the methods described here were partly known previously in connection with special problems, for instance in the radiation theory given by Gora,[5] a general treatment has not yet been published. We have given not only a simple derivation of the conventional perturbation theory, but also a new treatment of the problem of degeneracy and of the general problem of splitting the secular equation.

ACKNOWLEDGMENTS

The author should like to express his sincere gratitude to Professor Hertha Sponer, Department of Physics, Duke University, for many valuable discussions and for the great hospitality he has enjoyed during his stay in Durham, North Carolina.

APPENDIX. SYMBOLIC DERIVATION OF THE BASIC FORMULAS

The right-hand member of (9) is simply a geometrical series in the matrix h' belonging to the class (B), and it is therefore easy to give a sufficient condition for its convergency.[18] The form of the series also indicates that there might exist another simple derivation, and here we will therefore try to give a more direct derivation of (9) by using operator calculus and symbolic expansions.[19]

In order to separate the secular equation $Hc=Ec$ into two parts, we write the quadratic matrix H and the column matrix c in the form

$$H=\begin{bmatrix}A & \beta\\ \beta^* & B\end{bmatrix},\qquad c=\begin{bmatrix}a\\ b\end{bmatrix}, \tag{33}$$

and then we obtain

$$\begin{cases}Aa+\beta b=Ea,\\ \beta^*a+Bb=Eb.\end{cases} \tag{34}$$

Solving b from the latter equation, we get

$$b=\frac{1}{E-B}\beta^*a, \tag{35}$$

and

$$\Big(A+\beta\frac{1}{E-B}\beta^*\Big)a=Ea. \tag{36}$$

If we confine the indices of U^A to the class (A), we have therefore

$$U^Aa=Ea, \tag{37}$$

$$U^A=A+\beta\frac{1}{E-B}\beta^*. \tag{38}$$

It is now immediately seen how the geometrical series in (9) arises. Dividing B in its diagonal and nondiagonal parts, B_d and B', and expanding $(E-B_d-B')^{-1}$ in a power series in B', we obtain

$$U^A=A+\beta\frac{1}{E-B_d}\beta^*+\beta\frac{1}{E-B_d}B'\frac{1}{E-B_d}\beta^*+\cdots, \tag{39}$$

which is nothing but (9). Equation (37) gives then (12), and Eq. (35) gives (13). In this way all our basic formulas are derived.

[18] See, for instance, Courant-Hilbert, *Methoden der Mathematischen Physik*, I (Verlag. Julius Springer, Berlin, 1931), p. 16, footnote 1.

[19] Compare Gora, reference 5. For the symbolic treatment given here, the author is indebted to a discussion with Dr. G. Goertzel, Columbia University.

Excluded Volume Effect in Polymer Chains. I*

H. L. FRISCH† AND F. C. COLLINS, *Department of Chemistry, Polytechnic Institute of Brooklyn, Brooklyn, New York*

AND

B. FRIEDMAN, *Institute of Applied Mathematics and Mechanics, New York University, New York, New York*

(Received June 8, 1951)

The number of allowed configurations of a polymer chain is considered on the basis of a random walk on an arbitrary "regular" lattice. Upper and lower bounds for the number of nonoverlapping configurations in various lattices have been derived by means of a recursion formula method. The probability density function and its moments for the "head-to-tail" distance for short-range nonoverlapping chains are shown to the calculable by the use of a generating function. The order of the logarithm of the number of nonsuperposable ring polymer chains has been shown to be directly proportional to the number of segments composing the ring.

INTRODUCTION

THE elastic behavior of chain polymers and the theory of polymer solutions are strongly dependent on the geometrical configurations assumed by the polymer. The accepted theories of viscoelastic behavior and the theory of solutions of high polymers do not prohibit configurations in which several atoms exist concurrently in the same element of volume. This leads to a greater number of configurations and smaller root-mean-square lengths for such hypothetical polymer models than those of real polymers.

This paper deals with statistical methods for the calculation of the average configurations of polymer chains on regular lattices first treated by Montroll.[1] The present discussion employs the usual random walk method of handling the configurations of N connected segments, and includes the added restriction that the segments may not overlap each other. Configurations of such chains on the planar square, the planar hexagonal, and the diamond lattice have been studied. The calculation of the following quantities have been investigated: (a) The total number of allowed configurations satisfying the nonoverlap restriction for chains of N segments. (b) Root-mean-square "head-to-tail" distance of such chains. (c) The total number of allowed nonsuperposable configurations of simple ring polymers.

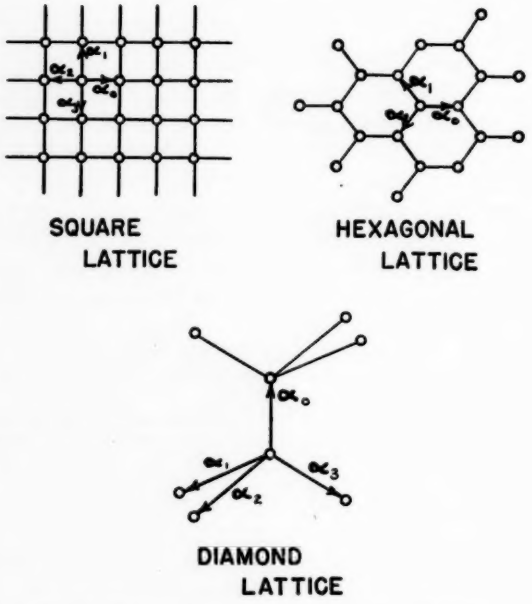

FIG. 1. Vector representations in various lattices.

A general method of calculation has been developed for the number of allowed configurations of N segments which do not overlap in any subsequence of M segments on any regular space lattice. This method has been used in the calculation of the number of configurations on the following lattices: (a) A square lattice with no overlaps in either four or twelve segments, (b) a hexagonal lattice with no overlap in six segments, and (c) a diamond lattice with no overlap in six segments. In addition, a simple method of calculation of a lower bound for the number of configurations of chains with no overlaps is presented. This lower bound may be used in connection with the calculation of the entropy of fusion of normal alkanes.

A distribution function has been derived for the probability of a chain on a square lattice having a given "head-to-tail" distance with no overlaps within fewer than a sequence of twelve segments. The method can be applied in principle to polymer chains which do not overlap throughout their length.

Consider a regular lattice in space, i.e., a tessellation. Choose an arbitrary lattice point as origin, call it 0. Let all points a unit distance away from 0 be called "nearest neighbors." Connect these points to the origin 0 by directed line segments which we will denote by $\alpha_0, \alpha_1, \cdots \alpha_{p-1}$, respectively. Let $\mathbf{w}$ be the transformation which carries α_0 into α_1, $\cdots$, α_{p-2} into α_{p-1}, and α_{p-1} into α_0, i.e.,

$$\mathbf{w}\alpha_0=\alpha_1, \quad \cdots, \quad \mathbf{w}\alpha_{p-2}=\alpha_{p-1}, \quad \mathbf{w}\alpha_{p-1}=\alpha_0$$
$$\mathbf{w}^j\alpha_k=\alpha_{j+k}=\alpha_l;$$

* Part of the dissertation of H. L. Frisch submitted in partial fulfillment of the requirements for the degree of Doctor of Philosophy at the Polytechnic Institute of Brooklyn.

† Dow Chemical Company Research Fellow, 1949–1950.

[1] E. W. Montroll, J. Chem. Phys. 18, 734 (1950).

where $j+k\equiv l(\mathrm{mod}\,p)$. Let $\mathbf{w}^{-1}$ be the inverse to $\mathbf{w}$, i.e.,

$$\alpha_0=\mathbf{w}^{-1}\alpha_1,\quad\cdots,\quad\alpha_{P-2}=\mathbf{w}^{-1}\alpha_{p-1},\quad\alpha_{p-1}=\mathbf{w}^{-1}\alpha_0$$

where $\mathbf{w}\mathbf{w}^{-1}=\mathbf{w}^{-1}\mathbf{w}=\mathbf{1}$ the identity transformation, $\mathbf{1}\alpha_k=\alpha_k\mathbf{1}=\alpha_k$.

Hence,

$$\alpha_l+\alpha_k=\alpha_k+\alpha_l=\mathbf{w}^k\alpha_0+\mathbf{w}^l\alpha_0=\mathbf{w}^k\alpha_0(\mathbf{1}+\mathbf{w}^{l-k}).$$

By a path of n steps from a given origin is meant an open, or closed circuit (polygon), through the points 0, $A_1\cdots A_{n-1}$ where A_1 is a nearest neighbor of 0, $\cdots$ and A_{n-1} a nearest neighbor of A_{n-2}. Such a path is called open if all the A's are distinct, and otherwise is designated as closed or overlap. We can represent any such path $P(n)$ by the sum

$$P(n)=\sum_{i=1}^{n}\sum_{j=1}^{p-1}\epsilon_{ij}\alpha_j$$

where $\epsilon_{ij}=\pm1$, 0, and $\epsilon_{ij}\neq0$ for only one value of j. We shall stipulate that no path retrace its last step. In general for a lattice which has p unit vectors there are under the above restriction $p(p-1)^{n-1}$ of the $P(n)$'s.

A necessary and sufficient condition that the ith step of a path $P(n)$ overlaps with the jth step that

$$\sum_{k=i}^{j}\sum_{c=1}^{p-1}\epsilon_{kl}\alpha_l=0$$

which is equal in turn to

$$\sum_{k=i}^{j}\sum_{c=1}^{p-1}\epsilon_{kl}\mathbf{w}^l=0,$$

since $\alpha_0\neq0$. In particular, we are interested in the following lattices (see Fig. 1): (1) square lattice on a plane, (2) hexagonal lattice on a plane, (3) diamond lattice in space. In the square lattice $\mathbf{w}$ is a rotation through 90° which is equivalent to multiplication by i. We will define two kinds of paths $P(n)$ and $P^*(n)$,

$$P(n)=\sum_{i=1}^{n}\sum_{j=1}^{p-1}\epsilon_{ij}\alpha_j,$$

where $j=0, 1, 2, 3=p-1$, and $\epsilon_{ij}\neq0$ for only one value of j, ϵ_{ij} is equal to one when i and j have the same parity, and zero otherwise.

The $P^*(n)$ are defined by

$$P^*(n)=\sum_{i=1}^{n}\sum_{j}\epsilon_{ij}{}^*\alpha_j,$$

where $\epsilon_{ij}=\epsilon_{ij}{}^*$, if $j\neq2$ and $\epsilon_{i2}=0$ for all values of i. (See Fig. 2.)

In the planar hexagonal lattice $\mathbf{w}$ is a rotation through 120°, which is equivalent to multiplication by cube root of unity ($e^{i\pi/3}$). We again define two kinds of paths, $P(n)$ and $P^*(n)$:

$P(n)=\sum_i\sum_j\epsilon_{ij}\alpha_j$ where $j=0, 1, 2.$

$\epsilon_{ij}=-1$ for some j, if i is even, otherwise $\epsilon_{ij}=0$.

$\epsilon_{ij}=0$ if $\epsilon_{i-1,\,j}=1$,

$\epsilon_{ij}=-1$ for some j, if i is odd, otherwise $\epsilon_{ij}=0$.

$P^*(n)=\sum_i\sum_j\epsilon_{ij}{}^*\alpha_j$, $j=0, 1, 2$ where

$\epsilon_{ij}{}^*=\epsilon_{ij}$, except when i is even and $j=0$ then $\epsilon_{i0}=0$.

In the diamond lattice in space $\mathbf{w}$ is a rotation through a solid tetrahedral angle. We again define two kinds of

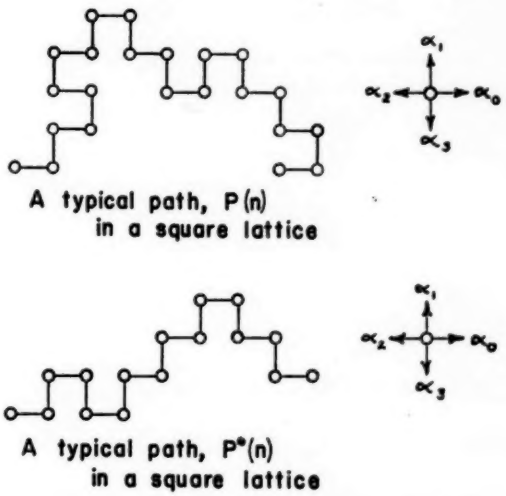

FIG. 2. Types of paths in the square lattice.

paths $P(n)$ and $P^*(n)$:

$P(n)=\sum_i\sum_j\epsilon_{ij}\alpha_j$ with $j=0, 1, 2, 3,$

$\epsilon_{ij}=-1$ for some j, when i is odd and $j=0, 1, 2, 3.$

$\epsilon_{ij}=-1$ for some j, when i is even and $j=0, 1, 2, 3.$

$\epsilon_{ij}=0$ if $\epsilon_{i-1,\,j}=1$, and

$P^*(n)=\sum_i\sum_j\epsilon_{ij}{}^*\alpha_j$, where

$\epsilon_{ij}=\epsilon_{ij}{}^*$, except when i is even and $j=0, 1$. Then

$\epsilon_{i0}=0$ and $\epsilon_{i1}=0$.

It can be shown by an elementary argument that all the simple closed polygons in the square, hexagonal, and diamond lattices formed by $P(n)$ or parts thereof have the following numbers of sides: (1) square=4, 12, 16, $\cdots$, $4l$, $\cdots$, (2) hexagonal=6, 10, 12, 14, $\cdots$, $2l$, $\cdots$, and (3) diamond=6, 8, 10, 12, $\cdots$, $2l$, $\cdots$.

Furthermore, should we restrict ourselves to allowing only those paths in (1) a square lattice where we never take an α_2 step, (2) a hexagonal lattice where we never take a $-\alpha_0$ step, and (3) a diamond lattice where we

never take a $-\alpha_0$ and $-\alpha_1$, step, then all these paths thus chosen contain no overlaps, and are identical with the $P^*(n)$.

Let $\Phi(n)$ be the total number of $P(n)$ paths of n steps from an arbitrary origin of some regular lattice, and $\Phi^*(n)$ be the number of $P^*(n)$'s; then it is clear that

$$\Phi^*(n) \leqslant \Phi(n) \text{ for all } n \geqslant 0.$$

The lower bounding functions $\Phi^*(n)$ are easily calculated for the three lattices which concern us most.

SQUARE LATTICE

Let $\varphi_0(n)$ be the number of $P^*(n)$ which end in an α_0 step, and similarly define $\varphi_1(n)$, $\varphi_2(n)$, $\varphi_3(n)$,

$$\Phi^*(n)=(\varphi_0+\varphi_1+\varphi_2+\varphi_3).$$

For n odd $\varphi_0(n)=\Phi^*(n)$, and for n even $\Phi^*(n)=\varphi_1(n)+\varphi_3(n)$, by the definition of the $P^*(n)$.

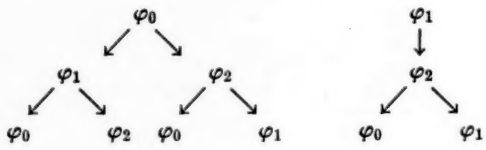

Whence we find

$$\varphi_0(2m-1)=2\varphi_0(2m-3)+\varphi_1(2m-3)+\varphi_2(2m-3)$$
$$\varphi_1(2m-1)=\varphi_0(2m-3)+\varphi_1(2m-3)$$
$$\varphi_2(2m-1)=\varphi_0(2m-3)+\varphi_2(2m-3).$$

Setting $(2m-1)=n$ and solving for $\Phi^*(n)=(\varphi_0+\varphi_1+\varphi_2)$ we find $\Phi^*(n)=3\Phi^*(n-2)$; the solution of this difference equation being

$$\Phi^*(n)=A_H(3^{\frac{1}{2}})^n+B_H(-3^{\frac{1}{2}})^n$$
$$\sim C_H(3^{\frac{1}{2}})^n; \quad C_H>0.$$

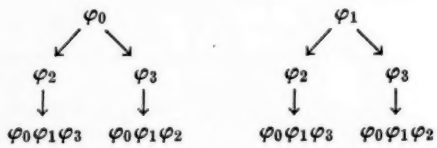

Whence

$$\varphi_0(2m-1)=2\varphi_0(2m-3)+2\varphi_1(2m-3)+\varphi_2(2m-3)+\varphi_3(2m-3)$$
$$\varphi_1(2m-1)=2\varphi_0(2m-3)+2\varphi_1(2m-3)+\varphi_2(2m-3)+\varphi_3(2m-3)$$
$$\varphi_2(2m-1)=\varphi_0(2m-3)+\varphi_1(2m-3)+\varphi_2(2m-3)$$
$$\varphi_3(2m-1)=\varphi_0(2m-3)+\varphi_1(2m-3)+\varphi_3(2m-3).$$

Let $2m-1=n$, solving for $\Phi^*(n)$ we find

$$\Phi^*(n)=5\Phi^*(n-2);$$

Consider the $(2m-2)$nd step; then,

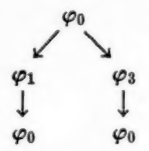

Whence $\varphi_0(2m)=2\varphi_0(2m-2)$, let $2m=n$; then $\Phi^*(n)=2\Phi^*(n-2)$, the solution of this difference equation being

$$\Phi^*(n)=A_s(2^{\frac{1}{2}})^n+B_s(-2^{\frac{1}{2}})^n$$
$$\sim C_s(2^{\frac{1}{2}})^n; \quad C_s>0.$$

HEXAGONAL LATTICE

Let us define again $\varphi_0(n)$, $\varphi_1(n)$, $\varphi_2(n)$ as in the preceding example, where now $\Phi^*(n)=\varphi_0(n)+\varphi_1(n)+\varphi_2(n)$. Consider the $2m-3$rd step:

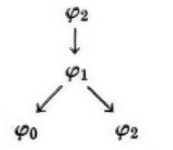

DIAMOND LATTICE

Let as before $\Phi^*(n)=\varphi_0(n)+\varphi_1(n)+\varphi_2(n)+\varphi_3(n)$. Consider the $2m-3$rd step, and from the definition of $P^*(n)$ we find:

the solution is given by

$$\Phi^*(n)=A_D(5^{\frac{1}{2}})^n+B_D(-5^{\frac{1}{2}})^n$$
$$\sim C_D(5^{\frac{1}{2}})^n; \quad C_D>0.$$

In general to find a better upper bound for $\Phi(n)$ other than $p(p-1)^{n-1}$, we proceed as follows. Let the 1st, $\cdots$, $r-2$nd, $r-1$st, rth$\cdots$ simple overlap (simple closed polygon) in some regular lattice have a, $\cdots$, k, l, $m\cdots$ sides, respectively. We will consider all paths of n steps from an arbitrary origin which do not overlap in m steps. Let the number of such paths, $P(n, m)$, be $\Phi_m(n)$; $n>m$. Then we have that

$$\Phi_a(n) \geqslant \cdots \geqslant \Phi_m(n) \geqslant \Phi(n),$$

for all $n \geqslant 0$. Construct all "basic" paths of $m-1$ steps

from a given origin 0 which have no overlaps in l, k, $\cdots a$ steps; let us call these paths $q_j(m-1)$ where $j=1, 2, \cdots L'$. Here L' is the number of such paths. For convenience in counting we need consider only $1/p$ of these $q_j(m-1)$, namely, only those which start with an α_0 step, i.e.,

$$q_j(m-1)=\alpha_0+\sum_{i=2}^{m-1}\sum_{k=1}^{p-1}\epsilon_{ik}\alpha_k=\alpha_0[1+\sum_{i=2}^{m-1}\sum_{k=1}^{p-1}\mathbf{w}^k\epsilon_{ik}],$$

$$j=1, 2, \cdots L; \quad L=L'/P.$$

Assume we have constructed all paths of $n-1$ steps which do not overlap in m, l, k, $\cdots a$ steps. Consider one such given by the sum

$$\epsilon_{1s}\alpha_s+\cdots+\epsilon_{n-m,\,t}\alpha_t+\cdots+\epsilon_{n-1,\,u}\alpha_u=\epsilon_{1s}\alpha_s+\cdots$$
$$+\epsilon_{n-m,\,t}\mathbf{w}^t\alpha_0[1+\sum_{i=n-m+1}^{n-1}\sum_{k}^{p-1}\epsilon_{ik}/\epsilon_{n-m,\,t}\mathbf{w}^{k-t}].$$

But by hypothesis,

$$\alpha_0[1+\sum_i\sum_k\epsilon_{ik}/\epsilon_{n-m,\,t}\mathbf{w}^{k-t}]$$

is some $q_j(m-1)$, since

$$\epsilon_{ik}/\epsilon_{n-m,\,t}=\pm 1.$$

Let it be the jth. Then we define

$$P_j(n-1, m)=\epsilon_{1s}\alpha_s+\cdots+\epsilon_{n-m,\,t}\mathbf{w}^t q_j(m-1),$$

where $0\leqslant s, u, t\leqslant p-1$. Let the number of $P_j(n-1, m)$ be $\varphi_j(n-1, m)$. We wish to find the number of $P(n, m)$ formed from the $P_j(n-1, m)$ by the addition of another step, say, $\epsilon_{n,\,q}\alpha_q$ such that $P(n, m)$ does not overlap in $m, l, k\cdots a$ steps. On the nth step the path may do one and only one of the following:

I. Overlap in m, l, $k\cdots a$ steps corresponding to a rth, $r-1$st, $\cdots 1$st overlap, respectively. (One and only one of these), II.(a) overlap in w, v, $\cdots$ etc., steps, where $m<w<v$, $\cdots$, $<n$, (b) not overlap. This will depend on the choice of α_q. We can decide which case occurs by using the relation

$$\sum_{i=0}^{d}\sum_{k}^{p-1}\epsilon_{ik}\alpha_k=0$$

for an overlap of the cth and dth step. Since we are concerned only with paths which do not overlap in m or less steps, we can group II(a) with II(b) and collectively call it II. For some path $P_j(n-1, m)$, let $\alpha_q{}^*$ be those α_q which correspond to case I but not to case II. Then we may write

$$P_j(n-1, m)+\epsilon_{nq}\alpha_q=\epsilon_{1s}\alpha_s+\cdots$$
$$+\epsilon_{n-m,\,t}\mathbf{w}^t q_j(m-1)+\epsilon_{n,\,q}\alpha_q;$$

where α_q is not a member of the set $\{\alpha_q{}^*\}$. Then

$$\epsilon_{1s}\alpha_s+\cdots+\epsilon_{n-m,\,t}\alpha_t+\cdots+\epsilon_{n,\,q}\alpha_q=\epsilon_{1s}\alpha_s+\cdots$$
$$+\epsilon_{n-m+1,\,k}\mathbf{w}^k\alpha_0[1+\sum_{i=n-m+2}^{n}\sum_{q=1}^{p-1}\epsilon_{nq}/\epsilon_{n-m+1,\,k}\mathbf{w}^{q-k}]$$
$$=P_i(n, m);$$

where

$$q_i(m-1)=[1+\sum_{i=n-m+2}^{n}\sum_{q=1}^{p-1}\epsilon_{nq}/\epsilon_{n-m-1,\,k}\mathbf{w}^{q-k}].$$

Thus all $P_i(n, m)$ are obtained from one or more $P_j(n-1, m)$; j, $i=1\cdots L$ by a suitable nth step, the choice depending only on the nature of the $m-1$ *step* ending of $P_j(n-1, m)$, $q_j(n-1)$, and is completely independent of n. We have by induction

$$\varphi_i(n, m)=\sum_j\gamma_{ij}\varphi_j(n-1, m); \quad i=1, \cdots, L$$

where $\gamma_{ij}=1$ if some α_k step exists which added $P_j(n-1, m)$ gives a $P_i(n, m)$, and otherwise $\gamma_{ij}=0$. Furthermore,

$$\Phi_m(n)=\sum_{i=1}^{L}\varphi_i(n, m),$$

since every $P_i(n, m)$ ends in some $q_i(m-1)$. The system of L simultaneous first-order difference equations can be solved by considering the $\varphi_i(n, m)$ to be the components of a vector $\varphi(n, m)$. Thus we find

$$\varphi(n, m)=\|\gamma_{ij}\|\varphi(n-1, m),$$

where $\|\gamma_{ij}\|$ is the matrix of γ_{ij}'s, i.e.,

$$\begin{Vmatrix}\gamma_{11} & \gamma_{12}\cdots\gamma_{1L}\\ \cdot & \cdot & \cdot\\ \cdot & \cdot & \cdot\\ \cdot & \cdot & \cdot\\ \gamma_{L1} & \gamma_{L2}\cdots\gamma_{LL}\end{Vmatrix}.$$

Assume a solution of form

$$\varphi(n, m)=\lambda^n\begin{pmatrix}\beta_1\\ \cdot\\ \cdot\\ \cdot\\ \beta_L\end{pmatrix},$$

substituting into the difference equation we find that λ must be one of the roots of the polynomial

$$0=\begin{vmatrix}\gamma_{11}-\lambda, & \gamma_{12}, & \cdots, & \gamma_{1L}\\ \gamma_{21}, & \gamma_{22}-\lambda, & \cdots, & \gamma_{2L}\\ \cdot & & \cdot & \cdot\\ \cdot & & \cdot & \cdot\\ \cdot & & \cdot & \cdot\\ \gamma_{L1}, & \gamma_{L2}, & \cdots, & \gamma_{LL}-\lambda\end{vmatrix}.$$

If we are concerned with only an asymptotic solution for $\varphi(n, m)$ we find

$$\varphi(n, m)\sim(\lambda_{\max})^n\{\beta_i\},$$

and thus

$$\Phi_m(n)\sim C_m(\lambda_{\max})^n.$$

In practice it is usually easier to remove linear factors from the system of difference equations, to obtain a system of equations of higher order, but the determinant which specifies $\lambda_{\max}$ will be of lower order. $\Phi(n)$ may by this method be calculated to any desired degree of accuracy; needless to say, as m increases so does the labor of the calculation.

To illustrate the method we will consider the calculation of $\Phi_4(n)$ in the square lattice. The "basic" paths $q_j(3)$ are:

$$(1+w+w^4)=q_1(3)$$
$$(1+w+w^2)=q_2(3)$$
$$(1+w^3+w^4)=q_3(3)$$
$$(1+w^3+w^2)=q_4(3)$$

with $w^4=1$, we find

$$\|\gamma_{ij}\|=\begin{Vmatrix}0, & 1, & 1, & 0\\ 0, & 0, & 1, & 0\\ 1, & 0, & 0, & 1\\ 1, & 0, & 0, & 0\end{Vmatrix},$$

where

$$\varphi_i(n,4)=\sum_{j=1}^{4}\gamma_{ij}\varphi_j(n-1,4)$$

and $\lambda_{\max}$ must satisfy

$$0=\begin{vmatrix}-\lambda, & 1, & 1, & 0\\ 0, & -\lambda, & 1, & 0\\ 1, & 0, & -\lambda, & 1\\ 1, & 0, & 0, & -\lambda\end{vmatrix},$$

which gives

$$\lambda^4-\lambda^2-2\lambda-1=0=(\lambda^2-\lambda-1)(\lambda^2+\lambda+1)$$

and $\lambda_{\max}=\frac{1}{2}+\frac{1}{2}(5)^{\frac{1}{2}}$ and thus $\Phi_4(n)\sim C_4(1.62)^n$ which agrees with the exact solution given by Montroll.[1]

We have found by this method that (1) in the square lattice $-\Phi_{12}(n)=C_{12}(1.46)^n$, (2) in the hexagonal lattice $\Phi_6(n)=C_6(1.81)^n$, and (3) calculations are in progress for $\Phi_6(n)$ in the diamond lattice.

We can summarize the results in the following manner:

Square lattice:

$$C_{12}(1.46)^n\gtrsim\Phi(n)\gtrsim C_S(1.41)^n,$$

Hexagonal lattice:

$$C_6(1.81)^n\gtrsim\Phi(n)\gtrsim C_H(1.73)^n,$$

Diamond lattice:

$$\gtrsim\Phi(n)\gtrsim C_D(2.24)^n.$$

In the next few paragraphs we shall be concerned with the problem of determining the probability of reaching a given point in n steps without overlapping in a square lattice. Should we not be concerned with overlaps, the desired probability could be written for sufficiently large n as

$$Pr^0(r,n)^N\frac{2}{\pi n}\exp[-r^2/2n].$$

It has been assumed in deriving this result that the probability of going a unit step to the right is equal to the probability of a unit step to the left; the same applies for unit steps up or down.

As a first approximation to the desired probability, let us calculate the probability of reaching a given point in n steps, by paths which do not overlap in 4 steps, in the square lattice.

Let $\epsilon_1, \epsilon_2, \cdots, \epsilon_n$ be a sequence of ±1's. Let α_k, $(k=1, 2, \cdots, n)$, be the distance moved during the kth step. Then $r_n=\sum_k\epsilon_k\alpha_k$ is the point reached during some path of n steps. In the square lattice, we are interested in paths where $\alpha_1=\alpha_3=\cdots=1$ and $\alpha_2=\alpha_4=\cdots=i$.

Define

$$F_n(\alpha_1,\cdots,\alpha_n)=\sum_{\text{paths}}\exp[t(\epsilon_1\alpha_1+\cdots+\epsilon_n\alpha_n)]Pr(\epsilon_1,\cdots,\epsilon_n)$$

where $Pr(\epsilon_1,\cdots,\epsilon_n)$ is the desired probability, and the sum is taken over all paths which do not overlap in 4 steps. t is a positive parameter.

Call a path a "G-path" if $\epsilon_n=\epsilon_{n-2}$; otherwise, if $\epsilon_n=-\epsilon_{n-2}$, it is a "$B$-path."

Now let

$$G_n(\alpha_1,\cdots,\alpha_n)=\sum_{G\text{-paths}}\exp[t(\epsilon_1\alpha_1+\cdots+\epsilon_n\alpha_n)]Pr(\epsilon_1,\cdots,\epsilon_n)$$

$$B_n(\alpha_1,\cdots,\alpha_n)=\sum_{B\text{-paths}}\exp[t(\epsilon_1\alpha_1+\cdots+\epsilon_n\alpha_n)]Pr(\epsilon_1,\cdots,\epsilon_n),$$

and note that

$$F_n=B_n+G_n.$$

Now, a "G-path" $\epsilon_1,\cdots,\epsilon_n$ where $\epsilon_{n-2}=\epsilon_n$ can come from either a "G-path" $\epsilon_1,\cdots\epsilon_{n-1}$, where $\epsilon_{n-1}=\epsilon_{n-3}$ or from a "B-path" $\epsilon_1,\cdots,\epsilon_{n-1}$ where $\epsilon_{n-1}=-\epsilon_{n-3}$. However, a "$B$-path" of n steps must come from a "G-path" of $n-1$ steps, otherwise we overlap in 4 steps.

Hence, consider

$$\begin{aligned}G_n(\alpha_1,\cdots,\alpha_n)&=\sum_{G\text{-paths}}\exp[t(\epsilon_1\alpha_1+\cdots+\epsilon_n\alpha_n)]Pr(\epsilon_1,\cdots,\epsilon_n)\\&=\sum_{G\text{-paths}}\exp[t(\epsilon_1\alpha_1+\cdots+\epsilon_{n-1}\alpha_{n-1})]\\&\quad\times\exp[t\epsilon_{n-2}\alpha_n]Pr(\epsilon_1,\cdots,\epsilon_n)\\&=\tfrac{1}{2}\sum_{\substack{G\text{-paths}\\ n-1\text{ steps}}}\exp[t(\epsilon_1\alpha_1+\cdots+\epsilon_{n-1}\alpha_{n-1})]\\&\quad\times\exp[t\epsilon_{n-2}\alpha_n]Pr(\epsilon_1,\cdots,\epsilon_{n-1})\\&\quad+\sum_{\substack{B\text{-paths}\\ n-1\text{ steps}}}\exp[t(\epsilon_1\alpha_1+\cdots+\epsilon_{n-1}\alpha_{n-1})]\\&\qquad\times\exp[t\epsilon_{n-2}\alpha_n]Pr(\epsilon_1,\cdots,\epsilon_{n-1})\end{aligned}$$

$$G_n(\alpha_1, \cdots, \alpha_n)=\tfrac{1}{2}G_{n-1}(\alpha_1, \cdots, \alpha_{n-2}+\alpha_n, \alpha_{n-1})$$
$$+B_{n-1}(\alpha_1, \cdots, \alpha_{n-2}+\alpha_n, \alpha_{n-1}).$$

Similarly,

$$B_n(\alpha_1, \cdots, \alpha_n)$$
$$=\sum_{B\text{-paths}} \exp[t(\epsilon_1\alpha_1+\cdots+\epsilon_n\alpha_n)]Pr(\epsilon_1, \cdots, \epsilon_n)$$
$$=\sum_{B\text{-paths}} \exp[t(\epsilon_1\alpha_1+\cdots+\epsilon_{n-1}\alpha_{n-1})]$$
$$\times\exp[-t\epsilon_{n-2}\alpha_n]Pr(\epsilon_1, \cdots, \epsilon_n)$$
$$=\tfrac{1}{2}\sum_{\substack{G\text{-paths}\\ n-1\text{ steps}}} \exp[t(\epsilon_1\alpha_1+\cdots+\epsilon_{n-1}\alpha_{n-1})]$$
$$\times\exp[-t\epsilon_{n-2}\alpha_n]Pr(\epsilon_1, \cdots, \epsilon_{n-1})$$
$$=\tfrac{1}{2}G_{n-1}(\alpha_1, \cdots, \alpha_{n-2}-\alpha_n, \alpha_{n-1}).$$

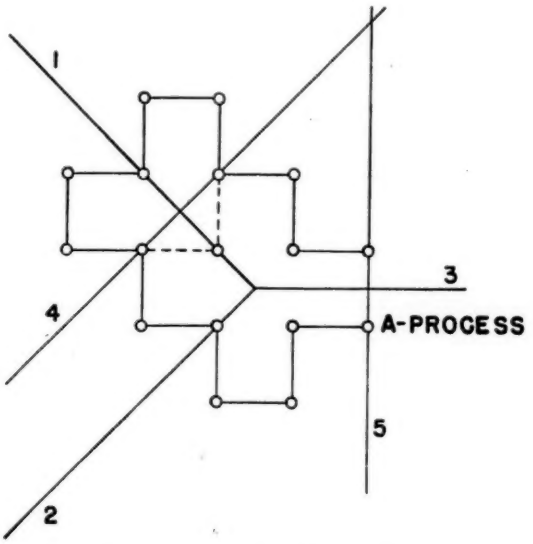

FIG. 3. "A-Process" for generating a simple closed path of a larger number of sides from one of a smaller number of sides.

But then,

$$B_{n-1}(\alpha_1, \cdots, \alpha_{n-2}+\alpha_n, \alpha_{n-1})$$
$$=\tfrac{1}{2}G_{n-2}(\alpha_1, \cdots, \alpha_{n-3}-\alpha_{n-1}, \alpha_{n-2}+\alpha_n),$$

so that

$$G_n(\alpha_1, \cdots, \alpha_n)=\tfrac{1}{2}G_{n-1}(\alpha_1, \cdots, \alpha_{n-2}+\alpha_n, \alpha_{n-1})$$
$$+\tfrac{1}{2}G_{n-2}(\alpha_1, \cdots, \alpha_{n-3}-\alpha_{n-1}, \alpha_{n-2}+\alpha_n).$$

If this recursion formula is solved for $G_n(\alpha_1, \cdots, \alpha_n)$, then $F_n(\alpha_1, \cdots \alpha_n)$ may be solved.

Considering now F as a function of t, we have

$$[\partial F/\partial t]_{t=0}=E(r_n),$$
$$[\partial^2 F/\partial^2 t]_{t=0}=E(r_n^2),$$

and in general,

$$[\partial^u F/\partial t^u]_{t=0}=E(r_n{}^u).$$

Also, there are inversion formulas for finding the probability distribution from F_n. Certain generalizations of the equations here derived exist for higher overlaps; also it may be possible to generalize these characteristic functions for any regular lattice.

Particular solutions for the recurrence relation satisfied by G are not too difficult to find. For let

$$G_1=\cosh\alpha_1 t,$$
$$B_1=0,$$

then we find

$$G_2=\cosh\alpha_1 t\cosh\alpha_2 t,$$
$$B_2=0,$$
$$G_3=\tfrac{1}{2}\cosh t(\alpha_1+\alpha_3)\cosh\alpha_2 t,$$
$$B_3=\tfrac{1}{2}\cosh t(\alpha_1-\alpha_3)\cosh\alpha_2 t,$$
$$G_4=\tfrac{1}{4}\cosh t(\alpha_1+\alpha_3)\cosh t(\alpha_2+\alpha_4),$$
$$+\tfrac{1}{2}\cosh t(\alpha_1-\alpha_3)\cosh t(\alpha_2+\alpha_4),$$
$$B_4=\tfrac{1}{4}\cosh t(\alpha_1+\alpha_3)\cosh t(\alpha_2-\alpha_4),$$
$$G_5=\tfrac{1}{8}\cosh t(\alpha_1+\alpha_3+\alpha_5)\cosh t(\alpha_2+\alpha_4)$$
$$+\tfrac{1}{4}\cosh t(\alpha_1-\alpha_3-\alpha_5)\cosh t(\alpha_2+\alpha_4)$$
$$+\tfrac{1}{4}\cosh t(\alpha_1+\alpha_3+\alpha_5)\cosh t(\alpha_2-\alpha_4),$$

etc.

Substituting $\alpha_{2n-1}=1$ and $\alpha_{2n}=i$, we find for G_4:

$$G_4=\tfrac{1}{4}\cosh 2t\cos 2t+\tfrac{1}{2}\cos 2t,$$

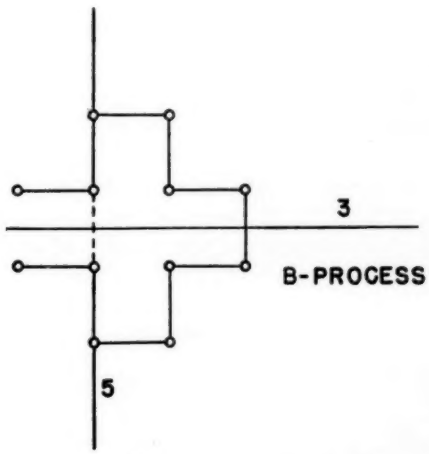

FIG. 4. "B-Process" for generating a simple closed path of a larger number of sides from one of a smaller number of sides.

and for B_4:

$$B_4=\tfrac{1}{4}\cosh 2t$$

and hence $F_4=B_4+G_4$ is given by

$$F_4=\tfrac{1}{4}\cosh 2t(1+\cos 2t)+\tfrac{1}{2}\cos 2t,$$

and hence

$$E(r_4) \quad \text{and} \quad E(r_4^2)$$

is given by

$$[\partial F_4/\partial t]_{t=0}=E(r_4)=0$$
$$[\partial^2 F_4/\partial t^2]_{t=0}=E(r_4^2)=-1.$$

$E(r_n^2)$ should not be confused with $E[(Re r_n)^2+(Im r_n)^2]$ where $Re r_n$ is the real part of r_n and $Im r_n$ is the imaginary part of r_n; $E(r_n^2)$ is given by

$$E(r_n^2)=E[(Re r_n)^2-(Im r_n)^2+2i(Re r_n)(Im r_n)].$$

Further work on these methods is in progress.

Again let us restrict ourselves to paths in a square lattice. Choosing an arbitrary origin we ask how many simple closed polygons can be formed by paths of $4y$ steps which cannot be superposed. Let the desired number be $q(y)$ where y is any one of the following in-

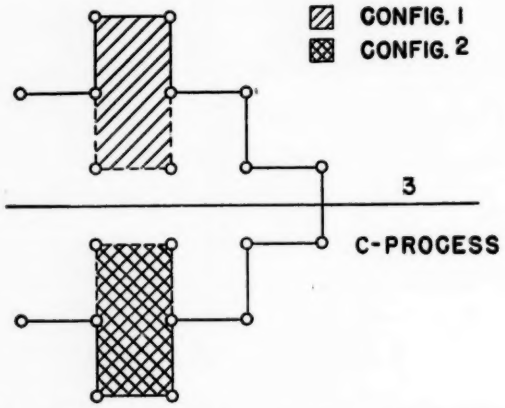

FIG. 5. "C-Process" for generating a simple closed path from one of the same number of sides.

tegers 1, 3, 4, 5, $\cdots$. Clearly, if we have one such configuration, say $0A_1A_2\cdots A_{4y-1}0$, we can obtain $4y$ more by starting from A_j as origin rather than 0; these configurations may be superposed. Also, we can complete the circuit of vertices of the simple closed polygon in either a clockwise or counter clockwise direction; this gives us twice as many configurations which may be superposed. An upper bound is easily

TABLE I.

Process	Number of sides added	Number of unit areas added
A	4	3
B	8	4
C	0	2

found. Consider an unrestricted random walk which may take a unit step to left or right on every odd step, and a unit step up or down on every even numbered step. Since the walk is unrestricted, we can consider it as composed of two independent one-dimensional walks. We will be interested in the number of walks of $4y$ steps which terminate at the origin. The number is

$$w=(2y!)^2/(y!)^4\sim\frac{1}{\pi y}2^{4y};\quad y>10,$$

and hence

$$q(y)\leqslant w/8y\leqslant\frac{2^{4(y-2)}}{\pi y^2}.$$

To find a lower bound for $q(y)$ we construct a class of simple closed polygons $q^*(y)$ where

$$q(y)\geqslant q^*(y).$$

We will build up these configurations by starting with a simple closed polygon of twelve steps; there is only one nonsuperposable isomer, by three processes:

Process A: consists of deleting two sides of the configuration and adding six sides, along line 1. (See Fig. 3.) Notice that no overlaps can occur since line 4 divides the plane into two distinct regions, for only below and on this line can lie vertices of the original configuration.

Process B: consists of deleting one side and adding nine new sides to the configuration along line 3. (See Figs. 3 and 4.)

Process C: consists of deleting three sides from a configuration obtained by a B process and adding three sides. (See Fig. 5.) At least two new configurations can be obtained in this way.

In Table I we summarize these processes:

Any closed configuration produced by A, B, C of $4y$ sides can be thought to consist of $12-4x$ sides (x an integer), i.e., $x=y-3$.

Thus the number of $q^*(x)$ is equal to the number of $q^*(x-1)$ which yield a $q^*(x)$ by an A-process plus the number of $q^*(x-2)$ which yield a $q^*(x)$ by a B-process. Furthermore, for every $q^*(x)$ produced by a B-process we can obtain two other configurations by a C-process.

Hence

$$q^*(x)=q^*(x-1)+3q^*(x-2),$$

where

$$q^*(0)=1\quad\text{and}\quad q^*(1)=1,$$

$$q^*(y)\sim k(1.52)^{2y}.$$

We conclude that as $y\to+\infty$

$$k_1y\geqslant\ln q(y)\geqslant k_2y;$$

where k_1 and k_2 are positive constants.

CONCLUSION

The results obtained indicate that the sequence of numbers $\Phi_a(n)$, $\Phi_b(n)$, $\cdots$, $\Phi_m(n)$ converges fairly quickly to $\Phi(n)$ in the two planar lattices considered, as can be seen from the magnitude of the lower bounds From the lower bound on the diamond lattice we have a fair estimate of the logarithmic order of $\Phi(n)$ in that lattice. The method of generating functions has been applied to the determination of the probability of reaching a given point in a square lattice without overlapping in 4 steps. Further work on this problem and generalizations thereof will be presented later. An

estimate of the logarithmic order of the number of simple nonsuperposable closed polygons in the square lattice indicates that it varies with n, the number of steps in the simple closed polygon. It is expected that this will hold true for the hexagonal planar lattice and the diamond space lattice.

ACKNOWLEDGMENT

It is the pleasant duty of the authors to express their appreciation to Dr. Turner Alfrey, Jr., of The Dow Chemical Company and to Professor H. Mark of the Polytechnic Institute of Brooklyn for their interest and helpful discussions of this problem.

THE JOURNAL OF CHEMICAL PHYSICS VOLUME 19, NUMBER 11 NOVEMBER, 1951

Sum Rules for the Vibration Frequencies of Isotopic Molecules

J. C. Decius* and E. Bright Wilson, Jr.†
Department of Chemistry and Chemical Engineering, University of Washington, Seattle, Washington
(Received July 30, 1951)

The squares of the frequencies of isotopically related molecules obey certain simple sum rules. Whenever there exists a chemical exchange reaction involving only isotopic variations of a single type of molecule, such that the reaction is balanced at each atomic position of the molecule, then a relation of identical form exists between the sums of the squares of the frequencies. Thus

$$\Sigma\nu^2(H_2O)+\Sigma\nu^2(D_2O)=2\Sigma\nu^2(HDO) \quad \text{and} \quad \Sigma\nu^2(N^{14}H_3)+\Sigma\nu^2(N^{15}D_3)=\Sigma\nu^2(N^{14}D_3)+\Sigma\nu^2(N^{15}H_3).$$

If, as in the latter example, the molecules all have the same symmetry, the sum rule may be applied separately to each factor of the secular equation. When forms of lower symmetry appear (as in the example involving the water molecule), symmetry factoring may or may not be possible. In such cases it is necessary to employ certain group-theoretical considerations; the possible factoring is not in general identical with that appropriate for the product rule.

Examples of the application of the sum rule are given, involving the acetylene, water, methane, and hydrocyanic acid molecules. The existence of higher order isotope rules, intermediate between the sum and product rules, is pointed out.

INTRODUCTION

THE product rule[1] of Redlich and Teller, which relates the vibration frequencies of isotopic molecules, has proved very useful in confirming the assignments of the vibration frequencies to the various symmetry species. In addition to the product rule, however, there exist certain sum rules, which are remarkably easy to apply, and which yield independent information. As in the case of the product rule, these sum rules apply exactly only when the frequencies have been corrected for anharmonicity.

As an elementary example, consider the molecules HOH, DOD, and HOD. The rule states that the sums of the squares of the frequencies are related by

$$\sum\nu^2(\text{HOD})+\sum\nu^2(\text{DOH})=2\sum\nu^2(\text{HOD})=\sum\nu^2(\text{HOH})+\sum\nu^2(\text{DOD}). \quad (1)$$

A second type of relation exists between isotopic molecules such as $N^{14}H_3$, $N^{14}D_3$, $N^{15}H_3$, and $N^{15}D_3$, namely,

$$\sum\nu^2(N^{15}H_3)+\sum\nu^2(N^{14}D_3)=\sum\nu^2(N^{14}H_3)+\sum\nu^2(N^{15}D_3). \quad (2)$$

Both types of relation can be incorporated in one rule. Number the atomic positions, distinguishing thereby between positions even if occupied by identical kinds of atoms. Thus the formula for ethane would be:

$$C_1C_2H_3H_4H_5H_6H_7H_8$$

where the numerical subscripts have an agreed-upon geometric meaning. Then write the exchange reaction in the form

$$\sum_\alpha n_\alpha(C_1C_2H_3H_4H_5H_6H_7H_8)_\alpha=0, \quad (3)$$

where the subscript α identifies an isotopic form with specified isotopic atoms in each of the identified atomic positions, n_α is an integer which is positive for reactants and negative for products, and the whole expression constitutes a chemical isotopic exchange reaction which is balanced *at each atomic position separately*. In many cases it will be necessary to include as separate terms molecules which differ only in orientation, as HOD and DOH. The rule states that

$$\sum_\alpha n_\alpha\sum_k\nu_{\alpha k}^2=0, \quad (4)$$

where the sum is over the molecular forms (α) and over the fundamental modes of vibration (k). Degenerate frequencies must be counted the appropriate number of times.

There exists a certain set of symmetry operations common to every molecule in Eq. (3) (identified with

---

* Oregon State College, Corvallis, Oregon.
† Harvard University, Cambridge, Massachusetts. The work herein reported was supported in part by the ONR under Contract N8 ONR 52010.

[1] O. Redlich, Z. physik. Chem. B. **28**, 371 (1935). E. Teller, quoted in W. R. Angus *et al.*, J. Chem. Soc., 1936, p. 971.

respect to the fixed numbering scheme for atomic positions), which form a group K which is a subgroup of the point group for the isotopic form of highest symmetry. The transformations of molecular coordinates will form a representation of this group which can be reduced by constructing suitable symmetry coordinates. If these coordinates occur in more than one symmetry species of the group K, the secular equation for each of the molecules can be factored into the same blocks or factors, involving the same symmetry coordinates. (Some of the molecules may factor further but this is

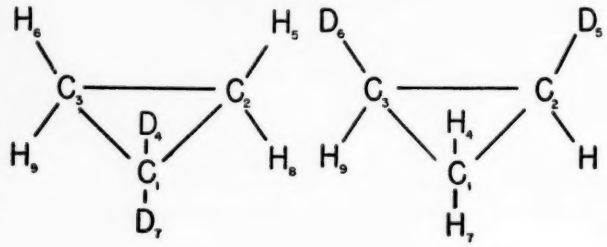

FIG. 1. Numbering scheme, geometry, and two isotopic forms for cyclopropane.

irrelevant for the present purpose.) Then the above rule (4) can be applied separately to the normal modes of each of the species of the group K.

For example, consider the exchange reaction

$$CD_3CH_3+CH_3CD_3-C_2H_6-C_2D_6=0.$$

In this case, every molecule has at least the symmetry C_{3v}, so that $C_{3v}=K$. The common symmetry, may however, be lower than that of any individual molecule.

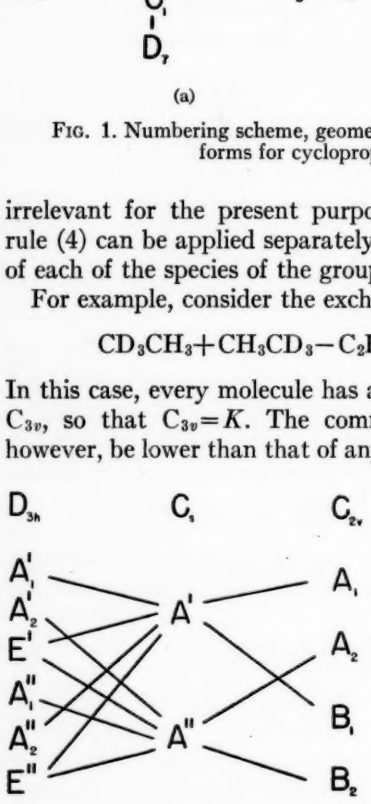

FIG. 2. Correlation between species of D_{3h} and C_s and between C_{2v} and C_s.

Thus in the exchange reaction,

$$3(p-C_6H_4D_2)-2C_6H_6-C_6D_6=0,$$

each of the dideuterobenzenes (with deuterium in the para positions) has the symmetry V_h, but when the superposition is made, the deuteriums must successively occupy the 1,4, the 2,5, and the 3,6 positions. Therefore the twofold axes lying in the molecular planes are not the same for all three orientations, and, in fact, the common operations constitute $K=C_{2h}$.

As a final example, consider the following exchange reaction for the cyclopropane species, in which the numbering is as in Fig. 1.

$$C_1C_2C_3D_4H_5H_6D_7H_8H_9+C_1C_2C_3H_4D_5D_6H_7H_8H_9$$
$$+C_1C_2C_3H_4H_5H_6H_7D_8D_9-2C_1C_2C_3H_4H_5H_6H_7H_8H_9$$
$$-C_1C_2C_3D_4D_5D_6D_7D_8D_9. \quad (5)$$

Each atom position is balanced; e.g., at position 6 the atoms are H+D+H−2H−D=0. Furthermore all five molecules display a plane of symmetry passing through atoms 1, 4, 7. The group K is thus C_s and the sum rule

$$\sum \nu_k^2(C_3H_4D_2)+2\sum \nu_k^2(C_3H_2HDHD)$$
$$-2\sum \nu_k^2(C_3H_6)-\sum \nu_k^2(C_3D_6)=0 \quad (6)$$

can be applied separately to the modes symmetrical to the plane and antisymmetrical to the plane, these being the two species of the group C_s. Note that the second two molecules in (5) are the same except for orientation, i.e., except for the numbering. Nevertheless they must be distinguished in determining the symmetry operations common to all molecules, although they of course have the same frequencies.

TABLE I. Application of the sum rule to C_2H_2, C_2D_2, and C_2HD.

	C_2H_2		C_2D_2		C_2HD	
k	ω_k(cm^{-1})	ω_k^2(10^6 cm^{-2})	ω_k	ω_k^2	ω_k	ω_k^2
1	3373.7	11.38	2700.5	7.29	3334.8	11.12
2	1973.8	3.90	1762.4	3.10	1851.2	3.42
3	3287	10.80	2427	5.89	2584	6.69
		26.08		16.28		21.23
				$(\frac{1}{2})[\sigma(C_2H_2)+\sigma(C_2D_2)]$=		21.18
5	611.8	0.3743	505	0.2550	518.8	0.2692
6	729	0.5314	539.1	0.2906	683	0.4665
		0.9057		0.5456		0.7357
				$(\frac{1}{2})[\sigma(C_2H_2)+\sigma(C_2D_2)]$=		0.7256

If it is known in which way the normal modes for each molecular form divide into symmetry species under the group for that form, the relation of these to the factoring under the subgroup K can be found from so-called correlation tables.[2] Thus in the above example the molecule C_3H_6 has symmetry D_{3h} and its frequencies fall into the six species or irreducible representations A_1', A_2', E', A_1'', A_2'', E''. These flow into the two species A′ and A″ of C_s as shown in Fig. 2. Also shown is the correlation of C_{2v} and C_s, the former applying to $C_3H_4D_2$. Then the frequencies of C_3H_6 of species A_1', E' (counted once each), A_2'' and E'' (counted once each) will appear in the sum of species A′ of C_s, while A_2', E' (once), A_1'' and E'' (once) will appear in A″.

If all molecules are of the highest symmetry, as in (2), the regular factoring for the group of highest symmetry can be used. In other cases, no factoring at all may be possible in the application of the sum rule.

[2] See for example G. Herzberg, *Infrared and Raman Spectra of Polyatomic Molecules* (D. Van Nostrand Company, Inc., New York, 1945), p. 237.

TABLE II. Application of the sum rule to H_2O, D_2O, and HDO.

	H_2O		D_2O		HDO	
k	ω_k(cm^{-1})	ω_k^2(10^6 cm^{-2})	ω_k	ω_k^2	ω_k	ω_k^2
1	3652	13.337	2666	7.108	2719	7.393
2	1595	2.544	1179	1.390	1402	1.966
3	3756	14.108	2789	7.779	3655[a]	13.360
		29.989		16.277		22.719
				$(\frac{1}{2})[\sigma(H_2O)+\sigma(D_2O)]=23.133$		

[a] Calculated by product rule from H_2O.

Thus this is true for

$$4CH_3D=3CH_4+CD_4. \quad (7)$$

When the four different orientations of CH_3D which are required are examined, it is seen that they possess no common symmetry operation at all, except the identity operation.

PROOF OF THE RULE

The secular equation can be set up in terms of Cartesian coordinates, S_1, $S_2\cdots S_{3N}$ in the form

$$\begin{vmatrix} (F_{11}/m_1)-\lambda & F_{12}/(m_1m_2)^{\frac{1}{2}} & \cdots & \cdots \\ F_{21}/(m_2m_1)^{\frac{1}{2}} & (F_{22}/m_2)-\lambda & \cdots & \cdots \\ \cdots & \cdots & \cdots & \cdots \\ \cdots & \cdots & \cdots & (F_{3N3N}/m_{3N})-\lambda \end{vmatrix} = 0 \quad (8)$$

in which the F's are the force constants in terms of Cartesian coordinates, the m's are the masses of the atoms associated with these coordinates, and $\lambda_k=4\pi^2\nu_k^2$. The sum σ of the roots of such an equation is known to be

$$\sigma_\alpha=\sum_k\lambda_k^{(\alpha)}=\sum_j F_{jj}/m_j^{(\alpha)} \quad (9)$$

in which the superscript (α) refers to the isotopic molecular form. Each index j is associated with a given atomic position. The sum rule, Eq. (4), can now be written

$$4\pi^2\sum_\alpha\sum_k n_\alpha\nu_{\alpha k}^2=\sum_\alpha\sum_k n_\alpha\lambda_k^{(\alpha)} =\sum_j F_{jj}\left(\sum_\alpha n_\alpha/m_j^{(\alpha)}\right)=0 \quad (10)$$

because $\sum_\alpha(n_\alpha/m_j^{(\alpha)})=0$ for every atomic position j. The fact has been used that the force constants $F_{jj}^{(\alpha)}$ are independent of α, the isotopic form.

Furthermore, if the coordinates S_j are Cartesian symmetry coordinates which reduce the group K, all the above equations will apply to a single factor of the secular equation corresponding to a given species of K. Each position on the diagonal of the secular equation, for each isotopic form, is labelled by the same coordinate S_j, has the same force constant F_{jj} (now in terms of symmetry coordinates), and has associated with it a mass $m_j^{(\alpha)}$ which behaves in the required manner.

SOME EXAMPLES OF APPLICATION OF THE SUM RULE

At the outset, it must be emphasized that the sum rule as here stated‡ can only be applied to three or more isotopic molecules, whereas the product rule can be applied to any pair. Table I shows the application to C_2H_2, C_2D_2, and C_2HD. The data for this and the succeeding examples (except $DC^{13}N$) have been taken from Herzberg.[2] The summations are extended over two classes of frequencies, namely the motions parallel and perpendicular, respectively, to the axis. No attempt is made to correct for anharmonicity.

The sum rule is applied in Table II to the molecules H_2O, D_2O, and HDO. According to Herzberg,[2] the frequency ω_3 of HDO has not been positively identified owing to overlapping by ω_1 of H_2O. By application of the product rule, a value of 3655 cm^{-1} is found for ω_3 of HDO, employing the frequencies of H_2O. Had this same frequency been calculated by the sum rule, a result of 3711 cm^{-1} would have been obtained. A more elaborate application, involving all the deuterated methanes, is given in Table III. The checks seem quite

TABLE III. Application of the sum rule to CH_4, CH_3D, CH_2D_2, CHD_3, and CD_4.

	CH_4		CH_3D		CH_2D_2		CHD_3		CD_4	
k	ω_k(cm^{-1})	ω_k^2(10^6 cm^{-2})	ω_k	ω_k^2	ω_k	ω_k^2	ω_k	ω_k^2	ω_k	ω_k^2
1	2914.2	8.491	2204.6	4.862	2139	4.575	2141.1	4.583	2084.7	4.347
2a	1526	2.329	1476.7	2.182	1450	2.103	1299.2	1.687	1054	1.111
2b	1526	2.329	1476.7	2.182	1285.6	1.654	1299.2	1.687	1054	1.111
3a	3020.3	9.120	2982.2	8.892	2974.2	8.845	2992.0	8.952	2258.2	5.099
3b	3020.3	9.120	3030.2	9.181	3020	9.120	2268.6	5.148	2258.2	5.099
3c	3020.3	9.120	3030.2	9.181	2255	5.085	2268.6	5.148	2258.2	5.099
4a	1306.2	1.706	1306.4	1.706	1034.4	1.069	982	0.964	995.6	0.991
4b	1306.2	1.706	1156.0	1.336	1235.2	1.525	1046	1.094	995.6	0.991
4c	1306.2	1.706	1156.0	1.336	1090.2	1.188	1046	1.094	995.6	0.991
			$(\frac{3}{4})\sigma(CH_4)+(\frac{1}{4})\sigma(CD_4)=40.480$				$\sigma(CH_3D)=40.857$			
			$(\frac{1}{4})\sigma(CH_4)+(\frac{3}{4})\sigma(CD_4)=30.036$				$\sigma(CD_3H)=30.360$			
			$\sigma_A=\omega_1^2+\omega_{2a}^2+\omega_{2b}^2+\omega_{3a}^2+\omega_{4a}^2$							
			$\sigma_B=\omega_{3b}^2+\omega_{3c}^2+\omega_{4b}^2+\omega_{4c}^2$							
			$(\frac{1}{2})\sigma_A(CH_4)+(\frac{1}{2})\sigma_A(CD_4)=18.317$				$\sigma_A(CH_2D_2)=18.245$			
			$(\frac{1}{2})\sigma_B(CH_4)+(\frac{1}{2})\sigma_B(CD_4)=16.916$				$\sigma_B(CH_2D_2)=16.919$			

‡ However, see the special rule stated subsequently.

TABLE IV. Application of the sum rule to $HC^{12}N$, $DC^{12}N$, $HC^{13}N$, and $DC^{13}N$.

	$HC^{12}N$		$DC^{13}N$		$DC^{12}N$		$HC^{13}N$	
	ω_k (cm^{-1})	$\omega_k^2(10^6$ $cm^{-2})$	ω_k	ω_k^2	ω_k	ω_k^2	ω_k	ω_k^2
1	2089	4.364	1916	3.671	1928	3.717	2055[a]	4.221
3	3312	10.969	2585	6.682	2629.3	6.913	3295	10.857
		15.333		10.353		10.630		15.078

$\sigma(HC^{12}N)+\sigma(DC^{13}N)=25.686$
$\sigma(DC^{12}N)+\sigma(HC^{13}N)=25.708$

[a] Calculated from $HC^{12}N$ by the product rule.

reasonable, and, in particular, it would be quite hard to reassign the CH_2D_2 frequencies and still satisfy the sum rule.

As a final illustration[3] of the application of the sum rule, the stretching frequencies for the superposition

$$(HC^{12}N)+(DC^{13}N)=(DC^{12}N)+(HC^{13}N) \quad (13)$$

are considered in Table IV. The frequency ω_1 for $HC^{13}N$ has not been observed but was calculated from ω_1 of $HC^{12}N$ by the product rule.

AN ADDITIONAL RULE

It is apparent from the previous discussion that the sum of the roots for any isotopic form of less than the maximum symmetry can always be expressed in terms of the sums for molecules of the maximum symmetry (CH_3D in terms of CH_4 and CD_4, etc.). Since the sums for the latter types of molecules can be written

$$\sum_k \lambda_k=\sum_j F_{jj}/m_j=\sum_{s=1}^{d} C_s\mu_s, \quad (14)$$

where $\mu_s=1/m_s$ and the summation over s is over the non-equivalent sets of atoms, it is apparent that if there are d such sets of atoms in the most symmetrical form of the molecule, then the sum of all roots for any isotopic form whatsoever can be expressed in terms of the sums for d suitably chosen forms of the maximum symmetry. Suppose the sum $\sum\lambda_k$ for the "unsubstituted" molecule is designated as σ_0, that for the molecule in which the first equivalent set is entirely substituted as σ_1 (but no other set is changed), etc. Then from (14)

$$\begin{aligned} C_1&=(\sigma_0-\sigma_1)/(\mu_1-\mu_1') \\ C_2&=(\sigma_0-\sigma_2)/(\mu_2-\mu_2') \\ &\cdots\cdots\cdots\cdots\cdots\cdots \\ C_{d-1}&=(\sigma_0-\sigma_{d-1})/(\mu_{d-1}-\mu_{d-1}') \\ C_d&=[\sigma_0-(C_1\mu_1+C_2\mu_2+\cdots C_{d-1}\mu_{d-1})]/\mu_d, \end{aligned} \quad (15)$$

where the unprimed reciprocal masses refer to the unsubstituted molecule. Once the C_s are known, the σ for any other molecule of the maximum symmetry can be immediately calculated. In conclusion, there can be only d independent sums of roots.

In the ammonia example, where the nitrogen and the three hydrogens constitute the $d=2$ distinct sets, it is therefore possible to express σ for all forms in terms, say, of the σ for $N^{14}H_3$ and $N^{14}D_3$, instead of requiring all four isotopic species as employed in (2).

HIGHER ORDER ISOTOPE RULES

In addition to the sum rule and the product rule, there will exist connections between the frequencies of isotopic molecules based on other combinations of frequencies, such as the sum of the products of roots (λ_k) by pairs. In the latter case, one obtains

$$\sum_{kl}\lambda_k\lambda_l=\sum_{ij}A_{ij}\mu_i\mu_j \quad (16)$$

in which the A_{ij} are independent of isotopic composition because they depend only on the force constants and geometry. In simple cases, the number of independent A_{ij} may be sufficiently small so that enough isotopic forms are available to make possible their evaluation, but in most cases this will require an impractical number of forms. These higher rules will not therefore be considered further here.

[3] W. S. Richardson, J. Chem. Phys. **19**, 1213 (1951).

A Reduced Equation of State for Gases and Liquids*

SIDNEY W. BENSON AND ROBERT A. GOLDING†
Departments of Chemistry and Chemical Engineering University of Southern California, Los Angeles 7, California
(Received May 8, 1951)

An empirical, reduced equation of state is presented which holds with reasonable accuracy for both liquids and gases. Liquid densities of non-associated substances are predicted to within 4 percent, vapor pressures to within 25 percent, heats of vaporization to within 10 percent and gas isotherms reproduced to within 10 percent. The values predicted for the coefficients of thermal expansion and compressibility are not better than 30 percent. With the exception of the latter which are incapable of good representation by any such reduced equation, the equation represents a marked improvement over the van der Waals and Berthelot equations.

THAT there should exist a reduced equation of state capable of representing the properties of both gases and liquids seems evident from both theoretical considerations[1] and experimental data.[2] The present paper discusses such an equation which was developed empirically employing the following criteria:

1. The equation must not contain more than 3 constants (including R).
2. It must approach the ideal gas law at low densities.
3. It should approximate to the following experimental data: (a) Trouton's rule: $E_{vap}/RT=9.5$. (b) Critical ratio: $1/Z_c=RT_c/P_cV_c=3.70$. (c) Liquid density rule: $1/\phi_b=2.72$ (at the boiling point). (d) The coefficients of thermal expansion and compressibility at the normal boiling points were about 1.3×10^{-3}/°K and 1.5×10^{-4}/atmos respectively.[3]

Two algebraic forms were investigated:

$$P=RT/(V-bV^{-s}T^{-n})-a/(V^mT^p), \quad (1)$$

$$P=RT/V+aT^n/V^m-bT^x/V^y, \quad (2)$$

TABLE I. Comparison of Van der Waals, Berthelot, and modified equations.

Physical property	Mean exp. value	Modified equation	Van der Waals equation	Berthelot equation
Critical ratio $1/Z$	3.70	3.624	2.67	2.67
Reduced limiting volume at high pressures*	0.26	0.29	0.33	0.33
Trouton constant H_{vap}/RT_b at $T_b=0.625T_c$	10.5	10.95	5.0	16
Reduced liquid density at $\theta=0.625$	2.75	2.838	2.26	2.60

* At very high pressures the limiting volume of gases approaches a value of about $0.26V_c$ which is practically temperature independent. See J. P. Kuenen, *Handbuch der Allgemeinen Chemie* (Akademische Verlagsgesellschaft, Leipzig, 1919), Vol. 3, p. 259.

in which the various exponents could be evaluated by fitting to the above requirements.[4] Only the first (Eq. (1)) will be discussed here.[5]

The best choice of exponents is shown in the following,

$$P=RT/(V-bV^{-\frac{1}{3}})-a/V^{5/3}T^{\frac{1}{3}}, \quad (3)$$

where $a=0.9099RT_c^{5/3}V_c^{\frac{1}{3}}$; $b=0.1567V_c^{\frac{1}{3}}$ and in reduced form:

$$P/P_c=\pi=3.624[\theta/(\phi-0.1567\phi^{-\frac{1}{3}})-0.9099/\phi^{5/3}\theta^{\frac{1}{3}}]. \quad (4)$$

Various physical quantities calculated from this equation are listed in Table I along with corresponding values calculated from the Van der Waals and Berthelot equations.

At temperatures near or below the normal boiling point, the pressure may be ignored compared to the other terms in the equation of state. This approximation

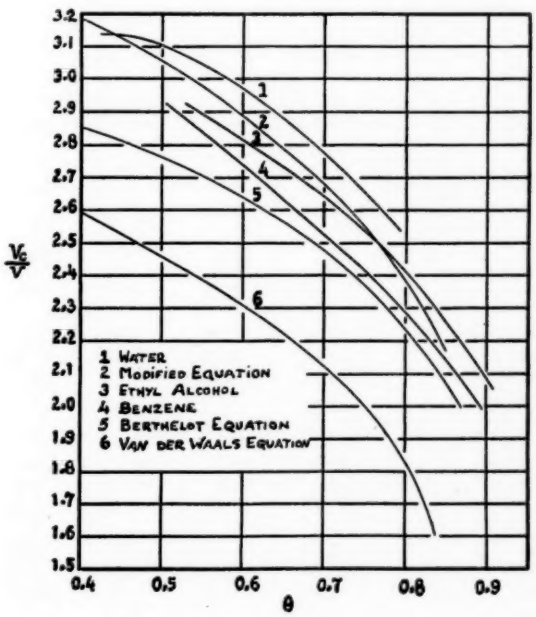

FIG. 1. Reduced liquid densities.

* Part of the contents of this paper are taken from the Master's Thesis of Robert Golding presented to the Graduate School of the University of Southern California, August 1950.

† Present address, Shell Chemical Company, California.

[1] J. deBoer and A. Michels, Physica **5**, 945 (1938); K. S. Pitzer, J. Chem. Phys. **7**, 583 (1939).

[2] S. W. Benson, J. Phys. and Colloid Chem. **52**, 1060 (1948).

[3] These values show a spread of some 10–50 percent depending on the class of liquids investigated. They are not therefore a reliable guide.

[4] Equation (1) was first reported by S. W. Benson (S. W. Benson and E. Gerjuoy, J. Chem. Phys. **18**, 215 (1950)).

[5] S. W. Benson made an extended investigation of the second form (Eq. (2)) and found that it will not represent the gas and liquid as well as Eq. (1).

TABLE II. Physical properties computed from modified equation.

Reduced temperature θ	Reduced liquid density Δ_l	$\frac{E_{vap}}{RT_c}$	Reduced vapor pressure π	Reduced coeff. of therm. exp. αT_c	Reduced coeff. of comp. $\times 10^3$ βP_c	Supersat. ratios	Reduced liquid tensile strengths
0.400	3.182	9.06	9.23×10^{-6}	0.364	2.09	—	18.8
0.420	3.158	8.73	3.2×10^{-5}	0.385	2.43	—	17.3
0.440	3.133	8.42	9.5×10^{-5}	0.407	2.81	350 (at	15.88
0.460	3.107	8.13	1.4×10^{-4}	0.430	3.24	$\theta=0.45$)	14.7
0.480	3.080	7.86	3.8×10^{-4}	0.454	3.73	—	13.6
0.500	3.051	7.60	0.000750	0.480	4.28	88	12.9
0.520	3.021	7.35	0.0014	0.508	4.92	—	11.1
0.540	2.990	7.12	0.0025	0.537	5.64	30	10.2
0.560	2.957	6.90	0.0037	0.569	6.47	($\theta=0.55$)	9.2
0.580	2.922	6.69	0.00638	0.605	7.43	—	8.3
0.600	2.886	6.48	0.00940	0.644	8.55	13	7.548
0.620	2.848	6.29	0.0139	0.687	9.84	—	6.80
0.640	2.808	6.10	0.0202	0.734	11.4	7.5	6.12
0.660	2.762	5.91	0.0252	0.787	13.1	($\theta=0.65$)	5.40
0.680	2.721	5.73	0.0356	0.847	15.3	—	4.79
0.700	2.673	5.56	0.0456	0.916	17.9	4.9	4.22
0.720	2.623	5.39	0.0589	0.997	21.0	—	3.69
0.740	2.568	5.21	0.074	1.093	25.0	3.4	3.16
0.760	2.510	5.04	0.090	1.207	30.0	($\theta=0.75$)	2.66
0.780	2.447	4.88	0.101	1.353	36.7	—	2.23
0.800	2.378	4.70	0.133	1.533	45.4	—	1.81

permits great simplification of calculation in this region.[6]

The following equations were derived from Eq. (1) by means of this approximation:

A. Liquid Density: (by numerical solution of resulting equation).

B. Energy of Vaporization:

$$E_{vap}/RT_c=2.275/(\theta\phi)^{\frac{3}{2}}. \quad (5)$$

C. Vapor Pressure:[7]

$$Ln\pi=-1-1.446/\theta^{5/3}\phi^{\frac{3}{2}}-Ln[3.403/\theta^{1/9}\phi^{13/9}]. \quad (6)$$

D. Coefficient of Thermal Expansion:

$$\alpha=5/3T_c[(\theta\phi)^{\frac{3}{2}}/(1.365-2.167\theta^{5/3}\phi^{\frac{3}{2}})]. \quad (7)$$

E. Coefficient of Compressibility:

$$\beta=\theta^{\frac{3}{2}}\phi^{5/3}/3.297P_c[1.365/\theta^{5/3}\phi^{\frac{3}{2}}-2.167]^{-1}. \quad (8)$$

TABLE III. Comparison of vapor isotherms.[a]

Pressure atmos.	Reduced temp.	ϕR_{dW}	Oxygen ϕ_{ber}	Oxygen ϕ_{eq3}	Oxygen ϕ_{obs}	Ethane ϕ_{eq3}	Ethane ϕ_{obs}	Carbon dioxide ϕ_{eq3}	Carbon dioxide ϕ_{obs}	Water ϕ_{eq3}	Water ϕ_{obs}
1	$\theta=1.1$	145	145	194	186	188	195	287	298	904	1030
5		28.5	28.6	36.8	36.5	35.7	38.2	55	59.7	162	206
10		13.9	14.0	17.6	17.7	17.0	18.7	26.9	29.8	83	102
50		2.01	2.21	2.43	2.57	2.32	2.74	4.19	4.84	15.2	19.5
100		0.673	0.805	0.750	0.765	0.730	0.765	1.42	1.59	6.94	9.13
150		0.578	0.630	0.576	0.590	0.570	0.630	0.735	0.810	4.15	5.62
200		0.537	0.569	0.517	0.520	0.513	0.583	0.603	0.671	2.79	3.82
500		—	—	—	—	0.409	0.484	0.449	0.516	—	—
1	$\theta=1.5$	199	199	268	255	260	266	392	407	1180	1410
5		39.7	39.8	52	50.6	51	53.2	77	81.4	234	249
10		19.5	19.8	26.9	25.1	25.8	26.2	38.6	40.7	117	141
50		3.55	3.84	4.55	4.65	4.42	4.88	7.00	7.65	22.8	26.4
100		1.58	1.90	2.10	2.13	2.01	2.26	3.23	3.62	10.8	13.6
150		0.99	1.28	1.33	1.35	1.30	1.45	2.05	2.34	6.98	8.94
200		0.78	1.00	0.980	1.03	0.95	1.09	1.47	1.70	5.07	6.46
500		—	—	—	—	0.521	0.627	0.646	0.780	—	—

[a] Values listed are reduced vapor volumes.

[6] S. W. Benson and E. Gerjuoy, J. Chem. Phys. **17**, 914 (1949).

[7] The vapor pressure equation was derived from the condition that $\pi(\phi_g-\phi_l)=\int_{\phi_l}^{\phi_g}\pi d\phi$ which is equivalent to equating the chemical potentials of gas and liquid. Ignored terms become important for $\theta\geq0.800$.

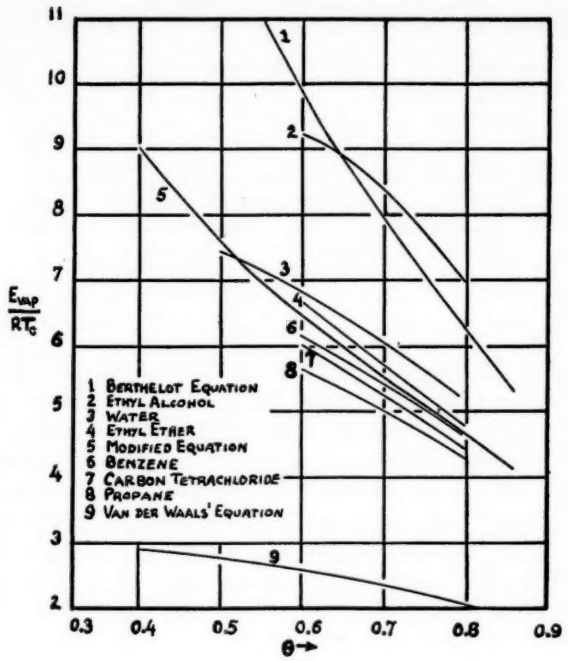

FIG. 2. Energies of vaporization.

In addition, it was possible to calculate exactly, from the maximum and minimum in each isotherm, supersaturation ratios[4] and liquid tensile strengths.[6] As a severe check on the behavior of the equation in the vapor region, gas isotherms were calculated for $\theta = 1.1$ and 1.5. These calculations together with others made from the above equations are shown in Tables II and III.

A comparison of the present equation, with the Van der Waals and the Berthelot equations with respect to liquid densities is shown in Fig. 1. Some comparisons of energies of vaporization are made in Fig. 2 and some typical vapor pressures are shown in Fig. 3.

The coefficients of thermal expansion predicted by Eq. (1) are about 20 percent lower than the experimental

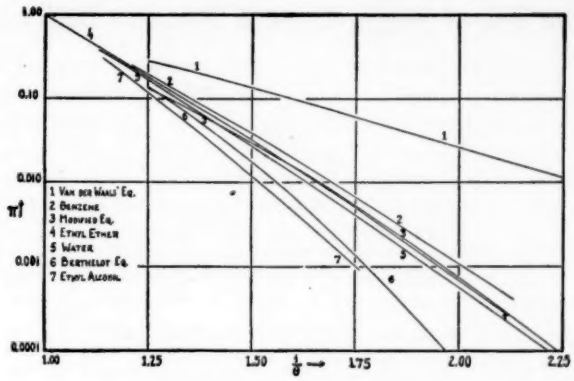

FIG. 3. Reduced vapor pressures.

values. They tend to be nearly correct for the alcohols and too high for the strongly bonded liquids such as water. The calculated coefficients of compressibility tend to be high by anywhere from 40–50 percent for the paraffins, 10 percent high for the aromatics and halides and are low by some 10–30 percent for alcohols and acids.[8] It is clear that these coefficients show much greater variation than other liquid properties.

The superiority of the present equation to other reduced equations holds also in the gas and vapor regions. Table III compares the vapor volumes predicted by the various equations with some observed values. The Van der Waals and Berthelot values are shown only for oxygen, values in the other cases showing the same agreement or worse.

[8] It is actually impossible to make a choice of exponents in Eqs. (1) or (2) that will meet the requirements listed and simultaneously give good values for the coefficients of compressibility and thermal expansion. In fact the form of these equations is such that it is impossible to get good values for both the coefficients of compressibility and thermal expansion at the same time. The choice made here was to obtain better values for the latter. It is not surprising that there is so much difficulty in fitting these coefficients. They constitute a very sensitive test for any equation of state.

The Use of Single-Crystal Neutron Diffraction Data for Crystal Structure Determination*

S. W. Peterson and Henri A. Levy
Oak Ridge National Laboratory, Oak Ridge, Tennessee

(Received August 30, 1951)

Intensities of neutron reflections from single crystal specimens of several substances have yielded structure factors in close agreement with calculation and with those measured by the usual powder method. Specimens whose dimensions were in the millimeter range were used. Three materials yielded low results, probably because of extinction in the single crystal specimens. The use of single crystal neutron reflections for crystal structure determination appears practical in many cases.

NEUTRON diffraction has in recent years become a valuable supplement to x-ray diffraction for studying structures of crystals. To date only the powder method has been applied. Because available neutron beams are of low intensity, it has not been possible to construct spectrometers of high resolution. Typical line widths in powder patterns are of the order of one degree at small scattering angle and increase rapidly as the scattering angle increases. Thus only simple, highly symmetric crystals give powder patterns sufficiently resolvable to yield data useful for crystal structure determination.

These limitations would largely disappear in a single-crystal method, which, as in the x-ray case, has inherently greatly enhanced resolution. The practicability of single-crystal methods has, however, been questioned because of extinction. Bacon and Lowde[1] have made a theoretical examination of this question; they conclude that in crystals sufficiently large for use in neutron crystallography, i.e., large enough to permit the observation of many reflections with a single specimen, secondary extinction would be of overriding importance, intensities being more strongly dependent on the mosaic spread of the specimen than on the structure factors. These authors concluded that, in general, crystal specimens would have to be thinner than about 0.1 mm to avoid these difficulties.

We have been led to question the generality of this conclusion by the following considerations. Many crystals do not show as high a degree of perfection or as large values of Q, the integrated reflection per unit volume, as MgO, the crystal Bacon and Lowde chose as an example for detailed calculation. For example, if their "thin crystal" criterion is applied to the (200) reflection of NaCl, using a mosaic spread parameter of 10′ and a wavelength of 1.16A, a limiting thickness of 1 mm is computed; this thickness is adequate for obtaining extensive neutron data. Further, even if the strongest crystal reflections were to be severely reduced by extinction, weaker reflections may well not be so affected and therefore give useful data. Finally, if a few strong reflections are subject to appreciable extinction, it should be possible, as in the x-ray case, to make empirical corrections by the method of Darwin.[2]

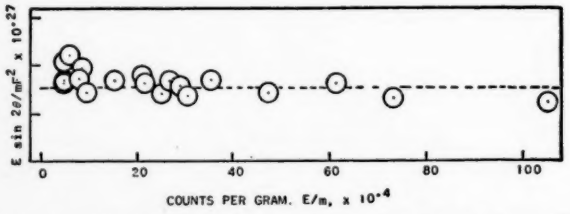

FIG. 1. A plot of the ratio of observed single crystal intensities for NaCl to the calculated value of $F^2/\sin 2\theta$ against observed intensity, expressed as counts per gram.

We report here preliminary results of a series of empirical tests on the feasibility of utilizing single crystal neutron diffraction data. We find that intensities from NaCl, KCl, KBr, KHF, and NH_4Cl single crystals yield correct structure factors without extinction corrections to an accuracy ample for structural purposes. However, intensities from the strong reflections of CaF_2, $CaCO_3$, and LiF yield structure factors which are substantially low and appear to be significantly affected by extinction.

The spectrometer used is similar to one described by Wollan and Shull.[3] Each single crystal specimen was mounted on a fine glass fiber set on a goniometer head in the usual fashion, and was bathed in neutron radiation monochromated by reflection from a (111) face of a single crystal of copper. The wavelength was 1.16A. Integrated reflections were measured by recording total neutrons counted as the crystal was rotated, usually at 8° per hour, through the reflecting position, while the counter was rotated synchronously at twice this angular velocity. Background intensity measured with the crystal and counter set just off the reflecting position was subtracted from the count.

In Fig. 1 are the results of measurements on 19 reflections from NaCl. The abscissa is the observed intensity expressed as counts per gram of crystal and the ordinate is the ratio of this quantity to the calculated value of $F^2/\sin 2\theta$. These calculated values utilize the scattering amplitudes of Shull and Wollan[4] and incorporate separate factors for Na and Cl as evaluated from careful

* This work was performed for the AEC.

[1] G. E. Bacon and R. D. Lowde, Acta Cryst. **1**, 303 (1948).

[2] R. W. James, *The Optical Principles of the Diffraction of X-rays* (G. Bell and Sons, Ltd., London, 1948), p. 292.

[3] E. O. Wollan and C. G. Shull, Phys. Rev. **73**, 830 (1948).

[4] C. G. Shull and E. O. Wollan, Phys. Rev. **81**, 527 (1951).

TABLE I. Single crystal neutron reflections from NaCl.

Indexes	Structure factor × 10^{12} Observed[a]	Calculated	Observed reflection, counts per gram × 10^4 Specimen 1	Specimen 2	Specimen 3
111	2.45	2.50	30.2	31.8	28.9
200	4.89	5.12	105.2	100.3	78.3
220	4.80	4.91	73.2	81.0	···
311	2.35	2.30	15.3	···	···
222	4.80	4.72	61.3	···	···
400	4.48	4.56	47.5	47.4	···
331	2.12	2.14	9.9	10.2	···
422	4.18	4.22	35.6	34.1	···
333	2.02	1.98	8.04	7.8	7.22
511	2.10	1.98	8.65	7.6	···
440	(3.90)	3.90	28.8	28.7	26.0
600	3.70	3.75	24.9	25.4	17.5
442	3.84	3.75	26.8	···	···
533	1.85	1.69	6.07	5.0	···
622	3.51	3.48	21.9	···	···
444	3.44	3.33	21.1	···	···
711	1.59	1.56	4.52	4.3	···
551	1.60	1.56	4.56	···	···
553	1.55	1.44	4.44	···	···
Weight of specimen, mg			10.5	15.8	72.9

[a] From reflections from specimen 1. No corrections for absorption were made. These data were normalized to make (440) agree with calculation.

x-ray measurements by Waller and James.[5] In the absence of extinction, there should be no trend in the ratio with the intensity of the reflection. A mild deviation of the strongest reflections from a horizontal line suggests that these reflections may be subject to a small extinction effect which is, however, not over 15 percent of the observed intensity. The dotted line indicates the ordinate value chosen to establish the incident beam intensity and subsequently used to convert observed values for this and other crystals to absolute structure factors. Table I compares observed and calculated structure factors for this sodium chloride crystal, and also compares observed integrated reflections for three specimens on a counts-per-gram basis. The strong reflections of the larger specimens show deviations which are very likely due to extinction, but even here the effects are not so severe as to make the data useless for structure determination.

Table II compares a few structure factors measured from single crystal reflections from a number of substances with those measured from the usual powder intensities. Calculated structure factors without temperature corrections are also listed. Approximate corrections for absorption in the single crystals were estimated, treating each specimen as that cylinder parallel to the rotation axis which most nearly approximated its actual form. The corresponding correction was applied to the NaCl data used as standard. The usual absorption corrections were applied to the powder data. Good agreement is obtained for KCl, KBr, KHF_2, and NH_4Cl, while LiF, $CaCO_3$, and CaF_2 show deviations probably assignable to extinction in the single crystal. These last three materials are known to crystallize with a high degree of perfection.

[5] I. Waller and R. W. James, Proc. Roy. Soc. (London) **A117**, 214 (1927).

Also listed in Table II are calculated limiting thicknesses for a number of the reflections according Bacon and Lowde's thin crystal criterion. The formu a was applied for the case of symmetrical transmission and the cosine of the angle of the incident beam with respect to the normal to the surface was taken as unity. We have assigned the mosaic spread parameter for all specimens the low value of 5′ in the absence of more detailed knowledge. These calculated thicknesses should be roughly applicable to specimens differing from parallel plates if compared to the maximum dimension in the section parallel to the incident and scattered beams. The values of this dimension for our specimens, also listed in the table, are in general larger than the thin crystal limit even in those cases which gave little or no extinction. However, considering that the mosaic spreads may be larger by a factor of two or three than that assumed, this does not invalidate the theoretical criterion of Bacon and Lowde. It is nevertheless apparent that the limiting thickness of 0.1 mm postulated by Bacon and Lowde does not have any general significance, and that in many cases it is possible to use crystals with thicknesses in the millimeter range for structural work.

In addition to the foregoing data, a large number of intensities have been measured from a single crystal of KHF_2 in order to establish the hydrogen atom parameter and the temperature factors. The excellent agreement between experimental and calculated structure factors for the complete list of reflections examined, with no extinction corrections, is additional strong evi-

TABLE II. Comparison of structure factors from single crystal and powder measurements.

Substance	Indexes	Structure factor × 10^{12} Obs. from powder	Obs. from single crystal	Calc.[a]	Thin crystal limit,[b] mm	Thickness,[c] mm
KBr	(111)	1.29	1.27	1.28		
	(200)	4.04	4.09	4.08	1.6	1.9
KCl	(111)	2.40	2.37	2.56		
	(200)	5.04	4.71	5.36	0.7	1.8
KHF_2	(121)	3.09	3.08	3.06[d]	2.3	2.8
NH_4Cl	(110)	1.34	1.27	···	0.8	2.0
LiF	(111)	2.80	1.63	2.92	0.2	1.8
	(200)	1.51	1.04	1.48		
	(400)	1.49	1.19	1.48		
CaF_2	(111)	1.74	1.57	1.95		
	(200)	2.45	2.13	2.44	0.4	1.7
	(220)	6.17	3.17	6.36		
$CaCO_3$	(211)[e]	3.29	2.39	3.46	0.5	1.6

[a] No temperature correction included except as noted.
[b] According to the "thin crystal" criterion of Bacon and Lowde.
[c] Approximately the largest dimension of the specimen in the section normal to the rotation axis.
[d] Includes temperature factors.
[e] Cleavage plane. Indexes and structure factor based on primitive rhombohedral unit.

dence that extinction is not a serious problem in many crystal specimens of moderate size. A complete description of this work will appear separately.

We may conclude that single crystal neutron reflections should be useful for structure determinations in many cases. Inherent advantages of the method include greatly increased resolution and greatly reduced sample size. A corollary to the latter feature is that incoherent scattering is greatly reduced relative to the intensity of Bragg reflections; this will be of great importance in crystals containing hydrogen and will make unnecessary the preparation of deuterated specimens, usually required in the powder method. It is clear that many relatively complex crystals, including those containing several hydrogen atoms, are now open to attack by neutron diffraction.

THE JOURNAL OF CHEMICAL PHYSICS VOLUME 19, NUMBER 11 NOVEMBER, 1951

Experimental Determination of Even-Odd Character of Excited Electronic States of Molecules with a Center of Symmetry

JOHN R. PLATT
Physics Department, University of Chicago, Chicago, Illinois
(Received September 24, 1951)

Even-even transition intensities increase with monosubstitution but decrease with opposed disubstitution. Even-odd transition intensities which increase with monosubstitution must increase further with opposed disubstitution.

Determination of parity in this way may settle disputed assignments. Thus the $^1A_{1g}-^1E_{2g}$ π-transition of benzene is probably at 1700 A. The first singlet absorption of naphthalene is $^1A_{1g}-^1B_{1u}$ or $^1A_{1g}-^1B_{2u}$ and cannot be $^1A_{1g}-^1A_{1g}$ even though the cancellation of transition matrix elements (from configuration interaction, in the one-electron approximation) gives it an intensity and vibrational structure similar to those in a forbidden transition. The visible bands of porphine are even-odd ($a_{2u}\rightarrow e_g$ $^1A_g-^1Q_u^0$).

Intensities in the 2100 A transition of phenyl derivatives are being remeasured to settle its assignment in benzene, since existing data give conflicting results.

IN molecules with a center of symmetry, transitions from an even ground state to an even excited state are forbidden, but may become allowed if substitution perturbs the symmetry. The intensity of the observed absorption then increases, especially in the 0—0 vibrational band. However, disubstitution by the same substituents at exactly opposite positions restores the symmetry and reduces the intensity again to nearly its original value, if the vibrational interaction which makes the absorption visible is not too greatly altered by the substitution. The "spectroscopic moments"[1] of equal substituents at opposed positions therefore exactly *cancel* for an even-even transition.

Similarly, by first-order perturbation theory, the spectroscopic moments of equal substituents at opposed positions must *add* for an even-odd transition, giving approximately four times the intensity change produced by one substituent alone.[1]

These differences make possible the unambiguous determination of the parity of every spectroscopically observed excited state of a centrally symmetric molecule. In many cases, this information alone will settle disputes over assignment of the states to theoretically predicted wave functions.[2]

Thus, the 2100A transition of benzene which was long assigned as $^1A_{1g}-^1B_{1u}$[3] has recently been proposed to be $^1A_{1g}-^1E_{2g}$.[4] This proposal has been made in the implicit faith that certain approximate energy level calculations including configuration interaction must give the correct *sequence* of excited states, even though the absolute values of energies given by calculations of this kind are frequently in error by 2 ev and more, and the differences between the different approximations used by different computers are often much greater than this.[4]

Unfortunately the available data in the literature on intensities of the corresponding transitions in mono- and di-substituted benzenes with moderately strong substituents such as OH, NH_2, and COOH are scanty and conflicting. They are also partially invalidated by use of polar solvents at unspecified pH values. We are now engaged at this laboratory in remeasuring some of these intensities in nonpolar solvents in order to settle the assignment of this transition.

Pending the outcome of these measurements, it seems more likely that the forbidden $^1A_{1g}-^1E_{2g}$ phenyl π-electron transition is the relatively weak peak near 1700–1730A which is not clearly seen in benzene itself but appears in toluene and in o- and m-xylene, becoming weak again with opposed disubstitution in p-xylene.[5]

[1] J. R. Platt, J. Chem. Phys. **19**, 263 (1951).
[2] J. R. Platt, J. Chem. Phys. **19**, 101 (1951), especially pp. 115–6.
[3] C. C. J. Roothaan and R. S. Mulliken, J. Chem. Phys. **16**, 118 (1948).
[4] D. P. Craig, Proc. Roy. Soc. (London) **200**, 401 (1950); Parr, Craig, and Ross, J. Chem. Phys. **18**, 1561 (1950).
[5] J. R. Platt and H. B. Klevens, Chem. Revs. **41**, 301 (1947).

Such intensity behavior indicates that the observed peak is probably even-even, supporting this assignment, which was proposed for it earlier[6] because it lay on a smooth sequence with the other even-even $e \rightarrow g$ $^1A - {}^1C_b$ transitions[6] in naphthalene and anthracene which showed the same kind of increase of intensity with loss of central symmetry.

The intensity of this 1730A peak (f about 0.3 in the xylenes) seems too great for a Rydberg transition (f about 0.03 in ethylene),[7] especially an even-even one, but is reasonable for an even-even π-electron transition.[6] And its position is within 2000 cm^{-1} of the position predicted for $^1A_{1g} - {}^1E_{2g}$ by either the free-electron or the LCAO-overlap method (with $\beta_{spect} = 20{,}000$ cm^{-1}; and assuming the singlet-triplet separation is 4000–10,000 cm^{-1}). This is significant because these methods are successful to this accuracy in predicting some 50 excited states of other ring systems.[6, 8, 9]

Similarly, the lowest singlet transition in naphthalene is certainly even-odd as shown by its increases of intensity in 1,5- and 2,6-dichloronaphthalenes.[1] This confirms its assignment as $^1A_{1g} - {}^1B_{1u}$[10] or $^1A - {}^1L_b$[6] (or possibly $^1A_{1g} - {}^1B_{2u}$)[10] and makes impossible its assignment as $^1A_{1g} - {}^1A_{1g}$,[11] in spite of its low intensity and apparently forbidden type of vibrational structure.[12] This shows clearly that the "accidental" cancellation of transition matrix elements in a formally-allowed one-electron transition (such as this one is if it is even-odd), because of the effect of configuration interaction[10] in producing a high "effective angular momentum" in the excited state,[6] can make such an allowed transition mimic the appearance of a forbidden one, not only in its low intensity but also in its vibrational structure. Therefore, in a complex molecule neither the intensity nor structure can be relied on for proof that an observed transition would not be formally allowed in the one-electron approximation. Since the theoretically predicted energies or sequence of energies is evidently also no more than a rough guide in assignments, the perturbation method or comparison method emerges as an especially useful guide to classification of electronic states, at least when the observed changes can be interpreted, as in these cases.

The visible bands of porphine are believed to represent another case of a formally-allowed one-electron transition which is relatively weak and presumably "accidentally" forbidden by the same mechanism[13–15] and which has a weak 0–0 band (especially in the salts or hydrochlorides,[16] where the D_{4h} symmetry is strictly obtained) but which is nevertheless certainly even-odd, as shown by di- and poly-substitution effects on intensities in the porphyrins.[17] If we treat the removal of a double bond from the porphine ring as a perturbation, the addition of the resultant spectroscopic moments for bacteriochlorophyll, with two opposite double bonds removed, accounts for the fact that its first red band is about four times as intense as the first band in the chlorins which have only one double bond removed. This demonstrates the even-odd character of the transition and shows the approximate validity, even with these drastic changes, of the first-order perturbation theory.

[6] J. R. Platt, J. Chem. Phys. **17**, 484 (1949), especially p. 491.
[7] Platt, Klevens, and Price, J. Chem. Phys. **17**, 466 (1949).
[8] H. B. Klevens and J. R. Platt, J. Chem. Phys. **17**, 470 (1949).
[9] J. R. Platt, J. Chem. Phys. **18**, 1169 (1950).
[10] J. Jacobs, Proc. Phys. Soc. (London) **62**, 710 (1949).
[11] D. P. Craig, Disc. Faraday Soc. **9**, 5 (1951).
[12] H. Sponer and G. P. Nordheim, Disc. Faraday Soc. **9**, 19 (1951).
[13] W. T. Simpson, J. Chem. Phys. **17**, 1218 (1949).
[14] H. Kuhn, Chimia **4**, 203 (1950).
[15] Longuet-Higgins, Rector, and Platt, J. Chem. Phys. **18**, 1174 (1950).
[16] J. G. Erdman and A. H. Corwin, J. Am. Chem. Soc. **68**, 1885 (1946).
[17] J. R. Platt, "Electronic structure and excitation of polyenes and porphyins," Chapter 4 in *Radiation Biology* (edited by Sterling Hendricks) (McGraw-Hill Book Company, Inc., New York, to be published), vol. III.

Viscosity of Neopentane

M. K. PHIBBS*
Division of Chemistry, National Research Council Ottawa, Canada
(Received May 21, 1951)

The viscosity of neopentane has been measured between −15°C and 30°C. These results are consistent with published work covering the temperature range 30°C to 150°C. The viscosity data for neopentane have been compared with similar data for the other pentanes. This comparison has provided an example of the importance of molecular shape for viscosity behavior. The possible significance of molecular shape for the interpretation of viscosity curves of binary mixtures is noted. Finally, it has been suggested that further work on liquids composed of spherical molecules might be worthwhile.

THE viscosity of neopentane has been measured between 30°C and −15°C in a viscometer of the Ostwald type modified to permit "sealing off" and designed so that the driving head remained independent of temperature. N.B.S. standard samples of hexane and neopentane were used for calibration of the instrument and the measurements, respectively. The viscometer was filled by evacuating it completely and then distilling into it 5 cc of air free liquid. The temperature was controlled to within 0.05°C during a measurement. A "sealed off" dilatometer of standard design with a small dead space of known volume was used for the density determinations of neopentane.

The only other viscosity data for neopentane were obtained between 30°C and 150°C under moderately high pressure.[1] Linear extrapolation of these latter data on a pressure *versus* viscosity plot gave η (coefficient of absolute viscosity) at one atmosphere pressure for each temperature. The extrapolated values and the present results are plotted in Fig. 1. The latter results are also given in Table I. Viscosity data[2] for *n*-pentane, isopentane, and cyclopentane are included for comparison.

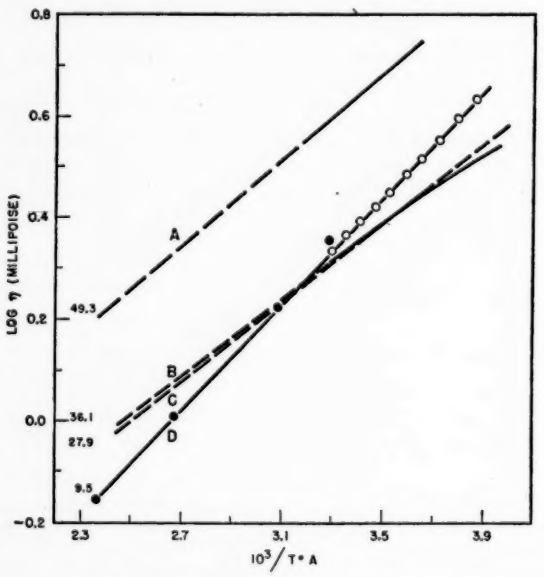

FIG. 1. Viscosity of pentanes: A. cyclopentane; B. pentane; C. isopentane; and D. neopentane. ○ our data. ● data from reference 1. Broken portions of lines represent extrapolation. The boiling points of the respective pentanes in °C are included at the left of the figure.

There seems to be no theory of viscosity sufficiently developed to help with an interpretation of the data in Fig. 1 but some qualitative remarks can be made. The graph for neopentane is a good straight line from −15°C (M.P. −16.6°C) to 149°C ($T_c \sim 3/2 T_B{}^0 A$ = 150°C). It is unusual that the functional form $\eta = A \exp(B/T)$ is correct over most of the accessible liquid range. Because neopentane is a spherical nonpolar molecule, any deviations from this functional form shown by other liquids might be attributable to asymmetry of either molecular shape or electrical field of force.

A comparison of the data in Fig. 1 for the pentanes reveals some interesting trends. At high temperature η increases with the T_B (boiling point) of the corresponding substance. The T_B are approximately a measure of the overall intermolecular forces of attraction.† At high temperatures thermal agitation has become severe enough to remove any trace of ordered arrangement in the liquid and the basic correspondence between η and T_B is revealed. At the low temperature end of the plot the correspondence between η and T_B has disappeared because the value of $d \log\eta/d(1/T)$ increases up the series pentane, isopentane, and neopentane. This is just the order of approach to spherical molecular shape. Ewell and Eyring[3] noted that the symmetrical molecules CCl_4, cyclohexane, and benzene fell into a special category. This trend toward larger values of $d \log\eta/d(1/T)$ is not restricted to spherical molecular shape. There seems to be a regular increase in $d \log\eta/d(1/T)$ within a group of isomers as the molecular shape approaches the sphere. For example, the order of increasing slope ($d \log\eta/d(1/T)$) within each group of isomers is butane, isobutane; hexane, 2,3-dimethylhexane; heptane, 2,2,3-trimethylbutane; *n*-butyl bromide, *t*-butyl bromide; *n*-butyl chloride, *t*-butyl chloride

* Present address: E. I. du Pont de Nemours and Company, Wilmington, Delaware.

[1] W. R. van Wijk and W. A. Seeder, Physica **7**, 45 (1940).

[2] J. M. Geist and M. R. Cannon, Ind. Eng. Chem. Anal. Ed. **18**, 611 (1946).

† A study of molecular models of the pentanes suggests that the differences among the T_B are probably determined largely by the possible area of contact between adjacent molecules in each case.

[3] R. H. Ewell and H. Eyring, J. Chem. Phys. **5**, 726 (1937).

and *n*-butanol, isobutyl alcohol, *t*-butyl alcohol. Within each group of isomers η and T_B are related at the high temperature end of the plot, as found for the pentanes.

The value of dV/dT (V=molar volume) increases in the same order as $d\log\eta/d(1/T)$ for the series pentane, isopentane, and neopentane. Because the value of dV/dT is largely a reflection of changes in the free volume $V_f=V-V_s$ (V_s molar volume of unexpanded solid phase) the above correspondence supports the familiar concept that η is closely dependent on V_f. It seems then that the absolute value of viscosity at high temperature is determined primarily by intermolecular forces of attraction but that the differences between values of $d\log\eta/d(1/t)$ among isomers are attributable to a free volume factor dependent on molecular shape. An explanation for this shape effect must be found before viscosity data can be properly interpreted.

The concept that neopentane molecules can pack three dimensionally whereas *n*-pentane molecules may pack two dimensionally like a bundle of logs may lead to asymmetrical and possibly smaller thermal expansion for the latter. One might suspect that the greater flexibility of *n*-pentane (adaptation of shape to flow situation) is important but the behavior of cyclopentane (see later) does not support this possibility. On the other hand it is conceivable that liquid neopentane is not quite a model liquid (cell or cage model) if there is any element of semi long range cooperative packing of molecules. However, the argument for cooperative effects is rather weak.‡

‡ Neopentane, like other substances composed of spherical molecules, is characterized by a solid phase with an abnormally high melting point which is attributed to the fact that the molecules rotate in the solid phase. Such solids are unusually soft and can be extruded extremely easily. The neopentane solid phase then is one in which the molecules have considerable freedom to rotate and to change position yet long-range order is maintained. It is normally considered that on melting a substance loses all vestiges of long-range order. However the existence of the "liquid crystalline" phase indicates that semi long-range order is not incompatible with a liquid phase. A gradual decrease in possible semi long-range order in neopentane with increasing temperature might then be the reason for a high value of $d\log\eta/d(1/T)$. However, cooperative phenomena are normally characterized by their abrupt disappearance at one temperature even for the liquid crystalline phase.

TABLE I. Viscosity of neopentane.

Temperature °C	30	25	20	15	10	5	0	−5	−10	−15
Viscosity (cps)	0.216	0.231	0.247	0.264	0.281	0.303	0.328	0.356	0.393	0.431

The behavior of cyclopentane is surprising because its value of $d\log\eta/d(1/T)$ is similar to that for *n*-pentane whereas cyclohexane and benzene, also disk-shaped molecules, behave more as though they had spherical molecular shape ($d\log\eta/d(1/T)$ large and abnormally high melting points which are unusually sensitive to pressure). The cyclopentane molecule is a flat disk which may be asymmetrical enough to prevent free rotation whereas cyclohexane with a puckered ring and benzene with π-electron orbitals $\perp$ to the ring plane may have enough symmetry to explain their behavior as spheres.

Any interpretation of viscosity curves of binary liquid mixtures of which one component is composed of spherical molecules must take account of this shape factor. For instance, addition of a little ethanol to CCl_4 at 5°C lowers the viscosity whereas addition of a little CCl_4 to ethanol increases the viscosity. An *S*-shaped curve of this type suggests first that CCl_4 and C_2H_5OH form a molecular compound and secondly that CCl_4 is associated.§ It seems more likely that the spherical shape of CCl_4 is the cause of this apparent association rather than that CCl_4 is an associated liquid.

Further information about this shape factor might be obtained by a study of the liquids CCl_4, methyl chloroform, 2,2-dichloropropane, tertiary butyl chloride along with neopentane. This set of model liquids could then serve as standards with which to compare the corresponding isomers.

§ This apparent association might be attributable to a difference of internal pressure between the two liquids and the association of ethanol but for the fact that the *S*-shape is peculiar to the viscosity and molar volume binary curves and does not appear in the vapor pressure curve of this binary system.

Letters to the Editor

THIS section will accept reports of new work, provided these are terse and contain few figures, and especially few half-tone cuts. The Editorial Board will not hold itself responsible for opinions expressed by the correspondents. Contributions to this section should not exceed 600 words in length and must reach the office of the Editor not later than the 15th of the second month preceding that of the issue in which the letter is to appear. No proof will be sent to the authors. A publication charge of $10.00 per Letter is made which, when honored, will entitle the Institution to 100 free reprints.

Note on the Hydrogen-Deuterium Isotope Effect in Crystals

CHRISTER E. NORDMAN AND WILLIAM N. LIPSCOMB
School of Chemistry, University of Minnesota, Minneapolis, Minnesota
(Received September 13, 1951)

THE hydrogen-deuterium isotope effect in crystals has been the subject of considerable experimental investigation. It has been found that substitution of D for H in LiH produces a shortening of the unit cube edge,[1] whereas in crystals with short hydrogen bonds a considerable expansion of the O−H−O distance results.[2] In the case of long hydrogen bonds no appreciable effect has been observed.[3]

A consideration of the difference between the probability distribution functions for H and D in these three cases suggests a simple explanation of the observed facts.

In a 3-body system O−H−O the hydrogen may be considered approximately as moving in a one-dimensional potential field U between the two end atoms. Assuming further that the latter are located at $x=\pm d$, it is seen that U is of the form,

$$U(d, x)=V(d+x)+V(d-x),$$

where $V(r)$ is the O−H potential function. The equilibrium value of d is determined by the condition,

$$\int_{-\infty}^{+\infty} P(x, d, m, T)[\partial V(d+x)/\partial x]dx-f(d)=0, \qquad (1)$$

where $f(d)$ is the repulsive O−O interaction force, and

$$P(x, d, m, T)=[1/Q(d, m, T)]\Sigma_n \exp(-E_n/kT)\cdot\psi_n^2(x, d, m)$$

is the probability distribution fuction for the H atom of mass m.

At a given temperature, let (1) be satisfied by $P(m)$ in Fig. 1, and let $P(m')$ be the distribution function for a particle of mass m'. Since the repulsive part of V is generally steeper than the attractive part, it follows that d must be slightly increased in order for $P(m')$ to satisfy (1). This increase will produce an additional widening of $P(m')$ arising from the slight widening of $U(d, x)$, it is however clear that an equilibrium value d' corresponding to $P(m')$ exists, which is $\gtrless d$ depending on whether $P(m')$ is broader or sharper than $P(m)$, that is, depending on the mean amplitudes of m' and m. Thus, in order to explain the observed isotope effects it is necessary to investigate the change in the probability distribution function produced by isotopic substitution.

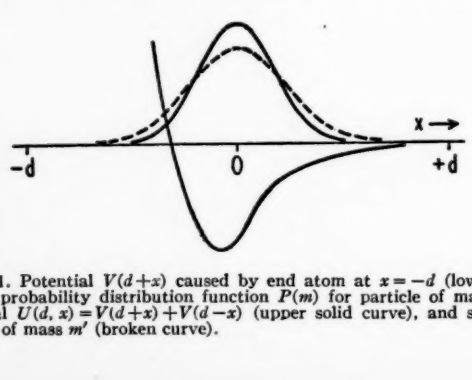

FIG. 1. Potential $V(d+x)$ caused by end atom at $x=-d$ (lower solid curve), probability distribution function $P(m)$ for particle of mass m in potential $U(d, x)=V(d+x)+V(d-x)$ (upper solid curve), and same for particle of mass m' (broken curve).

In lithium hydride $U(d, x)$ may be assumed to be closely parabolic. Since for a harmonic oscillator[4]

$$P(x, d, m, T)=(F/\pi)^{\frac{1}{2}}\exp(-Fx^2),$$

where $F=(4\pi^2m\nu/h)\tanh(h\nu/2kT)$, with $\nu(d, m)$ closely proportional to $m^{-\frac{1}{2}}$, it follows that an increase in m increases F in agreement with the observed decrease in Li−Li distance.

In short, O−H−O bonds $U(d, x)$ may be described as a steep-walled and more or less flat-bottomed well, with or without a small central maximum. As a preliminary approximation we have computed the mean amplitudes of H and D in the potential $U=A/(c-|x|)^2$. For a given c it can be shown that a value of A can be found at which the isotope effect reverses its sign, that is, for large A the function $P(x, m_D)$ is "sharper" than $P(x, m_H)$, the reverse being true when A is small. Particularly, when A goes to zero U approaches a potential "box," in which case it is easy to verify that the D-distribution is broader. On this basis we feel that the isotope effect in short hydrogen bonds can be explained in terms of the "box"-like form of the potential function.

In long hydrogen bonds the probability distribution function has two distinct peaks corresponding to the two minima in U. One peak will nearly coincide with the minimum of $V(d+x)$, the other will be approximately in the region of the minimum of $V(d-x)$, where, however, the derivative of $V(d+x)$ almost vanishes. It will be seen from (1) that the change in d produced by isotopic substitution will be small.

[1] E. Zintl and A. Harder, Z. physik. Chem. **28B**, 478 (1935).
[2] J. M. Robertson and A. R. Ubbelohde, Proc. Roy. Soc. (London) **170A**, 222 (1939); A. R. Ubbelohde, *ibid.* **173A**, 417 (1939); A. R. Ubbelohde and I. Woodward, *ibid.* **179A**, 399 (1942); D. H. W. Dickson and A. R. Ubbelohde, Acta Cryst. **3**, 6 (1950).
[3] J. M. Robertson and A. R. Ubbelohde, Proc. Roy. Soc. (London); A. R. Ubbelohde, *ibid.*; H. D. Megaw, Nature **134**, 900 (1934).
[4] P. Debye, J. Chem. Phys. **9**, 56 (1941). An error in this paper has been corrected by Y. Morino, *ibid.* **18**, 395 (1950).

Color Centers in Glass

R. K. SHELINE,* D. E. SHARP, AND W. J. ARNER
Libbey-Owens-Ford Glass Company, Research Division, Toledo, Ohio
(Received September 5, 1951)

A NUMBER of investigators[1-5] have shown that glass on exposure to the radiations of radium discolors to violet, yellow, or brown. Most of the observers were familiar with the fact that the depth of color increases with the increase of intensity of radiation or with the increase of the time of exposure to the radiation. It was also well known that the glass could be restored to its original color by heating and that luminescence occurred during the heating.

It is the intention of the authors to suggest that this discoloration is the result of the formation of color centers similar to those produced in the alkali halides when bombarded by x-rays or cathode rays.[6-8]

In 1922, 43 spent radiation emanation tubes having total weight of 1.7 grams were added to 1450 grams of a borosilicate glass having the following calculated composition.

SiO_2	68.9
K_2O	16.9
Na_2O	5.2
CaO	1.9
B_2O_3	7.0
As_2O_3	0.1

A quantitative spectrochemical analysis of this glass showed the presence of iron in quantities between 0.1 and 0.01 percent and

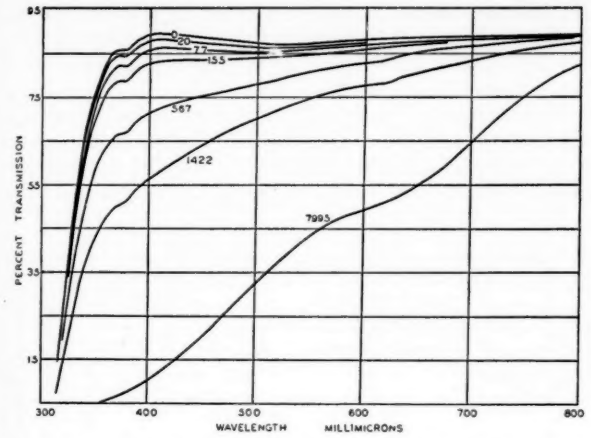

FIG. 1. The visible and ultraviolet spectrum of a radium containing borosilicate glass 0.221 inch thick: age in days shown on curve.

showed that there was less than 0.005 percent manganese present. In addition, there was approximately 0.1 percent chloride present as impurities in the sodium and potassium carbonate. No spectrometer was available to measure quantitatively the extent of the decolorization and the attendant absorption until May, 1944. At this time the following procedures were followed. Pieces of glass which had been discolored by the radium radiations were heated up to 350° for two hours and then cooled. During this time there was a considerable luminescence of the glass and the glass was rendered transparent and colorless to visible observation. The transmission of this glass was then run using a Beckman spectrophotometer. This is shown in Fig. 1 and is the curve marked 0. The transmission of this glass was again determined in 20, 77, 155, 567, and 1422 days as shown in Fig. 1. The transmission of a piece of glass, which was not decolorized by the heat treatment with a total life of 7995 days since fabrication, is shown in Fig. 1 and is marked 7995. The absorption maximum in the region of 5100 angstroms can be destroyed by heating for longer times at approximately 510°C.

The absorption at 3800 angstroms is present in spite of all heating, and it appears that this absorption is not in any way related to color centers but is instead related to the ferrous-ferric oxide equilibrium in glass. When glasses containing iron are prepared under conditions producing excellent chemical reduction, this absorption appears only as a shoulder. When the reduction is less perfect, a deeper absorption is shown.

In addition to this peak, three other peaks are present in Fig. 1—one at approximately 6175 angstroms, a second at approximately 5100 angstroms, and the third at less than 4000 angstroms. A maximum of this last-named peak does not seem to be attained at the cutoff in the transmittance of glass.

It is our belief that these three bands result from color centers which are produced by the alpha-, beta-, and gamma-rays from radium. These alpha-, beta-, and gamma-rays move through the glass network producing photoelectrons in the solid which move through the glass network at a high rate of speed producing secondary electrons and holes. It is the disposition of these secondary electrons and holes which results in the color centers in glass. Since lattice defect type color centers have not been suggested as occurring in vitreous solids previously, it is perhaps advisable to discuss the reasons one might expect to observe them in glass.

In vitreous quartz, oxygen tetrahedra serves to build a coherent but irregular network. The presence in glass of network modifiers (Na_2O, K_2O, and CaO) make the structure even more irregular by breaking the oxygen bridges between adjacent polyhedra.[9] The presence of these irregularities, together with the open network nature of glass, builds into the glass the imperfections which are potential color centers. In view of the complexity of the composition of the glass used in this experiment, it is not possible to assign particular bands to particular type color centers; however, it is possible to suggest which color centers are possibilities. These include the *F* center which is a negative ion vacancy in which an electron is trapped; the *F'* center which is a negative ion vacancy which has trapped two electrons; the *V* center which is a hole trapped by a positive ion vacancy; the *M* center which is an *F* center combined with a pair of vacancies; and the *R* center which is probably two negative ion vacancies in which one or two electrons are trapped. It would appear both from the composition of the glass and from the position of the absorption bands that *V* centers should be considered most probable. From the experiment it is not possible to determine if the maximum at 5100 angstroms is a secondary color center, the result of heating some of the primary color centers, or if it is a primary color center itself which is not as easily destroyed by heat. However, since thermal energy destroys two of the color centers much easier than the one at 5100 angstroms, it is probable that these color centers are of at least two fundamentally different types.

The fact that the absorption bands reported in this communication are broader than the normal type *F* bands is probably explained by the chemical complexity of the glass. Thus Gnaedinger[10] showed that the width of *F* bands increased when mixed crystals were irradiated with x-rays. The luminescence which occurs when the discolored glass is heated probably results from the fact that the electrons from the color centers are ejected into the conduction band by the increased thermal agitation of surrounding ions. This ionization is then followed by emission in the form of luminescence.

In summary then, the fact that heating destroys the discoloration and with varying degrees of efficiency, the fact that luminescence can be explained in terms of color centers, and the fact that the structure of glass is consistent with the formation of color centers, lead us to postulate their existence in glass incorporated with radium.

* Now at Florida State University, Tallahassee, Florida.

[1] E. Rutherford, *Radioactive Substances* (Cambridge University Press, London, 1913), p. 307.
[2] Doetler, Le Radium **7**, 58 (1910).
[3] C. L. Ross, Phys. Rev. **26**, 108 (1926).
[4] C. W. Parmelee, J. Soc. Glass Technol. **13**, 279 (1929).
[5] M. Berthelot, Compt. rend. **145**, 710 (1907).
[6] R. W. Pohl, Physik. Z. **39**, 36 (1938).
[7] F. Seitz, Revs. Modern Phys. **18**, 384 (1946).
[8] N. F. Mott and R. W. Gurney, *Electronic Processes on Ionic Crystals* (Oxford University Press, New York, 1940).
[9] J. Biscoe and B. E. Warren, J. Am. Ceram. Soc. **21**, 287 (1938).
[10] R. Gnaedinger, Thesis, University of Chicago, June, 1951.

Critical Phenomena in the Cyclohexane-Aniline System*

ROBERT W. ROWDEN AND O. K. RICE
Department of Chemistry, University of North Carolina, Chapel Hill, North Carolina
(Received September 5, 1951)

THERE has recently been much interest in critical phenomena in binary liquid mixtures in particular with respect to two questions:[1–6] (1) Does the coexistence curve have a finite horizontal portion at the critical mixing temperature? (2) In the region of homogeneous mixtures immediately beyond this temperature do the isotherms show a constant fugacity over a range of concentrations? The scanty experimental evidence has recently been reviewed by Rice,[3] and more recently Zimm[7] has concluded that for the perfluoromethylcyclohexane-carbon tetrachloride mixture the answer to both of these questions is "no," the critical phenomena being of the classical type. To get further evidence on these questions a study has now been made of the cyclohexane-aniline system. The total vapor pressure was taken as a measure of the fugacity, and this system was chosen because one component, the cyclohexane, contributes practically all of the pressure.[8]

The sample tube was made so that the mixture could be distilled into it in vacuum, the mixture frozen out with liquid air and

pumped off, and the tube sealed while under vacuum. The sample tube was also provided with a break seal. Thus it was possible to fasten the sample tube to a differential manometer or to continue its purification in vacuum or in an atmosphere of its own vapor. To repurify, the mixture was distilled through the break seal into a chamber containing freshly ignited CaO, melted, and allowed to remain in contact with the CaO (to remove residual water) for several hours. Finally the mixture was distilled into another sample tube and sealed off in the manner already mentioned.

The results of the study of the coexistence curve are shown in Fig. 1. The system was found to be extremely sensitive to impurities.[3] Although carefully purified materials were used, it was found necessary to make repeated purifications of each mixture to remove residual water. The change in transition temperature as the water was removed is shown. The three circles with tails indicate no change in transition temperature after repurification. It will be noted that two other mixtures changed less than 0.01° on repurification, and the excellent consistency of the experimental results is evidence that final purification was obtained in all cases. All eleven samples were placed in a thermostat and observed simultaneously. On cooling from above the critical temperature the transition was from clear to blue opalescence (with intensity increasing) to blue-white opalescence to distinct cloudiness to appearance of the meniscus. The two mixtures on the outside did not go through the blue-white opalescence stage. The transition temperature was taken as that temperature at which, on cooling, the opalescence changed to distinct cloudiness. The critical temperature, T_m, was thus found to be 29.63°C. The meniscus was not visible until about 0.015° lower but appeared, as nearly as discernible, simultaneously in the center portion of the six mixtures shown on the flat portion of the coexistence curve; all these thus appear to be critical mixtures. In the two samples to the right of the flat portion the meniscus appeared and disappeared at the top while in the three samples to the left of the flat portion, it appeared and disappeared at the bottom. There appeared to be no measurable difference in the transition temperatures whether approached by cooling or by heating. In the neighborhood of T_m the mixtures were cooled at a rate less than 0.01° per hour. The maximum range of transition temperatures is believed to be less than 0.003° for the six critical mixtures, and it is therefore concluded that the coexistence curve does have a flat portion for the cyclohexane-aniline mixture.

Four pairs, as indicated in Fig. 2, of the samples were attached to differential manometers (polyethylene glycol was the manometric fluid), break seals opened, and the pressure differences measured as a function of temperature. Two of the pairs were outside the critical region and the other two inside. (The mixture at 0.419 mole fraction became a critical mixture on attaching to the manometer, because of the slight change in composition resulting from distillation of cyclohexane vapor into the dead space above the break seal.) In all cases there was a small amount of gas present (noncondensable with liquid air) which caused a constant pressure difference to be observed in the two-phase (liquid) region as the temperature was changed. This is believed to have been caused by the fact that it was impossible to outgas the apparatus at elevated temperatures and in the sealing process some gas was given off the glass. This constant pressure difference (of the order of 0.1 to 0.2 mm Hg) was subtracted from the observed differences and the resultants divided by the difference in mole fraction of the two samples. The resulting slopes are plotted in Fig. 2. Except for the highest temperature all slopes are mean values of two or three readings. The slope is zero below T_m and appears to increase approximately linearly with temperature above T_m. The agreement between pairs is within experimental error. Obviously the experimental error will increase with a decrease in difference in concentration such that the error would be greatest for those pairs inside the critical region. If a constant fugacity region exists above 29.63°C, the experimental evidence indicates it would have to be below 29.80°C for the pair just inside the critical region and below 29.90°C for the pair well inside the critical region. Probably little significance can be attached to the relative positions of the slopes to each other at a given temperature although there seems to be a slight indication that the pressure difference increases more outside the critical region than inside.

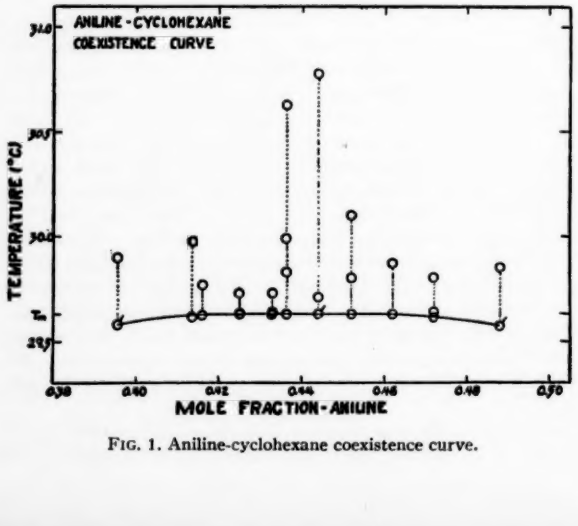

FIG. 1. Aniline-cyclohexane coexistence curve.

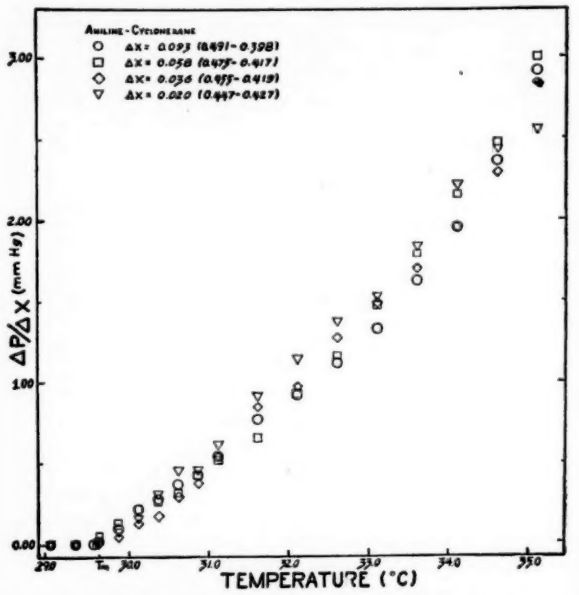

FIG. 2. Pressure differences divided by mole fraction differences for pairs of samples plotted against temperature.

We wish to thank the American Petroleum Institute and the National Bureau of Standards for the cyclohexane, and Dr. A. T. Schramm of the National Aniline Division of Allied Chemicals and Dye Corporation for a special sample of aniline.

* Work supported by the ONR..

[1] J. E. Mayer and S. F. Harrison, J. Chem. Phys. **6**, 87, 101 (1938).
[2] O. K. Rice, J. Chem. Phys. **15**, 314 (1947).
[3] O. K. Rice, Chem. Revs. **44**, 69 (1949).
[4] O. K. Rice, J. Phys. Coll. Chem. **54**, 1293 (1950).
[5] B. H. Zimm, J. Chem. Phys. **19**, 1019 (1951).
[6] J. E. Mayer, J. Chem. Phys. **19**, 1024 (1951).
[7] B. H. Zimm, J. Phys. Coll. Chem. **54**, 1306 (1950).
[8] H. Schlegel, J. Chim. Phys. **32**, 215 (1935).

A Note on the Scattering of Ions by Molecules

VERNON MYERS
Pennsylvania State College, State College, Pennsylvania
(Received September 13, 1951)

SIMONS[1] and his co-workers have made some intensive investigations of the scattering of ions in gases and find in some instances that the scattering is much larger than that expected for an attractive force caused by polarizability or a permanent moment. This would be expected in the scattering of H^+ in H_2 or H^+ in He since H_3^+ and HeH^+ are stable ions. In the scattering of protons by molecular hydrogen, for example, one of the electrons normally associated with H_2 would spend part of its time in the field of the proton.

Actual ion capture was not observed in these experiments, but it may be of interest to set an upper limit to the cross section for ion capture and subsequent photon emission. It follows from the method of detailed balancing[2] that

$$\sigma_{cap}p_1^2=\sigma_{dis}p_2^2, \tag{1}$$

where σ_{cap} is the cross section for the capturing of the ion by the molecule, σ_{dis} is the cross section for the breaking up of the molecule ion, p_1 is the momentum of the ion in the center-of-mass system, and p_2 is the momentum of the photon. Statistical weighting factors have been neglected in Eq. (1). These factors are of the order of unity. In particular, for the H_2-H^+ interaction, σ_{cap} is the cross section for the formation of H_3^+, and σ_{dis} is the cross section for the photodisintegration of H_3^+ into H_2 and H^+. For H_2-H^+ one finds

$$\sigma_{cap}/\sigma_{dis}=1\cdot10^{-9}E_2^2/E_1, \tag{2}$$

where E_2 is the photon energy in ev, and E_1 is the energy of H^+ in in ev relative to the laboratory coordinates. $E_2=\frac{2}{3}E_1+\Delta$, where Δ is the energy required for dissociation of H_3^+ into H_2 and H^+. Δ is estimated from Hirschfelder's[3] calculations to be of the order of 3 volts. The lower limit on E_1 set by experiment is about 1 volt. The cross section for photodisintegration of H_3^+ would be expected to be less than the "area" of the molecule. Taking the upper limit on σ_{dis} to be $1\cdot10^{-15}$ cm^2 and E_1 to be 1 volt, the result is

$$\sigma_{cap}\lesssim2\cdot10^{-23}\text{ cm}^2. \tag{3}$$

This cross section is insignificant in comparison to the scattering cross section for the proton by H_2 ($4\cdot10^{-15}$ cm^2 at this energy).

[1] Simons, Fontana, Muschlitz, and Jackson, J. Chem. Phys. **11**, 307 (1943).
[2] H. A. Bethe, *Elementary Nuclear Theory* (John Wiley and Sons, Inc., New York, 1947), p. 61.
[3] J. Hirschfelder, J. Chem. Phys. **6**, 795 (1938).

A Second Water Structure for Inert Gas Hydrates

W. F. CLAUSSEN
Illinois State Water Survey, Urbana, Illinois
(Received September 5, 1951)

A STRUCTURE for the water molecules in inert gas hydrates was recently proposed by the author,[1] and this structure was subsequently verified by the x-ray technique by von Stackelberg and Müller.[2] This x-ray investigation also yielded the result that there must exist two distinct hydrate structures corresponding to (1) hydrates of small molecules or gases such as Cl_2, CH_3SH, H_2S, Br_2, SO_2, etc., with a cubic cell constant of 12A, and (2) hydrates of large molecules, such as $CHCl_3$, C_2H_5Cl, etc., with a cubic cell constant of 17A. The water structure of the latter type of hydrate agreed with that earlier proposed by the author. The author is now in a position to propose a water structure for hydrates of the smaller molecules having the 12A cell.

This second water structure for inert gas hydrates is a modified body centered cubic lattice, at each of the corners, and in the center of the cube there is a pentagonal dodecahedral array of 20 water molecules. The dodecahedra at the corners of the cube are joined to adjacent corner dodecahedra by two additional water molecules to form hexagons of water molecules (see Fig. 1, which represents part of the unit cell). The body centered dodecahedron is attached to all of the 8 corner dodecahedra through single hydrogen bonds, and is also attached to 12 of the added "hexagon" water molecules. The resulting structure has another, new void, besides the pentagonal dodecahedron, namely, a tetrakaidecahedron (Fig. 2). This figure has 2 opposite hexagonal faces and 12 pentagonal faces. The volume of this figure must be slightly larger than that of the dodecahedron and quite a bit smaller than the hexakaidecahedron of the earlier described hydrate structure. We might term this void the medium sized void, while the other two may be termed large and small voids. The lattice constant of the unit cubic cell should be about 12A, in agreement with the x-ray data.

Some data on the unit cubic cell are as follows:

Total number of water molecules	46
Number of small holes or voids (dodecahedra) (at 000, $\frac{1}{2}\frac{1}{2}\frac{1}{2}$)	2
Number of medium sized holes (14-hedra) (at $\frac{1}{4}0\frac{1}{4}$, $\frac{3}{4}0\frac{1}{4}$, $0\frac{1}{4}\frac{1}{4}$, $0\frac{3}{4}\frac{3}{4}$, $\frac{1}{4}\frac{1}{4}0$, $\frac{3}{4}\frac{3}{4}0$)	6
Hypothetical hydrating numbers	
Filling all holes	$46/8=5\frac{3}{4}$ H_2O
Filling only medium holes	$46/6=7\frac{2}{3}$ H_2O

In Table I are listed the hydrating numbers of various molecules as assembled by Schroeder[3] and reclassified according to the described scheme.

TABLE I.

Small molecules (filling all holes)			Medium-sized molecules (filling only medium holes)		
Ar	4.5	H_2O	C_2H_6	7	H_2O
CH_4	6.3	H_2O	C_2H_4	7.4	H_2O
C_2H_2	5.7	H_2O	C_2H_5F	8.27	H_2O
PH_3	5.9	H_2O	*SO_2	8	H_2O
*H_2S	5.7	H_2O	*CH_3Cl	7.2	H_2O
CO_2	6	H_2O	*Cl_2	6.91	H_2O
N_2O	6	H_2O	*Br_2	10	H_2O
H_2Se	5.87	H_2O			

Hydrates of molecules labeled with an asterisk in Table I have been studied by one of Professor M. v. Stackelberg's students, H. R. Müller,[4] and have been found to fall in the 12A cell class. It is assumed that all of the hydrates in Table I have this same water structure.

The author wishes to express appreciation to Dr. A. M. Buswell and Dr. W. H. Rodebush, whose interest in the structure of water substances provided the impetus for this investigation. The author

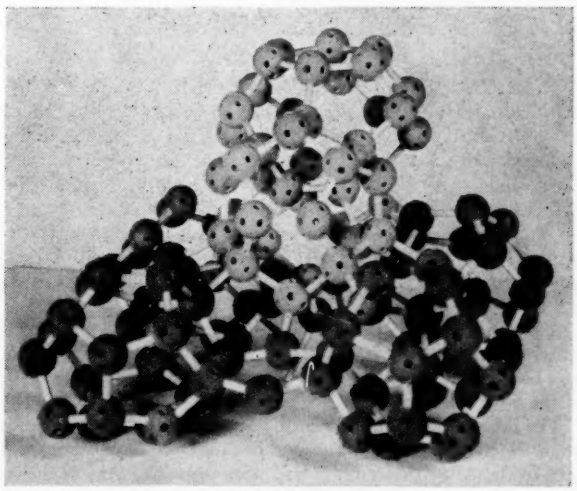

FIG. 1. Body centered cubic pentagonal dodecahedral lattice, showing base and center of unit cell. Each ball represents one water molecule.

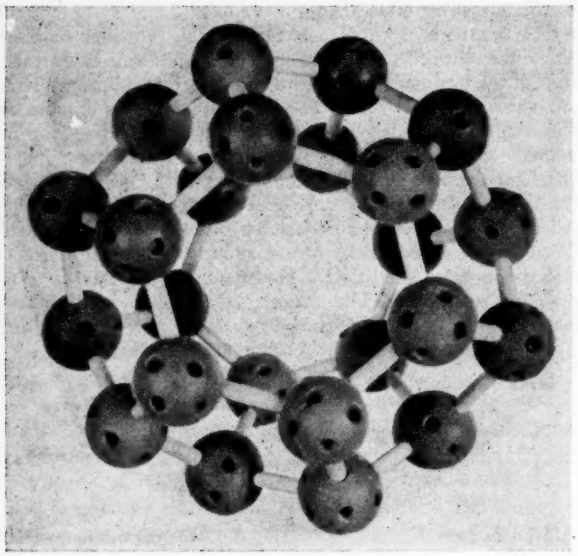

FIG. 2. Tetrakaidecahedron.

gratefully acknowledges the help given by Professor M. v. Stackelberg and Mr. H. R. Müller by providing the original x-ray data and conclusions on some hydrates, which conclusions prompted the author into making a renewed search for the structure of the 12A unit cell.

This work was made possible by a grant from the ONR, on a project pertaining to the properties of watery substances.

[1] W. F. Claussen, J. Chem. Phys. **19**, 259–260, 662 (1951).
[2] M. v. Stackelberg and H. R. Müller, J. Chem. Phys. **19**, 1319 (1951).
[3] W. Schroeder, Ahren's Sammlung chemischer und chemischer-technischer Vortrage, 1926–28, p. 76.
[4] H. R. Müller, "X-ray investigation of gas hydrates," Thesis, Rheinischen Friedrich-Wilhelms-Universitat zu Bonn, July, 1951.

Carrier-Free Radioisotopes from Cyclotron Targets. XIX. Preparation and Isolation of $Pt^{191,193}$ from Osmium*

JEANNE D. GILE, WARREN M. GARRISON, AND JOSEPH G. HAMILTON
Crocker Laboratory, Radiation Laboratory, and Divisions of Medical Physics, Experimental Medicine, and Radiology, University of California, Berkeley and San Francisco, California
(Received September 7, 1951)

RADIOACTIVE platinum produced by bombardment of osmium with 38-Mev alpha-particles has been isolated without addition of isotopic carrier. The following two radioisotopes of platinum are produced by (α, n), $(\alpha, 2n)$, and $(\alpha, 3n)$ reactions with alpha-particles of this energy: 3-day Pt^{191} and 4.3-day Pt^{193}. The carrier-free radio-platinum was separated from the target element and from the possible radioisotopes of Ir (from α, pn reaction) and Re (from n, p reaction) by a solvent-extraction procedure based on the solubility of chloroplatinous acid in ethyl ether.

A 2-mm layer of C.P. osmium† powder, supported on a grooved water-cooled aluminum target plate by a 0.25-mil tantalum foil, was bombarded for 40 μa-hr at an average beam intensity of 7 μa, in the 60-in. cyclotron at Crocker Laboratory.

The bombarded osmium was dissolved in aqua regia, additional 16 N HNO_3 was added, and the osmium was volatilized as the tetraoxide. After the osmium had been volatilized the HNO_3 was destroyed with excess of 12 N HCl. The acid solution containing the active $Pt^{191,193}$ was diluted with distilled water to make the solution 3 N in HCl, 1 ml of 10 percent $SnCl_2$ was added, and the chloroplatinous acid was extracted with ethyl ether which had previously been saturated with 3 N HCl. Under these conditions over 95 percent of the carrier-free radio-platinum is recovered in the organic phase. The ether layer was washed with 6 N HCl and the activity was quantitatively retained in the organic layer. Twenty mg of NaCl were added to the ether phase and the mixture was evaporated to dryness on a steam bath. The carrier-free $Pt^{191,193}$ was redissolved quantitatively in 2 ml of distilled water at pH 6 to give an isotonic saline solution for biological experiments.

The radio-platinum was identified by half-life determinations, absorption measurements, and chemical separation with carrier. The decay was followed for 40 days and showed the 3.0-day Pt^{191},[1] and the 4.3-day Pt^{193}.[1] Seven days after bombardment the activity showed predominately the 4.3-day period. Aluminum and lead absorption measurements two days after bombardment showed the 0.5-Mev conversion electron and the 0.57-Mev gamma-ray previously reported[2] for Pt^{191}. An aliquot of the solution was added to a solution containing carrier amounts of Os, Ir, Re, and Pt. The radioactivity was quantitatively recovered in the Pt fraction following chemical separation.[3]

We wish to thank Professor G. T. Seaborg for helpful suggestions, the staff of the 60-in. cyclotron and Crocker Laboratory for bombardments, and Miss Margaret Gee for technical assistance in counting.

* This document is based on work performed under Contract No. W-7405-eng-48-A for the AEC.
† The osmium was obtained from Johnson Mathey and Company. Pt was not detected by spectrographic analysis.
[1] G. T. Seaborg and I. Perlman, Revs. Modern Phys. **20**, 585 (1948).
[2] G. Wilkinson, Phys. Rev. **73**, 252 (1948).
[3] A. A. Noyes and W. C. Brag, *A System of Quantitative Analysis for The Rare Elements* (The Macmillan Company, New York, 1927).

Carrier-Free Radioisotopes from Cyclotron Targets. XX. Preparation and Isolation of $Ru^{97,103}$ from Molybdenum*

JEANNE D. GILE, WARREN M. GARRISON, AND JOSEPH G. HAMILTON
Crocker Laboratory, Radiation Laboratory, and Divisions of Medical Physics, Experimental Medicine, and Radiology, University of California, Berkeley and San Francisco, California
(Received September 7, 1951)

ALPHA–PARTICLE bombardment of molybdenum produces the 2.8-day Ru^{97} and the 42-day Ru^{103} by the nuclear reactions, $Mo(\alpha, xn)Ru^{97}$, and $Mo^{100}(\alpha, n)Ru^{103}$.[1] This paper reports a method of isolating this activity in the carrier-free state from the target element and from radioisotopes of Tc (from α, pxn reactions) which are produced concurrently by the 40-Mev alpha-particles from the 60-in. cyclotron at the Crocker Laboratory.

The target was a block of C.P. molybdenum metal, silver-soldered to a water-cooled copper target plate. It was bombarded with 40-Mev alpha-particles for a total of 70 μa-hr at an average beam intensity of 8 μa. The bombarded surface was removed by milling off approximately 0.5 g of Mo. The Mo chips were fused with 5 g of KOH and 0.5 g of KNO_3 in a nickel crucible at 500°C for 15 minutes. The fused mass was dissolved in a minimum amount of hot water and centrifuged to remove insoluble material. The strongly basic solution was transferred to an all-glass distilling flask,[2] a stream of Cl_2 was bubbled through the solution, and the active ruthenium was distilled as the RuO_4 which was collected in a trap containing 12 N HCl cooled with ice. Under these conditions the technetium isotopes remain in the distilling flask with the target material. The acid distillate containing the radio-ruthenium was evaporated to a small volume, made basic with NaOH, and redistilled into a trap containing 12 N HCl. The second distillation was done to insure complete separation from the target material. The final HCl solution was evaporated to dryness on 20 mg of NaCl and the activity dissolved quantitatively with the addition of 2 ml of distilled water.

An aliquot of the preparation was added to a solution containing

carrier amounts of Mo and Ru. The activity was quantitatively recovered in the Ru fraction following chemical separation. The radiation characteristics were obtained by aluminum and lead absorption measurements and showed the 0.2-Mev conversion electron and the 0.23-Mev gamma-ray previously reported[3] for Ru^{97}. The activity showed the 2.8-day period for nearly 15 half-lives at which time it began to lengthen to a period of approximately 40 days, presumably because of Ru^{103}.

We wish to thank Professor G. T. Seaborg for helpful suggestions, the staff of the 60-in. cyclotron for bombardments, and Miss Margaret Gee for technical assistance in counting.

* This document is based on work performed under Contract No. W-7405-eng-48-A for the AEC.

[1] *Nuclear Data* (National Bureau of Standards, September 1, 1950).
[2] L. A. Scherrer, J. Research Natl. Bur. Standards **21**, 95 (1938).
[3] D. T. Eggen and M. L. Pool, Phys. Rev. **74**, 57 (1948).

Carrier-Free Radioisotopes from Cyclotron Targets. XXI. Preparation and Isolation of $Tl^{200,201,202}$ from Mercury*

JEANNE D. GILE, WARREN M. GARRISON, AND JOSEPH G. HAMILTON
Crocker Laboratory, Radiation Laboratory, and Divisions of Medical Physics, Experimental Medicine, and Radiology, University of California, Berkeley and San Francisco, California
(Received September 7, 1951)

THIS paper reports a procedure used in isolating radio-thallium in the carrier-free state from a mercury target which had been bombarded with 19-Mev deuterons in the 60-in. cyclotron at Crocker Laboratory. At this energy deuteron bombardment of mercury produces[1] $Tl^{200,201,202}$ by the nuclear reactions $Hg^{199}(d,n)Tl^{200}$, $Hg^{200}(d,2n)Tl^{200}$, $Hg^{200}(d,n)Tl^{201}$, $Hg^{201}(d,2n)Tl^{201}$, $Hg^{201}(d,n)Tl^{202}$, and $Hg^{202}(d,2n)Tl^{202}$. Other shorter-lived radioisotopes of thallium, notably the 7-hr Tl^{199}, were allowed to decay out prior to chemical separation.

The target chamber[2] was made from a 100-ml Pyrex flask and had a concave glass window approximately 4 cm in diameter and 0.15 mm in thickness with a total volume of 30 ml. The target flask was connected to a small reflux condenser and the flask was cooled by a stream of air during bombardment. The target was filled with liquid mercury† and bombarded with 19-Mev deuterons for a total of 30 μa-hr at an average beam intensity of 3.5 μa. After removal of the mercury from the target, it was found that the radio-thallium had deposited quantitatively on the walls of the glass flask. The mercury was discarded and the flask was washed twice with 16 N HNO_3. The HNO_3 solution which contained the radio-thallium, and traces of mercury which had adhered to the glass surface, was evaporated to 2 ml, treated with excess 12 N HCl to destroy the HNO_3, and diluted to approximately 3 N HCl. This solution was then extracted with ethyl ether which had previously been equilibrated with 3 N HCl. Over 95 percent of the carrier-free radio-thallium was removed from the aqueous phase. The ether fraction was washed with water to remove HCl and the activity was quantitatively retained in the organic phase. Fifty mg of NaCl was added to the ether solution and the mixture evaporated to dryness on a steam bath. The carrier-free $Tl^{200,201,202}$ redissolved quantitatively in 5 ml of distilled water and was adjusted to pH 6 to give an isotonic saline solution for biological investigation.

The radio-thallium was identified by half-life determinations, absorption measurements, and by a chemical separation procedure in which Au, Hg, and Tl were used as carriers. The decay curve was followed for 60 days and showed three periods: 27-hr Tl^{200}, 72-hr Tl^{201}, and 11.8-day Tl^{202}. Eleven days after bombardment the activity showed only the 11.8-day period. The aluminum absorption measurements four days after bombardment showed an end point of ~130 mg/cm².[3] Lead absorption measurements showed the 0.4-Mev gamma-ray assigned to Tl^{202}.[1] Milligram amounts of Au, Hg, and Tl were added to an aliquot from the preparation and 98 percent of the activity was recovered in the Tl fraction, using a standard chemical procedure for isolation of the Tl.[4]

We wish to thank Professor G. T. Seaborg for helpful suggestions, Mr. B. Rossi and the staff of the 60-inch cyclotron at Crocker Laboratory for the bombardments, and Miss Margaret Gee for technical assistance in counting.

* This document is based on work performed under Contract No. W-7405-end-48-A for the AEC.

[1] G. T. Seaborg and I. Perlman, Revs. Modern Phys. **20**, 585 (1948).
[2] Garrison, Haymond, and Hamilton, "Carrier-free radioisotopes from cyclotron targets; preparation of F^{18} from water" (unpublished data).
† The mercury was C.P., triple distilled, thallium-free.
[3] R. S. Krishnan and E. A. Nohum, Proc. Camb. Phil. Soc. **36**, 490 (1940).
[4] A. A. Noyes and W. C. Brag, *A System of Quantitative Analysis for The Rare Elements* (The Macmillan Company, New York, 1927).

Carrier-Free Radioisotopes from Cyclotron Targets. XXII. Preparation and Isolation of Pb^{203} from Thallium*

HERMAN R. HAYMOND, WARREN M. GARRISON, AND JOSEPH G. HAMILTON
Crocker Laboratory, Radiation Laboratory, and Divisions of Medical Physics, Experimental Medicine, and Radiology, University of California, Berkeley and San Francisco, California
(Received September 7, 1951)

THE 52-hr Pb^{203}, produced by the reaction $Tl^{203}(d,2n)Pb^{203}$ has been isolated in the carrier-free state from a Tl target without the addition of stable lead carrier.

The target consisted of a 2-mm layer of Tl_2O_3 powder held on a grooved water-cooled copper plate by a 0.25-mil platinum foil and was bombarded with 19-Mev deuterons in the 60-in. cyclotron at the Crocker Laboratory. Lead was not detected by spectrographic analysis (less than 0.01 percent) in the Tl_2O_3 powder used for the target. The beam current was limited to 5 μa to avoid volatilization of the target powder from over-heating during bombardment.

After bombardment, the Tl_2O_3 powder was dissolved in 1 N HNO_3. The solution was saturated with SO_2 gas to reduce the thallic ion to the thallous state, following which the solution was heated to expel the excess SO_2. Ten mg of ferric ion were added and the solution was made basic by the addition of NH_4OH. The precipitated $Fe(OH)_3$, which carried most of the Pb^{203}, was removed by centrifugation, washed twice with dilute NH_4OH and once with water, and dissolved in 1 N HNO_3. Five mg of inert thallic ion were added to the solution as holdback carrier and the whole process was repeated. The process was repreated again without the addition of inert thallium. The third $Fe(OH)_3$ precipitate was dissolved in 6 N HCl and the iron removed by four extractions with equal volumes of ethyl ether. After the addition of 25 mg of NaCl the solution was heated to dryness and then dissolved in water to give a solution of isotonic saline at pH 4 containing the carrier-free radio-lead, which was subsequently used for biological investigations.

Identification of the isolated activity was confirmed with an aliquot of the preparation by a chemical separation using milligram quantities of thallium, lead, and mercury. The decay curve, over a period of four half-lives, and the absorption curves in aluminum and lead agreed with published data.[1-3] The 68-min. Pb^{204} which results from deuteron bombardment of thallium,[3,4] was allowed to decay out prior to this separation.

We wish to thank Professor G. T. Seaborg for reviewing the manuscript, Mr. T. Putnam, Mr. B. Rossi, and the staff of the 60-in. cyclotron for bombardments, and Miss Margaret Gee for technical assistance.

* This document is based on work performed under Contract No. W-7405-eng-48-A for the AEC.

[1] G. T. Seaborg and I. Perlman, Revs. Modern Phys. **20**, 585 (1948).
[2] *Nuclear Data* (National Bureau of Standards Circular 499, September, 1950).
[3] Templeton, Howland, and Perlman, Phys. Rev. **72**, 766 (1947).
[4] K. Fajans and A. F. Voigt, Phys. Rev. **60**, 619 (1941).

Carrier-Free Radioisotopes from Cyclotron Targets. XXIII. Preparation and Isolation of $Rh^{100,101,102,105}$ From Ruthenium*

JEANNE D. GILE, WARREN M. GARRISON, AND JOSEPH G. HAMILTON
Crocker Laboratory, Radiation Laboratory, and Divisions of Medical Physics, Experimental Medicine, and Radiology, University of California, Berkeley and San Francisco, California
(Received September 7, 1951)

RADIOACTIVE rhodium, produced by the bombardment of ruthenium with 19-Mev deuterons, has been isolated without added isotopic carrier. Several radioisotopes of rhodium[1] are produced by (d, n) and $(d, 2n)$ reactions with deuterons of this energy: 19-hr Rh^{100}, 4.3-day Rh^{101}, 210-day Rh^{102}, and 37-hr Rh^{105}, and short-lived Rh^{103} and Rh^{104}. The target was aged a few days to allow Rh^{103} and Rh^{104} to decay out prior to chemical separation. Small amounts of technetium are also produced concurrently by (n, p) reaction.

A 2-mm layer of C.P. ruthenium powder,† supported on a grooved water-cooled copper plate by a 0.25-mil platinum foil, was bombarded for 35 μa-hr at an average beam intensity of 5.5 μa. The ruthenium powder was fused with 10 g of Na_2O_2 in a nickel crucible at 300°C for 30 minutes. The small amount of Tc produced is lost in this step. The fused mass was dissolved in aqua regia with heating and the insoluble material centrifuged out. The solution was made basic with KOH, heated to approximately 100°C, and Cl_2 gas was bubbled through to volatilize the target ruthenium as RuO_4. The residue containing the radioactive rhodium and nickel which was dissolved from the crucible during fusion was centrifuged out and found to carry 95 percent of the radio-rhodium. The precipitate of nickel hydroxide was washed with water and dissolved in a minimum volume of dilute HNO_3. Five mg of Fe^{+3} were added to the acid solution and the $Fe(OH)_3$ precipitated with NH_4OH, which carried the active rhodium quantitatively and left the nickel in solution as $Ni(NH_3)_6^{++}$. The $Fe(OH)_3$ was reprecipitated twice, carrying the activity completely each time. The iron was dissolved in 6 *N* HCl and extracted with ethyl ether. The aqueous phase containing HCl and the active rhodium was evaporated to dryness on 50 mg of NaCl and dissolved quantitatively in 5 ml of distilled water.

The decay curve was followed for 200 days and showed three periods:[2] 37-hr Rh^{105}, 4.3-day Rh^{101}, and 210-day Rh^{102}. Twenty days after bombardment the decay curve showed the single period of 210-day Rh^{102}. Mass absorption measurements in aluminum and lead two days after bombardment showed the 0.78-Mev beta-particles of Rh^{105}, and the 0.35-Mev and 0.33-Mev gamma-rays of Rh^{101} and Rh^{105}, respectively. Milligram amounts of Ru and Rh were added to an aliquot of the preparation. The rhodium fraction was separated chemically and contained 98 percent of the activity.

We wish to thank Professor G. T. Seaborg for helpful suggestions, Mr. B. Rossi and the staff of the 60-in. cyclotron at Crocker Laboratory for bombardments, and Miss Margaret Gee for technical assistance in counting.

* This document is based on work performed under Contract No. W-7405-eng-48-A for the AEC.
[1] G. T. Seaborg and I. Perlman, Revs. Modern Phys. 20, 585 (1948).
† Spectrographic analysis of Ru powder showed less than 0.017 percent Rh.
[2] Sullivan, Sleight, and Gladrow, P.P.R., CC-1493 (1944).

The Lower Excited States of Carbon Dioxide

JOSEPH F. MULLIGAN*
Physics Department, The Catholic University of America, Washington, D.C.
(Received September 13, 1951)

CALCULATIONS of LCAO (linear combination of atomic orbitals) molecular orbitals and ionization potentials, using Roothaan's LCAO SCF (self-consistent field) method, have been recently reported for the electronic ground state of carbon dioxide.[1] These calculations have now been extended to the lower excited states of CO_2.

The method used was to assume that the lower excited MO's were identical with the unfilled MO's obtained from the ground-state calculations, and given in Table VI of reference 1. These orbitals satisfy the requirements of symmetry and orthogonality, and are the simplest that can be obtained without carrying out a separate variational calculation for each excited state. Roothaan[2] has given convenient formulas for calculating the energies of the excited states, consistent with this assumption.

The lower excited states of CO_2 correspond to the excitation of an electron from one of the degenerate $1\pi_g$ orbitals to the higher $3\sigma_g$, $3\sigma_u$, and the degenerate $2\pi_u$ orbitals. The excited states resulting from these transitions and their calculated energies are given in Table I. In the case of Π_g, Π_u, and Σ_u^-, the calculated

TABLE I. Results of LCAO SCF calculation of lower excited states of carbon dioxide.

Transition[a]	Excited state[b]	LCAO SCF energies (ev)		Mean
$1\pi_g \rightarrow 3\sigma_u$	$(^1\Pi_u)$	16.3		16.3
	$^3\Pi_u$	16.3		
$1\pi_g \rightarrow 3\sigma_g$	$^1\Pi_g$	14.6		14.6
	$^3\Pi_g$	14.6		
$1\pi_g \rightarrow 2\pi_u$	$(^1\Sigma_u^+)$	22.1		11.0
	$^1\Delta_u$	9.5	13.6	
	$^1\Sigma_u^-$	9.2		
	$^3\Sigma_u^-$	9.2		
	$^3\Delta_u$	8.4	8.4	
	$^3\Sigma_u^+$	7.6		

[a] The molecular orbitals are numbered as in reference 1, following R. S. Mulliken, J. Chem. Phys. 3, 720 (1935).
[b] Parentheses indicate states to which transitions are permitted from the $^1\Sigma_g^+$ ground state. All energies are with respect to the ground state.

singlet-triplet splitting was zero within the accuracy of the calculations. In the case of Σ_u^+ the splitting was abnormally large. This too-large singlet-triplet splitting is consistent with previous calculations on similar transitions in molecules with conjugated double bonds.[3,4] In these cases it has been suggested that the "center of gravity" of the singlet-triplet system might be in agreement with experiments, even when the calculated singlet-triplet splitting is bad. For this reason mean values are given for the singlet-triplet systems. Six excited states arise from the $1\pi_g \rightarrow 2\pi_u$ transition, and the method used here cannot be expected to represent the splitting with great accuracy. For this reason the "center of gravity" of the whole $1\pi_g \rightarrow 2\pi_u$ system may have more physical significance.

The experimental data on the lower excited states of CO_2 are inconclusive. There is not one electronic level whose energy is known with certainty, since these states are all high in energy above the ground state and their band systems fall in the experimentally difficult vacuum-ultraviolet region. Thus gaseous CO_2 is transparent to wavelengths longer than 1712A (7.2 ev). The initial absorption appears to correspond to a forbidden transition, and has a maximum at about 1495A (8.3 ev).[5] The results of the LCAO SCF calculation are in qualitative agreement with this, since they indicate no excited states less than 7.6 ev above the ground state, with the lowest states all corresponding to forbidden transitions. Mulliken[6] has pointed out that this initial absorption probably corresponds to excitation to the $^1\Pi_g$ state, and this assignment has received some confirmation from Price and Simpson's[7] comparison of the spectra of CO_2, COS, and CS_2. If this is correct, the LCAO SCF value of 14.6 ev for this state is much too high.

The center of gravity of the $1\pi_g \rightarrow 2\pi_u$ system corresponds to about the same energy (11.3 ev) as the upper state in Rathenau's[8] "strong" series. Of course, this series may correspond to the allowed transition to the $^1\Pi_u$ state, which the calculations put at 16.3 ev above the ground state. This is perhaps more probable, since previous LCAO SCF calculations have always given energies

which are too large for the lower excited states. Mulliken[4] has also pointed out that it is to be expected that Roothaan's LCAO SCF method will give poor results for highly antibonding excited states, and all the lower excited states in CO_2 are highly antibonding.

It is probable that better agreement with experiment would be obtained if LCAO MO's were used which minimized the energy of the desired excited state, rather than that of the ground state, and if exact values were available for the many integrals that had to be approximated in this calculation. Recent work also indicates that configuration interaction may have a considerable effect on the energies of these excited states.[9]

The atomic orbitals used throughout these calculations were Slater orbitals with $n^*=2$, and $Z^*=3.25$ for carbon, $Z^*=4.55$ for oxygen. Kohlrausch[10] recently has pointed out that better results are obtained for a number of atomic properties by the choice: $n^*=1.944$, $Z^*=2.03$ for carbon; $n^*=1.924$, $Z^*=2.38$ for oxygen. It is clear that if these should turn out to be the better values for molecular problems, the results of these calculations would be changed considerably.

The author wishes to thank Dr. C. C. J. Roothaan for helpful correspondence during the course of this work.

* Now at Woodstock College, Woodstock, Maryland.
[1] J. F. Mulligan, J. Chem. Phys. **19**, 347 (1951).
[2] C. C. J. Roothaan, Ph.D. thesis, University of Chicago, 1950.
[3] R. G. Parr and R. S. Mulliken, J. Chem. Phys. **18**, 1338 (1950).
[4] R. S. Mulliken, J. Chim. Phys. **46**, 497, 675 (1949).
[5] P. S. Wilkinson and H. L. Johnston, J. Chem. Phys. **18**, 190 (1950).
[6] R. S. Mulliken, J. Chem. Phys. **3**, 720 (1935); Revs. Modern Phys. **14**, 204 (1942).
[7] W. C. Price and D. M. Simpson, Proc. Roy. Soc. (London) **A169**, 501 (1938).
[8] G. Rathenau, Z. Physik **87**, 32 (1933).
[9] Parr, Craig, and Ross, J. Chem. Phys. **18**, 1561 (1950); Coulson, Craig, and Jacobs, Proc. Roy. Soc. (London) **A206**, 297 (1951).
[10] K. W. F. Kohlrausch, Acta Phys. Austriaca **3**, 452 (1949); see also O. Theimer, *ibid.* **4**, 1 (1950).

A Possible Relation between the Nuclear Relaxation Time, T_2, and Molecular Structure*

C. S. Clay,† R. S. Bradford,‡ and Ellis Strick§
Department of Physics, University of Wyoming, Laramie, Wyoming
(Received September 7, 1951)

It has been shown that transient solutions of the Bloch equations[1] have two experimentally measurable parameters T_1, T_2. The reciprocal of T_2 can be considered as an uncertainty in the Larmour precession frequency because of the spread in the effective values of the static component of the internal magnetic fields plus the reciprocal of the finite state life time (T_1), i.e., $1/T_2=\gamma(\Delta H)+1/T_1$. If it is assumed that T_1 is very large (our qualitative experimental observations support $T_1>T_2$ for liquid hydrocarbons) and that random motions of the molecules average out static interactions among molecules, then T_2 can be a measure of the spread of magnetic fields at the hydrogens of the molecule. This would indicate that T_2, a measure of the half-width of the proton resonance line, is also a measure of the symmetry of the molecule with respect to the hydrogens, i.e., protons. A long T_2 would indicate a small spread of internal magnetic field, averaged for all hydrogens in the molecule and a large spread for short T_2.

Measurements of T_2 for several related hydrocarbons (shown in Table I) were made using the steady-state transient technique.[2,3]

Discussion of results.—(a) The different relaxation times for dimethyl propane (neopentane), *n*-pentane, and 2-methyl butane show that there is a strong dependence of T_2 upon the particular molecular structure for the same number of hydrogens and carbons.

(b) Another illustration of the isomeric effect is the variation of T_2 as the two methyl groups are moved in the dimethyl pentanes. Qualitatively one would expect that 3,3-dimethyl pentane would have more symmetry than 2,4-dimethyl pentane, or 2,2-dimethyl pentane. The large T_2 for 3,3-dimethyl pentane as compared to the other dimethyl pentanes appears to support this.

TABLE I.

Sample[a]	Structural formula	T_2 in milliseconds	$(\Delta H)=1/T_2$ milligauss
2,2-dimethyl propane	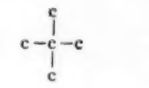	30±2	1.1 ±07
2,2-dimethyl butane	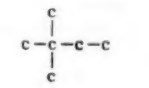	18±2	2.05±0.2
2,2-dimethyl pentane	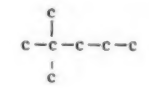	3±1	11 ±3
2,3-dimethyl pentane	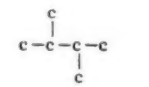	5±1	7.4±1.5
2,4-dimethyl pentane	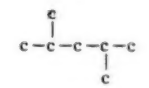	6.3±1	5.9 ±1
3,3-dimethyl pentane	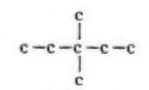	10±1	3.7 ±0.4
n-pentane		20±3	1.8 ±0.3
2-methyl butane	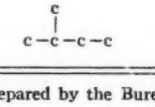	12±2	3.1 ±0.5

[a] All samples were prepared by the Bureau of Standards and have less than 1 percent impurity.

(c) Dimethyl propane had the longest T_2 of all liquid hydrocarbons measured. This hydrocarbon also possibly has the most symmetry of any investigated (i.e., it can be called tetramethyl methane). As successive CH_2 groups are added to the basic propane, one would expect that the symmetry would reduce. From Table I, 2,2-dimethyl pentane, 2,2-dimethyl butane, and 2,2-dimethyl propane show, respectively, increasing T_2's and from 3-dimensional chemical models increasing symmetry.

The relaxation time, T_2, appears to be strongly related to molecular structure of the simpler hydrocarbons. It is believed that T_2 can give information concerning the gross structure of hydrocarbons, and these measurements appear to strengthen the T_2-symmetry arguments. A paper is in preparation for *The Physical Review* that describes the method of measurement and will report values of T_2 for many more related liquid hydrocarbons.

* Assisted in part by the AEC.
† Now at Carter Oil Research Laboratory, Tulsa, Oklahoma.
‡ Now at Institute for Industrial Research, Denver University, Denver, Colorado.
§ Now at Shell Exploration and Research, Houston, Texas.
[1] Bloch, Phys. Rev. **70**, 460–474 (1946).
[2] Bradford, Clay, and Strick, Phys. Rev. **84**, 157 (1951).
[3] Strick, Bradford, Clay, and Craft, Phys. Rev. **84**, 363 (1951).

Erratum: Fast Electrode Reactions

[J. Chem. Phys. **19**, 1065 (1951)]

J. G. Barredo
Jones Laboratory, University of Chicago, Chicago, Illinois

Equations (3) and (4) should read

$$I^{-\alpha+1}=2K_2(1-\alpha)(nF)^{1-\alpha}\Sigma^{-\alpha}I^1, \quad [3]$$

$$\Sigma=2^{1/\alpha}K_2^{1/\alpha}(1-\alpha)^{1/\alpha}I^{(\alpha-1)/\alpha}I^{1/2\alpha}n^{(1-\alpha)/\alpha}F^{(1-\alpha)/\alpha}, \quad [4]$$

respectively.

Conformal Solution Theory and Dipole Interaction

J. A. BARKER
Division of Indistrial Chemistry, Commonwealth Scientific and Industrial Research Organization, Melbourne, Australia
(Received September 10, 1951)

THE theory of conformal solutions[1] provides an ingenious method for differentiating the phase integral for a solution, and so permits the expression of the properties of the solution in terms of those of the pure (nonpolar) components. This note indicates that a similar method can be applied to solutions in which a weak dipole interaction occurs.

A binary solution of N_p polar molecules and N_s nonpolar molecules is considered. The polar molecules have a point dipole of strength μ located at the center, but are otherwise spherically symmetrical (pseudo-spherical molecules).

The energy of the solution in a given configuration is supposed to be

$$U=U^1+U^E, \tag{1}$$

where

$$U^1=\sum_{r,s} f_{rs}u(g_{rs}R_{rs}) \quad \text{(summed for all molecular pairs)},$$

$$U^E=\sum_{\kappa,\lambda}\frac{\mu^2\Phi(\kappa,\lambda)}{R_{\kappa\lambda}^3} \quad \text{(summed for all pairs of polar molecules)}.$$

The dispersion and induction energies are included in U^1, $u(\rho)$ is a universal function, f_{rs} and g_{rs} depend only on the chemical nature of the molecules r and s and are supposed to be close to unity. U^E represents the energy of the dipole-dipole interaction, and the function $\Phi(\kappa,\lambda)$ depends on the orientations of the molecules κ and λ.

The energy U^E is regarded as a perturbation and the phase integral may be explained in the following way (classical statistics are assumed):

$$\Omega(T,V)=\frac{\dfrac{1}{N_p!N_s!}\int\int\exp(-U^1/kT)\exp(-U^E/kT)(dx)(d\theta)}{\int(d\theta)}$$

$$=\Omega^1\left(1-\frac{(U^E)_{Av}}{kT}+\frac{(U^E)_{Av}^2}{2(kT)^2}\right).$$

The average values are defined as integrals over the unperturbed configurations, (dx) and $(d\theta)$ refer to integration over positional coordinates of all molecules and orientational coordinates of polar molecules, respectively. Terms higher than that in $(U^E)_{Av}^2$ are neglected.

Integration over orientational coordinates gives the following results:

$$(U^E)_{Av}=0$$

$$(U^E)_{Av}^2=\frac{\frac{2}{3}u^4\int\exp(-U^1/kT)(\Sigma R_{\kappa\lambda}^{-6})(dx)}{\int\exp(-U^1/kT)(dx)}.$$

If the special form shown by Eq. (2) is assumed for $u(\rho)$, then $\Sigma R_{\kappa\lambda}^{-6}$ is determined by Eq. (3).

$$u(\rho)=\frac{6}{m-6}E_m\left[\left(\frac{\rho_0}{\rho}\right)^m-\frac{m}{6}\left(\frac{\rho_0}{\rho}\right)^6\right] \tag{2}$$

(m, Em, ρ_0 are constants),

$$\sum_{\kappa\lambda}R_{\kappa\lambda}^{-6}=-\frac{1}{mf_{pp}E_md^6}\left(mf_{pp}\frac{\partial U^1}{\partial f_{pp}}+g_{pp}\frac{\partial U^1}{\partial g_{pp}}\right). \tag{3}$$

In Eq. (3) the abbreviation $d=\rho_0/g_{pp}$ has been made. Using Eq. (3) it follows that

$$(U^E)_{Av}^2=\frac{\frac{2}{3}u^4kT}{mf_{pp}E_md^6}\left(mf_{pp}\frac{\partial}{\partial f_{pp}}+g_{pp}\frac{\partial}{\partial g_{pp}}\right)\log\Omega^1.$$

If F is the Helmholtz free energy of the actual solution, F^1 that of a corresponding solution in which the dipole-dipole interaction is reduced to zero, then

$$F-F^1=-kT\log(\Omega/\Omega^1)$$

$$=\frac{kT}{3mf_{pp}E_m}\left(\frac{u^2}{kTd^3}\right)^2\left(mf_{pp}\frac{\partial}{\partial f_{pp}}+g_{pp}\frac{\partial}{\partial g_{pp}}\right)F^1.$$

Using the results of the conformal solution theory and transforming to constant pressure conditions, the Gibbs free energy of the solution is found to be given by Eq. (4), in which terms of order $(f-1)^2$, $(g-1)^2$, $(f-1)(u^2/kTd^3)^2$, $(g-1)(u^2/kTd^3)^2$ have been neglected.

$$G(T,p)=G_0+RT(x_p\log x_p+x_s\log x_s)$$
$$+E_0[x_p^2(f_{pp}-1)+2x_px_s(f_{ps}-1)+x_s^2(f_{ss}-1)]$$
$$+3(RT-pV_0)[x_p^2(g_{pp}-1)+2x_px_s(g_{ps}-1)+x_s^2(g_{ss}-1)]$$
$$+\frac{\gamma T}{3mT_0^c}\left(\frac{u^2}{kTd^3}\right)^2[mE_0+3(RT-pV_0)]x_p^2.$$

In this expression, G_0, E_0, V_0 are the Gibbs free energy, energy, and volume, respectively, of a pure reference liquid in which the molecular interactions are given by Eq. (2). The energy E_m has been related to the critical temperature T_0^c of the reference liquid by the equation

$$\gamma E_m=kT_0^c.$$

According to Lennard-Jones and Devonshire[2] $\gamma\simeq1.3$. The length d is the diameter of the polar molecules (more strictly the equilibrium separation of two molecules under the influence of dispersion and induction forces). The quantities f_{rs}, g_{rs} depend on the dipole moment and the polarizabilities as well as on the magnitude of the dispersion forces.

Equation (4) can be used to determine the effect of the dipole interaction on the thermodynamic properties of both the pure polar liquid and the solution. The general requirement for validity is that $(u^2/kTd^3)<1$.

[1] H. C. Longuet-Higgins, Proc. Roy. Soc. (London) **A205**, 247 (1951).
[2] J. E. Lennard-Jones and A. F. Devonshire, Proc. Roy. Soc. (London) **A163**, 53 (1937).

Solvent Effects for the Ultraviolet Spectra of Aromatic Hydrocarbons

ROBERT SCHNURMANN AND WILLIAM FRANCIS MADDAMS
Physics Department, Manchester Oil Refinery, Ltd., Manchester, England
(Received September 9, 1951)

ATTENTION was drawn some time ago to a solvent effect on the band positions and absorption intensities of phenanthrene in various solvents.[1] Recently Coggeshall and Pozefsky[2] claimed a dependence of the frequency of naphthacene on the refractive index of the solvent where they considered solvents consisting of mixtures of a paraffinic material and of a number of atomatic hydrocarbons in order to vary the n_D-values between 1.39 and 1.62.

From hitherto unpublished data on the solvent effect on anthracene, naphthacene, chrysene, pyrene, triphenylene, 1,2-benzanthracene, and 3,4-benzphenanthrene, it would appear that the magnitude of the wavelength shift was not a regular function of n_D. In all cases but that of triphenylene the transition from isooctane to ethylalcohol as the solvent yielded a red-shift of the absorption bands. Triphenylene also showed a red-shift on passing from isooctane to chloroform as the solvent, whereas its band positions and intensities were similar in ethylalcohol and in isooctane.[3] This would suggest that the portion of Bayliss' formula[4] relating wavelength shift to refractive index was not in accordance with the experimental evidence.

The employment of the refractive index values for the relevant wavelengths in place of the n_D-values would increase this discrepancy.

The purity of the aromatic hydrocarbons might be considered to be important for the assessment of the solvent effect on the ultraviolet spectra. It is evident that Coggeshall and Pozefsky's phenanthrene[2] contained some anthracene, and that this impurity

has given rise to an error in assignment of the electronic transitions. Therefore, unless attention is paid to the purity of the aromatic hydrocarbons, any attempts at discriminating between ^1L_a- and ^1L_b-transitions[5] for these spectra appear to be premature.

[1] W. F. Maddams and R. Schnurmann, J. Chem. Phys. **17**, 108 (1949).
[2] N. D. Coggeshall and A. Pozefsky, J. Chem. Phys. **19**, 980 (1951).
[3] This point seems to be worthy of note since the change in n_D-values between isooctane ($n_D^{20}\approx1.392$) and ethylalcohol ($n_D^{20}\approx1.362$) involves a negative increment.
[4] N. S. Bayliss, J. Chem. Phys. **18**, 292 (1950).
[5] J. R. Platt, J. Chem. Phys. **17**, 484 (1949).

A Note on the Paper "On the Latent Heat of Fusion and the Hole Theory," N. R. Mukherjee

[J. Chem. Phys. 19, 502 (1951)]

A. K. Mukherjee
College of Engineering and Technology, Bengal, Calcutta, India

(Received September 24, 1951)

THE note by Mukherjee presents a theoretical attempt at the calculation of latent heats of fusion of substances at their respective melting points. But it appears that the attention of the author should be drawn to certain points which apparently go against presently accepted views.

(1) Frenkel's formula for the size of a hole has been used by the author in his calculations. But, as Frenkel[1] himself points out, to use this formula we must assume that the surface tension of a hole must, in general, be much smaller than its (liquid) normal value in a free surface. But the author in the present case appears to have overlooked these observations by Frenkel, and has assumed the surface tensions of a hole and of a free surface to be equal.

(2) Eyring[2] has shown that in the calculations of viscous flow in liquids the volume of a hole comes out to be only a fraction of the volume of a molecule while the author assumes them to be equal.

(3) To explain the serious discrepancies between the calculated and observed values of the latent heats of fusion the author claims that the substitution of the radius of a single atom for that of a molecule will bring about an agreement between these two values. But this is not evident from the data presented in Table II which render the acceptance of such an arbitrary assumption unnecessary.

(4) The equation derived by the author is claimed to be applicable to the case of monatomic liquids. But the observed and calculated values of the latent heats of fusion of mercury do not support this claim.

(5) Casually also it may be said that in the sentence, "Again, the sum total of the attractive and repulsive forces, U, . . ." etc., in paragraph 6, the word "force" should be replaced by "energy," so that $(U-U^*)/RT$ may become a dimensionless quantity.

[1] J. Frenkel, *Kinetic Theory of Liquids* (Clarendon Press, Oxford, 1946), pp. 179–180.
[2] Glasstone, Laidler, and Eyring, *The Theory of Rate Processes* (McGraw-Hill Book Company, Inc., New York, 1941), pp. 508–510.

On the Principle of Thermal Interaction

P. Mazur
Faculté des Sciences de l'Université Libre de Bruxelles, Brussels, Belgium

(Received September 24, 1951)

IN a recent paper[1] H. Holtan introduces a new hypothesis "the principle of thermal interaction" in order to give a description of the interaction between different transport phenomena in non-isothermal systems by means of known thermodynamic functions only. Without going into the details of the rather intricate thermodynamic derivations, it seems interesting to examine more closely the basic ideas involved.

We would like to point out first that the mutual phenomenological coefficient R_{12}[2] is related directly, in the case of a binary mixture, to the so-called thermal diffusion coefficient.[3,4] It is obvious and well known from the theory of non-uniform gases[5] that this coefficient can only be evaluated by means of a kinetic treatment based on a peculiar law of interaction. In this respect there is no difference between R_{12} and the coefficients R_{11} and R_{22}, which are related to the ordinary diffusion coefficient and the coefficient of heat conductivity.

For gaseous thermocells, the coefficients R_{12} is related to the Knudsen coefficient in the case of a narrow connecting tube between the two parts of the cell. Again, however, a general evaluation of this coefficient can be given only on a kinetic basis, as all intermediate cases between the limiting Knudsen case and the normal case, where R_{12} reduces to zero, are possible. The value of R_{12} depends, as is well known, on the ratio of the tube width and the mean free path of the particles; therefore no general purely thermodynamic expression can be given for this coefficient.[6]

Another illustration of the fact that mutual phenomenological coefficients cannot be expressed in terms of known thermodynamic functions only is given by Saxén's relation between streaming potential and electroosmosis.[7] Here R_{12} is a function of such quantities as the viscosity of the medium, the dielectric constant, and the ζ-potential of the electric double layer.

As Holtan states, the result of his principle is that any particle will tend to move against the temperature gradient. For one-component continuous systems the macroscopic motion of the particles is described by an equation of motion containing the divergence of the pressure tensor. According to the theory of non-uniform gases,[5] this pressure tensor does not depend explicitly upon the temperature gradient in the second approximation of Chapman-Enskog, that is, in the region of validity of the thermodynamics of irreversible processes when applied to continuous system.[8] Holtan's hypothesis is in contradiction with this result of the kinetic theory of gases and cannot be accepted as a new general principle of irreversible thermodynamics.

The aim of irreversible thermodynamics is not the evaluation of kinetic quantities, but the establishment of general relations between different irreversible processes, e.g., transport phenomena. The importance of Onsager's reciprocal relations is to be found in the reduction of the number of unknown kinetic coefficients. Further analysis of these coefficients requires a kinetic treatment, just as statistical mechanics is required in order to evaluate thermodynamic quantities in classical thermodynamics.

[1] H. Holtan, Jr., J. Chem. Phys. **19**, 520 (1951).
[2] See reference 1, Eq. (6).
[3] I. Prigogine, *Thermodynamique des phénomènes irréversibles* (Ed. Desoer, Liège, 1947).
[4] S. R. de Groot, *Thermodynamics of Irreversible Processes* (North Holland Publishing Company, Amsterdam, Holland, 1951).
[5] Chapman and Cowling, *Mathematical Theory of Nonuniform Gases* (Cambridge University Press, Cambridge, 1939).
[6] S. Weber, Commun. Leiden Suppl. 716; Rapports et Communications sixième Congrès international du Froid, Buenos Aires; Commun. Leiden 246 d; Rapports et Communications, Septième Congrès international du Froid, Ia Haye-Amstérdam, 1936.
[7] P. Mazur and J. Th. G. Overbeek, Rec. trav. chim. **70**, 84 (1951).
[8] I. Prigogine, Acad. roy. Belg. Bull. classe sci. [5] **34**, 789 (1948), Physica **15**, 272 (1949).

Infrared Spectra of CD_2CO and CHDCO*

William H. Fletcher and William F. Arendale
University of Tennessee, Knoxville, Tennessee

(Received September 12, 1951)

THE infrared spectrum of CH_2CO has been observed and discussed by several investigators recently.[1–3] There is complete agreement on the assignment of the parallel fundamentals, but it has not been possible to arrive at a satisfactory assignment of the perpendicular fundamentals. In order to find the correct assignment of these bands and to resolve some of the uncertainties in overtone assignments, the spectra of CD_2CO and CHDCO have been observed. A Perkin-Elmer Model 12-C spectrometer with potassium bromide, rocksalt, and calcium fluoride prisms was used. The positions of the parallel fundamentals and the two most prominent overtones are given in Table I. The corresponding bands for CH_2CO which have been already reported are included for comparison.

An interesting case of Fermi resonance is observed between the energy levels ν_4 and $2\nu_9$. The isotopic shift which affects ν_4 much

TABLE I. Observed parallel bands of ketene.

	CD_2CO	CHDCO	CH_2CO
ν_1	2267 cm^{-1}	3126 cm^{-1}	3068 cm^{-1}
ν_2	2117	~2150	2151
ν_3	1229	1293	1388
ν_4	862	1046	1120
$2\nu_3$	2457	2583	
$2\nu_9$	927	1003	1062

more than ν_9 causes a reversal of the relative magnitudes of ν_4 and $2\nu_9$ in going from CH_2CO to CD_2CO. Fermi resonance is strongest between these two levels in CHDCO. It is probable that interaction between these levels exists also in CH_2CO. Quite strong Fermi resonance occurs between ν_1 and ν_2 in CD_2CO, and the two are of much more nearly equal intensity than they are in CH_2CO.

The perpendicular bands of CD_2CO are not nearly as prominent as in CH_2CO. The antisymmetric CD stretching band is almost completely covered by the adjacent parallel bands ν_1 and $2\nu_3$. The lower end of one band (probably ν_6) appears on the side of ν_4. Another perpendicular band lies between 750 cm^{-1} and 650 cm^{-1} and is not overlapped by any other fundamentals. Its form suggests that it is subject to rather strong perturbations. The two skeletal bending frequencies are below 550 cm^{-1} in the KBr region. They are badly overlapped and strongly perturbed as they are in CH_2CO.

Not much can be said about the perpendicular bands of CHDCO, since all of these gas samples contained large amounts of CH_2CO and CD_2CO.

A detailed investigation of the parallel and perpendicular bands of CH_2CO and CD_2CO is being made with the grating spectrometer in the University of Tennessee Physics Department.† Band analyses and more complete assignments will be reported as the work progresses.

* This work is being supported by a Frederick Gardner Cottrell grant from the Research Corporation.

[1] Frederick Halverson and Van Zandt Williams, J. Chem. Phys. **15**, 552 (1947).

[2] W. R. Harp and R. S. Rasmussen, J. Chem. Phys. **15**, 778 (1947).

[3] L. G. Drayton and H. W. Thompson, J. Chem. Soc., 1416 (1948).

† The completion of this spectrometer was made possible by a Frederick Gardner Cottrell grant from the Research Corporation.

Structure-Optical Studies. III. Smeared X-Ray Layer Lines from Periodide Crystals

C. D. WEST
Polaroid Corporation, Cambridge, Massachusetts
(Received September 14, 1951)

THE periodides form an extensive class of crystalline solids, few of which have been measured crystallographically, and many of which have compositions not falling into any simple system. In an x-ray diffraction survey of selected crystalline periodides, chiefly with polar organic molecules, and characterized by strong positive dichroism, we find numerous examples of smeared layer lines superposed on typical spot-diffraction patterns. These effects are attributed to diffraction by mixed structures containing three-dimensional gratings and line gratings. The period of the line gratings in all of these crystalline periodides is constant at 3.1A. This is just the same value as was reported for well-oriented addition compounds of iodine with polar linear high polymers, which likewise have strong positive dichroism.[1] The implication is that linear polyiodine has a stable existence in solid association with two different kinds of polar molecules, namely high polymers molecules and molecules of ordinary dimensions. Examples of positive-dichroic periodide crystals which show the smeared layer lines are cinchonidine herapathite, benzamide plus HI_3, coumarin plus KI_3, and piperin plus NH_4I_3. There also exist positive-dichroic periodide crystals which do not exhibit smeared layer lines. Examples are quinine herapathite, purpureo cobalt sulfate tri-iodide, and the ethyl oxalate alkali tri-iodides.

The foregoing paragraph is the abstract, slightly revised, of a talk presented with E. J. Weichel before the American Society for X-Ray and Electron Diffraction in June, 1947. The periodide crystals examined were all formed from solution and none was analyzed chemically. Of the four periodides named the smearing is most distinct in the case of the benzamide plus HI_3 crystal. A rotation picture of this crystal has distinct spots on the equator and first layer line, which is not smeared, and which shows a period of 3.75A; beyond this is a uniformly blackened continuous layer line of period 3.10A. Similar pictures made with the crystal stationary show it to have a fibrous structure, and some intensity maxima appear on the continuous layer lines.

[1] C. D. West, J. Chem. Phys. **15**, 689(L) (1947); **17**, 219(L) (1949). F. Cramer recently reported similar observations on the oriented addition compound of iodine with α-dextrin (Naturwiss. **38**, 188 (1951)). Another recent example is the oriented addition compound of iodine with polyvinylene, which provides the first dichroic polarizer for the near infrared: *cf.* Blake, Makas, and West, J. Opt. Soc. Am. **39**, 1054(A) (1949).

The Molecular and Crystal Structure of Nitric Oxide Dimer

WILLIAM J. DULMAGE,* EDWARD A. MEYERS, AND WILLIAM N. LIPSCOMB
School of Chemistry, University of Minnesota, Minneapolis, Minnesota
(Received September 24, 1951)

CRYSTALLINE nitric oxide has been known for some time to be diamagnetic[1] and to have a residual entropy[2] of very nearly $\frac{1}{2}R\ln 2$ per mole of NO. These facts strongly suggest a dimer, N_2O_2. Some spectroscopic evidence has been advanced[3] regarding the existence of this dimer, and further conclusions relating to its structure have been presented.[4] We have nearly completed an x-ray diffraction investigation of single crystals of nitric oxide, and have determined the structure of the dimer as described below.

The crystals are monoclinic, with two molecules of N_2O_2 in a cell with $a=6.64$, $b=3.93$, $c=6.52$A, and $\beta=128.0°$. The space group is $P2_1/a$, which requires that the dimer must have a center of symmetry, at least statistically if not actually. The atoms are in general positions of this space group, and, with the origin chosen at a symmetry center, preliminary values of the parameters are

$$x_1=0.227 \qquad x_2=0.159$$
$$y_1=0.117 \qquad y_2=-0.100$$
$$z_1=0.194 \qquad z_2=0.242.$$

These parameters were obtained from the resolved electron density projections along [100] and [001], and have been corrected for termination of the series. A complete least-squares treatment of the $\{hk0\}$, $\{0kl\}$, $\{h0l\}$, $\{hk\bar{h}\}$, and $\{hk\bar{k}\}$ zones is now in progress.

The molecule is approximately a rectangle with the dimensions,

N←2.38A→O
↑
1.10A
↓
O N.

The residual entropy is accounted for by the two possible orientations

N O O N
and
O N N O,

in the crystal. The essentially identical electron densities of N and O, obtained in our electron density maps, tend to support this interpretation.[5] The distance of the strong bond, 1.10A, is in good agreement with the predicted value of 1.10A obtained with the use of double and triple bond distances[6] of 1.19A and 1.07A if one assumes 50 percent triple-bond character. Thus it is probable that the dimer has mainly the electronic structure represented by the resonance hybrid.

This interpretation suggests that the rather unusual long bond is partly ionic, but some degree of covalency could be achieved by the use of double bonds only for the short bonds, thus making available a vacant orbital on the nitrogen atom. It is interesting that the bond distance of 2.38A would suggest only three percent of a covalent single bond if one uses Pauling's equation[7] for bond order,

$$d = d_1 - 0.6 \log n.$$

However, dispersion, polarization, and other electrostatic forces would probably be of greater importance than the covalent forces in this dimerization. The presence of such weak bonds is at least consistent with the low value,[8] 4000 cal/mole of N_2O_2 or less, of the heat of dissociation of the dimer.

In view of these results and of the long N−N bond of 1.64A observed[9] in N_2O_4, it would be reasonable to expect a long bond in N_2O_3, which is now under investigation.

Support of this work by the Office of Naval Research is gratefully acknowledged.

* Present address, Electric Reduction Company of Canada, Ltd., Buckingham, P. Q., Canada.

[1] E. Lips, Helv. Phys. Acta **8**, 247 (1935).
[2] H. L. Johnston and W. F. Giauque, J. Am. Chem. Soc. **51**, 3194 (1929).
[3] Vodar, Jardillier, and Mayence, Compt. rend. **222**, 1343 (1946).
[4] Smith, Keller, and Johnston, J. Chem. Phys. **19**, 189 (1951).
[5] A statistically arranged dimer with the short NO groups parallel within any given molecule would also satisfy the data, but would require nearly equivalent long bonds between NN and OO, would appear to give unfavorable electronic distributions of charge, and may show a permanent dipole moment, though small, sufficient to order the solid.
[6] W. Gordy, J. Chem. Phys. **15**, 81 (1947). The resonance curve given by Pauling, *Nature of the Chemical Bond* (Cornell University Press, Ithaca, 1940), second edition, p. 174, was modified to correspond to the double-bond distance of 1.35A.
[7] L. Pauling, J. Am. Chem. Soc. **69**, 542 (1947).
[8] A. Eucken and L. d'Or, Nachr. Ges. Wiss. Göttingen, Math.-physik. Kl. 107 (1932). Also O. K. Rice, J. Chem. Phys. **4**, 367 (1936).
[9] J. S. Broadley and J. M. Robertson, Nature **164**, 915 (1949).

On the Three- and Four-Center Integrals in Molecular Quantum Mechanics

KLAUS RÜDENBERG*
Department of Physics, University of Chicago, Chicago, Illinois
(Received September 5, 1951)

THE integrals which arise if one expands the electronic wave functions of molecules in terms of atomic orbitals have recently been studied by several authors, Coulson, Löwdin, Kotani, Kopineck, Roothaan, Rüdenberg, and others. The object of the present note is to point out a relation between the three- and four-center electron repulsion integrals on the one hand and the two-center integrals on the other hand. Approximate relations of this type had been assumed intuitively by A. London and R. S. Mulliken; the derivation below is related to the formula of Mulliken.[1]

Let

$$\chi_{a1},\ \chi_{a2},\ \cdots\ \chi_{ak}\ \cdots \tag{1}$$

be a complete set of *orthogonalized* real orbitals on center a—analogously

$$\left.\begin{array}{llll}\chi_{a1}, & \chi_{b2}, & \cdots & \chi_{bk}\ \cdots,\\ \chi_{c1}, & \chi_{c2}, & \cdots & \chi_{ck}\ \cdots,\\ \chi_{d1}, & \chi_{d2}, & \cdots & \chi_{dk}\ \cdots,\end{array}\right\} \tag{2}$$

on the centers b, c, d, respectively. We consider the integral

$$[\chi_{a\alpha}\chi_{b\beta}|\chi_{c\gamma}\chi_{d\delta}] = \int dV_1 \int dV_2 \chi_{a\alpha}(1)\chi_{b\beta}(1)(1/r_{12})\chi_{c\gamma}(2)\chi_{d\delta}(2). \tag{3}$$

If

$$S_{mn} = \int dV \chi_m \chi_n \tag{4}$$

denotes the overlap integral between the orbitals χ_m and χ_n, then we have the expansions

$$\chi_{a\alpha}(1) = \sum_{k=1}^{\infty} S_{a\alpha,\,bk}\chi_{bk}(1), \tag{5}$$

$$\chi_{b\beta}(1) = \sum_{k=1}^{\infty} S_{b\beta,\,ak}\chi_{ak}(1), \tag{6}$$

whence:

$$\chi_{a\alpha}(1)\chi_{b\beta}(1) = \tfrac{1}{2}\sum_{k=1}^{\infty} \times\{S_{a\alpha\ bk}\chi_{b\beta}(1)\chi_{bk}(1) + S_{b\beta,\,ak}\chi_{a\alpha}(1)\chi_{ak}(1)\}. \tag{7}$$

Insertion of (7) and the analogous formula for the centers c, d in (3) yields

$$\left.\begin{aligned}[\chi_{a\alpha}\chi_{b\beta}|\chi_{c\gamma}\chi_{d\delta}] = \tfrac{1}{4}\sum_{k=1}^{\infty}\sum_{j=1}^{\infty} &\times\{S_{a\alpha,\,bk}S_{c\gamma,\,dj}[\chi_{bk}\chi_{b\beta}|\chi_{dj}\chi_{d\delta}]\\ &+S_{a\alpha,\,bk}S_{d\delta,\,cj}[\chi_{bk}\chi_{b\beta}|\chi_{c\gamma}\chi_{cj}]\\ &+S_{b\beta,\,ak}S_{c\gamma,\,dj}[\chi_{a\alpha}\chi_{ak}|\chi_{dj}\chi_{d\delta}]\\ &+S_{b\beta,\,ak}S_{d\delta,\,cj}[\chi_{a\alpha}\chi_{ak}|\chi_{c\gamma}\chi_{cj}]\}\end{aligned}\right. \tag{8}$$

Equation (8) expresses the four-center integral in terms of two-center coulomb integrals and overlap integrals.

The convergence in (7) will be good if the two centers a and b are not too far apart, since

$$S_{a\alpha,\,ak} = \delta_{\alpha k}, \quad S_{b\beta,\,bk} = \delta_{\beta k}. \tag{9}$$

In this case the largest term in (7) is given by

$$\chi_{a\alpha}(1)\chi_{b\beta}(1) \approx \tfrac{1}{2}\{S_{a\alpha,\,b\alpha}\chi_{b\alpha}(1)\chi_{b\beta}(1) + S_{b\beta,\,a\beta}\chi_{a\alpha}(1)\chi_{a\beta}(1)\}. \tag{10}$$

If in addition one has $\alpha = \beta$, i.e., if the orbitals on the atoms a and b are the same except for their respective center points, then Eq. (10) simplifies to

$$\chi_{a\alpha}(1)\chi_{b\alpha}(1) \approx \tfrac{1}{2}S_{a\alpha,\,b\alpha}\{\chi_{a\alpha}(1)\chi_{a\alpha}(1) + \chi_{b\alpha}(1)\chi_{b\alpha}(1)\}, \tag{11}$$

or, omitting α and β,

$$\chi_a(1)\chi_b(1) \approx \tfrac{1}{2}S_{ab}\{\chi_a(1)\chi_a(1) + \chi_b(1)\chi_b(1)\}, \tag{12}$$

which, upon substitution in (3), yields the formula of Mulliken.[2] Analogous arguments hold, of course, for the centers c and d.

If the centers a and b are farther apart from each other, then another term of the expansion (7) may prove to be the most important one upon substitution in (3).

If the centers a and c are close to each other, and if the same holds for the centers b and d, then it may be that a better convergence is obtained by taking

$$\chi_{a\alpha}(1)\chi_{c\gamma}(2) = \tfrac{1}{2}\sum_{k=1}^{\infty} \times\{S_{a\alpha,\,ck}\chi_{ck}(1)\chi_{c\gamma}(2) + S_{c\gamma,\,ak}\chi_{a\alpha}(1)\chi_{ak}(2)\} \tag{13}$$

and the analogous formula for the pair b, d. Thus the four-center integral is reduced to two-center exchange integrals and overlap integrals:

$$\left.\begin{aligned}[\chi_{a\alpha}\chi_{b\beta}|\chi_{c\gamma}\chi_{d\delta}] = \tfrac{1}{4}\sum_{k=1}^{\infty}\sum_{j=1}^{\infty} &\times\{S_{a\alpha,\,ck}S_{b\beta,\,dj}[\chi_{ck}\chi_{dj}|\chi_{c\gamma}\chi_{d\delta}]\\ &+S_{a\alpha,\,ck}S_{d\delta,\,bj}[\chi_{ck}\chi_{b\beta}|\chi_{c\gamma}\chi_{mj}]\\ &+S_{c\gamma,\,ak}S_{b\beta,\,dj}[\chi_{a\alpha}\chi_{dj}|\chi_{ak}\chi_{d\delta}]\\ &+S_{c\gamma,\,ak}S_{d\delta,\,bj}[\chi_{a\alpha}\chi_{b\beta}|\chi_{ak}\chi_{bj}]\}\end{aligned}\right. \tag{14}$$

The largest term of Eq. (13) in the case $\alpha = \gamma$, namely,

$$\chi_{a\alpha}(1)\chi_{ca}(2) \approx \tfrac{1}{2}S_{a\alpha,\,ca}\{\chi_{ca}(1)\chi_{ca}(2) + \chi_{a\alpha}(1)\chi_{a\alpha}(2)\}, \tag{15}$$

corresponds to Eq. (11) and, upon insertion in (3), yields a formula analogous to the one of Mulliken.

A correct information on the convergence can be obtained only by calculating concrete cases. It may be instructive to expand, by virtue of (7), two-center exchange integrals in terms of two-center coulomb integrals, overlap integrals, and one-center integrals or, by virtue of (13), to expand two-center coulomb integrals in terms of two-center exchange integrals, overlap integrals, and one-center integrals. For, in these cases, the approximate values obtained by the method described in this note could be compared with the exact values, which are independently accessible.[3]

* Work assisted by the ONR.
[1] R. S. Mulliken, J. Chim. Phys. **46**, 500 and 521 (1949).
[2] Mulliken reported good results with this approximation.
[3] See the recent work of C. C. J. Roothaan and the present author.

Errata: A Two-Path Method for Measuring Flame Temperatures and Concentrations in Low-Pressure Combustion Flames

[J. Chem. Phys. 19, 272–280 (1951)]

S. S. PENNER
Jet Propulsion Laboratory, California Institute of Technology, Pasadena, California

IN Eq. (A1) the factor log2 should be replaced by 2.303 log2. Hence the Doppler half-width becomes $\alpha_D \sim 7\times10^{-3}$ cm^{-1}. Equation (A2) should read

$$\alpha_c=(1/\pi)(3.8\pi kT)^{\frac{1}{2}}N_T p p^2[(m_1+m_2)/m_1m_2]^{+\frac{1}{2}}, \qquad \text{(A2)}$$

and the quantity $(m_1+m_2)/m_1$ appearing on page 280 should be replaced by $(m_1+m_2)/m_1m_2$. Also $\alpha_c \sim 1\times10^{-3}$ cm^{-1}. The integrand in Eq. (A13) should be multiplied by the factor cos$S$. The quantity $N_T\pi e^2/3\mu c$ should be multiplied by the factor $\omega^*/\omega_e=\nu_{0\to1}/\omega_e\simeq0.988$ wherever it appears in Sec. IV. Also $\gamma=h/4\pi^2Ic\omega_e$. All other numerical values and equations remain unchanged.

Pure Quadrupole Spectra: the Substituted Methanes*

RALPH LIVINGSTON
Chemistry Division, Oak Ridge National Laboratory, Oak Ridge, Tennessee
(Received September 12, 1951)

THE pure quadrupole spectra of Cl isotopes in a number of substituted methanes have been measured in the manner already described.[1] Two or more closely spaced lines, presumed to originate from different Cl symmetry groups in the crystal lattice, are frequently found. In such cases the average frequency is used to compute an average coupling, taken to be twice the frequency.[2] Only the magnitudes of the couplings are considered, the sign not being determined by this method.

The observed frequencies at three temperatures and computed nuclear quadrupole couplings at 20°K for Cl^{35} are given in Table I. The interaction of lattice vibrations with the spin system is expected to cause an increase in frequency with a decrease in temperature.[2] A small frequency increase is observed in all cases in cooling from 77°K to 20°K, while further cooling to 4°K, for the few cases studied, gives very little additional increase. A preliminary measurement on $CHCl_3$ at 4°K similarly gave about 0.01 Mc increase over the 20°K value. Cooling to 4°K gives a noticeable increase in relaxation time as evidenced by a loss of sensitivity in the equipment.

There are regularities in trend of the couplings in Table I. Progressively replacing the hydrogen atoms by Cl in CH_3Cl gives rise to smooth coupling increases averaging about 4.5 Mc for each Cl added. Similarly the complete replacement of H by F in CH_3Cl, CH_2Cl_2, and $CHCl_3$ gives rise to an average coupling increase of 2.9 Mc for each F added. These changes in coupling may be explained in terms of two opposing effects in the molecular binding. When H is replaced by a halogen the C−Cl bond becomes less ionic in character because of a polarization by the electronegative halogen, causing a coupling increase.[3] This effect should decrease

TABLE I. Observed frequencies and quadrupole couplings for Cl^{35}.

Compound	Observed frequency, Mc 77°K	20°K	4°K	$\lvert eqQ\rvert$ av. Mc 20°K
CH_3Cl	34.029	34.199	34.206	68.40
CH_2Cl_2	35.991	36.233	36.243	72.47
$CHCl_3$	38.254 38.308	38.486 38.490		76.98
CCl_4	40.46[a] 40.52 40.54 40.61 40.64 40.65 40.72	41.139 41.109 41.045 41.022 40.972 40.965 40.918 40.895 40.888 40.831 40.826 40.800 40.794 40.732		81.85
CHF_2Cl		35.249		70.50
CF_3Cl	38.089	38.790		77.58
$CHFCl_2$	36.479 36.508	36.752 36.775		73.53
CF_2Cl_2	38.450	39.078		78.16
$CFCl_3$	39.161 39.517 39.703	39.537 39.867 40.046		79.63
CF_2BrCl	38.342	38.675		77.35
Cl_2	54.248	54.476[b]		108.95

[a] Fourteen very weak closely spaced lines were observed. Approximate frequencies are given for seven of them.
[b] The Cl^{37} frequency was measured at 20°K and that for Cl^{35} computed from the quadrupole moment ratio. Both isotopes were measured at 77°K and the ratio agreed with the published value (see reference 1).

in the order F, Cl, and Br corresponding to the Pauling electronegativity values 4.0, 3.0, and 2.8, respectively. Comparison of the couplings for CF_2BrCl, CF_2Cl_2, and CF_3Cl indicates that the substitution of Br for Cl is consistent with this concept. The substitution of F for Cl, however, gives a decrease in coupling. This and the small increase when H is replaced by F (as compared with Cl) may be explained by contributions of the resonant structure $X^-C{=}Cl^+$ [4] which will decrease the coupling.[3] This effect should be largest, for F. Pauling[5] has applied this concept in discussing the bond lengths in the fluorochloromethanes and fluoromethanes. Admittedly the previous considerations need further refinement.

Some of the couplings may be compared with values determined by other methods. The coupling value for Cl^{35} in Cl_2 at 20°K should be somewhat better than that previously published.[6] It is 0.7 percent lower than the recently remeasured value for atomic chlorine.[7] The coupling for CF_3Cl is 0.6 percent lower than the microwave value of 78.05 Mc.[8] On the other hand the value for CH_3Cl is 9.0 percent lower than the microwave value of 75.13 Mc[9] much like Dehmelt and Krüger's[2] values for Br in solid CH_3Br which is 8.3 percent lower than the microwave value and I in CH_3I which is 9.3 percent low.[10] These differences seem to be indicative of a change in character of the carbon-halogen bond on going from the gaseous to the solid state.

I have benefited from helpful discussions with H. A. Levy and the cooperation of R. Erickson on the liquid hydrogen aspects of the work.

* This work was performed for the AEC.
[1] R. Livingston, Phys. Rev. **82**, 289 (1951).
[2] H. G. Dehmelt and H. Krüger, Z. Physik **129**, 401 (1951).
[3] C. H. Townes and B. P. Dailey, J. Chem. Phys. **17**, 782 (1949).
[4] The use of this resonant structure was first suggested to me by C. H. Townes.
[5] L. Pauling, *The Nature of the Chemical Bond* (Cornell University Press, Ithaca, New York, 1944), second edition.
[6] R. Livingston, J. Chem. Phys. **19**, 803 (1951).
[7] V. Jaccarino and J. G. King, Phys. Rev. **83**, 471 (1951).
[8] D. K. Coles and R. H. Hughes, Phys. Rev. **76**, 858 (1949).
[9] Gordy, Simmons, and Smith, Phys. Rev. **74**, 243 (1948).
[10] H. G. Dehmelt, Naturwiss. **37**, 398 (1950).